UNIVERSITAT POLITÈCNICA DE VALÈNCIA

DOCTORADO EN INGENIERÍA Y PRODUCCIÓN INDUSTRIAL

TESIS DOCTORAL

"Use of wool reinforcements for biodegradable materials"

Autor:

Franciszek Józef Pawlak

Directed by:

Dr. Juan López Martínez

Dr. Miguel Aldás Carrasco

Date of presentation:

October 2024

UNIVERSITAT POLITÈCNICA DE VALÈNCIA

DOCTORADO EN INGENIERÍA Y PRODUCCIÓN INDUSTRIAL

TESIS DOCTORAL

"Uso de refuerzo de la lana para materiales biodegradables"

Franciszek Józef Pawlak

El Dr. Juan López Martínez, Catedrático del Departamento de Ingeniería Mecánica y de Materiales de la Universitat Politècnica de València (UPV, Valencia, España) y el Dr. Miguel Fernando Aldás Carrasco, Profesor a tiempo completo del Facultad de Ingeniería Química y Agroindustria, Escuela Politécnica Nacional (EPN, Quito, Ecuador), en calidad de directores de la Tesis Doctoral (modalidad Doctorado Internacional) presentada por D. Franciszek Józef Pawlak, con el título **"Uso de refuerzo de la lana para materiales biodegradables"** (Use of wool reinforcements for biodegradable materials"),

CERTIFICAN

Que la presente memoria, **"Uso de refuerzo de la lana para materiales biodegradables"**, para aspirar al grado de Doctor por la Universitat Politècnica de València, reúne las condiciones adecuadas para constituir la tesis doctoral de D. Franciszek Józef Pawlak (modalidad Doctorado Internacional).

Asimismo, certifican que la citada tesis doctoral se ha realizado en el Instituto de Tecnología de Materiales de la Universitat Politècnica de València.

Y para que conste a los efectos oportunos, firman la presente en Alcoy a 2 de octubre de 2024.

LOPEZ MARTINEZ JUAN - 22690214R

Firmado digitalmente por LOPEZ MARTINEZ JUAN - 22690214R
Fecha: 2024.10.03 10:04:14 +02'00'

ALDAS CARRASCO MIGUEL FERNANDO - 29572618T

Firmado digitalmente por ALDAS CARRASCO MIGUEL FERNANDO - 29572618T
Fecha: 2024.10.02 07:37:35 -05'00'

Fdo.

Dr. Juan López Martínez

Fdo.

Dr. Miguel Fernando Aldás Carrasco

pol. "...Bo nie jest światło, by pod korcem stało,
Ani sól ziemi do przypraw kuchennych,
Bo piękno na to jest, by zachwycało
Do pracy, praca, by się piękno zmartwychwstało..."

esp. "...Pues la luz no está destinada a permanecer bajo la jarra,
Ni la sal de la tierra para las especias de cocina,
Porque la belleza está destinada a encantar para el trabajo,
Y el trabajo, para que la belleza resucite..."

C.K. Norwid, Promethidion

A mi familia

AGRADECIMIENTOS

En primer lugar, me gustaría agradecer a la Universitat Politècnica de València (UPV) y al Instituto Universitario de Tecnología de Materiales (IUTM) del Departamento de Ingeniería Mecánica y Materiales por acogerme como estudiante de doctorado y permitirme llevar a cabo la investigación presentada en la presente tesis doctoral.

Específicamente, quiero expresar mi agradecimiento al Prof. Dr. Juan López Martínez por la oportunidad que me brindó y por confiar en cada paso antes y durante mis estudios de doctorado. Agradezco también al Dr. Miguel Fernando Aldás Carrasco por su apoyo en la investigación y la co-dirección del estudio.

A la Prof. Dra. Dana Luca Motoc de la Universitatea Transilvania din Brașov (UniTBv) le agradezco por recibirme durante mi estancia internacional y por su ayuda en la investigación.

Al grupo de investigación completo, profesores, personal técnico, investigadores y colegas de la Escuela Politécnica Superior de Alcoy (EPSA), específicamente del Instituto Universitario de Tecnología de Materiales en Alcoy, les agradezco su presencia y colaboración.

A mis amigos, doctores, Cris, Sandra, Harrison, Diego, Vero, Miguelito, Martín, Mado, Pelayo, Dani, Vincent, Octavio y otros que probablemente olvido mencionar, les agradezco por acompañarme durante mi estancia en Alcoy y por los buenos recuerdos.

A mis colegas, de trabajo en Atos, Thyssenkrupp, Eviden; a Marta, Mateusz, Tomek, Marcin, Stanisław, Agnieszka, Gosia, Sandra, Sebastian, Monika, Kuba, Przemek, Katie, Kasia, Sebastian, y otros que probablemente olvido mencionar, les agradezco por la motivación.

Finalmente, gracias a Wiktoria, a mis padres, Albina y Jan, y a mi familia cercana, Halina, Jan, Agnieszka, Łukasz, Marysia, Stanisław, Ania, Maria, por su apoyo incondicional y su paciencia.

RESUMEN

“Uso de refuerzo de la lana para materiales biodegradables”

En esta tesis doctoral se examina el uso de fibras de lana de oveja, derivadas de la industria láctea, como refuerzo sostenible para materiales poliméricos biodegradables. La tesis doctoral se divide en cinco capítulos principales que abordan la introducción, los objetivos y la planificación, la parte experimental, los resultados y la discusión, y las conclusiones. Estos capítulos se complementan con referencias y un apéndice al final de la disertación. El primer capítulo, denominado introducción, cubre una revisión general de la literatura sobre el tema principal discutido en la tesis doctoral, que incluye fibras, bioplásticos, materiales poliméricos biodegradables, polímeros reforzados con fibras y un subcapítulo dedicado al modelado computacional. El segundo capítulo aborda el propósito de la investigación, los objetivos específicos de la tesis doctoral y el plan de investigación para lograrlos. El tercer capítulo detalla la metodología experimental, las técnicas de caracterización aplicadas y los materiales utilizados. El cuarto capítulo presenta, analiza y discute los resultados adquiridos en la tesis doctoral, divididos en seis secciones. Finalmente, el quinto capítulo aborda la sección de conclusiones, proporcionando conclusiones generales y conclusiones específicas para cada trabajo de investigación. Como requisito para obtener el título de Doctor con la mención "Doctorado Internacional", al menos una sección del capítulo de resultados y discusión, el resumen y las conclusiones se redactaron en inglés.

El objetivo general de la tesis doctoral se logró mediante la realización de seis trabajos de investigación, que se dividieron en objetivos específicos de la tesis doctoral, uno para cada estudio realizado. Estos trabajos se separaron en dos grupos, donde cuatro estudios principales se centraron en la preparación de materiales y su caracterización en laboratorio, y dos estudios complementarios se centraron en modelado de aprendizaje automático de las características previamente obtenidas. Antes de la investigación diseñada para la tesis doctoral, se recopilaron varias observaciones generales basadas en investigaciones realizadas en el grupo de investigación y en la literatura del campo de estudio. Entre ellas, se considera que la modificación del aceite natural o la modificación superficial de las fibras son un buen enfoque para obtener polímeros reforzados con fibras (FRPs). Los estudios de caracterización de materiales se llevaron a cabo para investigar varias variables que influyen en las características de los FRPs, centrándose en la composición del material, la interacción y tratamiento superficial, el preprocesamiento del material o la estabilidad en condiciones específicas. Por otro lado, los estudios complementarios se realizaron para proporcionar un nuevo enfoque de modelado mejorado por inteligencia artificial para predicciones de propiedades de materiales en relación con diferentes composiciones o tratamientos superficiales.

El estudio presentado en el primer capítulo se centró en la elaboración de mezclas de ácido poliláctico/aceite de linaza maleinizado reforzadas con fibras de lana de oveja. Para este fin, se aplicaron varios agentes de acoplamiento de silano y alquiloxi a fibras cortas de lana para aumentar el número de grupos funcionales en la superficie de la fibra. Entre los grupos funcionales adheridos por el tratamiento superficial se distinguen aminas primarias, secundarias y terciarias, epoxi y grupos vinílicos. Las fibras modificadas se aplicaron a una concentración única a la mezcla de ácido poliláctico/aceite de linaza maleinizado previamente establecida. El tratamiento

superficial con diferentes agentes de acoplamiento resultó en cambios principalmente en propiedades mecánicas y térmicas. Se descubrió que el tratamiento de alquiloxi de las fibras de lana de oveja con isopropóxido de titanio (IV) (trietanolamina) fue el más efectivo en cuanto a propiedades mecánicas de tracción, mientras que el tratamiento de silano con trimetoxi (2-(7-oxabiciclo(4.1.0)hept-3-yl)etil)silano resultó en altas mejoras en la resistencia al impacto entre los agentes de acoplamiento probados. En cuanto al impacto del tratamiento superficial de la lana en las propiedades térmicas, se encontró que dichas modificaciones resultaron en un aumento de las temperaturas de cristalización en frío y en un menor grado de cristalinidad. Sin embargo, la modificación de alquiloxi con isopropóxido de titanio (IV) (trietanolamina) disminuyó la estabilidad térmica, a diferencia de otros modificadores superficiales, determinación que se hizo estudiando la temperatura de pérdida de masa del 5%.

En el estudio descrito en el segundo capítulo es una continuación del estudio sobre el impacto del tratamiento superficial en las características de los FRPs. Entre los tratamientos superficiales previamente probados, se seleccionó para un examen detallado el silano tris(2-metoxietoxi)(vinilo). El estudio tenía como objetivo descubrir la influencia de concentraciones más altas de fibras de lana de oveja en formulaciones poliméricas y concentraciones más altas del agente de tratamiento superficial con respecto a las fibras de lana de oveja. Basándonos en la experiencia del estudio anterior, la reacción de tratamiento superficial se llevó a cabo en un entorno ligeramente ajustado, incluyendo un aumento de la temperatura de reacción en 15°C. En cuanto a los resultados obtenidos, en el rendimiento mecánico, un aumento en el contenido de fibras de lana de oveja produjo una reducción de las propiedades de tracción. Esto se esperaba hasta cierto punto sabiendo que el ácido poliláctico no interactúa de manera adecuada con la superficie de la lana de oveja. Sin embargo, la aplicación del tratamiento de silano a las fibras compensó parcialmente el efecto negativo observado en el caso de las fibras de lana no modificadas. El impacto de la mejora con el aumento de la concentración del tratamiento de silano se observó principalmente en el módulo de Young o en la elongación en el punto de rotura. La concentración de fibras de lana afectó la estabilidad térmica de las formulaciones a base de ácido poliláctico, ya que la fibra de lana de oveja presenta una menor resistencia a las temperaturas elevadas. Sin embargo, la resistencia térmica es suficiente para el procesamiento con la mayoría de los polímeros termoplásticos biodegradables, como el ácido poliláctico.

El tercer capítulo se centró en un paso adicional de preprocesamiento de las fibras de lana de oveja con tratamiento de plasma y su impacto en las propiedades finales del material, entre otras propiedades mecánicas y térmicas. El tratamiento de plasma se conoce por sus aplicaciones de limpieza, que en el caso de la lana se puede utilizar para eliminar los lípidos presentes en la superficie de la fibra. Sin embargo, el tratamiento prolongado con plasma se conoce por su influencia destructiva en la superficie de la fibra de lana, por lo tanto, el pretratamiento se aplicó en poco tiempo. El estudio se centró en un estudio exhaustivo de la mezcla de ácido poliláctico/aceite de linaza maleinizado reforzada con fibras de lana no tratadas y fibras de lana con tratamiento de plasma aplicado. En cuanto a las propiedades térmicas, el pretratamiento de plasma de las fibras de lana mostró una temperatura de transición vítrea reducida y afectó la cristalización del ácido poliláctico reforzado con las fibras. Además, dado que la mayor resistencia a la tracción se encontró para el ácido poliláctico puro, la adición de refuerzo de fibra de lana no modificada redujo la propiedad de tracción. Sin embargo, se encontró que el pretratamiento con plasma fue beneficioso en esa área, lo que resultó en una elongación mejorada en el punto de rotura.

El siguiente capítulo de la tesis doctoral se centró en investigar los aspectos del envejecimiento físico del ácido poliláctico con el tiempo. El ácido poliláctico, como bioplástico, se conoce por mostrar cambios en sus características con el tiempo, incluso sin el impacto del entorno externo, conocido como envejecimiento acelerado. Como resultado, se compararon las características de las formulaciones basadas en ácido poliláctico/aceite de linaza maleinizado entre la preparación inicial del material y después de cuatro años de envejecimiento físico. El estudio se centró en formulaciones reforzadas con dos concentraciones de fibra de lana, sin tratamiento y con tratamiento de silano tris(2-metoxietoxi)(vinilo). Se evaluaron los cambios en la estructura cristalina y las temperaturas de transición del ácido poliláctico, así como el rendimiento mecánico mediante curvas de esfuerzo-deformación.

Los dos últimos capítulos experimentales, que desempeñan un papel complementario en la investigación de laboratorio. Estos se centraron en el uso de un enfoque de modelado basado en inteligencia artificial para la predicción de propiedades de materiales. El entrenamiento del modelo se realizó en función de algoritmos de regresión seleccionados y datos experimentales preprocesados derivados de la caracterización en el laboratorio. A medida que los modelos entrenados fueron evaluados con el coeficiente de determinación y métricas estadísticas medias y relativas, se implementaron para su uso en la predicción de propiedades. El objetivo de los estudios era proporcionar características predichas para un espectro más amplio de formulaciones. El primer estudio computacional se centró en las predicciones de resistencia a la tracción y pérdida de masa del 5% para el ácido poliláctico modificado con diferentes concentraciones de aceite de linaza maleinizado, diferentes concentraciones de fibra de lana de oveja, diferentes tratamientos superficiales y sus concentraciones. El segundo estudio computacional se centró en las predicciones de propiedades mecánicas y características basadas en calorimetría diferencial de barrido para el ácido poliláctico modificado con diferentes concentraciones de aceite de linaza maleinizado y diferentes concentraciones de fibra de lana de oveja.

Los resultados obtenidos en la tesis doctoral proporcionaron una mejor comprensión del refuerzo de lana de oveja en el polímero biodegradable representado por el ácido poliláctico. Un aspecto fundamental de la disertación es el uso de materiales de origen biológico en la mayor cantidad posible, donde el ácido poliláctico, el aceite de linaza maleinizado y las fibras de lana que, en su estado puro, son abundantes en la naturaleza. Además, como parte complementaria de la tesis, se investigó el enfoque computacional del modelado de aprendizaje automático aplicado para limitar el consumo de materiales y energía requerido para la investigación de un vasto espectro de concentraciones de componentes de mezcla. Como un valor añadido a la ciencia, es necesario señalar que la disertación contiene varios enfoques para investigar la interacción entre las fibras de lana de oveja y el biopolímero, además de centrarse en la aplicación a largo plazo de dichos materiales. Las amplias características mecánicas, térmicas, microestructurales y de superficie abren posibilidades para aplicaciones de materiales en diversos sectores industriales, como automotriz, aeroespacial, agricultura o aplicaciones a corto plazo. Finalmente, el trabajo abre nuevas líneas de investigación para el uso de fibras de lana como subproducto y proporciona enfoques para su utilización.

RESUM

“Ús de reforç de la llana per a materials biodegradables”

A la tesi doctoral s'examina l'ús de fibres de llana d'ovella derivades de la indústria làctia com a reforç sostenible per a materials polimèrics biodegradables. La tesi doctoral es divideix en cinc capítols principals que aborden la introducció, els objectius i la planificació, la part experimental, els resultats i la discussió, i les conclusions. Aquests capítols es complementen amb referències i un apèndix al final de la dissertació. El primer capítol, anomenat introducció, cobreix una revisió general de la literatura sobre el tema principal discutit a la tesi doctoral, que inclou fibres, bioplàstics, materials polimèrics biodegradables, polímers reforçats amb fibres i modelatge computacional. El segon capítol aborda el propòsit de la investigació, els objectius específics de la tesi doctoral i el pla de recerca per aconseguir-los. El tercer capítol detalla la metodologia experimental, les tècniques de caracterització aplicades i els materials utilitzats. El quart capítol presenta, analitza i discuteix els resultats adquirits a la tesi doctoral, dividits en sis seccions. Finalment, el cinquè capítol aborda la secció de conclusions, proporcionant conclusions generals i conclusions específiques per a cada treball de recerca. Com a requisit per a obtenir el títol de Doctor amb la menció "Doctorat Internacional", almenys una secció del capítol de resultats i discussió, el resum i les conclusions es van redactar en anglès.

L'objectiu general de la tesi doctoral es va assolir mitjançant la realització de sis treballs de recerca, que es van dividir en objectius específics de la tesi doctoral, un per a cada estudi realitzat. Aquests treballs es van separar en dos grups, on quatre estudis principals es van centrar en la preparació de materials i la seva caracterització en laboratori, i dos estudis complementaris es van centrar en el modelatge d'aprenentatge automàtic de les característiques prèviament obtingudes. Abans de la investigació dissenyada per a la tesi doctoral, es van recopilar diverses observacions generals basades en investigacions realitzades al grup de recerca i en la literatura del camp d'estudi. Entre elles, es considera que la modificació de l'oli natural o la modificació superficial de les fibres són un bon enfocament per obtenir polímers reforçats amb fibres (FRPs). Els estudis de caracterització de materials es van dur a terme per investigar diverses variables que influeixen en les característiques dels FRPs, centrant-se principalment en la composició del material, la interacció i el tractament superficial, el pre-processament del material o l'estabilitat en condicions específiques. D'altra banda, els estudis complementaris es van realitzar per proporcionar un nou enfocament de modelatge millorat per la intel·ligència artificial per a prediccions de propietats de materials en relació amb diferents composicions o tractaments superficials.

L'estudi presentat en el primer capítol es va centrar en l'elaboració d'estudis anteriors en els quals es van investigar barreges d'àcid polilàctic/oli de lli maleïtzat reforçades amb fibres de llana d'ovella. Amb aquesta finalitat, es van aplicar diversos agents d'acoblament de silà i alquiloxi a fibres curtes de llana per augmentar el nombre de grups funcionals en la superfície de la fibra. Entre els grups funcionals afegits pel tractament superficial es distingeixen amines primàries, secundàries i terciàries, epoxi i grups vinílics. Les fibres modificades es van aplicar a una concentració única a la barreja d'àcid polilàctic/oli de lli maleïtzat prèviament establerta. El tractament superficial amb diferents agents d'acoblament va provocar canvis principalment en les propietats mecàniques i tèrmiques. Es va descobrir que el tractament d'alquiloxi de les fibres de

llana d'ovella amb isoproxid de titani (IV) (trietanolamina) va ser el més efectiu pel que fa a les propietats mecàniques de tracció, mentre que el tractament de silà amb trimetoixi (2-(7-oxabiciclo(4.1.0)hept-3-yl)etil)silà va resultar en les majors millores en la resistència a l'impacte entre els agents d'acoblament provats. Pel que fa a l'impacte del tractament superficial de la llana en les propietats tèrmiques, es va trobar que aquestes modificacions van provocar un augment de les temperatures de cristal·lització en fred i una menor grau de cristal·linitat. No obstant això, com es va observar per a la temperatura de pèrdua de massa del 5%, la modificació d'alquiloxi amb isoproxid de titani (IV) (trietanolamina) va disminuir la estabilitat tèrmica, a diferència d'altres modificadors superficials.

En l'estudi descrit en el segon capítol, que és una continuació de l'estudi sobre l'impacte del tractament superficial en les característiques dels FRPs. Entre els tractaments superficials prèviament provats, es va seleccionar per a un examen detallat el silà tris(2-metoxietoxi)(vinil). L'estudi tenia com a objectiu descobrir la influència de concentracions més altes de fibres de llana d'ovella en formulacions polimèriques i concentracions més altes de l'agent de tractament superficial respecte a les fibres de llana d'ovella. Basant-nos en l'experiència de l'estudi anterior, la reacció de tractament superficial es va dur a terme en un entorn lleugerament ajustat, incloent un augment de la temperatura de reacció en 15°C. Pel que fa als resultats obtinguts, en el rendiment mecànic, un augment en el contingut de fibres de llana d'ovella ha causat una reducció de les propietats de tracció. Això era esperat fins a cert punt sabent que l'àcid polilàctic no interactua de manera adequada amb la superfície de la llana d'ovella. No obstant això, l'aplicació del tractament de silà a les fibres ha compensat parcialment l'efecte negatiu observat en el cas de les fibres de llana no modificades. L'impacte de la millora amb l'augment de la concentració del tractament de silà es va observar principalment en el mòdul de Young o en l'elongació en el punt de trencament. La concentració de fibres de llana va afectar l'estabilitat tèrmica de les formulacions a base d'àcid polilàctic, ja que la fibra de llana d'ovella presenta una menor resistència a les temperatures elevades. No obstant això, la resistència tèrmica és suficient per al processament amb la majoria dels polímers termoplàstics biodegradables, com l'àcid polilàctic.

El tercer capítol es va centrar en un pas addicional de pre-processament de les fibres de llana d'ovella amb tractament de plasma i el seu impacte en les propietats finals del material, entre altres propietats mecàniques i tèrmiques. El tractament de plasma és conegut per les seues aplicacions de neteja, que en el cas de la llana es pot utilitzar per eliminar els lípids presents en la superfície de la fibra. No obstant això, el tractament prolongat amb plasma és conegut per la seua influència destructiva en la superfície de la fibra de llana, per tant, el pretractament es va aplicar en poc temps. L'estudi es va centrar en un estudi exhaustiu de la barreja d'àcid polilàctic/oli de lli maleïtzat reforçada amb fibres de llana no tractades i fibres de llana amb tractament de plasma aplicat. Pel que fa a les propietats tèrmiques, el pretractament de plasma de les fibres de llana va mostrar una temperatura de transició vítrea reduïda i va afectar la cristal·lització de l'àcid polilàctic reforçat amb les fibres. A més, atès que la major resistència a la tracció es va trobar per a l'àcid polilàctic pur, l'addició de reforç de fibra de llana no modificada va reduir la propietat de tracció. No obstant això, es va trobar que el pretractament amb plasma va ser beneficiós en aquesta àrea, la qual cosa va resultar en una elongació millorada en el punt de trencament.

El següent capítol de la tesi doctoral es va centrar en investigar els aspectes de l'envelliment físic de l'àcid polilàctic amb el temps. L'àcid polilàctic, com a bioplàstic, és conegut per mostrar canvis en les seues característiques amb el temps, fins i tot sense

l'impacte de l'entorn extern, conegut com envelliment accelerat. Com a resultat, es van comparar les característiques de les formulacions basades en àcid polilàctic/oli de lli maleïtzat entre la preparació inicial del material i després de quatre anys d'envelliment físic. L'estudi es va centrar en formulacions reforçades amb dues concentracions de fibra de llana, sense tractament i amb tractament de silà tris(2-metoxietoxi)(vinil). Es van avaluar els canvis en l'estructura cristal·lina i les temperatures de transició de l'àcid polilàctic, així com el rendiment mecànic mitjançant corbes d'esforç-deformació.

Els dos últims capítols experimentals, que juguen un paper complementari en la investigació de laboratori, es van centrar en l'ús d'un enfocament de modelatge basat en intel·ligència artificial per a la predicció de propietats de materials. L'entrenament del model es va dur a terme en funció d'algoritmes de regressió seleccionats i dades experimentals pre-processades derivades de la caracterització en el laboratori. A mesura que els models entrenats van ser avaluats amb el coeficient de determinació i mètriques estadístiques mitjanes i relatives, es van implementar per al seu ús en la predicció de propietats. L'objectiu dels estudis era proporcionar característiques predites per a un espectre més ampli de formulacions. El primer estudi computacional es va centrar en les prediccions de resistència a la tracció i pèrdua de massa del 5% per a l'àcid polilàctic modificat amb diferents concentracions d'oli de lli maleïtzat, diferents concentracions de fibra de llana d'ovella, diferents tractaments superficials i les seues concentracions. El segon estudi computacional es va centrar en les prediccions de propietats mecàniques i característiques basades en calorimetria diferencial d'escombrada per a l'àcid polilàctic modificat amb diferents concentracions d'oli de lli maleïtzat i diferents concentracions de fibra de llana d'ovella.

Els resultats obtinguts en la tesi doctoral van proporcionar una millor comprensió del reforç de llana d'ovella en el polímer biodegradable representat per l'àcid polilàctic. Un aspecte fonamental de la dissertació és l'ús de materials d'origen biològic en la major quantitat possible, on l'àcid polilàctic, l'oli de lli maleïtzat i les fibres de llana, que en el seu estat brut són abundants en la naturalesa. A més, com a part complementària de la tesi, es va investigar l'enfocament computacional del modelatge d'aprenentatge automàtic aplicat per limitar el consum de materials i energia requerit per a la investigació d'un ampli espectre de concentracions d'ingredients. Com a valor afegit a la ciència, cal assenyalar que la dissertació conté diversos enfocaments per investigar la interacció entre les fibres de llana d'ovella i el biopolímer, a més de centrar-se en l'aplicació a llarg termini d'aquests materials. Les àmplies característiques mecàniques, tèrmiques, microestructurals i de superfície obren possibilitats per a aplicacions de materials en diversos sectors industrials, com ara automoció, aeroespacial, agricultura o aplicacions a curt termini. Finalment, la feina obre noves línies de recerca per a l'ús de fibres de llana com a subproducte i proporciona enfocaments per a la seua utilització.

ABSTRACT

"Use of wool reinforcement for biodegradable materials"

The doctoral thesis examines the use of sheep wool fibers derived from the dairy industry as a sustainable reinforcement for biodegradable polymeric materials. The doctoral thesis has been divided up into five main chapters: introduction, objectives and planning, experiment, results and discussion, and conclusions. Those chapters were supplemented with references and an appendix at the end of the dissertation. The first chapter, referred to as the introduction, has covered a general literature review of the main topic discussed in the doctoral thesis concerning fibers, bio-plasticizers, biodegradable polymeric materials, fiber-reinforced polymers, and computational modeling. The second chapter covers the research purpose, specified objectives of the doctoral thesis, and research plan addressing their achievement. The third chapter details experimental methodology, applied characterization techniques, and used materials. The fourth chapter covers the presentation, analysis, and discussion of acquired results across the doctoral thesis and is divided into six sections. Lastly, the fifth chapter covers the conclusion section, providing a general conclusion and separate, specific conclusions for each research work. As a requirement for the title of Doctor with the “International Doctorate,” mention at least one of the sections in the result and discussion chapter; the summary and the conclusions were written in English.

The general objective of the doctoral thesis was accomplished by conducting six research works, which were further separated into specific objectives of the doctoral thesis, each specific objective for each conducted study. The research mentioned above was separated into two groups, where four primary studies were concerned with materials preparation and their laboratory characterization, and two supplementary studies were concerned with machine learning modeling of prior obtained materials characteristics. Before the investigation was designed for the doctoral thesis, a comprehensive review was conducted based on research conducted in the investigation group and on literature in the field of study, and several general observations were gathered. Among them, using natural oil or surface modification of fibers is a promising approach for obtaining fiber-reinforced polymers (FRPs). The material characterization studies investigated several variables influencing FRP`s characteristics, mainly focusing on material composition, surface interaction, treatment, material preprocessing, or material stability in specific conditions. On the other hand, supplementary studies were conducted to provide a novel approach to artificial intelligence-enhanced modelling for material properties predictions concerning different material compositions or surface treatments.

The study in the first chapter concerned the elaboration of prior studies where polylactic acid/maleinized linseed oil blends reinforced with sheep wool fibers were investigated. For this purpose, several silane and alkoxide coupling agents were applied to short wool fibers to enhance the number of functional groups on the fiber`s surface. Among functional groups attached by surface treatment are distinguished primary, secondary, and tertiary amines, epoxy, and vinyl groups. Modified fibers were applied at a single concentration to the previously established polylactic acid/maleinized linseed oil blend. Surface treatment with different coupling agents mainly changed mechanical and thermal properties. An alkoxide treatment of sheep wool fibers with titanium (IV) (triethanolaminate)isopropoxide was found to be most effective concerning tensile

properties, whereas silane treatment with trimethoxy (2-(7-oxabicyclo(4.1.0)hept-3-yl)ethyl)silane resulted in highest impact strength improvements among tested coupling agents. Concerning the impact of wool surface treatment on thermal properties, such modifications resulted in increased cold crystallization temperatures and a lower degree of crystallinity. However, as observed for the temperature of 5% mass loss alkoxide modification with titanium (IV) (triethanolaminate)isopropoxide has lowered thermal stability, differently to other surface modifications.

The study described in the second chapter is a continuation of the study on the impact of surface treatment on FRP characteristics. Among prior tested surface treatments, tris(2-methoxyethoxy)(vinyl) silane was selected for detailed examination. The study aimed to discover the influence of higher concentrations of sheep wool fiber in polymer-based formulations and higher concentrations of surface treatment agents in sheep wool fibers. Based on experiences from previous studies, surface treatment reaction was carried out in a slightly adjusted environment, including increased reaction temperature by 15°C. Concerning the results obtained, in the case of mechanical performance, an increasing content of sheep wool fiber has caused reduced tensile properties. This was expected to some point, knowing that polylactic acid does not interact with sheep wool surface well. However, applying the silane treatment to the fibers has a partially compensated negative effect, as observed in the case of unmodified wool fibers. The impact of improvement with increasing silane treatment concentration was mostly spotted for Young modulus or elongation at break. The concentration of wool fiber impacted the thermal stability of polylactic acid-based formulations, as sheep wool fiber presents lower resistance to elevated temperatures. However, the thermal resistance is sufficient for processing most bio-based thermoplastic polymers, such as polylactic acid.

The third chapter focused on an additional step of sheep wool fiber preprocessing with plasma treatment and its impact on final material properties, among other mechanical and thermal properties. Plasma treatment is known for its cleaning applications, which, in the case of wool, can be used to remove lipids present on a fiber surface. However, prolonged plasma treatment is known for its destructive influence on the wool fiber surface; therefore, the pretreatment was applied quickly. The study concerns a comprehensive study of polylactic acid/maleinized linseed oil blends reinforced with untreated wool and wool fibers with applied plasma treatment. Concerning thermal properties, plasma pretreatment of wool fibers showed reduced glass transition temperature and affected crystallization of polylactic acid reinforced with the fibers. Furthermore, as the highest tensile strength was found for neat polylactic acid, adding unmodified wool fiber reinforcement reduced the tensile property. However, prior plasma treatment was beneficial in that area resulting in improved elongation at break.

The next chapter of the doctoral thesis was addressed to investigate the physical aging of polylactic acid over time. Polylactic acid as a bioplastic is known for showing changes in its characteristics over time, even without the impact of the external environment, known as physical aging. As a result, characteristics of formulations based on polylactic acid/maleinized linseed oil were compared between initial material preparation and after four years of physical aging. The study concerned formulations reinforced with two concentrations of wool fiber without and with tris(2-methoxyethoxy)(vinyl) silane treatment. The changes in crystalline structure and transition temperatures of polylactic acid and mechanical performance were assessed through stress-strain curves.

The last two experimental chapters, supplementary to laboratory research, are concerned with using an artificial intelligence-based machine learning modeling approach for predicting material properties. Model training was performed based on selected regression algorithms and preprocessed experimental data derived from laboratory characterization. Trained models were evaluated with coefficient of determination, mean, and relative statistical metrics and deployed for their usage for properties predictions. The studies aimed to provide predicted characteristics for a broader spectrum of formulations. First, the computational study has concerned tensile strength predictions and 5% mass loss for polylactic acid modified with different maleinized linseed oil concentrations, sheep wool fiber concentrations, and different surface treatments and concentrations. The second computational study concerns tensile properties and characteristics predictions based on differential scanning calorimetry for polylactic acid modified with different maleinized linseed oil concentrations and sheep wool fiber concentrations.

The results obtained in the doctoral thesis provided a better understanding of sheep wool reinforcement of biodegradable polymer represented by polylactic acid. A fundamental aspect of the dissertation is using bio-derived materials in the highest possible amount, where polylactic acid, maleinized linseed oil, and wool fibers, which are in a raw state, are abundant in nature. Furthermore, a supplementary part of the thesis investigates the computational approach of machine learning modelling applied for the material and energy consumption limitation required to investigate a vast spectrum of ingredient concentrations. As an added value to the science, it has to be outlined that the dissertation contains several approaches for investigating the interaction between sheep wool fiber and biopolymer and is focused on the longer-term application of such materials. Broad characteristics of mechanical, thermal, microstructural, and surface properties open possibilities for material applications for multiple industrial sectors such as automotive, aerospace, agriculture, or short-term applications. Finally, the work opens new research lines for using by-product wool fibers and provides approaches for their usage.

LIST OF PUBLICATIONS

A list of publications derived from the current doctoral thesis is located below:

SCIENTIFIC PAPERS PUBLISHED IN INDEXED JOURNALS

1. **F. Pawlak**, M. Aldas, J. López-Martínez, M. D. Samper, “Effect of Different Compatibilizers on Injection-Molded Green Fiber-Reinforced Polymers Based on Poly(lactic acid)-Maleinized Linseed Oil System and Sheep Wool”, Polymers 11, no. 9: 1514, 2019. https://doi.org/10.3390/polym11091514
2. **F. Pawlak**, M. Aldas, F. Parres, J. López-Martínez, M. P. Arrieta, “Silane-Functionalized Sheep Wool Fibers from Dairy Industry Waste for the Development of Plasticized PLA Composites with Maleinized Linseed Oil for Injection-Molded Parts”, Polymers 12, no. 11: 2523, 2020. https://doi.org/10.3390/polym12112523

SCIENTIFIC PAPERS UNDER REVIEW

3. **F. Pawlak**, C. Pavón, M. Aldas, D.L.Motoc, J. López-Martínez, “New approach for processing thermoplastic starch/polyvinyl alcohol blends as injection-molded biodegradable materials”

SCIENTIFIC PAPERS IN PROGRESS

4. **F. Pawlak**, C. Pavón, M. Aldas, J. López-Martínez, “Plasma-Modified Wool Fibers in PLA Composites: A Comprehensive Study on Thermal, Mechanical, and Surface Properties”
5. **F. Pawlak**, C. Pavón, M. Aldas, M. D. Samper, J. López-Martínez, “Sustainable Biocomposites: Understanding the Aging Phenomenon in Wool Fiber Reinforced Polylactic Acid Materials”
6. **F. Pawlak**, M. Aldas, M. D. Samper, M. P. Arrieta, J. López-Martínez, “Predictive Modeling of Tensile Strength and Mass Loss Temperature in Wool-Reinforced PLA Composites Using Machine Learning”
7. **F. Pawlak**, C. Pavón, M. Aldas, J. Ferri, J. López-Martínez, “Modeling properties of maleinized linseed oil and wool fiber reinforcement for polylactic acid systems”

ARTICLES IN CONFERENCES

8. **F. Pawlak**, C. Pavón, M. Aldas, J. López-Martínez, “Enfoques para la modificación de fibra de lana para refuerzo de ácido poliláctico (PLA) y la influencia en las propiedades del material”, X Congreso I+D+i Campus de Alcoi. Creando Sinergias, p. 275-278, Universitat Politécnica de Valencia, Julio 2023, Alcoi – España

9. **F. Pawlak**, C. Pavón, M. Aldas, H. de la Rosa-Ramírez , “Uso de modelo de aprendizaje automático de datos para la agrupación de mezclas basadas en de alcohol polivinílico y almidón termoplástico con características similares”, IX Congreso I+D+i Campus de Alcoi. Creando Sinergias, p. 73-76, Universitat Politécnica de Valencia, Julio 2022, Alcoi – España

10. **F. Pawlak**, M. Aldas, M.P. Arrieta, J. López-Martínez, “Processing and characterization of new green material: PLA/compatibilized wool fiber reinforced polymer”, The 10th Conference on Green Chemistry and Nanotechnologies in Polymeric Materials GCNPM 2019, October 2019, Riga – Letonia.

11. **F. Pawlak**, M. Aldas, H. de la Rosa-Ramírez, C. Pavón, “The effect of coupling agents on thermal properties of a PLA/wool fiber reinforced polymer”, Zjazd Wiosenny SSPTChem 2019, Abril 2019, Ustroń – Polonia.

12. **F. Pawlak**, H. de la Rosa-Ramírez, C. Pavón, M. Aldas, J. López-Martínez, “The study of thermal properties of clusia rosea powder reinforced polyvinyl alcohol”, IX Wyjazdowa Sesja Naukowa Doktorantów Politechniki Łódzkiej, Abril 2019, Rogów – Polonia

13. **F. Pawlak**, M. Aldas, H. de la Rosa-Ramírez, C. Pavón, J. López-Martínez, “The Surface properties of thermoplastic starch/polyvinyl alcohol blends”, IX Wyjazdowa Sesja Naukowa Doktorantów Politechniki Łódzkiej, Abril 2019, Rogów – Polonia

INDEX OF CONTENTS

I. INTRODUCTION

1. Fibers as a reinforcement

1.1. Definition

The term 'fiber' is commonly used daily in many aspects of our lives. Terminology occurs in areas related to food and nutrition, character traits, and, most importantly, in work to material science and body structure. Therefore, the word 'fiber' is defined with the following meanings:

1) Material: "*any of the thin parts like a thread that form plant or artificial material, esp. those that can be made into cloth, or a mass of such parts twisted together"* [1]
2) Body: "*one of the many thin threads that form body tissue, such as muscle, and natural materials, such as wood and cotton"* [2]
3) Food: "t*he part of foods eaten that is not digested but that passes through the body and is excreted as waste"* [1]
4) Character: *"the quality of a person's character, esp. its moral strength"* [1]

Although fibers are associated with several fields of expertise, chemical, physical, and mechanical aspects are crucial from a material point of view. Fibers are composed of high-molecular compounds, which significantly influence their macroscopic properties. Among such properties are the ability of fiber to withstand tension, its capacity to return to its original shape, or its ability to maintain performance under varying temperatures. [3,4] Various fibers' chemical compositions indicate their types and characteristics for both natural and artificial fibers. Furthermore, fibers can be processed mechanically, providing tailored properties. Mechanical operations on fibers can be defined as spinning, knitting, weaving, etc. From a physical perspective, fibers are composed of high-molecular compounds. Therefore, their macroscopic properties and character depend on the properties of the compounds.[5]

Fibers are typically categorized according to their source, as presented in Figure 1. Fibers, whether synthetic or natural, exhibit variety of physical, chemical, and mechanical properties which determine their applications across different industries. [6] The next section of the chapter will provide an elaboration of the classification.

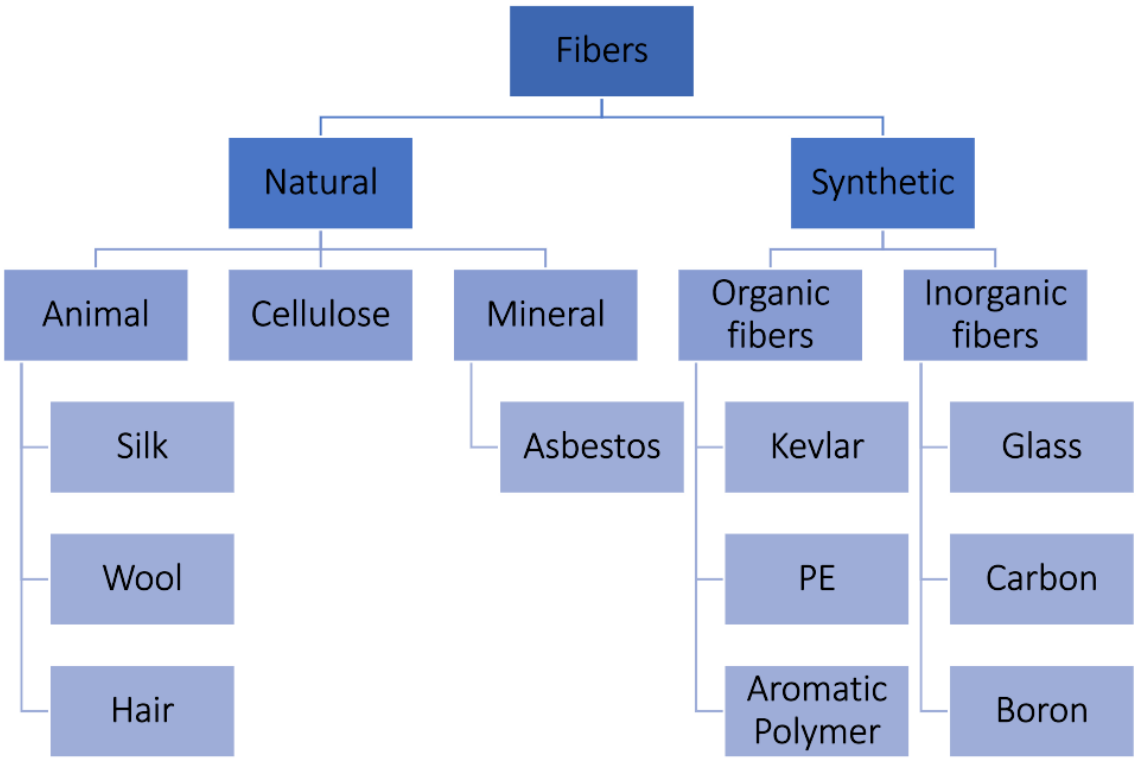

Figure 1 Classification of fibers

1.2. Natural fibers

Natural fibers are mainly consist of five key components: hemicellulose, cellulose, lignin, pectin and waxes. Their exact composition differs based on such factors like fiber type or geographical origin. The Fibers have recently been considered highly potential due to their environmental impact. A more complex composure of natural fibers allows them to adapt better, providing desired properties with less compromise on other properties. On the one hand, fabrics produced from chemically unmodified fibers, such as Merino wool, are resistant to water and windy conditions, making them customized for textile products. In contrast, natural fibers are recognized as biodegradable in both marine and land environments; therefore, they are advantageous as an alternative for synthetic fiber due to no post-usage environmental issues with microfiber pollution. [4,7]

Natural fibers are grouped into three primary types based on their origin: plant, animal, and mineral fibers. Fibers such as wool, silk, and feathers are derived from various animals, including sheep, rabbits, silkworms, and goats, leading to a wide range of application fields for these materials. Wool fibers are usually obtained from shaving sheep or goats, and as obtained material is known for its softness, warmth and ability to insulate. On the other hand, silk fibers, which are obtained from silkworms cocoons and known for their strength and smoothness. Fibers sourced from minerals, such as asbestos, ceramic, and metal fibers, can occur naturally or be slightly modified. Plant fibers mainly comprise cellulose, including cotton, linen, hemp, coir, jute, bagasse, and bamboo. Furthermore, plant fibers are divided into several types: seed, leaf, skin, fruit, and stalk. Cotton is derived from the seed hairs of a cotton plant and its fibers have excellent softness and are highly absorbent making them suitable for textiles. Linen

fibers are flex derived fibers which are known for their strength, moisture draining and durability. Natural fibers exhibit a range of properties and serve diverse purposes, including the production of yarn, fabric, packaging, and paper. Some fibers have higher tensile strength and are used for durable products. The classification and understanding of these fibers can aid in selecting the appropriate fiber for a specific application.[6,8–10]

1.2.1. Cellulose

Cellulose is a naturally occurring high-molecular carbohydrate compound. It is mainly derived from plants such as wood, cotton, hemp or agricultural residues from corn or wheat straw. Cellulose is a polymer with a hydrophilic surface constrained of a linear molecular chains of glucose units with alcoholic hydroxyl groups, the β-D-glucopyranose elements connected by the 1-4-glycosidic bond. In the Figure 2 is presented chemical structure of cellulose. Cellulose is the primary ingredient of vegetable fibers and comprises individual units of anhydrous d-glucose. These units contain 3 hydroxyl (-OH) functional groups, which create hydrogen bonds both within the individual cellulose macromolecule (intramolecular) and joining different macromolecules of cellulose (intermolecular). These hydrogen bonds promote strength and stability of cellulose fibers; however, the presence of the hydrogen bonds often significantly limits dispersibility of cellulose in solvents. These hydroxyl groups create intramolecular hydrogen bonding that give cellulose a high modulus of elasticity of 134 GPa in the axial way under humid environment.[11,12] Cellulosic fibers naturally absorb moisture, which can adversely impact the strength and durability of composites containing these fibers. [13] Cellulosic fibers consist of a hollow tube with multiple layers of cell walls, including a single outer layer, several inner layers, and the lumen. Each layer within the natural fiber contains cellulose, which is encased by hemicellulose and lignin. Investigation has shown that natural cellulosic fibers with higher levels of cellulose, increased polymerization, and a smaller microfibrillar angle exhibit superior tensile strength. [14,15]

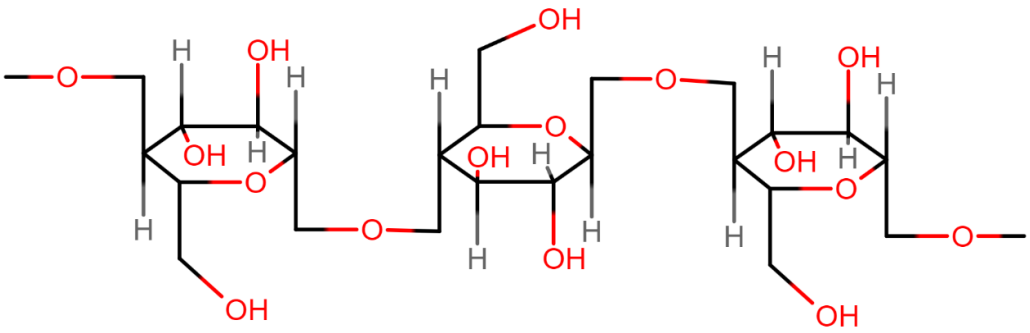

Figure 2 The structure of cellulose compound [16]

Cellulose, as biodegradable, biocompatible and renewable materials, is considered as attractive for variety of applications, also as it can be easily modified in

chemical way. However, cellulose is frequently restricted in its applications because of its limited thermal stability, susceptibility to flammability, and hydrophilic nature, which results in poor compatibility with hydrophobic polymers. To overcome such issues with low compatibility with polymers, several approaches are applied such as surface modifications, esterification or polymer grafting. [15]

1.2.2. Silk

Silk, a protein fiber delivered by spiders or silkworms, consists of a fibrous protein called fibroin, coated by a substance known as sericin. Similar to wool fibers, silk contains amino acids like glycine, alanine, and serine, which play a vital role in the formation of its fiber structure. Furthermore, the silk fibroin structure contains a significant amount of β-sheet crystalline formations, which enhance the mechanical performance of the fibers. Silk fibers are known for their favorable tensile properties and elasticity, allowing them to withstand significant stresses without rapture of fiber. However, there are several factors, such as source of the silk, processing methods, or degree of crystallinity, which may affect mechanical properties of specific silk fiber. Molecular biotechnology and protein engineering developments have led to the manufacture of moderate quantities of silks and silk-like biopolymers. However, due to a lack of proper spinning technology, 100% regenerated silk fibers have not been industrially produced. Silk is often produced in powder form for various uses, such as cosmetic materials, functional foods, and textile finishes. The powder form of silk fibroin protein has unique properties that make it useful for biomaterial applications and textile finishes, such as improving softness.[17–19]

Silk has been utilized in numerous medical fields, including tissue engineering, wound healing, surgical sutures, and drug delivery systems. Such applications are derived primarily due to biocompatibility of silk-based biomaterials, as silk is known for its ability to integrate well with biological tissues. Additionally, from medical perspective silk can be safely absorbed by human body over time, reducing surgical interventions related to removal of silk-based implants. Silk in eligible for chemical modifications for enhancement of its properties such as cell adhesion, degradation control, or enhancement of mechanical properties. This can be mainly achieved by techniques such as grafting, surface modification or cross-linking. [18,19]

1.3. Inorganic fibers

Inorganic fibers are fibers derived from natural resources, usually obtained through a synthesis from mineral or metallic compounds. Such fibers are usually characterized by high thermal stability, mechanical performance and chemical resistance. Due to high thermal stability, inorganic fibers can bear elevated temperatures without fiber degradation making them suitable for applications where high temperature is expected. Furthermore, high mechanical strength of inorganic fibers can contribute in improvement of material properties, once inorganic fiber is applied as a reinforcement. Therefore, inorganic fibers have become increasingly important, finding use in various industries, including construction, electronics, and aerospace. [20,21]

Inorganic fibers are classified as either natural or synthetic, depending on the specific type. As examples of naturally occurring inorganic fibers can be provided asbestos or basalt fibers. Due to health concerns related to use of asbestos currently its usage is limited; however, basal fibers, as fibers derived from volcanic rock, gain their industrial recognition as a fiber for reinforcement mainly due to its high strength, favorable thermal stability and natural origin. Towards synthetic inorganic fibers can be distinguished glass or ceramic fibers. Glass fibers are silica made synthetic fiber known for good tensile performance and low thermal conductivity. They are widely applied as material reinforcement in composites. Furthermore, ceramic fibers are usually based on alumina and silica and are synthesized to achieve exceptional thermal and chemical characteristics. They are commonly used for thermal insulation and aerospace components because of their excellent resistance to heat and chemicals, as well as their durability. [20,21]

Inorganic fibers are essential in modifying thermoplastics, where various inorganic fiber reinforcements are also being studied. Initially, glass fiber was one of the most applied inorganic fibers; however, relatively high production cost and environmental aspect have shifted use of such fiber as a method to reuse existing materials. Polymer reinforcement usually uses inorganic production wastes like dust, chips, or fibers, as they are significantly produced while manufacturing building components. Among these manufacturing by-products are glass and slate fibers, consisting primarily of various oxides like Al_2O_3, SiO_2, CaO, MgO, Fe_2O_3, and others, in differing proportions.[22,23]

1.4. Organic fibers

Organic fibers are materials composed of organic compound, where in case of synthetic fibers source for production of such fibers are petrochemicals. For production of synthetic organic fibers are commonly used synthetic polymers, such as polyolefins, polyester, nylon, or acrylic. Two main types can distinguish organic synthetic fibers. The first type of fiber is in the main macromolecular chain, whereas carbon atoms contain other elements such as oxygen or nitrogen. Such fibers can be obtained by polycondensation or cyclic compound polymerization, like in polyamide or polyester fibers. The other type is the fibers with leading macromolecular chains built only from carbon atoms. The fibers can be obtained with polymerization reactions. Among such fibers can be distinguished polyacrylonitrile, polyvinyl alcohol, or polyolefin fibers. [5,24]

From a chemical perspective, polyamide fibers are macromolecules containing acid-amino groups (-NH-CO-) separated by methylene groups in the main chain. Therefore, such fibers contain active amino and carboxyl group, but rather in a small number, as they occur only at the end of the molecular chain. Macromolecules in the polyamide fibers are interconnected due to hydrogen bonds presence created involving different acid-amino groups. Therefore, the interaction between adjacent macromolecules increases the stability of fiber properties. From a physical-mechanical perspective, polyamide fibers exhibit a favorable elongation at brake, elasticity, and abrasion resistance. The fiber is inconsiderably swelling in aqueous conditions, and the mechanical performance of a wet fiber is slightly reduced. Due to a hydrophilic group,

such fibers may absorb up to 4% of the humidity. Polyamide is a thermoplastic polymeric material that can withstand temperatures up to 120ºC. [5,25]

An example of polyester fibers is a polyethylene terephthalate fiber obtained through a condensation of dimethyl terephthalate and ethylene glycol. The fiber has a well-orientated internal structure, as between macromolecules occur van der Waals` forces. Polyethylene terephthalate fibers exhibit hydrophobic properties due to their dense structure and the minimal occurrence of hydrophilic groups located at the ends of the polymer chain. The hydrophobic properties do not allow the fiber to swell, making it unfavorable for dyeing. Additionally, static solid changes on the fiber's surface create difficulties during its mechanical processing and tend to boost its exploitation. [5]

The polyacrylonitrile fibers are manufactured from acrylonitrile or its copolymers; however, the main macromolecular chain consists of only carbon atoms and functional cyanide groups. Although the fiber occurs mainly in an amorphous structure, the macromolecules are highly orientated mainly due to numerous hydrogen bonds between macromolecules. Such interaction between macromolecules can be explained by the cyanide group's high polarity, which favors interaction with the hydrogen from the adjacent polymer chain. The nature of the polyacrylonitrile fibers is hydrophobic as fiber is not affected by humidity, and swelling is not aqueous, mainly due to the lack of hydrophilic groups observed only at the end of a macromolecular chain. The fiber shows high mechanical performance, abrasion resistance, and favorable properties in high temperatures up to 220ºC, which is the material softening temperature. In addition to mechanical performance, such fibers have good resistance to chemicals, as they have limited solubility in most solvents and are resistant to the action of most inorganic acids or oxidizing agents. [5,26]

Polyvinyl alcohol has the ability to be spun into fibers and is known for being hydrophilic and soluble in water. Moreover, the dissolution of polyvinyl alcohol macromolecules in water allows the production of such fibers and modification of the fiber in the solution, i.e., through cross-linking. However, cross-linking, or, in general, increasing macromolecule orientation in the fiber, may limit water solubility. Regarding mechanical performance, polyvinyl alcohol fiber shows weaker mechanical properties than previously mentioned polymer fibers; however, its properties remain considerably superior to natural fibers. The polymer's high content of hydroxyl groups attached to the macromolecular chain makes it particularly favorable for biodegradability. [5,27]

1.5. Wool fiber and its general description

Wool fiber is widely utilized in textiles due to its excellent heat and moisture-regulating properties. The value of the material can be associated, among others, with its particular inner structure. Wool has a more complex surface structure than other natural fibers, which can lead to technical difficulties, specifically regarding its wetting and dying ability.[28] The complexity of the wool fiber structure is shown in Figure 3. Furthermore, fiber's structure and chemical composition may differ, allowing diversity

and other material characteristics. In the current study, the superficial cortex layer is essential as a field for potential modification and complexity of inner structure.[7,29] Additionally, from the morphological perspective, wool fiber can be divided into the following parts: the hair bulb, the root, and the stem. The stem is given particular attention, as this part of the wool fiber is separated during shearing and utilized for various applications. Nevertheless, the remaining hair bulb and root play essential roles in connecting the fiber to the animal body or creating a protective layer of the stem. In further consideration, the phrase 'wool fiber' would describe the properties and functions of the sheared stem from wool hair structure. [5]

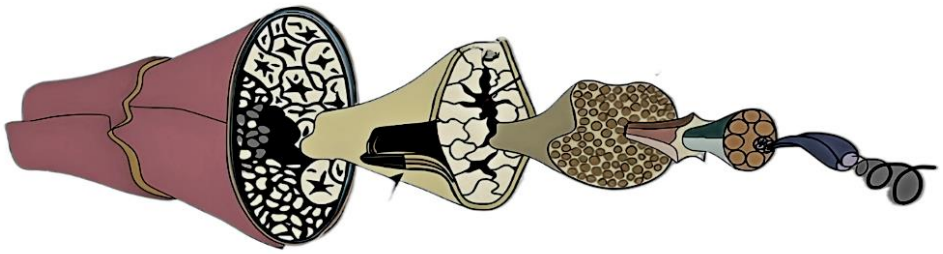

Figure 3: Structure of a wool fiber [21]

Wool can be characterized and described diversely:

- As a structure with heterogeneous histology, fiber is composed of an external cuticle surface structure, which covers the internal part, the cortex, with overlapping tiles. An additional third core layer called the medulla can be observed in coarse wool, indicating the softness of specific types of wool fiber. On the one hand, the cuticle cells anchor the fiber in animal skin or dirt particles in fiber towards its tip, but on the other hand, it is responsible for the fiber's softness, making it unique. Within the cortex, whose structure is fractal, can be distinguished further structures as cortical cells followed by microfibril, microfibril, and α-twisted molecular chain, respectively. The inner structure of the fiber refers to its performance properties.[5,7,30],
- as a composition of amino acids, where wool fiber may be a copolymer of 18 different amino acids, like glycine, alanine, serine, proline, valine, threonine, cysteine, leucine isomers, aspartic acid, glutamic acid, methionine, histidine, hydroxylysine, phenylalanine, arginine, tyrosine, and tryptophane. Among the proteins in the wool fiber, the highest levels are usually spotted for cysteine, serine, and methionine. The chemical structures of amino acids are presented in Figure 2a as a general amino acid structure. A structure of serine as a linear compound containing amino and carboxyl groups is shown in Figure 4b. Furthermore, compound examples of amino acids with sulfur linkage are shown in Figure 4c,d. Finally, proteins containing aromatic, heterocyclic, and simultaneously both groups are shown in Figure 4e,f,g. Natural fiber structures' complexity differs from synthetic fibers, which usually use two components to form a synthetic copolymer. [7,31]

- Composition of chemical elements, where the composition consists of various elements, but mainly five elements are usually characterized: the group of hydrogen (6-7%), carbon (50-52%), oxygen (21-25%), nitrogen (15-21%), which correspond to the structure of amino acids and sulfur (0-5%) which allows improvement of cystine's chemical resistance and physical mechanical properties. The sulfur content may differ as the chemical composition of various wool fibers is nearly the same. As sulfur linkages are present in a core canal of the fiber structure, a low amount of sulfur in coarse wool can be directly observed by the higher softness of the fiber. [5,7]

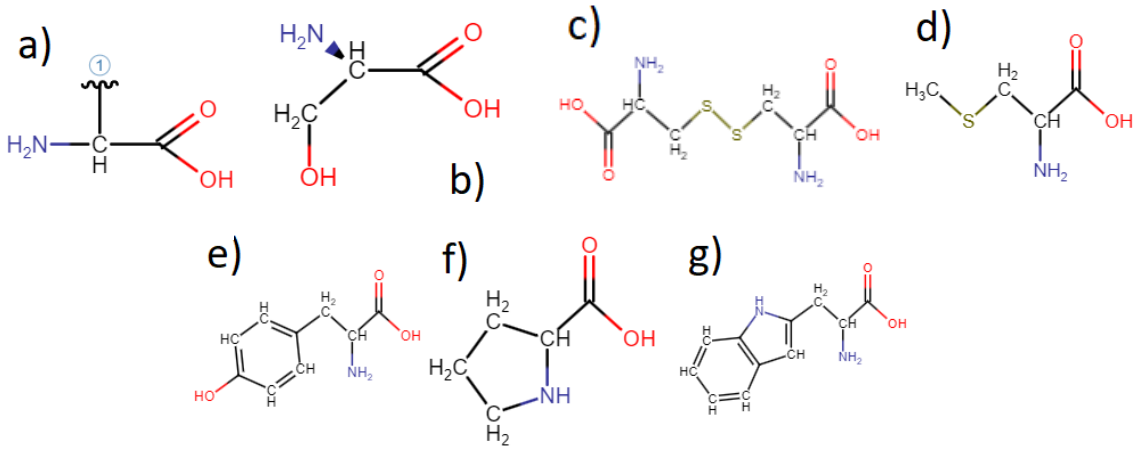

Figure 4: Chemical structures of a) amino acid, b) serine, c) cystine, d) methionine, e) tyrosine, f) proline, g) tryptophan

Wool's high quality and characteristic properties are linked to the fiber's chemical, supramolecular, and morphological structures. The histology of wool fibers can be described by explaining the fiber growth process. Protein-rich wool fiber is based on proteins, where the thiol group (–SH) containing keratin forms cells in the root region. During fiber growth, the cells migrate into the skin's surface with increasing compression and spindle shape. At that time, several chemical modifications are occurring, which allow for the formation of the stem of the fiber. Among chemical processes is the loss of initial substances, dehydration, or keratinization, described as the formation of disulfide cross-linkages. Furthermore, an external layer is created in scales arranged closely to a fiber surface. Scales partially cover adjacent areas and overlap each other, forming layers like shingles on a roof. [5,7,32,33]

The external, scale-containing layer called the cuticle represents 10-15% of the total weight of fine wool fiber. It consists of three separate fractions: the endocuticle, exocuticle, and epicuticle. The epicuticle forms a mantle providing high chemical stability, representing good resistance to chemical modifications with acids, oxidizing or reducing agents, and alkali. As the layer is composed of lipids, they define the hydrophobic properties of the cuticle surface layer. The epicuticle layer is bonded with adjacent exocuticle with covalent iso-peptide crosslinks; hence, the epicuticle layer can be eliminated by the action of alcoholic alkaline or chloride compounds. Within the middle exocuticle, the layer can be two different structures based on the amount of cystine rich in disulfide bonds. The outer exocuticle layer contains ca. 35% of cystine, and the inner exocuticle layer contains ca. 15% of cystine. Rich in disulfide bonds, the exocuticle layer, due to the presence of cysteine, plays the role of diffusion barrier to chemicals and is

favorable for chemical modifications. Finally, most inner cuticle structures are found in the endocuticle, which contains the lowest cystine concentration among cuticle layers. Additionally, the layer is adjacent to the intercellular cement. The detailed impact of various chemical modifications on cystine linkages is described in subsequent sections. [32]

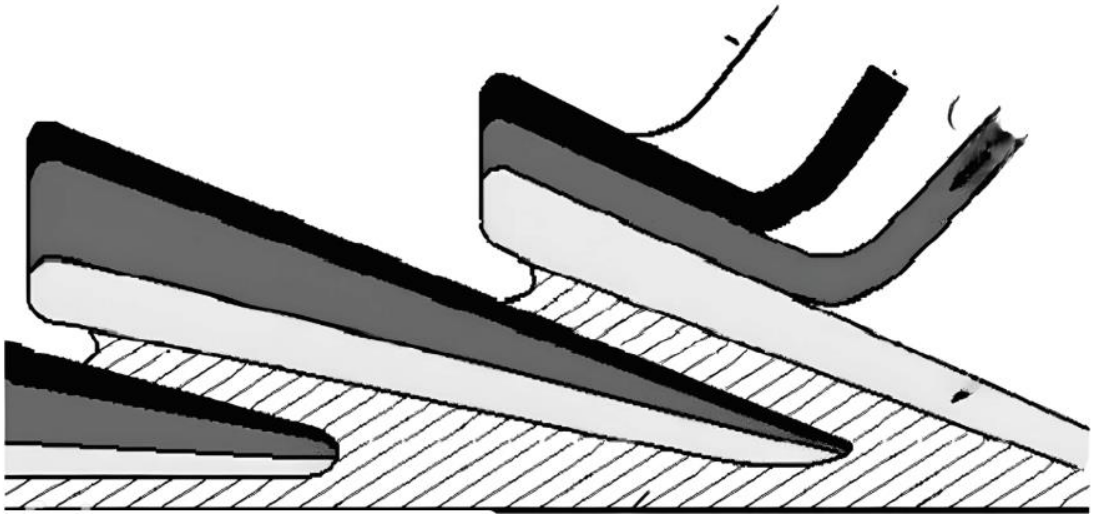

Figure 5 Scale structure of the cuticle

Directly under the scaly layer underlies the central part of wool fiber called the cortex, which occupies around 80-90% of the wool fiber. The structure of the cortex is composed of separate elongated cells. Like the external layer of the fiber, the cortex also undergoes chemical modification during stem growth. The spindle-shaped internal cells with an average 100µm length and 2.5µm diameter are disposed along each other in several parallel rows. Between individual spindle-shaped cells and under the cuticle layer occurs an intercellular cement called the complex of membrane cells (CMC), as presented in Figure 5. The CMC's role is to create a network for molecules diffusion into the wool fiber. Although the CMC consists mainly of lipids and proteins, its structure can distinguish carbohydrates and mineral components, like silicon compounds; further to the cells, they are composed of microfibrils, which are further composed of protofibrils in a particular ring-shaped order. Photofibril structure is described as two or three twisted molecular chains. [5,7,32]

For some fibers, an additional third layer called the medulla could be distinguished, which is an internal core structure with a different shape and contains air bubbles in interspaces between cells. Although the process of fiber growth can describe the general structure of the wool fiber, the cortex's chemical stability and other properties are not uniform in every part of the fiber. Differences during growth caused by unsymmetrical keratinization or slower keratinization of the cortex result in less resistance to chemical agents and enzymes in the orthocortex structure. However, the paracortex structure is chemically more stable due to the faster keratinization process. [5,7,32,34,35]

As previously mentioned, the wool fiber's histology comprises elements of photofibrils that are occurring linkages between single keratin compounds. As keratin itself is rich in diamino acids, dicarboxylic acids, and sulfur-containing cysteine, therefore

between polypeptide chains are occurring chemical and physical interactions in the form of salt linkages (i.e., between aspartic acid and lysine or arginine and glutamic acid), as well as cysteine linkage and hydrogen bonds. Examples of possible linkages between keratin chains are presented in Figure 6. [5]

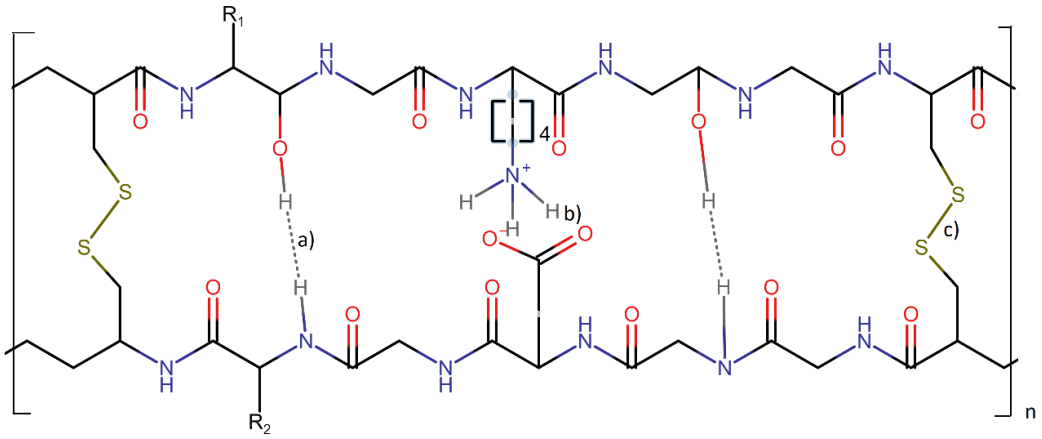

Figure 6 Structure of keratin cell with linkages: a) hydrogen bond, b) salt linkage, c) cystine linkage.

As presented in Figure 6, the polypeptide chain contains multiple groups; however, some residues are not linked and still acquire electric charges. That creates more complex interactions with adjacent chains or within the same polypeptide chain but between separate centers. That may occur for all types of linkages mentioned in Figure 6. Those interactions create considerable forces in the compound in the cross and longitudinal directions. As a result of the interaction, two phenomena can be observed: active side chains approach each other as closely as possible, and polypeptide chains tend to curve and bend. Due to the complex structure of keratin chains and the interaction described previously, the structure may differ, resulting in changes in the fiber's XRD pattern or principal properties. [5]

A wide variety of substances that build the wool fiber structure may influence a variety of substances that can be extracted as raw materials. Among the materials can be distinguished keratin, ceramides, lanoline, and peptone, whose chemical structure is presented in Figure 7. An overwhelming part of the fiber consists of keratin, a tough and insoluble material responsible for its structure. Furthermore, the compound exhibits favorable moisture sorption or thermal conductivity. Keratin is also a three-dimensional and stable compound due to disulfide bonds from cystine or inter- and intra-molecular bonds between amino acids. Keratin is broadly applied in the pharmaceutical, medicinal, and cosmetic industries to create various sponges, foams, films, gels, and drugs. Keratin is widely investigated and is advantageous for drug delivery, wound care, or tissue reconstruction. As an implantable sheet or scaffold, such biomaterial can be absorbed by adjacent tissue, helping to share the mechanical load and maintain a structure during the healing process. Further to keratin, wool fiber contains internal and external lipids in its structure with a high content of ceramides. In natural fibers, ceramides as an internal ingredient enhance barrier properties and allow high water-holding capacity. Such lipids are also broadly applied for pharmaceuticals and cosmetics, as they can be used without problems for skin or hair treatment. Its primary role is creating a protective layer that reduces moisture loss or the negative impact of pollutants. The next ingredient of wool that can be separated is a wool grease called lanoline. The wax is usually removed

during cleaning processes with detergents; however, it is considered beneficial for further usage. It is not only used for beauty care products but also for waterproof coatings and protective layers, i.e., for drug delivery. On the other hand, using lanoline for other purposes often requires complex processing, including discoloration or deodorization. Finally, peptones can be separated from wool fibers, which are considered one of the most expensive laboratory materials. Additionally, such microbial culture media is rich in key ingredients such as protein (over 67%) and ashes (over 29%); therefore, it is favorable for bacteria growth. Peptones, described as protein hydrolysates, provide a stable nitrogen source in a water-soluble form that does not coagulate upon heating. Numerous compounds derived from wool and their variety confirm the importance of wool fiber and make their usage reasonable for broader applications, indicating the importance of research in that area. [7]

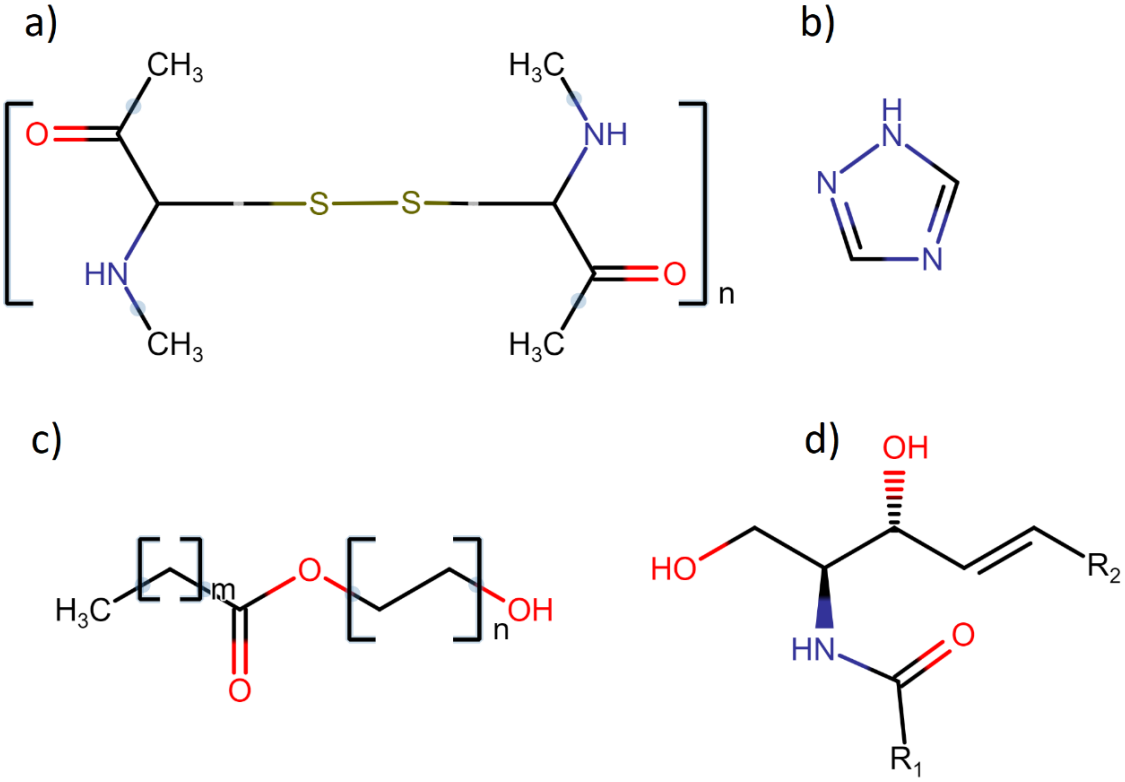

Figure 7: Chemical structure of a) keratin, b) peptone, c) lanoline, d) ceramide.

Wool fibers are the hair of animals, mainly sheared from sheep, which are grown in a renewable manner. Growth of the fibers strongly depends on animal nutrition, age of animals or season, atmospheric breeding conditions, or a place on the skin where it was shared.[36] An everyday nourishment that allows the fiber to grow continuously is grass. It also compensates for reduced fiber growth during animal pregnancy and offspring rearing. Ewe age also affects the growth rate of grown fiber, as young sheep typically present slower fiber growth, as proteins are used to build other tissues during severe animal growth. The most efficient wool growth is mainly achieved between the third and fifth year of breeding. Weather and breeding conditions are also essential factors in wool production, as exposure to cold and heat enhances wool fiber growth, especially in length. Wool fiber is also considered an inhomogeneous material, as its composition, shape or properties may differ depending on which part of skin fiber was collected. [7,34]

1.6. Wool processing and modification

One of the initial stages in wool processing is its purification. Raw wool is a dirty natural fiber with high grease, impurities, and vegetable or dirt contaminants. The purification of wool used several approaches, which can be separated into mechanical and chemical purification. Mechanical purification can be achieved by removing specks of dirt and vegetable residuals. However, this technique cannot deliver perfectly purified fiber; hence, it has to be followed by chemical purification in numerous cases. Depending on the impurities on specific fibers for purification, ethers, alcohol, water, alkalis, acids, and similar are commonly used. [5,33]

Chemical purification techniques include scouring, carbonizing, and bleaching wool. Wool scouring is applied to remove adhered or natural impurities, involving use of hot water and detergents to solubilize and wash off lanolin other contaminants. The process is performed as a batch process in an aqueous mixture of sodium carbonate and non-ionic surfactants. Furthermore, lanoline can be recovered as a by-product of such a process. The carbonizing process is applied to remove vegetable impurities from the wool fibers, as it is processed in 10% sulfuric acid and subsequently cured at 120ºC for 30 minutes. As an effect of acid treatment and heat, such a process may change the fiber color to yellowish. Finally, wool bleaching is carried out using hydrogen peroxide under mild conditions, a treatment commonly applied for purifying light-colored fibers, such as those used in baby clothing. The presence of an oxidizing agent, such a reaction is sensitive to high temperatures, which may cause damage to the wool fibers. [32,37]

One of the most crucial properties of wool is its hygroscopic characteristics, as depending on humidity and surrounding temperature, it adsorbs considerable moisture, mitigate its condensation and helps to control humidity in insulation materials. Moisture that is adsorbed on the wool fiber surface can be evaporated at the temperature of 100-105°C, which results in more rigid and less strong fibers. The softness and strength of fibers can be restored from repeated wetting. On the other hand, prolonged heating in the previously mentioned temperature for over 30 hours causes fiber degradation. Such destruction of fiber results in color changes into more yellowish and releases volatile byproducts such as hydrogen sulfide or ammonia. Other changes can be observed during wool combustion, which presents the characteristic smell of a burnt horn. Wool fibers show flame retardant properties, as burning ceases after the wool is removed from a flame, and porous ash beads are formed at the end of burnt fibers. Furthermore, wool fiber exhibits chemical activity due to its structure and the keratin content. The attendance of amino ($-NH_2$) and carboxyl (-COOH) groups determines the amphoteric properties of wool, as the amino substituent is capable of interaction in the form of dissemination or formation of dinitrophenyl derivatives, as well as carboxyl substituent is capable for reaction with alcohols, alkyl halides, dimethyl sulfate or epichlorohydrin. [5,38]

The keratin macromolecule in the wool fiber has two main conformations: helical, known as α-keratin, and rectal, known as β-keratin. These structures are stabilized by hydrogen bonds and disulfide linkages. The elastic nature of wool fiber is derived from the exocuticle structure, and several types of wool shrinkage can be observed for the fiber, such as felting, relaxations, consolidation, or swelling shrinkages. As polypeptide chains may stretch as a result of hot water or steam treatment, two types of structure are distinguished: α-keratin, where the main polypeptide chain forms regular folds, and β-keratin, where after the treatment, the main polypeptide chain is almost completely

straightened. The α-keratin is characteristic of fibers in their natural state. On the other hand, after stretching forces are applied, the α-keratin conformation is replaced by the β-keratin conformation. However, the β-keratin conformation is somewhat unstable, and the macromolecular chain structure tends to revert to its natural state. Differences in an α and β-keratin chain structure are shown in Figure 8. [5,32,34,39]

Furthermore, it was reported that stretching wool fibers causes a transformation in their secondary structure from an alpha form to a beta conformation, as indicated by the shift in the positions of two peaks of C-N-H and C=O bonds at lower wave numbers in stretched fibers compared to unstretched samples.[40]

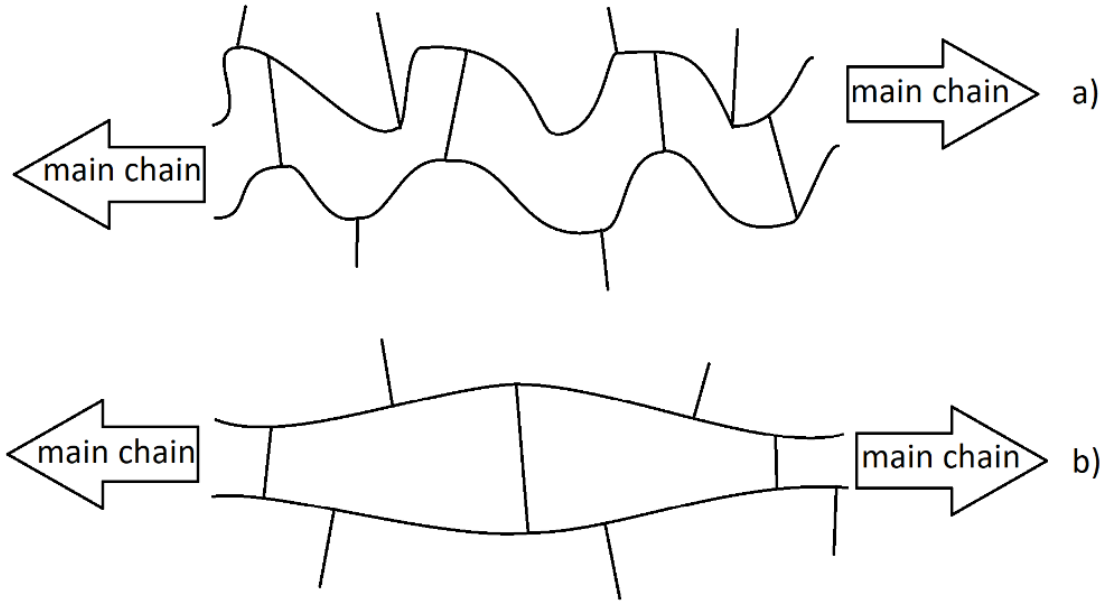

Figure 8 Structure of polypeptide chain of a) α-keratin and b) β-keratin.

The inherent hydrophilic nature of the surface of natural fibers poses a challenge by causing weak compatibility and adhesion with hydrophobic biopolymer matrices, making it a significant obstacle in developing high-performance fiber-reinforced materials. Applying natural fibers, such as flax, hemp, or jute, in bio-composites often creates challenges for interaction between polymeric matrix and hydrophilic fiber surface. This is derived from the occurrence of hydroxyl groups on the surface of natural fiber, which results in an ineffective interface between bio-composite phases and does not effectively allow biopolymer reinforcement. Fiber surface treatment is an effective method for compatibility improvement, where commonly peroxides, organic acid, or silane are applied. The function of the treatment is blocking the hydroxyl groups by reacting with surface treatment, therefore improving the effectiveness of phase interaction. [41,42]

1.6.1. Effect of water and steam

The moisture of wool fiber depends on the humidity of the surroundings. Although it is clear that higher humidity in the surroundings increases water content on the wool

surface, the kinetics of moisture content change on wool fiber is slightly faster for absorption than the desorption of water from the surface. Based on that, it is possible to state that dry fibers absorb a specific amount of moisture due to chemical interaction. The moisture causes fiber swelling, which can be observed in the change of fiber dimensions with increasing water content. However, as fully saturated wool can increase its length by 1-2%, the diameter of such fiber can increase significantly up to 20%. Furthermore, water on the wool fiber surface reduces internal interactions between polypeptide chains and their functional groups. A decrease in attraction between centers of salt linkages with opposite charges results in the straightening of a polypeptide chain, which causes a reduction in mechanical properties, especially fiber's tensile strength. Finally, in case of wool fiber, steam explosion was found to cleavage surface scales of wool and to form tiny grooves on fiber surface. [5,43]

As already mentioned, the presence of steam or boiling water allows for changes in the structure of polypeptide chains between α and β-keratin, causing the stretching of fibers. These reversible changes in chain structure are possible due to temperature in aqueous conditions, causing breakage of hydrogen bonds, salt and cystine linkages, and forming new bonds after the treatment. This is seen as the cleavage or removal of the outer cuticle scales, resulting in a reduction in the fiber's crystallinity. Water's presence is essential in reforming salt linkages and other chemical reactions, as shown in Figure 9. However, prolonged steam or boiling water treatment results in the hydrolytic destruction of wool. [5,44]

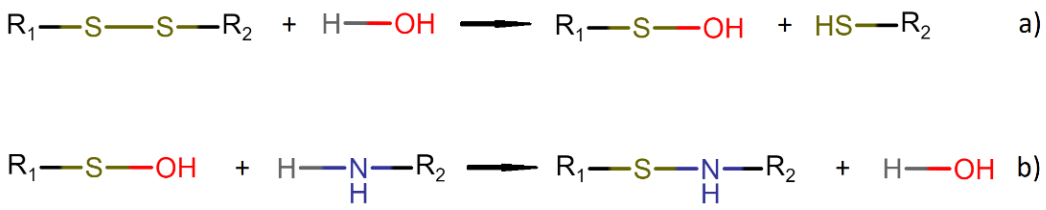

Figure 9 Chemical reactions occurring in steam-treated wool fiber: a)hydrolysis of cysteine; b) cystine-salt linkages

1.6.2. Effect of acids

Treatment with acid can modify the chemical structure of wool fibers involving organic acids, such as tannic acid. The modification with acid can enhance resistance to felting or antibacterial activity, as tannin acid treatment have resulted in improved antibacterial and odor of wool fibers. Acid treatment is a common method for modifying wool fibers; however, it can significantly affect the fiber's performance. Acid treatment, often carried out in an aqueous environment, leads to swelling and increased scale formation, which raises internal friction and improves the fiber's overall mechanical behavior. On the other hand, acids may interact with amino groups present in polypeptide chains, resulting in decreased internal linkages in and between polypeptide chains and decreasing mechanical performance from intramolecular interactions. Below pH=4, the effect of acids can be observed, as cross-chain salt linkages from the amino groups start to break and favor reaction with acid from the treatment. Although for higher than pH=4, no significant change of the pH value is observed, below the value, chemical and

mechanical properties of wool are changing, and fiber starts to uncurl or partially decompose. Furthermore, higher temperatures or prolonged treatment duration may further enhance such an effect. [5,45]

1.6.3. Effect of alkalis

The effect of alkali modification on wool fibers tends to break salt cross-linkages, similar to how acids act but with opposite charges. The alkali treatment, particularly with sodium hydroxide, is primarily used to alter the properties of sheep wool fibers by removal of impurities or disappearance of white patches. However, unlike the acid treatment, alkali treatment causes cystine's disulfide bonds to be impaired. An alkali treatment tends to result not only in the lower mechanical performance of the wool fiber but also in the change of fiber color into a yellowish and decrease of sulfur content through a dissolution of wool. The effect of alkali is considered to be more effective with a higher pH environment. The destructive effect on the wool of highly concentrated alkalis rather slowly penetrates inside the fiber, and in controlled conditions and at immediate neutralization after short-time treatment, only the superficial zones of wool become modified. Thus, wool sensitivity to alkali treatment can be explained mainly by the action of cystine linkages in the keratin structure, as the rapture is presented in two stages in Figure 10. A sulfenic acid created in the first stage is unstable in alkali conditions; hence, it decomposes to an aldehyde and volatile hydrogen sulfide. [5,46]

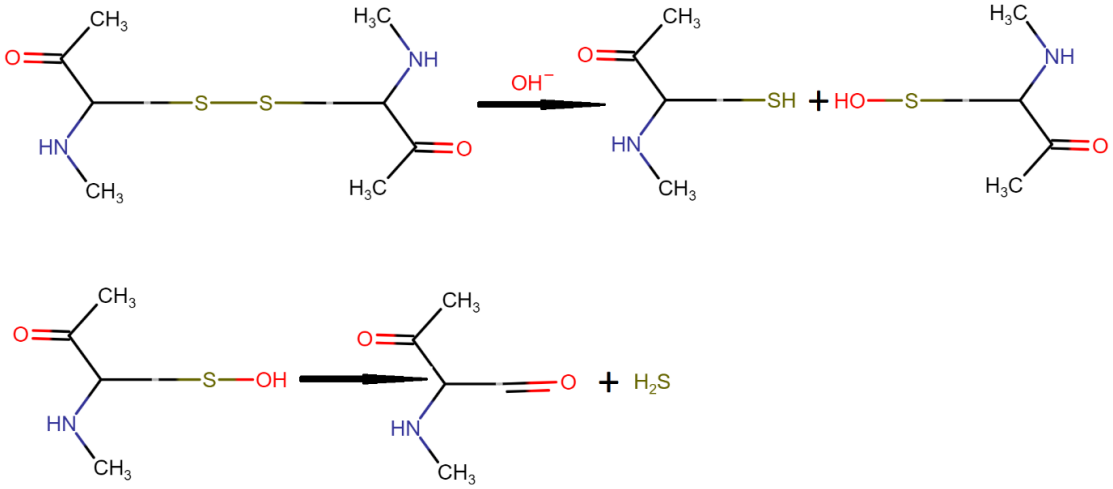

Figure 10 Effect of alkali treatment on cystine cross-linkages.

1.6.4. Effect of salts

The effect of salts on sheep wool fiber affects numerous material properties, influencing tensile strength, chemical resistance, moisture absorption, or an overall performance of the fibrous material. While prolonged boiling, wool fibers in aqueous conditions favor salt sorption in concentrations above 5%. Such sorption, especially in the presence of an acid, is known to cause the degradation of wool fibers, causing the

dissolution of keratin and decreased fiber strength or fiber coarsening. Additionally, wool boiling in hard water containing magnesium and calcium salts changes the wool color to yellowish. Furthermore, heavy metal salts can interact with wool in previously mentioned conditions, causing internal strains. On the other hand, chromium-based salts can act beneficially on fiber as a mordant during wool dyeing. [5]

Alkaline salts, such as potassium carbonate and sodium hydroxide, used for sheep wool fiber treatment may exhibit improved resistance to certain chemical environments. Alkaline solutions can enhance the fibers` durability when subjected to harsh, high-pH environments. On the other hand, chloride salts can affect wool fibers, as for concrete reinforcement treated wool fibers were found to reduce chloride penetration into concrete structure resulted in enhanced durability of composite materials. Such behavior was attributed to formation of dense structure and limitation of ability of chlorides movements within concrete composites. [38]

1.6.5. Effect of reducing agents

The structure of wool fiber can be influenced by reducing agents, especially in an alkaline environment. The treatment of L-cysteine/protease reducing agent was found to the scales structure of wool fibers, revealing their significant damage. Also a strong influence of such treatment can be observed in sodium sulfite acting as a reducing agent, where sodium hydroxide is released during hydrolysis, where the wool's structure and surface are impacted. As a result of such alkali action, salt and cysteine linkages are broken. In the reaction, sulfhydryl groups are also acidic, creating negative charges on keratin in alkaline solutions and resulting in swelling on the fiber's surface. The process can be summarized with a reaction shown in Figure 11. [5,47]

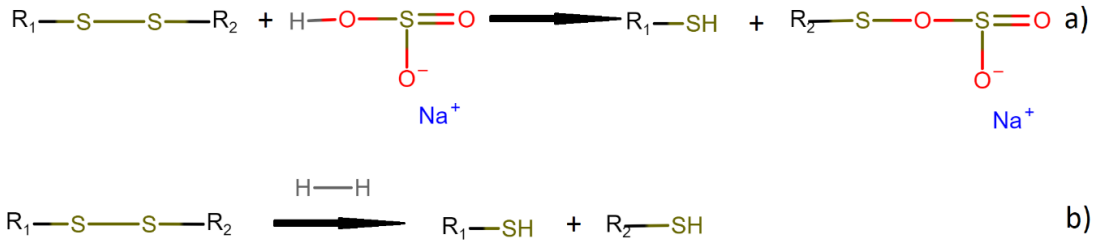

Figure 11 Effect of reducing agent on cystine cross-linkages a) with sodium bisulfite, b) hydrogen.

As it can be easily observed, cysteine linkages are susceptible to reducing agents and alkalis, breaking the disulfide bond. However, such sensitivity may improve wool stability by incorporating a bivalent metal between sulfur atoms or, with additional treatment trimethylene dibromide. As a result of such treatment, the prior raptured disulfide bond becomes linked again with an additional component, as presented in Figure 12. [5]

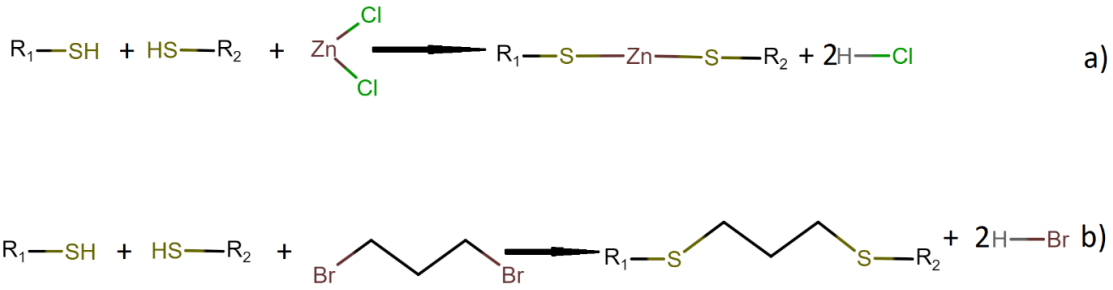

Figure 12 Reinforcement of cysteine disulfide linkages with a) zinc chloride, b) trimethylene dibromide

As a result of action of reducing agents on sheep wool fiber, main alterations can be spotted in chemical structure and forming of new groups within the structure. However, these changes lead to additional effects, where scale surface damage, confirmed by electron microscopy, results in a decrease in performance, including a reduction in elongation. This is happening, as comparing to raw wool, the modified wool is able to share lower load due to altered structure. Furthermore, modified chemical structure results in slight reduction of crystalline structure due to amino acid compositions changes. [47]

1.6.6. Effect of oxidizing agents

Oxidizing agents tend to affect cysteine's disulfide linkages, similar to other previously described reagents causing the disulfide bond rapture. This process can weaken the wool fiber structure and change its mechanical performance. The oxidation caused can decrease in tensile properties of wool fibers due to fibers` increased brittleness and lowered elasticity. Such oxidation may occur due to prolonged wool exposure to light and atmosphere or during treatment with 3% hydrogen peroxide above 3 hours. The breakage of sulfur linkages caused during light action on wool fiber forms sulfhydryl groups. Thus, the formation of compounds like cysteic acid can be observed as a result of treatment with an oxidizing agent. The two-stage reaction of oxidizing disulfide bond is shown in Figure 13. [5]

Partial oxidation of wool fiber occurs while treatment with halogens, resulting in the appearance of aldehyde groups and increasing a capacity for adsorbing. An example of such modification can be considered chlorination, where hypochlorous acid can be used for the treatment. Usually, such a reaction is performed in a no-moisture environment for better control of the reaction, as in aqueous solutions, the interaction between wool and active chlorine is intensive. Among the products of the reaction are water and hydrogen chloride, which promote further development of the reaction. Such modification is summarized by reactions shown in Figure 14. [5]

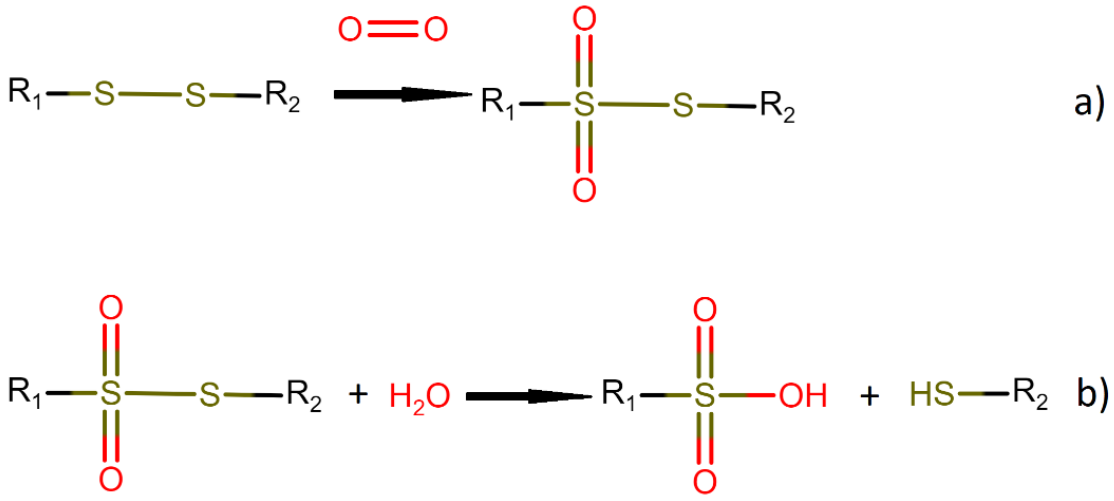

Figure 13 Breakage of the disulfide bond in reactions of a) oxidation and b) hydrolysis of disulfoxides.

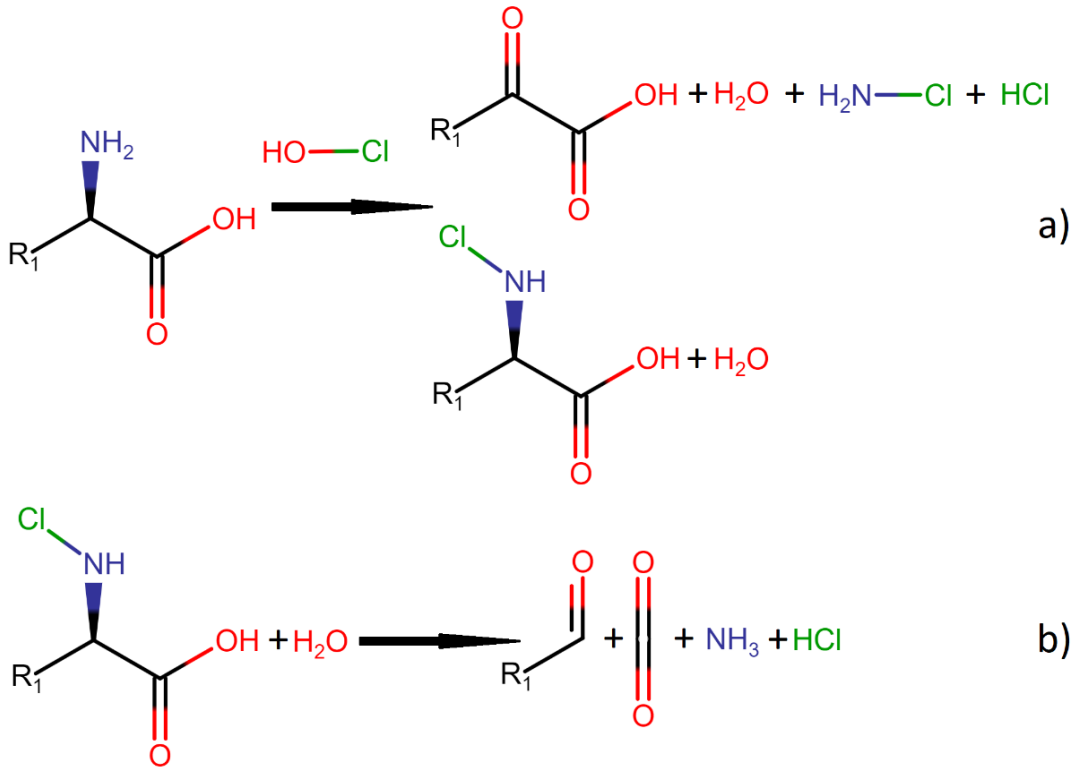

Figure 14 Wool fiber oxidation by a) reaction with hypochlorous acid and b) hydrolytic discomposure of keratin molecule.

Wool superficial oxidation can occur as a result of UV radiation of the fiber, which results in a alteration in its surface characteristics. Wool fiber absorbs UV radiation strongly at 350nm due to aromatic amino acids and cysteine residues. Surface oxidation with UV treatment increases the number of functional groups favorable for modification. Therefore, such treatment is often considered a precondition for fiber dyeing and improving the durability of modified fiber, especially for dyeing in dark and heavy shade colors. [32]

1.7. Wool fiber applications

People have favored wool fiber for a long time due to its excellent heat and moisture comfort properties. The fiber has been developed over millions of years by evolution to possess unique properties such as warmth-retaining, perspiration, and moisture absorption, which are difficult to replicate through synthetic means. The comfort of heat and moisture is derived from the wool's unique inner structure, which comprises a complex hierarchy of structures from alpha-keratin molecules to protofibril, microfibril, macrofibril, and cortex layers.[29,48] It has been a well-known material since ancient times, as it was already recognized in ancient China, Babylon, and Egypt, where it was applied for clothes manufacturing. In the early stages, the fibers were pulled out, but the development of the cutting tool in the Iron Age allowed for a change in the method of collecting fibers and introducing shearing, which has been practiced until the present. Further advancement in wool could be observed in the 14th century when on Spanish territory was bred Merino sheep distinguished for its wool softness. Moreover, in the subsequent centuries, wool production spread around the globe. [7]

Advancements in material science and techniques have expanded the range of applications for wool. Such fibers could be successfully used for building insulations or enhancing thermal and sound aspects. In application, wool fiber is a good replacement for glass and basalt fibers or aerogels. The fact that fiber acts as a sorbent for pollution and heavy metals is beneficial from the perspective of wool usage. Wool, as a natural protein fiber, can adsorb harmful gases and break down organic contaminants through its unique molecular composition and physical and chemical properties, resulting in substances that are not harmful to humans. Additionally, additional applications have recently been achieved through chemical modification by reducing wool disadvantages like low resistance to fire, microbes, or insects. [7,49,50]

Depending on various causes, some wool fibers are not eligible for textile application; therefore, they are used as an additive to, i.e., construction materials. The structure of natural wool fibers is prone to make a difference compared to fiberglass or mineral wool, not only due to its biodegradability and natural origin. Grow wool shows a porosity that affects fiber bulk density, which can be directly responsible for beneficial thermal insulating properties and tends to absorb sound in the material. Therefore, depending on final properties and material usage, wool fiber-based soft mats are competitive for roof and wall insulation, as a pure, entirely wool-based mat or as a composite panel with polyester for walls, but maintaining overwhelming wool volume. Furthermore, textile-undesired wool has found its potential for biochar modification. The biomaterial was mainly reinforced mechanically with wool; however, wool's addition and charring character allowed for smoke reduction and peak heat release rate. [7]

Wool is also investigated in the form of wool powder as a potential replacement for silk powder in some areas. Through a method for super-fine wool powder production with a size of 2μm and smaller than 0.1μm in diameter, it was possible to obtain smaller than other organic powders like silk powder and ramie powder. The wool powder is white due to the room temperature production method.[17]

An interesting wool modification approach is treating the fiber in alkaline conditions with orthosilicic acid. Due to silane elements in CMC interlayer within wool fiber structure, silane modification of wool fiber is worth considering to create active Si-O-Si connections and, therefore, modify properties of proteins in wool protein. It has been established that silane treatment masks a process of disulfide linkage bond and tends to

the protein present in the wool fiber to be less favorable for hydrolysis of the disulfide linkage. [34]

Wool fiber also has the potential to be modified with thin semiconductive or electrically conductive coatings of binary inorganic compounds to create new composite materials with varying properties. Growing interest was observed in using such composite materials with metal chalcogenide layers for solar radiation control, photovoltaic devices, gas sensors, and other applications. One approach to modifying wool fibers is through chemical surface treatment with thin coatings of a binary chalcogenide, such as copper selenide, which offers potential use as an optical recording material.[51]

1.8. Fiber as reinforcement

Wool fibers can be effectively utilized in industries including aerospace, civil engineering, sports equipment production, and more. Wool fiber-reinforced composites are as favorable as unreinforced plastics due to the enhancement of mechanical strength and flexibility and their resistance to a corrosive environment. Wool and other naturally derived fibers fulfill the role of decorative material in the automotive industry, especially for inner parts and seats. An aesthetic aspect can also be observed when wool is used as a reinforcement for cement composites for restoring historical buildings and ceilings. Towards mechanical properties, sheep wool fiber was found as an effective reinforcement for polymers such as polypropylene or polyester, as creation of polymeric composites reinforced among others with wool fibers lead to improved tensile, flexural, impact, and hardness characteristics compared to neat polymers. Therefore, in such applications, wool contributes positively to polymers by improving the durability and rigidity of the matrices.[7,52,53]

On the other hand, wool fibers have been incorporated into cementitious materials to enhance insulation, mechanical behavior, and durability. Several studies have explored the incorporation of wool fibers to improve cementitious materials. Research indicates that adding wool fibers can reduce the workability of concrete while increasing its ductility and flexural capacity. They can also reduce the composite's compressive strength due to the total binder reduction in the mix. Including wool fibers in cement-based mortars can also improve fracture toughness and reduce plastic shrinkage. Apart from material physical-mechanical characteristics, use of sheep wool fiber in concrete reinforcement is known to impact financial and safety aspects. On one hand use of wool is considered as a favorable replacement for more expensive admixtures resulting in reduced costs of materials. On the other hand, benefits gained from wool`s moisture absorption capacity result in improved workability and safety in construction applications. [54–56]

Finally, wool fibers as natural, biodegradable materials are considered as an attractive sustainable reinforcement option, especially for usage in polymers. Sheep wool fiber reinforced polymer composites are especially desired and wool allows to consider biodegradability aspect of final composite and act as eco-friendly alternative to synthetic fiber composites.[53]

1.9. Fiber waste disposal

An increasing amount of wool waste creates for farmers often a need for a rational, cost-effective solutions for solid waste management. Numerous applications of wool fibers are often correlated with strategies for waste disposal as a simultaneous way for material improvement and circular fiber economy. As a potential fields of wool waste disposal can be distinguished non-clothing sectors, including technical textiles or use of keratin extracts for cosmetics and medical application. Even though there are plenty of applications where wool fibers are desired, there will always be some fibers that do not fulfill the requirements for the tailored applications. Due to favorable biodegradability and natural origin, such residue from wool fibers can be used as fertilizer or ground reinforcement. Granules, blocks, or grids made from wool are broadly applied in soil, as they do not cause undesirable effects such as ground pollution, water contamination, or soil degradation. Utilizing wool may be beneficial as a source of desired for soil chemical elements as geotextiles help with water erosion and ground structure and as an adsorption material for toxic substances, preventing toxins accumulation in groundwater. As previously described, the wool fiber structure is generally assembled from various amino acids. Therefore, the elements from wool-based fertilizers are rich in carbon, nitrogen, and oxygen. Depending on the origin and detailed structure of the fertilizer, other elements, such as sulfur or phosphorus, can be provided; however, they are present in smaller quantities in the structure. The role of wool in fertilizer application is not limited to the role of a source of chemical elements. Hydrolyzed wool plays an active role in plant growth as a chelating agent, enhancing the utilization of microelements already present in the soil. While utilized in the ground, wool as a grid can be applied on slopes to protect drainages and gravel pits from undesired movement. After correct installation, wool-based geotextiles protect from land shifts and water erosion. [7,57]

Furthermore, such natural fiber plays the role of filter for catching toxic substances, preventing them from infiltrating water and accumulating in underground water and air pollutants remover. That correlates with another popular approach for wool fiber disposal, where mechanical and chemical methods for producing wool powders are applied. On one hand it allows to develop sustainable practices into other industrial processes, on the other hand it serves as recycled particles for textiles, biosorbents or biomaterials. Such application range is possible due to the porous wool structure and excellent sorbent properties. Wool fibers are known as pollutant removers from oil spills. A capability for oil removal concerns multiple types of substances, such as diesel fuel, vegetable, or motor oils. Another sorbent capability of sheep wool can be observed for disposing of silver (Ag) and copper (Cu) from industrial wastewater or steam. Such ability is possible due to the presence of cysteine (see Figure 4c), which allows it to build with the metals' stable mercaptides. "Caching" metal ions means the exchange of metal into hydrogen ions for the same binding sites. Furthermore, the fibers can lower levels of volatile organic compounds. The presence of keratin compound in wool fiber structure allows for the sorption of organic compounds like toluene, limonene, or dodecane, improving air quality and preventing health damage to indoor occupants. The variety of pollutant applications of sheep wool may be justified, as, among other sorbent materials, it has a low environmental impact. The impact is mainly caused by a reduced number of wool processing operations compared to conventional materials, which reduces energy consumption and CO_2 emissions. The changes in the environmental impact are caused by the requirement for material transportation, usage, recycling, or release of greenhouse gases, where sheep wool is considered good material. [7,58]

Finally, among recycling strategies for textile wool fiber wastes can be distinguished enzymatic recycling. The enzymatic treatment serves for selective degradation of wool fibers and recovering synthetic fibers from them. Further to enzymatic hydrolysis, amino acid from wool fibers can be extracted delivering nutrient sources and serving as a source in biogas production from wool waste. [59]

1.10. Surface modification of natural fibers

1.10.1. General information

Pretreatment of wool fibers can modify their physical-mechanical and mechanical properties to meet tailored requirements. Oxidizing or reducing agents are commonly used in pretreatment of wool fibers to make them reactive and ensure effective and uniform post-treatment results.[32]

Currently there is an increasing trend in searching for ways to modify the surface of wool and other textile fibers without damaging their excellent mechanical and bulk properties. Various chemical and physical modification methods are examined, such as treatment with enzymes and reagents, grafting of monomers, using supercritical carbon dioxide, microencapsulation techniques, corona discharge, gamma and ultraviolet irradiation, ultrasound vibration, and plasma functionalization. However, some of these methods are time-consuming, energy-intensive, and increase manufacturing costs. Additionally, it can be challenging to scale up these methods from laboratory to industrial level in the textile industry. [60,61]

Usually, before modification, wool fibers require a cleaning procedure, which removes the lanoline superficial layer. The surface modifications, observed by etching or damaging the wool fiber scales, are known to enhance hydrophilicity of the fiber surface. Removing the protective lipid layer on wool fibers reveals a protein-rich surface with various functional groups that can be used for attaching new molecular and nanoparticulate entities through surface treatments. To give wool unique surface properties like superhydrophobicity, it is necessary to have an activated surface with accessible functional groups for modification. By removing the lipid layer, it is possible to increase accessibility and functionality. Compounds attached to the wool surface through covalent bonding are expected to have a higher level of durability when it comes to wear and washing, as opposed to those applied by conventional techniques that rely on non-covalent or ionic forces.[62,63]

1.10.2. Plasma treatment

Plasma treatment is considered a rapid, non-toxic, and environmentally friendly process compared to chemical treatments. This method enables the activation, cleaning, or modification of the surface of diverse materials without the need for additional

chemical agents or the involvement of aqueous conditions. Plasma treatment induces microroughness on the surface, and the resulting hydrophobic or hydrophilic characteristics depending the specific type of plasma utilized. [64–66] The surface of wool fibers can undergo alterations, including changes in wettability or shrink resistance, because of plasma treatment. In addition to achieving the intended modifications on the fiber surface, plasma treatment proves advantageous, as it is perceived not to impact the core mechanical performance of the fiber. [66,67]

Plasma, as a fourth state of matter, allows for the creating of solid surfaces with improved properties that cannot be achieved through traditional methods. This modification technique focuses on the superficial of fibers without changing their bulk characteristics.[28] Plasma is generated through electrical discharge into a gas mixture, producing a combination of electrons and ions. The composition of wool fibers treated with plasma changes depending on the type of gas used. Plasma treatment alters the properties of textile fibers and enhances their wettability; as for wool fiber, it scratches the fatty acid deposit from the cuticle and parts of the exocuticle, leading to surface oxidation and the introduction of new anionic groups such as sulphonic and carboxylic acid groups. The treatment changes the chemical characteristics at the surface of the wool, such as increasing nitrogen and oxygen contents and decreasing carbon and sulfur contents. This increases the hydrophilicity of the wool fibers, reducing the hydrophobic effect between fibers. The wettability of wool fibers is enhanced noticeably when treated with plasma, which is considered beneficial for subsequent dyeing, printing, and chemical modification processes. The surface area of the fiber increases dramatically after plasma surface modification. Plasma treatments are an elegant approach to fiber modification to achieve shrink-resistance of wool, as they are surface-specific, totally waste-free, and environmentally friendly. However, such techniques still have to be commercially proven and broadly implemented. [12,32,68]

Plasma modification can serve as a preliminary process for subsequent modifications of wool fibers. Kan et al.[69] reported an exploration of low-temperature plasma treatment as a substitute pretreatment for chlorination in the context of subsequent polymer deposition on wool fibers. While plasma pretreatment demonstrated superior dyeability compared to chlorination alone, the most significant enhancement was observed when combining both pretreatment approaches. Plasma treatment can enhance wool fibers by improving their antifelting characteristics and increasing the adsorption and loading efficiency of nanoparticles. Additionally, it can improve the fiber cohesion and yarn-breaking force of wool fabrics. However, the specific effects of plasma treatment on wool fibers are not yet fully understood.[28]

Plasma treatment has been extensively studies for its influence on wool fiber properties. As the treatment changes the chemical functional groups on the wool fiber surface, it increases hydrophilicity and facilitates diffusion on fibers` surface due to conversion of ie. cystine into cysteic acid. Furthermore, several other wool properties are changed as an effect of plasma treatment, as modified fibers are less susceptible for felting, they present increased fiber friction and enhanced stability during processing. As several surface amino acids are changed due to treatment, it leads in enhancing functional and astatic properties of the wool. Finally, plasma treatment is considered as a cleaner alternative for traditional chlorine-based methods for wool fibers modification; therefore, its usage provides environmental benefits. [70–72]

1.10.3. UV radiation treatment

In general wool fibers possess low protection against UV radiation; therefore, there are several ways how the radiation can impact wool fiber properties. UV irradiation is known to cause a degradation of amino acids in wool structure, cause color change into yellowish and increase brittleness of fiber itself. Moreover, surface scale structure is impacted showing increased smoothness as an outcome of UV treatment. Wool typically has a beige color, which develops more pronounced yellow shades with prolonged exposure to UV irradiation. From mechanical perspective prolonged exposure to UV light causes reduces breaking strength of wool fibers as well as reduced surface friction. The changes are also more evident, the longer is impact of the UV irradiation. [73,74]

Investigations reported on wool fiber modification concluded that the impact of UV radiation on wool fabric modifies its surface features. The wool fiber's aromatic amino acids and cysteine residues strongly absorb UV radiation below 350nm, which justifies the modification capability. This leads to the oxidation of the surface fibers, which introduces more functional groups. Moreover, improved surface enhances the process of fiber dyeing, especially in dark shades such as black and navy blue.[32]

1.10.4. Enzyme treatment

Enzymes are large protein molecules that can react with substances to form products by decreasing the activation energy of a reaction. Enzyme treatment, a form of biological treatment, has been used to modify wool fiber surfaces. These treatments affect the lipid layer on the cuticle, selectively eroding or smoothing it. Additionally, these methods lead to the cystine amino acid split and the addition of anionic charge to the wool fibers, making the fibers more polar and increasing water permeability. The enzymatic treatment is considered as a cost-effective and reliable method for wool fiber surface modification, through enhancing its surface properties with simultaneous maintaining good wool quality. [28,75]

Enzyme reactivity is influenced by specific reaction factors, including pH, duration, and temperature. One notable application of enzymes is in wool fiber modification, particularly for wool finishing. Adding enzymes such as proteases and lipase to detergents increases the cleaning effect and decreases pollution. Enzymatic treatment is also considered as eco-friendly alternative to traditional chemical methods used in textile industry. On the other hand, using proteases tends to improve the softness of wool. Enzyme treatment can cause changes in the structure of wool fibers and weight loss at higher concentrations. A modification with protease enzymes results in the amorphous region of wool fibers being entered and causes swelling. This leads to changes in the disulfide region of cystine and promotes the chemical degradation process. As a result, the percentage of oriented alpha helix structure decreases and is converted to beta-sheet form during enzyme pretreatment.[32,76]

1.10.5. Electron beam treatment

The electron beam treatment is an eco-friendly, solvent-free treatment method used for altering wool fiber. Electron beam irradiation reaches deep into the fiber, altering its internal structure. As a result, such treatment results in formation of various reactive products such as cystine oxides or acids, and other similar protein-based compounds. Great importance of this modification method is gained due to its environmentally friendly modification process. Modification with electron beam treatment does not require use of additional chemical and does not derivate wastewater after modification, therefore it is considered as a sustainable alternative to traditional chemical treatment. [77,78]

The electron beam treatment of wool improves its sorption affinity towards some metal cations such as Cu(II), Co(II), or Cr(III) and can also be used as a method of modification for wool fibers. This method is being researched as a potential alternative to chemical modifying methods, as it does not produce hazardous waste. Although further examination is still necessary to understand the full potential of this method, environmental cleaning and material recycling are promising areas for improvement.[79]

1.10.6. Steam explosion

Another example of physical treatment used for bio-based materials is a steam explosion. The treatment occurs through instant steam discharge in a closed container under high pressure. The method is broadly applied for plant and starch separation, delignification of wood, or purification of cellulosic materials. However, the method tends to get a broader field of application as it was successfully applied for natural fiber surface modification. Although steam explosion is mainly used for cellulosic fibers, it was also successfully applied to silk or wool. Steam explosion is known to result in surface damage, especially visible on the wool fiber scale, where some fragments of scales were dislodged or damaged, resulting in a change of the surface and its contact area. Changes could also be observed in the wool fiber structure, where after wool fiber treatment, a lower amount of crystalline Structure and sulfur-containing compounds were better visible on the FTIR spectra. Sulfur linkages within the fiber were confirmed by the increased humidity absorption, as noted during thermal evaluation. [43]

1.10.7. Silane treatment

Silane coupling agent treatment is used to strengthen fibers in composites by enhancing the interaction between natural fibers and polymer macromolecules. Silane treatment is known to break hydrogen bonds within fibers and enhance surface roughness, resulting in improved mechanical interlocking. The treatment also increases the exposed fiber surface, thus increasing fiber surface reactivity. Studies have shown that silane treatment leads to reinforced polymers with enhanced tensile strength and improved thermal stability compared to other treatment methods. Silane treatment minimizes the impact of humidity on composites by boosting the chemical affinity

between fibers and the polymer, leading to improved tensile properties. It also enhances adhesion, contributing to greater composite strength.[80]

The treatment with silanes modifies surface characteristics of fibers, as silane coupling agent forms covalent bonds with hydroxyl functional groups from surface of natural fibers. Such coupling reaction results in formation of Si-O-C linkages modifying groups present on a surface of a fiber. Therefore, an improvement in adhesion involving fiber and polymer matrix it expected. Presence of such linkages reduces moisture regain of the fiber and improves hydrophobicity as result of incorporation of hydroxyl groups into the linkage forming reaction. As confirmed by electron microscopy observation, such modification causes increased roughness of the surface making the silane treatment suitable for improvement of mechanical performance in polymers reinforced with natural fibers. [81]

1.10.8. Alkaline treatment

Alkaline modification is a widely used technique to improve the performance of natural fibers in thermoplastic and thermoset applications. The treatment disrupts van der Waals forces within the fibers, increasing surface roughness and removing lignin, wax, or oils from the outer layer of the fiber. The addition of sodium hydroxide (NaOH) dissolved in water promotes the ionization of the hydroxyl functional group, affecting the cellulosic structure and degree of polymerization. Alkaline treatment enhances the strength and stiffness of natural fibers while also improving their impact resistance and the overall performance of fiber-reinforced composites. However, it is important to note that excessive alkali concentration can lead to the removal of lignin from the fibers, causing them to weaken or become damaged.[80,82]

1.10.9. Nanoparticle treatment

Natural wool fiber has excellent flexibility and hygroscopicity but can be prone to bacterial and mold growth during various production, storage, and processing stages. One of the methods for chemically modifying natural fibers involves the use of nanoparticles, such as silver nanoparticles. Antibacterial modification of wool fiber is a standard method to improve the quality of the fiber and prevent economic loss. The primary approach of such modification is combining favorable properties and a broad spectrum of application of the fibers, together with specific properties of nanoparticles, which can affect not only the esthetic part of the fiber but also increase the field of functionalities offered by the material. There were grafting Ag-loading SiO2 nano-antibacterial agents on ultraviolet-irradiated wool surface. The wool fiber's structural changes significantly impact mechanical properties and anti-shrinkage performance. [30,83]

Furthermore, clay nanoparticles mixed with polymers may be considered for modifying wool fibers. Different layered clays, such as mica, hectorite, and saponite, have been investigated, with bentonite particularly beneficial for commercial applications. The inner layers of clay consist of multi-sheets layer structure, which results

in a negative surface charge in water that can prevent modification with anionic dyes. Although recently, clay was investigated for cotton fiber coating to improve its flame resistance, thermal stability, and wrinkle resistance, a more complex wool fiber was not investigated.[60]

1.10.10. Maleate treatment

Maleated coupling agents, such as maleic anhydride, are a common approach for improving the strength and performance of polymer composites containing fillers and fiber reinforcements. These agents alter the fibers and matrix, like polypropylene, enhancing interfacial bonding and overall mechanical performance. Treatment with maleic anhydride forms strong chemical bonds, raising the fibers' surface energy and resulting in improved wettability and enhanced interfacial adhesion. This treatment can greatly enhance the flexural strength, stiffness, impact resistance, and overall hardness of composite material.[80]

1.11. The environmental aspect of surface modification

The process of raw wool purification into a textile material often involves either a long or water-dependent treatment process that includes washing, scouring, fulling, bleaching, and dyeing. These processes consume a lot of water and chemicals, resulting in high levels of toxic waste and a large amount of sewage. The usual wet-chemical treatments have a high energy consumption, causing environmental and economic concerns. Due to these issues, efforts have been made to acquire more ecologically friendly, water and energy-saving processes for wool. Research has shown that processes such as ultrasound waves during the cleaning of raw wool fibers and using natural dyes in conjunction with synthetic dyes can improve washing efficiency and decrease dye dosages, making wool textiles eco-friendlier. Additionally, reusing wastewater from natural dyes can result in cost savings.[33]

The surface properties of wool need to be modified for textile applications, but the most used method, wet chlorination, produces chlorinated liquid waste, which can be challenging to dispose of. Therefore, it is crucial to find alternative methods for the surface oxidation of wool that are more environmentally friendly, such as oxygen plasma treatment, lasers, or corona discharge.[84]

From the perspective of modification of natural fibers, although use of chemicals and impact on material end-of-life is considered, several positive outcomes can be outlined. Surface alteration of fibers used for reinforcement is known to enhance mechanical properties and durability of material, what leads to positive impact in longer service of products made from that materials, reduced frequency of product replacement and limited waste production. Furthermore, as modified fiber shows improved resistance to moisture, its degradation in environmental condition is expected after longer period of time. [85]

2. Bio-based plasticizers

2.1. General information

Due to the reduction of fossil fuels and increasing ecological concerns, exploring alternative, renewable sources for polymer production is crucial. Bio-based polymers that reduce dependence on petrochemicals can significantly impact environmental sustainability worldwide.[86] In recent years, the creation of thermosetting polymers for natural reinforcement composites has attracted considerable interest, with researchers utilizing vegetable oils like soybean, linseed, canola, karanja, and vernonia to produce epoxy resins. These resins can be crosslinked using various bio-based curing compounds, including amines, anhydrides, carboxylic acids, phenols, and polyphenols.[87]

2.2. Structure and role of plasticizers in polymer blends

Vegetable oils are a promising source of bio-based materials and additives for the polymer industry. They consist of a structure with multiple fatty acids linked to a glycerol base. Their key characteristic is unsaturation, which can be selectively transformed into various functional groups like hydroxyl and acrylate to adjust their reactivity for specific uses in polymer synthesis and industrial formulations.[87]

The role of a plasticizer is to increase reactivity and allow it to penetrate the polymeric matrix better. Chemical modifications result in a stronger plasticizing effect by increasing the intermolecular distance between polymer macromolecules and weakening their interactions, thereby creating more free volume for the oil to occupy.[88]

Modified vegetable oils are widely considered to interact with the thermoplastic polymer matrix. Such oils were widely found to act as plasticizers for polylactic acid blended with maleinized linseed oil [89], poly(butylene succinate) blended with maleinized linseed oil [90], polyvinyl chloride with epoxidized linseed oil [91], polylactic acid-polyhydroxybutyrate blend with both epoxidized corn oil and maleinized corn oil[92] and many others. The presence of modified vegetable oils in a polymer matrix provides a plasticization effect, resulting in lower energy required for material crystallization. This is explained by improved macromolecular chain mobility and compatibility due to easier crystallization processes.[93,94]

2.3. Synthetic plasticizers

Synthetic plasticizers are additives used for modification of polymers properties such as their flexibility, durability and workability. The plasticizer industry for use in plastics is currently facing several challenges, including restrictions on the use of

phthalate compounds due to their toxicity to humans and poor environmental degradation, as well as the negative perception of fossil fuels. In response, the chemical industry focuses on replacing non-renewable plasticizers with renewable compounds with low toxicity and migration levels. Synthetic modifiers like Bisphenol A (BPA) used in conventional epoxy resins in consumer products have been found to have negative impacts on human health as they can generate the migration of harmful substances. Renewable and sustainable alternatives are preferred as they are non-toxic and do not have the same negative impacts.[95]

2.4. Natural oils as plasticizers

Vegetable oils have gained attention in the polymer industry as a renewable source for polymer production and as additives for manufacturing various formulations. These oils, obtained from seeds, can act as compatibilizers, making them a valuable option in the packaging sector. Their high resistance to migration in food contact conditions makes them even more attractive. By modifying vegetable oils chemically, their interaction with polymeric chains can be increased, allowing for better compatibility in polymeric blends. An efficient plasticizer should have ester and aromatic groups that improve its compatibilizing impact. These present an opportunity to create sustainable plasticizers. Modified vegetable oils, like epoxidized and maleinized linseed oils, have proven effective in plasticizing and enhancing compatibility in polymer composites. These modifications have improved PLA-based composites' impact strength and general ductile material characteristics.

Additionally, incorporating maleinized cottonseed and linseed oils into PLA can increase the plastic's brittleness and speed up its decomposition during composting. The same has been observed using epoxidized karanja oil (EKO) as a plasticizer. However, adding acrylated epoxidized soybean oil (AESO) to PLA slightly speeds up disintegration. [96–98]

Vegetable oils are currently more often desired due to their abundance, as they are derived from agricultural resources and liquid at room temperature. Such oils are generally structured as triglycerides, where ether based on glycerol molecules contains fatty acid groups. The molecular chains in fatty acids are decisive in the properties of vegetable oils in terms of their molecular weight, ability for modification, or presence of functional groups.[99]

2.4.1. Chemical modification of natural oils

Vegetable oils are a potential source for polymer synthesis as they can be modified to produce thermosets. The degree of unsaturation of vegetable oil is essential in determining its suitability for this purpose. Epoxidation is the most common modification method, which uses peroxyacids, dioxirane, or hydrogen peroxide. The resulting epoxidized vegetable oils can be cross-linked by applying a hardener to produce materials that range from hard and stiff to soft and flexible thermosets. In addition to containing epoxide groups, epoxidized vegetable oils also possess other

functional groups, such as residual double bonds, ester groups, and allylic carbons, that can participate in curing.[86,100]

Within vegetable oils, from a chemical point of view, fatty acids present valuable unsaturated carbon bonds (C=C), which provide valuable metrics for vegetable oil application. An average amount of unsaturated bonds in oil can be classified with iodine value (g I_2/100g), whereas values above 100-150 are highly desired in terms of eligibility for modification. Among vegetable oils with many unsaturated carbon bonds are distinguished linseed, soybean, hemp, and chia oils, which make them highly desirable for industrial applications. [101]

Most vegetable oils have a triglyceride structure and are fatty acids containing molecular chains between 14 and 22 carbon atoms. The fatty acids usually contain between 0 to 3 unsaturated carbon bonds, which are valuable and enable vegetable oil for modification. Therefore, the high value of linseed oil is justified because, on average, this triglyceride contains more than six unsaturated bonds in fatty acid chains. That makes linseed oil eligible for further modifications, showing a higher distribution of unsaturated bonds, such as in corn, cottonseed, or soybean oils. [102]

One of the examples of modification through reaction with the bond is epoxidation. The epoxidation involves forming an oxirane ring in place of the carbon double bond. The epoxidation reaction is a known and widely applied approach for broadening applications of oils, also regarding vegetable oils. As a result, the oxirane ring provides a field for potential crosslinking with amines and anhydrides, reflecting modified oil applications in thermosetting materials or for compatibility improvement between material phases. [103,104]

The epoxidation of vegetable oils is a complex process commonly performed using the "Prileschajew route," which involves using peracids formed in situ. Performic and peracetic acids serve as typical oxidizers, with percarboxylic acid forming via a reaction between a carboxylic acid and hydrogen peroxide, catalyzed by Bronsted acid. The epoxidation involves multiple reactions, taking place both in the aqueous and organic phases. The primary reaction, the epoxidation of double bonds of the oil molecules, is very exothermic and requires reduced amounts of reactants to avoid thermal runaway. The process is usually performed in semi-batch mode, with a slow feed rate of reactants, and takes 8-10 hours to complete. Various unwanted reactions, including the degradation of epoxy rings, complicate the optimization of the process. Attempts have been made to optimize the process using alternative methods such as continuous operation and ultrasonic and microwave techniques, but these methods have not yet been developed for industrial use. ptimizing the process demands a thorough understanding of the kinetics of all reactions and the impact of heat and mass transfer.[105]

Maleinization involves incorporating maleic anhydride molecules into vegetable-derived oils that contain carbon-carbon (C=C) double bonds. This can be accomplished through methods including the "ene" reaction, which is the most commonly used. A schematic of the reaction is shown in Figure 15. The process occurs at approximately 200°C, leading to the attachment of anhydride groups to the allylic sites of the fatty acid.[95]

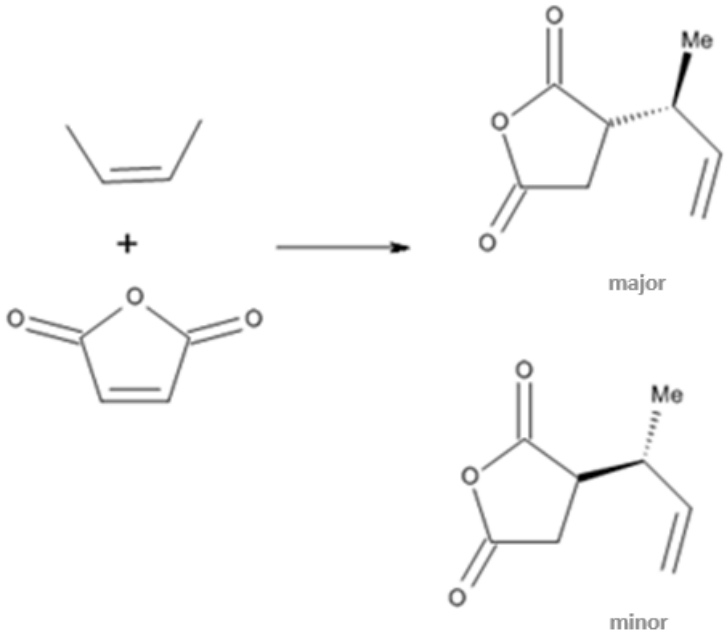

Figure 15 Schematic presentation of the "ene" reaction

2.5. Linseed Oil

Linseed oil, also known as flaxseed oil, is an edible vegetable oil primarily cultivated in colder regions of the world. It is made from the seeds of the linseed or flax plant and has a history of over 5000 years of use as a protein supplement and ingredient in products such as paint binder, putty, and wood finish. Linseed oil is a significant oil crop, producing approximately 2.4 million tons worldwide. It is grown in many countries, including the United States, Canada, and Argentina, with India being the third largest producer. Linseed oil is high in protein, contains 30-40% oil, and is rich in amino acids, dietary fiber, essential nutrients, minerals, lecithin, and flavonoids, making it a beneficial food supplement and medicinal ingredient.[106] Moreover, the chemical composition of linseed oil includes fatty acids like linolenic, oleic, linoleic, palmitic, or stearic acids, giving it modifiability attributed to the presence of unsaturated bonds, making it suitable for deployment as a plasticizer in polymer composites. The elongated hydrocarbon chains can enter the macromolecular structure, while the functional groups facilitate interaction and bonding with the macromolecule.

Linseed oil is extracted through a process that involves using different techniques, including hexane extraction of the press cake and pre-expelling. Linseed oil, derived from the dried seeds of the linseed plant, is available in several forms, including polymerized, sun-bleached, alkali-refined, sun-thickened, and cold-pressed varieties. The seeds must be crushed before being processed, and the extracted oil may contain up to 1% gums and waxes. The oil is then allowed to settle in tanks for three weeks before being heated to 110°C to remove additional impurities. Other methods of extraction include using other organic solvents or supercritical carbon dioxide.[106]

2.5.1. Modification process

One example of linseed oil modification involves maleinization, wherein maleic acid is the modifying agent. Linseed oil, characterized by unsaturated bonds in its fatty acid structure, exhibits reactivity for modification at sites where double bonds are present. Consequently, when subjected to reactive chemical modifiers, such as maleic acid, linseed oil undergoes a modification process. This process is executed at elevated temperatures exceeding 180°C for an extended duration, typically a few hours, to attain reaction equilibrium. The chemical structures showing linseed oil maleinization are illustrated in Figure 16.

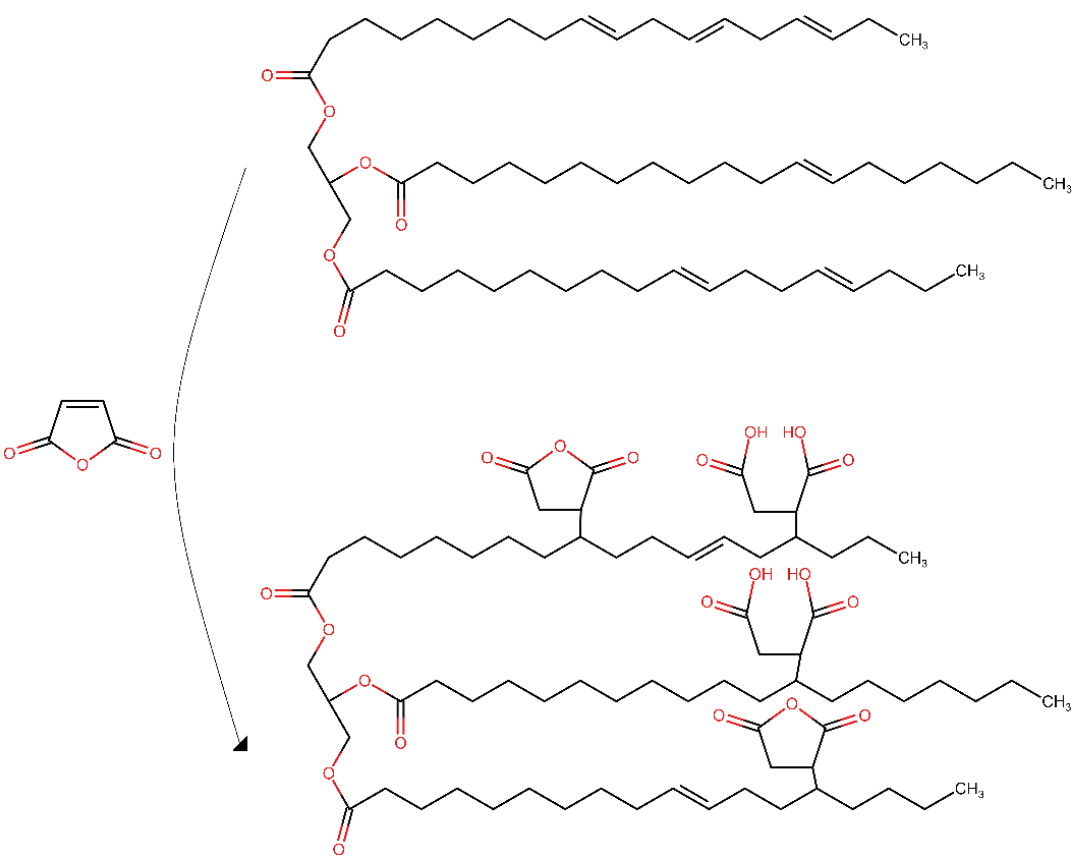

Figure 16 Maleinization of linseed oil

3. Biodegradable polymeric materials

3.1. General information

In an approach to decrease petroleum-based material dependence for short-term and disposable applications, biomaterials are considered to play an important role. A growing interest in using sustainable, eco-friendly materials has emerged, offering an alternative to traditional petroleum-based polymers. This approach focuses on increasing the use of biopolymers over petroleum-based alternatives, aiming to minimize petrochemical-origin materials and promote environmentally friendly options for disposable item. The aim is to use bioplastics to help reduce plastic waste, considered one of the main challenges for polymeric materials. [92,107,108]

3.1.1. Classification of plastics

Plastic materials composed of macromolecules, usually manufactured through chemical synthesis processes. Synthetic polymers, created through polycondensation, polyaddition, or polymerization of monomers, generally have a less complex structure than natural polymers. There are four classifications for plastics: elastomers, thermosets, thermoplastics, and synthetic fibers. Historically, these plastics were derived from petroleum, but there is an increasing demand for their production from renewable sources. Although all conventional plastics are technically degradable, they decompose slowly and are typically considered non-biodegradable. [109]

Bio-based resins are organic macromolecules derived wholly or partly from renewable materials. These resins can be produced from plant-based materials like starch and cellulose, or through the polymerization of plant-derived sugars and oils, as seen in polylactic acid (PLA), polyethylene terephthalate, and polypropylene. Bio-based polymers can be categorized into several key groups. One group includes materials derived entirely from plant biomass and are biodegradable, such as polyhydroxyalkanoates (PHA) and starch. Another group consists of materials that are also biodegradable but only partly derived from renewable sources, like cellulose and PLA. A third group includes materials that incorporate plant-based monomers but are non-biodegradable, such as bio-polyethylene terephthalate, bio-polyethylene, and bio-polypropylene. It has to be considered that not every bio-based material is biodegradable, and not every biodegradable material is bio-based. Polyethylene terephthalate (PET) can be made from fossil fuels or bioresources, but bio-based polyethylene terephthalate can persist in the environment without controlled composting conditions, just like its petrochemical counterpart. In contrast, plant-based polylactic acid is both recyclable and biodegradable.[13,110,111]

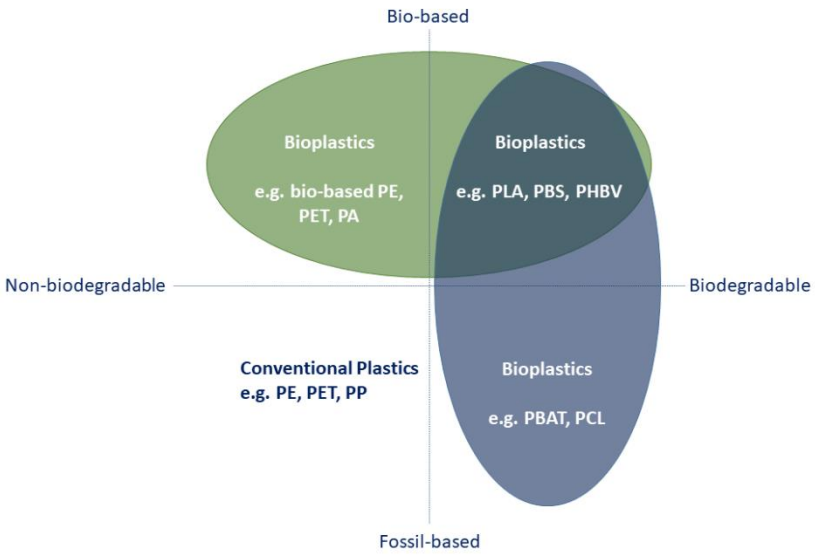

Figure 17 Classification of bioplastics

Biocomposites are classified in to subsets: fully “green” and partially “green” composites, indicating bio-content in materials. Partially “green” composites contains from petrochemical and bio-based resins mixtures, while fully “green” composites consist only from bio-based resins composition, where both types use natural fibers. It is important to recognize that although biopolymers are typically compostable, not all biodegradable and compostable polymeric materials are derived from biopolymers, with some being made entirely from synthetic resources. Due to their environmentally friendly nature, “green” composites are becoming ever more popular for engineering applications.[13]

Environmental matters and the push for sustainability have recently grown towards biocomposites. Plastic is a large part of our daily lives; however, the negative impact on ecosystems from plastic waste collected for recycling or landfill and the use of non-renewable resources like petroleum is a significant problem. The packaging sector uses the largest share of plastics, making up around 40% of total polymer usage in Europe. As a result, efforts are being directed toward developing materials derived from renewable sources or those that are biodegradable to tackle related environmental concerns.[95]

Bio-based materials often contribute to solving challenges with material, especially from environmental and economic perspectives. A short life cycle and high abundance make biomaterials desired in industry, as they are easy to reproduce and dispose of after usage. Bioplastics, in general, are susceptible to biodegradability, which allows material disintegration under the action of water, carbon dioxide, hummus, and microorganisms. That makes them an excellent alternative for non-renewable resources, at least from a short-term perspective, and creates a potential path for reducing scrap material pollution. [22,89,112,113] Another factor boosting the shift into biopolymers is increasing awareness of society's future climate-neutral materials used for production. Among polymers widely applied in industrial processing, besides polylactic acid (PLA), poly(hydroxybutyrate)-PHB and thermoplastic starch-TPS are distinguished poly

(hydroxybutyrate)- PHB. Such bioplastics present a group of materials derived from agro-resources. [89,99]

3.1.2. Aspect of circular economy

Plastic products offer numerous advantages in our everyday reality. The demand and production of plastic goods have significantly risen due to population growth, economic progress, increased commodity demand, and lifestyle changes. However, this has led to enormous amounts of plastic waste in developed and developing nations. Constantly increasing amounts of plastic waste brought critical issues concerning the management of disposal and recycling of the materials to the discussion. Nowadays, plastics form a significant non-biodegradable component of urban solid waste. Furthermore, most plastic waste are kept in landfills, soil, oceans, and waterways, posing a threat to plants, terrestrial and aquatic animals, and humans. [111]

Polymeric materials are broadly used because of their minimal material cost and diverse mechanical properties and applications, due to their long polymer chains structure. However, conventional plastics production involves fossil resources, and these plastics can rarely be recycled in a closed-loop system. Most of these fossil-based plastics are not biodegradable in a short period, causing harm to ecosystems. The life cycle of plastics is a significant concern due to the vast amount of plastic waste generated worldwide, with most plastics not being biodegradable. This has led to a shift towards more environmentally friendly polymeric materials, both in terms of the materials' origin and the potential for biodegradation or compost disintegration at the finish of the life cycle. This transition is particularly noticeable in the packaging sector, where an obstacle has increased due to the widespread use of single-use plastics.[96,114]

Comprehensively assessing the environmental impact of bioplastics and conventional plastics can be achieved by evaluating their entire life cycle from initial production to disposal. One evaluation method is the Life Cycle Assessment (LCA), where the environmental effects of these materials are compared throughout their lifespan. The LCA assesses the environmental impact of bioplastics at each phase of their life cycle, including sourcing of raw materials, manufacturing, and throughout their functional lifespan. Various scenarios of biowaste disposal, composting, or recycling help identify the best method based on the LCA assessment. The LCA analysis indicates that burning or landfilling bioplastic products is not a sustainable alternative to dispose of biowaste. On the other hand, bioplastic waste serves as a valuable alternative to petroleum-based plastics. For instance, PLA and thermoplastic starch are prone to significantly reducing carbon dioxide emissions by 50-70% compared to conventional petroleum-derived plastics. Nevertheless, to ensure the sustainable management of bioplastic waste, it is suggested that greenhouse gas emissions must be reduced to zero emissions. [115]

3.1.3. Bioplastics as an alternative to petroleum-based plastics

New polymers made from sustainable resources, like starch and lactic acid, are being utilized in natural fiber-reinforced composites. These bio-based polymers have advantages and drawbacks and are being studied alongside other bio-based polymers, such as soy-based biodegradable resin, polycaprolactone, and polybutylene succinate. While bio-based polymers have gained acceptance in the composites industry, weighing their pros and cons before deciding to use them is crucial.[116]

Bio-based polymers offer a range of advantages, including sustainability by reducing dependency on oil, being made from renewable sources, and being biodegradable. They are also promoted for recycled products, which are becoming more cost competitive as oil prices increase. Ongoing research is expected to lead to improved production techniques and more environmentally friendly products. Bio-based polymers also have some disadvantages, such as limited shelf life for some sustainable bioplastics, lesser performance compared to petroleum-based plastics, reliance on petroleum-based energy in the manufacturing process, variations in environmental impact among different bioplastics manufacturing methods, potential disruption of existing recycling methods, and higher production costs due to the newness of the market.[116]

Despite positive influence, bioplastics have their limitations and create technical challenges. For instance, products produced during bioplastic synthesis may pollute traditional plastics' recycling stream if they are not separated at the source. The biodegradation of bioplastics may require specific conditions to degrade effectively. Achieving the specific conditions necessary for the biodegradation of bioplastics, such as temperature, pH, and humidity, may not be sufficient in landfills for the complete composting of bioplastics. As a result, direct landfilling of biodegradable polymers may not be practical. Moreover, creating an environment for disposal of bioplastics requires land space, regular monitoring, simplified microbial creation, routine mining of intermediates and byproducts, and capital costs. Finally, bioplastics must be competitive with traditional petrochemical-based plastics regarding production costs, manufacturing scale, and compatibility with currently used production equipment. Furthermore, factors like waste management approaches, end-of-life remediation, social awareness, and spreading waste sorting strategies at the consumer level are crucial for assessing competitiveness.[111]

3.1.4. Aspect of biodegradation

The biodegradation of bioplastics is affected by their physical and chemical properties, such as polymer chains, functional groups, and crystallinity, along with the specific environmental factors like humidity, oxygen availability, temperature, and acidity. [109]

There exist various concepts regarding biodegradation. On the one hand, there are oxo-biodegradable plastics made by mixing petroleum-based polymers with a pro-degradant additive that catalyzes the degradation process of the plastic. The additive, typically a metal salt, enhances the abiotic degradation process of oxo-biodegradable plastics in the presence of oxygen. The time required to degrade biodegradable oxo-

products can be controlled during manufacturing; however, the degradation of oxo-biodegradable polymers usually takes months to years.[115]

Furthermore, hydrolysis is a commonly observed degradation process for hydro-biodegradable polymers that occurs when water diffuses through a polymer matrix, and a polymer backbone consisting of ester bonds is broken down by water molecules, thereby enhancing the hydrolysis mechanisms. The time required for degradation can vary depending on the material in question. For instance, polylactic acid degrades at a prolonged rate of around 11 months. Furthermore, the biodegradation rate can be affected by various factors, including disposal methods and fundamental physical conditions like moisture, oxygen availability, temperature, microorganisms, and light exposure. Hydrolysis reactions of PLA have been demonstrated in Figure 18 [109,115,117]

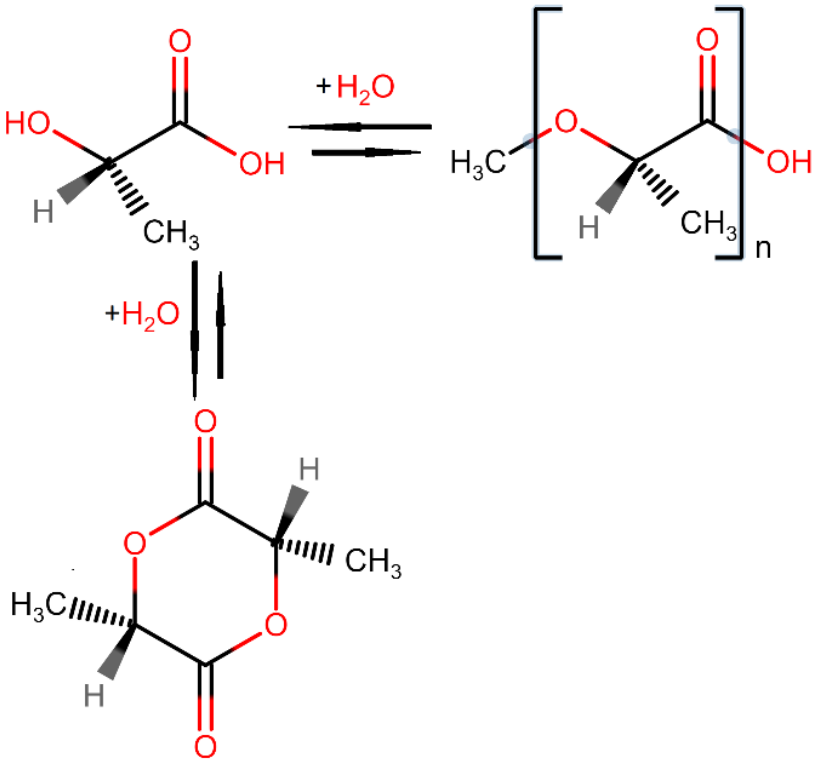

Figure 18 Hydrolysis of polylactic acid

Finally, biodegradation as an enzymatic reaction facilitated by microorganisms exists in various ecosystems. Biodegradation describes to the break of organic substance by microorganisms due to act of fungi, archaea, and bacteria. This process occurs under aerobic conditions, creating carbon dioxide and water as decomposition products. Microorganisms excrete extracellular enzymes to carry out the essential biodegradation processes for biopolymers, including hydrolysis of ester bonds to release monomers. To degrade biopolymers into smaller molecules, the process must occur outside of the microorganism since the substrate is typically too large to be taken up. Extracellular enzymes interact with the substrate's active site to form a complex and break off a portion. This more minor, soluble part can then be transported into the microorganism. [109,114]

3.2. Poly(lactic acid) (PLA)

Poly(lactic acid) (PLA) is a linear polymer created through the polymerization of lactic acid, which is sourced from materials such as corn starch, tapioca, and sugarcane. The structure of the PLA is presented in Figure 19. It is an abundant bioplastic currently applied in various industrial sectors due to its biodegradability, biocompatibility, market accessibility, and cost-effectiveness compared to other biopolymers. PLA is well suited for industrial manufacturing techniques such as injection molding, welding, thermoforming, and extrusion due to its thermal stability and capability to withstand the process. Its biodegradability makes it an ideal choice for packaging applications. Considering its mechanical properties, it is similar to non-degradable polymers commonly used in the industry, like polyethylene terephthalate or polystyrene. [88,95,115]

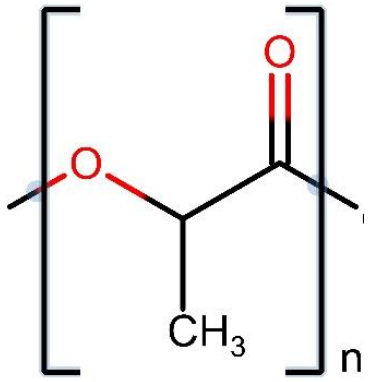

Figure 19 Chemical structure of polylactic acid

3.2.1. Synthesis of PLA

Polylactic acid is a synthetic polymer derived from lactic acid, produced through microbial fermentation of sugar-rich materials like cellulose and starches, using a process called ring-opening polymerization. [88,114] Polylactic acid (PLA) production starts with the conversion of glucose into lactic acid monomers through the homofermentative pathway, facilitated by Lactobacillus in a low oxygen, warm (38-42°C) and acidic (pH 5.4-6.4) environment. The monomers are then pre-polymerized into oligomers of the lactic acid, distilled to form lactide stereoisomers, and finally polymerized in a solvent-free synthesis to produce PLA macromolecules with monitored optical purity. The physical characteristics of the PLA is recognized by the fraction of lactic acid stereoisomers, with a range of amorphous (50-93% L-lactic acid) to semi-crystalline (above 93% L-lactic acid).[97]

L-lactic acid as a chiral organic acid can be present in L-lactic acid and D-lactic acid. The structure of lactic acid is shown in Figure 20. Carboxylic and hydroxyl groups make the molecule a potential monomer for chemical conversions. Due to its biodegradable nature, lactic acid gained attention as a precursor for PLA synthesis, a natural resource replacement to petroleum-based plastics. Synthesis of lactic acid can be achieved through either chemical means or microbial fermentation. The chemical

synthesis method produces a racemic L-lactic and D-lactic acid mixture. On the other hand, microbial fermentation offers either optically pure L-lactic acid or D-lactic acid. Thus, as previously mentioned, a ratio is essential in estimating the physical characteristics of PLA-based materials.[118]

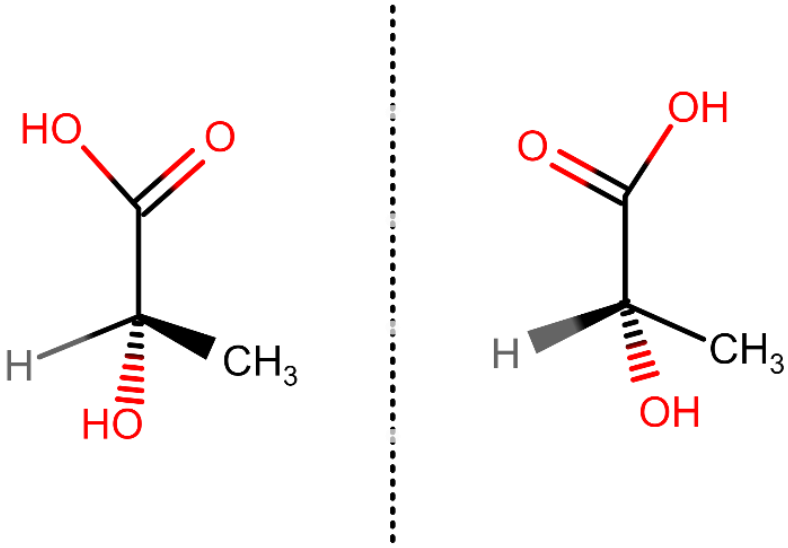

Figure 20 Enantiomers of lactic acid a) L-lactic acid, b) D-lactic acid

PLA production is a multistep process that includes the creation of lactic acid and the formation of the polymer, as shown in Figure 21. The synthesis of PLA typically involves three steps: microbial fermentation to produce lactic acid, its purification and cyclic dimer preparation, and polycondensation or ring-opening polymerization reactions. Polycondensation can be processed through solution or melt polymerization, but obtaining high molecular weight PLA through these methods is difficult. However, chain extension is an effective way to get greater molecular weight polymers. The polycondensation converts the lactic acid monomers into PLA by linking them together via reactions between the hydroxyl (-OH) and carboxyl (-COOH) groups. This process involves removing byproducts such as water and alcohol from the reaction system. Ring-opening polymerization is the most commonly used technique for synthesizing PLA macromolecules, involving a catalyst and the cyclic dimer form of lactic acid in the reaction. Furthermore, enzymatic polymerization is an environmentally friendly alternative to traditional chemical processes, carried out under mild conditions, and is not limited to the presence of pure monomers or anhydrous conditions, helping to avoid side reactions. Enzymatic reactions can also produce polymers with a fine structure using inexpensive raw materials, but these reactions still require more research to achieve a competitive production scale. For instance, lactic acid polymerizing enzymes used for PLA synthesis are lipase B from Candida antarctica and an ionic liquid (1-hexyl-3-ethylimidazoliumhexafluorophosphate). Furthermore, during PLA synthesis, chain extenders like isocyanates or epoxides can be used, but this affects the purity and quality of the material.[117–119]

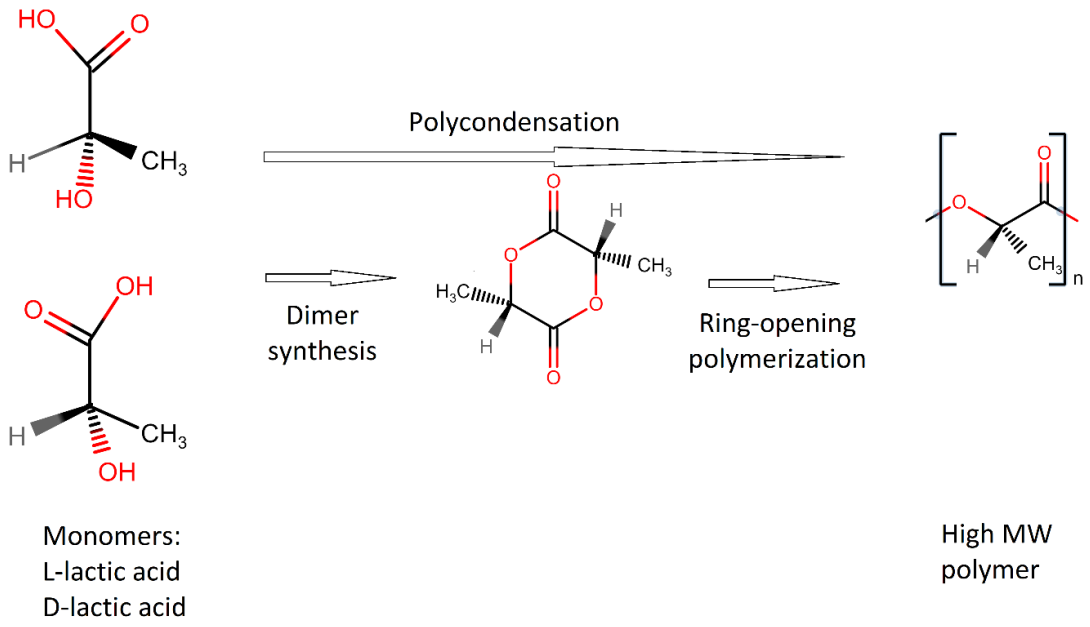

Figure 21 Synthesis routes of poly(lactic acid)

Another commonly used method to adjust material properties is copolymerization with glycolic acid, resulting in the well-known polylactic-co-glycolic random copolymer (PLGA). Copolymerization is also carried out with caprolactone, producing polylactic-co-caprolactone (PLCL). Another approach to enhance material hydrophilicity is synthesizing PLA and polyethylene glycol (PEG) block copolymers. Apart from synthesis methods, the preferred industrial approach for processing PLA involves physical mixing or blending. This method allows for the production of materials with customized characteristics and can be efficiently implemented using common manufacturing techniques like extrusion, injection molding, and film-forming.. In addition, PLA is vulnerable to moisture and often requires additional drying before material processing. [98,117,120]

In summary, different methods are currently applied or developed for PLA synthesis. The solution polycondensation is an economical and easy-to-control method performed in a single step, but it delivers a low-molecular-weight PLA with impurities and side reactions present during the polycondensation. A melt polycondensation is also a one-step method, but a higher reaction temperature and sensitivity to reaction conditions make the reaction more challenging to control, resulting in low-molecular-weight PLA. The ring-opening polymerization delivers a high molecular weight PLA; however, it requires strict lactide monomer purity and is related to higher production costs. Currently, modified techniques for PLA synthesis are also considered, where new catalysts are verified, offering efficient, non-toxic, and high molecular weight PLA production. Moreover, bioprocess/biosynthesis is a slow but efficient, non-toxic, low-cost, one-step method for obtaining PLA. It is worth noting that methods such as modified techniques or biosynthesis are being explored and have the potential to significantly impact PLA production in the market.[6]

3.2.2. Physical-chemical properties of PLA

The characteristics of PLA can be altered by adjusting its properties through various methods, such as selecting a specific molecular weight, copolymerization, blending, or developing more complex molecular structures. Properly adjusting the properties of the polymer can achieve the desired performance parameters such as tensile strength or release rate, over a suitable period without significant degradation reactions. Beyond the impact of synthesis on PLA characteristics, the degree of polymer crystallinity plays a crucial role in defining properties such as hardness, modulus, tensile strength, stiffness, and melting points. When the concentration of L-lactic acid in a polymer exceeds 90%, the polymer is considered semicrystalline. However, lower amounts of the monomer result in a lower optical purity and lead to an amorphous structure of PLA. [117]

PLA shows solubility in several solvents, such as dioxane, acetonitrile, chloroform, methylene chloride, 1,1,2-trichloroethane, and dichloroacetic acid. Partial solubility can be achieved in ethyl benzene, toluene, acetone, and tetrahydrofuran in a solvent's boiling temperature. Although partial solubility is observed for the solvents mentioned above, some of them, like acetone, ethyl acetate, or tetrahydrofuran, do not dissolve the crystalline structure of the PLA. PLA resists solvents such as water, alcohol, and linear hydrocarbons.[117]

Processing PLA can modify its properties, as thermal and mechanical stresses during the process influence the polymer's characteristics. PLA undergoes thermal degradation beyond 200°C, influenced by time, temperature, low molecular weight impurities, and the amount of catalyst used.[117]

The compatibility of PLA with other materials is a critical factor in processing them together. Compatibility, in this context, refers to the technical term that considers the properties of the mixture. If a blend has enhanced properties, like mechanical properties, it can be classified as compatible. Miscible and partially miscible polymer blends are considered compatible, while immiscible once are incompatible. An agent such as a compatibilizer may need to be added to enhance compatibility.[119]

3.2.3. PLA applications

PLA is a promising biopolymer widely used in various sectors, including the packaging industry, medical and pharmaceuticals, bioengineering, automotive and agriculture industries, additive manufacturing, and 3D printing. PLA is primarily used in the food industry to manufacture disposable tableware such as drinking cups, cutlery, trays, food plates, containers, and packaging for sensitive food products. However, PLA bioplastics are too brittle and cannot be utilized in other packaging production processes. Therefore, additives are necessary to increase the durability of PLA. Moreover, PLA exhibits poor thermal and barrier properties, which can restrict its suitability for demanding applications like 3D-printed parts. Additionally, PLA is highly valued for its printability and transparency, making it a popular material for food packaging. With a transparency rate of around 95%, PLA sheeting is preferred for consumers who need to see through the packaging. These properties have made PLA an ideal material for film production in food packaging applications. [88,96,97,115]

In recent times, the food industry has been observed to focus on packaging-related issues. This industry is continuously evolving to address the demands of food production, with the advancement of biopolymer-based packaging playing a key role in maintaining sustainability and quality standards within the sector. The industry can create more sustainable delivery chains by adopting such packaging from production facilities to consumer households. A compostable or degradable bioplastics approach for packaging applications offers an effective solution to the industry's demand for packaging with superior storage qualities, minimal environmental impact, and flexibility in design. While the use of packaging in the food industry still needs an improvement in its sustainability, numerous organizations are aware of the need for change and are willing to switch to bioplastics as much as possible.[109]

Many bioplastics, such as PLA, have limited agricultural applications, mainly nets, grow bags, or mulch films. Nets made from bioplastics are an ideal alternative to high-density polyethylene, helping improve crop quality, increase yield, and shield against birds, insects, and winds. Additionally, while traditional grow bags are typically made from low-density polyethylene, biopolymer-based alternatives provide biodegradability, root-friendly characteristics, and non-toxicity to nearby water sources. Biodegradable mulch films can play a key role in preserving soil structure, retaining moisture, controlling weeds, and preventing contamination, offering an eco-friendly alternative to traditional plastics.[109]

The biocompatibility of PLA to the human body caused extensive research for its use in medical applications. PLA is applied to medical products such as tissue-engineering scaffolds, covering membranes, delivery system materials, and various bio-absorbable medical implants. The versatility of PLA is strongly dependent on the ease of getting desired properties, which can be achieved with simple modifications to its physical-chemical structure, such as blending or copolymerization with other polymeric or non-polymeric components. Moreover, PLA is a polymer approved for use in human clinical sites. Among numerous applications, electrospun fibrous scaffolds are potential tissue-engineering materials for bone regeneration. However, cell adhesion to the polymer is challenging when constructing polymeric scaffolds. [117,118]

PLA is widely acknowledged as a highly suitable substitute for traditional polyethylene terephthalate (PET) since it exhibits numerous comparable properties, such as excellent stiffness, processability, and transparency. However, despite its many similarities to PET, PLA's inferior impact resistance remains a significant challenge. Although PLA may exhibit slightly poorer properties compared to traditional plastics, utilizing bio-composites is essential for driving innovation and broadening its range of applications. [109,121]

3.2.4. Recycling of PLA

Polylactic acid undergoes biodegradation, which results in the release of CO_2, water, and decomposed organic matter. Green plants can utilize organic matter, thereby minimizing their carbon footprint. Furthermore, polylactic acid does not emit toxic intermediates or byproducts upon oxygenation. Compared to other synthetic polymers, polylactic acid has a relatively lower rate of greenhouse gas emissions. For example, one ton of polylactic acid releases roughly 1600 kg of carbon dioxide, whereas

polypropylene, polyethylene terephthalate, and polyamide 11 produce approximately 2740, 4140, and 7150 kg of carbon dioxide per ton.[111]

PLA is a potentially recyclable material, but limited knowledge is currently on adequately disposing of biodegradable plastics. This can lead to PLA wastes contaminating traditional recycled plastics due to erroneous sorting in the recycling stream. However, it is predictable that recycling of PLA after its usage will become more feasible as commercial volumes increase. Compostability delivers a benefit for the end-life of PLA products, as aerobic fermentation can transform them into humus-rich soil. However, waste degradation in landfills through anaerobic fermentation takes longer and is less odorous than aerobic degradation.[97]

3.2.5. Physical aging of PLA

Bio-based polymers are generally recognized for their comparatively lower resilience to environmental stresses when compared to plastics derived from fossil sources. [122] To assess the viability of these materials over extended durations, it is customary to subject polymeric materials to aging tests, including accelerated aging. This investigative approach helps gain a comprehensive understanding of material behaviors over prolonged periods and facilitates practical deployment. Generally, aging is defined as altering material properties over time, induced by temperature, pressure, and other environmental variables. While standard aging studies necessitate prolonged exposure to these factors, accelerated aging enables comparable assessments within shorter timeframes and under heightened exposure conditions.[123,124]

Physical aging in polymers refers to alterations in material characteristics over time, manifested as modifications in their structure. Polylactic acid (PLA) properties can be affected by changes in crystal structure induced by various factors such as acidic environments, heightened temperature, or elevated moisture levels. [125,126] Physical aging primarily impacts the amorphous phase in glassy and partially glassy polymers. Notably, aging is discernible near the glass transition temperature as a mitigated polymer chain mobility. This transition is observable in the mechanical properties of polymers, resulting in phenomena like material shrinkage, augmented rigidity, and increased brittleness.

From an aging standpoint, including natural fibers as plastic reinforcement can diminish superficial interactions of the fiber and bioplastic within the composite. Specifically, natural fibers like wool can absorb water longitudinally, reducing adhesion involving the fiber and polymer matrix. Moreover, humidity absorption by wool fibers may engender fiber swelling, causing expansion into unoccupied spaces within the biocomposite. This, in turn, results in heightened stresses within the composite, potentially culminating in matrix cracking.[127,128]

To overcome the negative impact of aqueous conditions on the aging of wool fiber-reinforced polymers, a popular approach is a surface treatment of fiber with various chemicals such as silane, peroxide, and others. These treatments typically reduce the fibers' hydrophilicity, leading to lower water absorption, less swelling, and enhanced compatibility with the polymer matrix.

To counteract the negative effects of exposure to water on wool fiber-reinforced polymers, a commonly used approach is surface modification of the fibers with various chemicals, such as silane, peroxide, and similar agents. These treatments serve to moderate the hydrophilic character of naturally derived fibers, thereby leading to a reduction in moisture absorption, decreased fiber swelling, and enhanced compatibility of the fiber and polymer matrix[128]

Several reviews concerning the ageing of PLA-based materials are described in the literature. Cui et al. [125] have investigated the physical aging of PLA over time in conditioned laboratory conditions of controlled humidity and temperature (23°C, 50% RH). As a result of aging, ductile materials originally became brittle and had reduced deformability. Such change of properties due to physical aging was observed, most probably due to decreased free volume, as the change continued and had exponential characteristics. Furthermore, it was stated that increased internal stresses due to physical aging may result in micro-cracking in material structure, making the material brittle. Further to the DSC measurement, as concluded by Cui et al. [125], physical aging usually causes an increase in the temperature of glass transition thermal event as it decreased free volume and lower molecular mobility, which was observed in most research studies. However, among reviewed studies, both increase and decrease of the Tg were observed for physical aging studies of the PLA, which indicate that together with a decrease of free volume during PLA aging, additional processes, such as internal stresses, rate of cooling or sensitivity for the aging temperature, are present which determine the direction of change of the glass transition thermal event. Kumar et al. [123] have investigated accelerated thermal aging of biofiber-reinforced PLA with 12-hour temperature cycles between -20°C and 65°C with 12 weeks exposure. Initially, there was an improvement in tensile performance, but after 12 weeks of exposure, the tensile strength of fiber-reinforced PLA decreased..

The initial improvement caused by thermal conditioning could be related to the close conditioning temperature of the glass transition neat PLA. However, prolonged conditioning caused higher thermal stresses and structural deformation, resulting in decreased mechanical performance. Moreover, increasing stresses may relate to different thermal coefficients between PLA matrix and natural fiber reinforcement. Le Duigou et al. [127] have studied seawater-conditioned flax-reinforced PLA for two years. Moreover, samples were exposed to load-unload cycles for tensile properties to provide a broader understanding of damage analysis. As a result, immersion in the seawater causes a reduced Young modulus and strength at break derived from water uptake and damage of biocomposites upon aging. Akderya et al. [124] have investigated the long-term physical aging of chicken feather fiber-reinforced PLA and its influence on the thermal characteristics of the material. Aging is reflected in the chain structure of PLA, as recrystallization reduces chain mobility over the aging period. Through lamella thickening, PLA chains scission occurred, resulting in increased mobility of shorter macromolecules and formation of crystalline structures in lower temperatures. Moreover, the creation of novel crystalline structures after aging reflects on melting temperature by the presence of the shoulder peaks indicating melting of crystalline structure derived from scission macromolecular chains.

4. Fiber Reinforced Polymers (FRPs)

4.1. General information

Composites are materials made up combining two or more materials, where one material serves as a reinforcement and the other as a matrix. The reinforcement phase, typically fibers, sheets, or particles, is stiffer and more robust than the matrix phase and is responsible for bearing the loads. The matrix phase serves as a load transfer phase and delivers the composite toughness, protection, and other properties. Composites are extensively used for their superior strength and other advantages over individual materials. Modern construction, automotive, or aerospace industries are more often required to fulfill unusual requirements for products delivered by the industries. Such nonstandard demands often require specially designed materials. For materials design, one approach for creating tailored properties is reinforcement with fibers. For polymeric materials, such a group is fiber-reinforced polymers (FRPs). [129]

Natural fibers of various types are widely used worldwide. They are commonly found in everyday life and have been utilized by people for various purposes. Main key benefit of natural fibers is that they break down through composting or similar means at the end of their lifecycle. Natural fibers are increasingly recognized as reinforcement materials for their benefits, including affordability, lightweight nature, biodegradability, and non-abrasive characteristics, along with favorable specific properties. They are applied in several commercial applications, including deck surfaces, door components, windows, sports facilities, packaging and automotive industries, and furniture. They have similar properties to other reinforcing fibers and are readily available. However, they have certain downsides, such as low compatibility with hydrophobic polymers, a tendency to aggregate during manufacturing, and poor resistance to humidity that limit their potential as reinforcement in polymers.[14,130]

The creation of biodegradable and recyclable composites from natural materials holds promise for replacing non-renewable resources in industries like automotive and packaging. [131] Polyolefin-based fiber-reinforced polymers are widely utilized, with many composites being reinforced by materials such as glass, carbon, aluminum oxide, and other fibers or particles. Recently, natural fibers have been used as reinforcement in composites due to their benefits, positioning them as potential alternatives to glass fibers in composite materials.[80,132]

There remains significant interest in developing FRPs with natural fibers, which provide a promising alternative to inorganic fibers due to their biocompatibility and sustainability. Natural fibers are often cheap to obtain and easy to reproduce, which may significantly influence a final product's price. On the other hand, natural fibers are considered more complex in their structure than inorganic fibers; therefore often require an in-depth understanding of interaction with polymer matrix and innovative approaches for enhancing such interaction.[133,134]

Natural fiber polymers, such as coir, jute, cotton, bamboo, and hemp, have many advantages over traditional composites. They show several advantages such as eco-

friendly, low weight, favorable strength, renewability, low price, and biodegradability. They can reinforce thermosetting and thermoplastic matrices and potentially replace high-cost glass fibers in low-load-bearing applications. However, natural fibers absorb moisture, which can be addressed through chemical surface treatments. Advances in genetic engineering are also leading to improved natural fibers for composite materials. Natural fiber composites provide meaningful opportunities for sustainable materials with improved performance.[8,116]

4.2. Essential aspects of natural FRPs

4.2.1. Thermal stability of natural fibers

Thermal stability is a crucial aspect to consider for natural fibers usage when developing natural fiber reinforced materials. As an example of degradation of natural fibers, lignocellulosic fibers degrade usually at temperatures above 200°C and is a two-stage process, one in the temperature range of 220-280°C and another in the range of 280-300°C. The initial stage involves the breakdown of hemicellulose, while the later stage corresponds to the degradation of lignin. The decomposition of natural fibers structure can lead to degraded organoleptic appearance, odor and changes in color, as well worsen mechanical properties. Although various fibers can differentiate from each other, similarities in thermal stability and natural fibers degradation can still be observed. Therefore, efforts to coat the fibers and to graft the fibers with monomers to improve thermal stability is highly desired. The thermal degradation of fibers at processing temperatures releases volatiles, which can transform polymers into porous materials, reducing their density and mechanical performance.[130,135]

4.2.2. Moisture

Moisture content in natural fibers presents a significant challenge in the processing and performance of fiber-reinforced polymers. Natural fibers tend to absorb a high amount of humidity due to their hydrophilic properties, which leads to poor adhesion to hydrophobic polymer matrices. Very often, processing with such natural fibers requires additional drying procedures. Besides drying approaches to overcome this issue, various treatments, such as chemical treatments or grafting with vinyl monomers, can reduce the fibers' moisture gain. However, this can also affect other properties, such as mechanical properties and interfacial adhesion. Therefore, careful consideration must be taken when choosing the appropriate treatment method to optimize the performance of the composite.[130,135,136]

4.2.3. Biodegradability

Natural fibers have the favor due to their biodegradable character, which makes them a sustainable option for various applications. However, their resistance to biodegradation and UV radiation usually requires improvement by using chemical treatments or adding polymers to the cell matrix. This can increase their durability and longevity in specific applications, making them a more sustainable alternative to synthetic materials.[130]

Bio-based plastics are produced from renewable materials and have the potential to decompose through microbial activity. The biodegradability of biocomposites is affected by the presence of organisms with specific enzyme systems that can break down the carbohydrate polymers from the cell wall into smaller, digestible units. For example, the cellulose degradation process through oxidation, hydrolysis, and dehydration can also weaken the biocomposite. Several methods exist to improve natural fibers' resistance in biocomposites, including chemically modifying the cell wall polymers to reduce moisture content below the tolerance needed for microbial damage.[11,95]

4.2.4. Fiber modification

The primary challenge lies in the low compatibility between water-attracting natural fibers and water-repelling thermoplastic matrices. [131] From the perspective of natural fiber applications in polymeric materials, natural fibers tend to create aggregated additive phases and are unwilling to moisture as result of their hydrophilic surface. Various chemical modifications are used to enhance natural fibers' properties in polymer composites, including wax or lignin removal, bleaching, acetylation, and chemical structure grafting. These treatments aim to create a hydrophobic surface on the fibers and modify the interaction between the fibers and the surrounding polymer. Chemical modification can also be done using coupling agents such as silane, zirconate, or titanate, which helps effectively transfer stress across the interface. Overall, chemically modifying natural fibers plays a crucial role in advancing fiber-reinforced composites, enhancing their performance and broadening the range of potential applications for these bio-based materials. For instance, silane and alkali modifications are required to enhance the bond of natural fibers, which are hydrophilic in their nature, and the hydrophobic epoxy matrix. [14,130,135,137]

4.2.5. Dispersion in polymeric matrix

Adhesion of the fiber and matrix is a significant factor in determining the interface's response under stress. The dispersion of fibers in the matrix and the strength of the fiber/matrix interface are essential factors in determining the complete strength and integrity of the composite material. The importance of well-dispersed fibers in a polymer matrix is supported by a robust interface, ensuring that the composite can bear load even after fibers are broken.[138] Processing natural fibers with thermoplastics

often leads to poor fiber dispersion due to effective hydrogen bonding between fibers. Poor distribution of fibers in material may be reduced by using various processing aids or coupling agents such as stearic acid, mineral oil, and maleated ethylene. Using maleated polyolefins as a modifying agent improves the compatibility of natural fibers and thermoplastic material. This modification enhances the interactions between the maleated coupling agent's anhydride groups and the natural fibers' hydroxyl groups. [131]These additives are typically used at a concentration of around 1% by weight of fibers and can effectively improve the dispersion of the fibers by reducing fiber-to-fiber interaction and facilitating the disentanglement of individual fibers. On the other hand, the treatment of fibers with various methods, such as bleaching, grafting, and acetylation, can improve the adhesion of the fibers to the polymeric matrix. Additionally, compatibilizers or coupling agents can enhance stress transfer throughout the surface, recovering composite material properties.[130] The creation of fiber-matrix solid superficial bonding, thorough impregnation of fibers by the matrix, and effective transfer of stress from the matrix to the fibers are crucial for producing durable and environmentally friendly natural composites that obtain better mechanical properties and withstand changes caused by environment.[131]

4.2.6. Material processing techniques

Natural fiber-reinforced polymers are typically produced using well recognized methods like compounding, mixing, extrusion, injection molding, and compression molding. However, new technologies and processes are being researched to increase the strength and characteristics of the final product. Fiber type, fiber content, fiber orientation, and moisture content can significantly impact the manufacturing and properties of the final product. When choosing a suitable process for fabricating natural fiber composites, there must be factors such as desired properties, size, shape, processing attributes of raw materials, production rate, and total production cost. The production process includes essential steps such as mat production, slivers, fiber yarns, fiber preparation, and granule production.[116]

Subsequently, the properties of natural fiber-reinforced plastic composites are impacted by the processing technique, such as mixer-injection molding, mixer-compression molding, or direct compression molding. A mixer-injection molding leads to greater tensile and flexural strengths values than other processes. Compression molding also produces relatively lower material decomposition, which is favorable for the automotive sector. Most natural fiber-reinforced polymers are produced using injection molding, extrusion, compression molding, or sheet molding, but new equipment and processes such as pultrusion are being developed to improve feasibility. The size of the final product is a significant factor in determining the suitable manufacturing process to be used. Small to medium-sized components are typically produced through injection and compression molding for their simplicity and fast processing cycle, while large structures are typically manufactured by open molding.[116]

The choice of the optimal process technology for natural-fiber composite manufacturing is primarily based on the form of desired product, performance requirements, cost, and simplicity of manufacturing. Understanding the relationship between materials, raw ingredients, process technology, and final part design is essential for a quality, robust, repeatable manufacturing process. Factors that should be

considered in selecting a process include evenly distributed fiber within the matrix, compatibility between the matrix and fibers, minimal fiber attrition to maintain reinforcement, desired fiber orientation, thermal stability of the fiber, and desired moisture level to avoid swelling or distortion. [139]

Compounding methods that mix natural fibers with a thermoplastic matrix are becoming more popular as they offer a high stability in composition when provided in the pellet form. Compounding aims to manufacture a pelletized feedstock that can be further utilized using techniques such as injection molding, extrusion, or thermoforming. Different approaches of production are available, among others compounding processes, including extrusion, kneading, and high-shear mixers. Extrusion is a processing technique where compounded material is introduced into a heated container of an extruder and is heat up to facilitate thermoplastic flow. Different extruders are available, such as twin-screw, co-rotating, and counter-rotating, as well as planetary extruders, add in single-screw. All these extruders have the same purpose to feed material, heat it up, disperse, distribute, devolatilize, and extrude material through a die. Kneading is blending natural fibers with a thermoplastic matrix using continuous kneading mixers or batch-style kneading equipment. This process involves using two intermeshing rotors in a heated barrel to control mixing time, temperature, and energy consumption. Kneading can also be combined with an extruder and pelletizer to produce pellets, making it suitable for producing natural fiber-reinforced plastic composites. High-shear mixers employ robust mixing equipment, such as a thermal-dynamic batch-style machine.[139]

Injection molding is a popular method for manufacturing polymer composite products, especially when complex shapes are produced in high-volume. The benefits of injection molding consists of high tolerance for dimensions and short production cycles, but some challenges include producing consistent quality pellets. Using bio-based composites can result in parts that are 40% lighter than corresponding injection-molded specimens. However, challenging in injection molding natural fiber composites is producing pellets of uniform quality. This has been addressed by using the direct long-fiber thermoplastic molding process, a continuous process first developed for glass fibers. This process involves spooling the fibers and feeding them into a heating region, where the thermoplastic is mixed with the fiber packs. These packs are shorten to a selected length and supplied into an injection molding hopper to create parts.[139]

Thermoforming is a process usually used to manufacture natural-fiber-mat thermoplastic composites. It involves prefabricated layers of fiber or mats with a polymer sheet inserted into a heated up forming mold and consolidated as heat conducted to melted thermoplastic, allowing it to surround the fibers or mats. Pressure is employed during both heating and cooling cycles. As the melt temperature is achieved, the hybrid material is combined in melt state. The process is efficient, with low processing times possible through combined simultaneous heating-cooling presses.[139]

Compression molding is a process that uses thermoset polymer matrices to produce large parts, such as panels and structures, for the automotive industry. It offers advantages such as low fiber attrition and fast processing speed. Compression molding can be done using various methods, such as sheet molding compounds, and recent developments have combined it with extrusion for thermoplastic composites. However, it has high capitalization costs, which may hinder its large-scale adoption in the automotive sector.[139]

4.3. Natural fiber reinforced biopolymers

Natural fibers have recently gained attention as a potential reinforcement material in polymer composites based on their favorable cost, low density, and ability to degrade at certain conditions. However, specific weaknesses such as low compatibility with hydrophobic polymer matrix, affinity to make aggregates during manufacturing, and low moisture resistance can mitigate the capability of natural fibers as reinforcement in polymers. The fibers' properties, the fibers' aspect ratio, and the fiber-matrix interface play a key role in evaluating the performance of the composite. The thermal stability of the fibers and the surface adhesion characteristics are essential considerations in developing natural fiber-reinforced composites. Additionally, the dispersion of fibers in thermoplastic composites is vital for achieving regularity in the product.[130]

The mechanical properties of neat PLA polymers could be improved using various fibers like jute, flax, coir, kenaf, and bamboo fibers. The mechanical, rheological, and thermomechanical characteristics of PLA/fibers reinforced materials are also investigated concerning the chemical grafting on the fibers and the impact on manufacturing conditions. For instance, kenaf fibers treated with alkaline silane treatment demonstrated a high capability to enhance the mechanical characteristics of PLA. Nevertheless, comparatively less attention is observed for PLA blend/natural fiber composites, such as compatibilized PLA/LDPE blend reinforced with jute fibers.[119]

Coir fiber, derived from the husk of coconut fruit, has a high lignin content, making it a durable natural fiber. It can be reinforced with thermoset and thermoplastic resins to create polymeric materials with various industrial and socio-economic applications. The mechanical characteristics of coir fiber hang on the interfacial adhesion between the fiber and matrix material. Alkali treatment and fiber length can also alter the general properties of coir fiber-reinforced polymers. However, one limitation of coir fibers remains high moisture absorption, which may be controlled via chemical treatment. Coir fiber-reinforced composites are commonly applied for automotive interiors, building materials, and other applications.[8,140]

Kenaf, a plant from the hibiscus family, is a biodegradable crop that is an essential resource of fiber for composite and other fields of applications. Studies have shown that composites made from polyester resin with kenaf fiber have good mechanical properties. Historically, the fiber was applied to make ropes, but now it is utilized in producing clothing, toys, and shoes. The kenaf fiber is completely biodegradable, non-toxic, and can be reused.[141]

Jute fiber-reinforced composites are tested in variety of applications, such as doors, windows, furniture, corrugated sheets, and underground pipes. These composites have been made using polypropylene and epoxy matrices. Polymer reinforcement with jute fiber impacts mechanical properties by considering fiber treatment, fiber orientation, and the percentage of fibers in the polymer matrix. It has also been found that hybrid composites manufactured with jute and other naturally-derived fibers such as coir and sisal have improved mechanical properties and have potential applications in automotive, building, and aircraft sectors. Jute-coir hybrid composites have also been used in railway coaches and the transportation sector.[8]

Flax fibers have the prospective to be excellent reinforcing fillers in thermoplastic biocomposites. They can lower the usage of petroleum-based plastics in industries such as automotive, building, and appliances. Biocomposites containing thermoplastics and

modified flax fiber have mechanical properties comparable to glass fiber-based thermoplastic composites. Studies have been conducted on the mechanical characteristics of flax/polypropylene composites manufactured through batch processes like kneading and extrusion, and natural fiber mat applied in thermoplastic composites.[141]

Considering the environmental aspect of natural fiber-reinforced polymers, such materials are more environmentally friendly than glass fiber-reinforced polymers in tailored applications. The reasons for such a conclusion include lower environmental impact during production, higher fiber content, lower weight, and the ability to generate energy and carbon during end-of-life burning. However, it is essential to note that using fertilizer in natural fiber cultivation can increase nitrate and phosphate emissions and contribute to the eutrophication of local water bodies. Additionally, the environmental benefits of natural fiber-reinforced polymers may be reduced if they have a shorter lifespan compared to glass fiber-reinforced polymers. Natural fibers have a promising future for reinforcement applications as they are cheaper, lighter, and more environmentally friendly than glass fibers.[137,142]

5. Computational modeling

5.1. Artificial Intelligence (AI)

Artificial Intelligence (AI) is defined as a discipline wherein machines are designed to emulate human learning processes. AI systems can comprehend external data, integrate knowledge from the data, and employ this acquired knowledge to accomplish predefined objectives. The principal objective of the AI paradigm is to replicate human cognitive processes, encompassing learning, reasoning, and self-correction, to achieve specified goals. [143–146] This emulation is grounded in fundamental aspects of human learning, including observation and repetition, where the accumulation of multiple observations can interpret evident patterns. [147]

Artificial Intelligence (AI) is acknowledged as a fundamental element in the approaching industrial revolution. Recently, computational modeling methodologies have grown in significance for representing physical phenomena. The traditional trade-off between model accuracy and computational efficiency, primarily dictated by CPU and time constraints, is gradually retreating in importance within the modeling domain. This shift is mainly attributed to the rapid advancements in AI techniques and the corresponding infrastructure. Unlike the historical industrial transformations driven by manual production methods (Industry 1.0), the utilization of electrical energy (Industry 2.0), and digitalization (Industry 3.0), the imminent industrial revolution, denoted as Industry 4.0, is characterized by intelligent cyber-physical systems. Within material science, the contemporary industrial approach involves advancements in Big Data modeling for the processing, characterizing, and explaining of material properties. [148,149]

From a market perspective, Artificial Intelligence (AI) is undergoing rapid and widespread transformation across various daily planes, including technology, finance, industry, commerce, and entertainment. [143,144] Notably, AI techniques like machine learning are increasingly extending their applicability to complex engineering problem-solving in various domains. The appeal of these techniques lies in their capacity to facilitate data-driven conclusions, encompassing a comprehensive approach from material production to disposal, including factors such as transportation and others. [150] In material science, AI techniques serve as valuable tools for modeling the mechanical properties of materials, supplying models characterized by high reliability and reduced computational time. Despite the extensive influence and expanding applications of AI techniques, there remains a shortage of research studies exploring the integration of artificial intelligence in material science to investigate the complicated phenomena associated with materials. [151]

5.2. Machine learning

Machine learning (ML), a subgroup of Artificial Intelligence (AI), is characterized by its ability to enable a system to learn from available knowledge without predefined

relationships between input and output and explicit programming for such tasks. ML establishes associations between input and output without interpreting the nature of the interaction or the regulatory mechanisms governing the relationship. Moreover, ML models possess the capability to enhance their performance autonomously. The process involves postulating an unknown function based on environmental observations that are somehow linked to the output. Subsequently, the training of this function, using input data, adjusts the model to formulate potential relationships between input and output. [143,145,152] Machine learning involves constructing data models from sample inputs utilizing various algorithms, resulting in applicable estimates across diverse datasets.

Machine learning is a multidisciplinary domain encompassing various fields, including computer science, statistics, and complex algorithms. Machine learning classification primarily revolves around three main training approaches: supervised learning, unsupervised learning, and reinforcement learning. [143,150]

Supervised machine learning, a subcategory of machine learning, involves utilizing input and output information for model training to establish correlations between them. Essentially, a mapping between input and output is created as a function. In this context, supervision refers to the presentation of output data that corresponds to input data during the model training process. The training is an iterative procedure, continually adapting until the model accurately represents the relationship within the tagged data. This training process is similar to student learning under the guidance of an instructor. To validate the trained model, it undergoes testing on previously unseen data, and its performance is assessed by comparing the predicted results with the output data. A subset of data is specifically designated for evaluation, ensuring the alignment of prediction results with the output data from the trained model. The learning process concludes when the model achieves satisfactory predictions based on input data. Supervised learning is commonly employed in classification and regression models, especially for capturing non-linear and complex relationships between input and output. Algorithms such as Support Vector Machine, Linear Regression, Random Forest, or spam filtering are frequently applied in supervised machine learning. In this context, data labeling can be defined manually or through simulation. [143,147,153,154]

Unsupervised machine learning constitutes a subcategory within the field of machine learning wherein the model is trained only on input data without preceding guidance. Consequently, the data supplied to the model undergoes classification or categorization based on inherent patterns or features within the data. Such models can be trained to cluster information into predefined groups or identify predominant directions within high-dimensional space. Unsupervised learning algorithms aim to discover valuable insights by analyzing extensive datasets. A fundamental advantage of unsupervised machine learning lies in its ability to analyze data without needing pre-existing labels, easing the costs and time associated with the modeling process. Algorithms employed in unsupervised learning are broadly categorized into clustering, demonstrated by the K-means algorithm, and data association, represented by the a priori algorithm. [143,147,154]

In addition to supervised and unsupervised machine learning, a hybrid approach known as semi-supervised machine learning exists. This methodology involves incorporating labeled and unlabeled data for model training, primarily emphasizing utilizing the information from the unlabeled dataset. A representative example of such modeling is the graph neural network algorithm. [145,146]

Finally, reinforcement learning, a subcategory within machine learning, involves training a computational agent on a specific task, wherein the agent is permitted to undertake random actions to attain a predefined goal. Often referred to as feedback-based machine learning, reinforcement learning is characterized by a model that learns through iterative processes, receiving rewards for successful outcomes and penalties for failures. This approach enables the model to make decisions based on unstructured data. Typically, a Markov decision process is employed for such models, utilizing a scalar reward and its transition to the subsequent step, which is applied to system dynamics to maximize the desired return from the model. [143,145,153,154]

5.2.1. Machine Learning workflow

The conventional machine learning workflow comprises three fundamental phases: data preparation and feature extraction, ML algorithm selection involving model learning, and model validation, including evaluating its accuracy.[150] An illustrative representation of a machine learning workflow is shown in Figure 22, where the workflow elements are presented in an expanded format.

A critical factor for the efficacy of machine learning lies in the quality of the experimental data. Firstly, the data inputted into the model should be responsive for understanding and analysis by a machine learning algorithm, emphasizing that only adequate, well-suited experimental data can facilitate the modeling of the desired relationships. Secondly, before employing experimental data, preprocessing is essential, involving operations such as removing inaccurate or missing data, normalization, dimensionality reduction, or data category conversion. These operations contribute to optimizing the dataset's representativeness for machine learning modeling. [147]

Data acquisition involves systematically collecting data from published articles, technical reports, or proprietary experimental data. During this stage, a careful assessment of the data is necessary, as not all acquired data may prove valuable for subsequent use. Following data acquisition, the next step involves data preparation, wherein the previously collected data undergoes preprocessing involving formatting, cleaning, and sampling. Formatting demands the careful selection of data based on their applicability to predict the desired output, particularly in material science, where the relevance of selected input data to model predictions needs to be scrutinized. Cleaning the dataset involves the removal of inconsistent data concerning all input data, ensuring data quality. Subsequently, data sampling involves the conversion of raw data into information that is both relevant and easily interpretable for the algorithm. Such data manipulation enhances learning accuracy and improves clarity. [154]

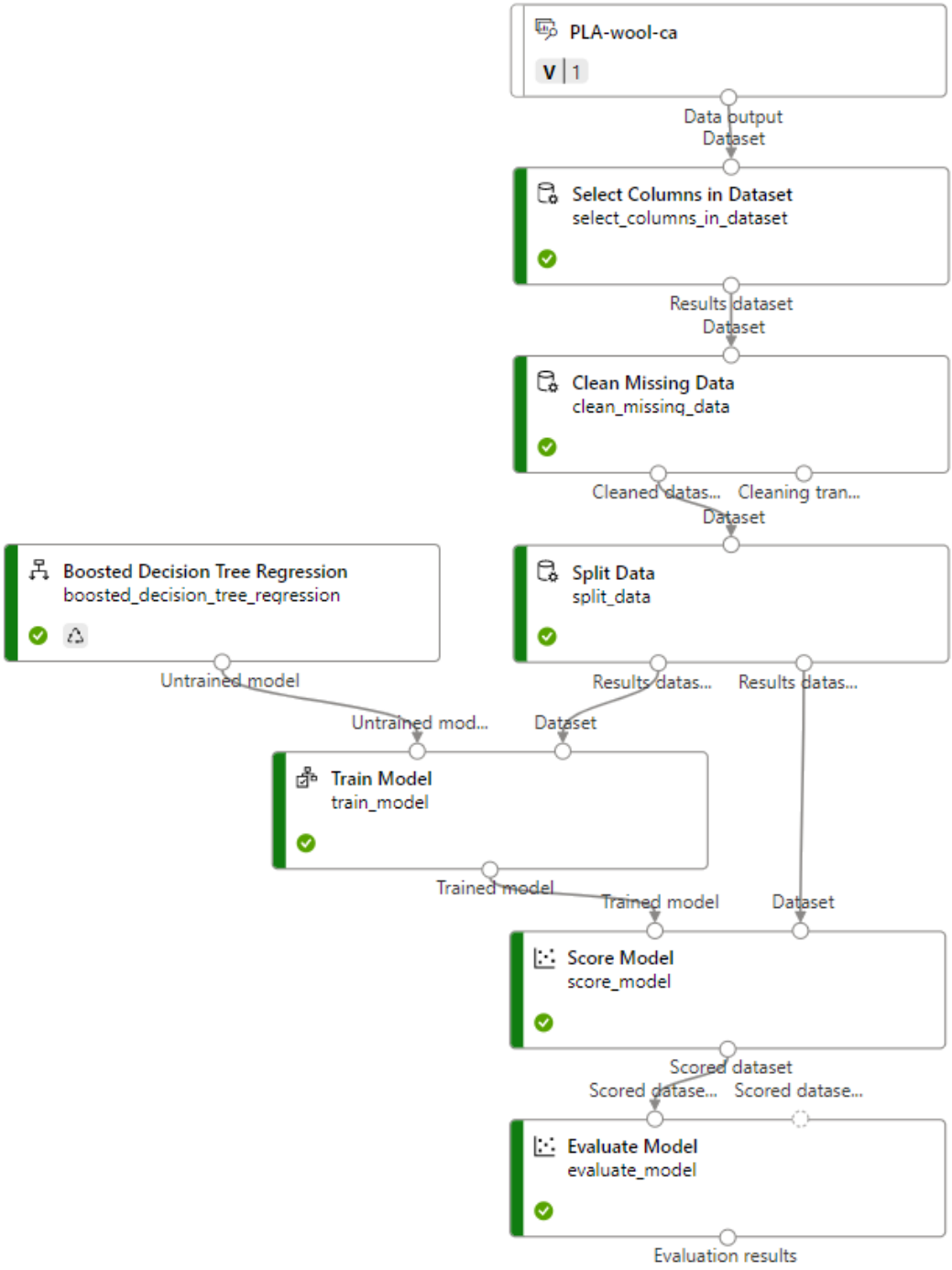

Figure 22 Machine learning experimental workflow obtained in Azure ML Studio

After completing data acquisition and preprocessing, the next critical step is the selection of an appropriate machine learning (ML) method to serve the defined hypothesis. Considering the expected outcome, whether in the form of classification or regression, and the type of modeling approach, a suitable algorithm is chosen for the modeling process. Given the variety of available models, verifying the same hypothesis using algorithms with slightly different approaches is practical. Once these prerequisites are fulfilled, the selected algorithm is employed for model training, typically divided into three stages: training, cross-validation, and testing. Consequently, the input dataset is

partitioned into subsets to facilitate model testing. Finally, the prepared model undergoes evaluation based on experimental data, and the outcomes are compared with the prediction data. This widespread process ensures the strength and effectiveness of the ML model. [154]

In the evaluation of models, various performance metrics are commonly employed, including mean absolute error (MAE), mean square error (MSE), root mean square error (RMSE), and the coefficient of determination (R^2) or others. These factors are formally stated by the following equations:[155]

Equation 1 $MAE = \frac{1}{n}\sum_{i=1}^{n} |Ai - Pi|$

Equation 2 $MSE = \frac{1}{n}\sum_{i=1}^{n} (Ai - Pi)^2$

Equation 3 $RMSE = \sqrt{MSE}$

Equation 4 $R^2 = 1 - \frac{SSr}{SSm}$

, where Ai stands for actual value, Pi stands for predicted value, SSr stands for squared sum error of the regression line, and SSm stands for squared sum error of the mean line.

5.2.2. Machine learning algorithms

Several methods characterized by distinct algorithms can be identified within the various categories of machine learning and their respective approaches to model training. Significant examples are artificial neural networks (ANN), support vector machines (SVM), decision trees, and random forests. [143] Adopting these algorithms is increasingly viewed as a new standard for cost reduction in manufacturing facilities. [156]

The K-Means algorithm is an iterative machine learning process that partitions data objects into several clusters.[144] Models based on this algorithm are recognized for their ease of implementation and rapid conjunction. However, they exhibit sensitivity to noise in the data feed. [150]

Artificial neural networks (ANN) represent a technique designed to emulate problem-solving like the human brain. ANN is one of the most promising and widely utilized algorithms, particularly in image analysis. [144] While suitable for capturing nonlinear relationships and exhibiting high fault tolerance, this algorithm necessitates learning numerous parameters and may result in unclear conclusions. [150] The ANN architecture is based on layers of neurons, where each layer's neurons are interconnected and transfer information. [147]

Deep learning (DL), a subcategory of machine learning, relies on computational models inspired by biological structures, utilizing multi-layer neural networks to address tasks. Its prominence lies in its ability to extract high-level features from data. Although extensively applied in web search, fraud detection, or financial risk modeling, deep learning garners increasing attention in diverse scientific fields such as chemistry, physics, or materials science. [145]

Decision trees (DT) are models that unite simple tests, comparing numerical and nominal attributes to determine possible outcomes. [147] While DT algorithms are recognized for their high efficiency and interpretability, they are susceptible to overfitting and may overlook feature correlations. These algorithms excel in representing knowledge and find applications in solving combinatorial optimization and event forecasting problems. Equally, boosted decision trees provide models with ranked feature importance. [150,155]

The Random Forest (RF) or decision forest algorithm is a variant of the decision tree method, focusing on classification using random vector values with average regression for forecasting. This model introduces a set of trees, allowing for correlation between decision trees, thereby reducing prediction variance. Additionally, each decision tree in the random forest is equally treated to contribute a similar representation to the final model.[147]

The Least Square regression model involves the machine learning transformation of independent variables into a multidimensional space, establishing relationships among them in a possibly linear function. Various mathematical functions, such as linear, polynomial, or Gaussian functions, can be employed for this approach. [157]

The Support Vector Machine (SVM) model is commonly utilized to optimize regression and classification tasks. The algorithm adjusts through vector optimization, seeking the hyperplane of separation between labeled data classes. [147]

In various machine learning technologies, linear regression, decision trees, and random forests are frequently employed to determine coefficients or parameters from structured data. Conversely, unstructured data, such as images, text, or graphs, often necessitate different approaches, as the techniques mentioned above may lack effectiveness in terms of time and scalability. For unstructured data, deep learning techniques, while requiring additional training effort, hold promise, as they enable the approximation of functions and expedite model conclusions.[145]

5.2.3. Machine learning applications

Materials science can generate data through theoretical simulations or experimental methods. Experimental data are acquired through characterization techniques that describe a material based on its structure, properties, and behavior. Furthermore, material characteristics may be associated with factors such as synthesis conditions, the type of substrate, or interactions with other particles.[147]

Machine learning models are valuable tools for designing materials with novel structures or predicting their properties. These models offer high accuracy without necessitating expensive tests. [158] The extensive datasets that train machine learning models create opportunities to establish relationships between materials, structures, and properties. As a result, these models can interpret how the structure of a material influences its properties. This approach facilitates the assessment of the behavior of produced polymer composites, concurrently reducing the need for extensive laboratory testing and addressing challenges inherent in traditional computational models. AI-based models find applications in predicting material properties and designing new polymer-based formulations. However, due to the numerous factors influencing material

properties, insufficient input data may lead to uncertain conclusions and incorrect predictions. [152]

The recent rapid development of machine learning techniques is attributed to their high efficiency in pattern recognition, making them practical alternatives to other methods. [159] In materials science research, traditional methods often involve designed experiments based on a trial-and-error approach with strong chemical intuition. While mathematical approaches such as density functional theory, molecular dynamics, or finite elements offer faster and cheaper alternatives to laboratory research, they are constrained by time limitations. Alternatively, AI techniques like deep learning provide faster results than traditional mathematical approaches, offering accuracy comparable to physics-based models. Simulations once considered impractical using traditional techniques are becoming realistic with AI-based models, indicating progress in material design and advancements in the fourth industrial revolution. [145,153]89]

Although AI techniques hold promise and are likely to be extensively used in the future, Rajasekaran et al. [121] demonstrated that traditional fuzzy logic functions achieved better predictions for cutting variables in carbon fiber-reinforced polymer composites compared to artificial neural networks. AI techniques were found to be less efficient due to longer modeling times, memory usage, and similar predictability, posing challenges in model creation.

Alternatively, AI techniques can be applied to design and model high-quality products. One method for designing new products is the design of experiments (DOE), where AI techniques within the machine learning category enable high-quality products with reduced optimization costs. [156]

An example of the use of supervised ML in materials science is the classification of alloy phases based on alloy contents and processing conditions. Based on a regression model, this results in predicting phase transformation temperatures, volume fractions, and formed phases. The early applications of artificial intelligence and machine learning in material sciences primarily focused on optimizing machining processes, evolving into modeling material design, processing, and characterization. [143] Another application of machine learning for polymeric materials is the prediction of fractional drug release from polymeric long-acting injectables, where crucial factors include drug erosion and diffusion from the polymeric matrix. [161]

5.3. Artificial Intelligence in material science

High entropy alloys (HEAs) have been recognized as promising materials for machine learning modeling due to their favorable mechanical performance and composition from five or more components. [143] Menou et al. [162] employed a genetic algorithm for optimization to model high entropy alloys, utilizing microscopic and elemental studies to design unique HEA properties such as hardness or density.

Gomes et al. [144] investigated sisal fiber reinforcement using a neural network-enhanced computer vision technique. Fiber segmentation was based on supervised training, where a supervisor defined the correct output for a given input. Based on images of fiber-reinforced composites, the resulting model was created to predict material properties, such as the modulus of elasticity or critical length of fiber. While some

algorithms like K-Means or Mask-RCNN did not provide consistent results, the U-Net algorithm exhibited precision levels up to 75%, presenting a promising alternative for material characterization.

Golkarnarenji et al. [163] explored machine learning-reinforced optimization of carbon fiber manufacturing regarding energy consumption. AI techniques, including artificial neural networks and support vector regression, were employed to optimize factors such as thermal stabilization or fiber density, ultimately reducing the energy required for fiber fabrication.

Malley et al. [160] applied artificial neural network deep learning techniques to construct machine learning models for predicting stress-strain curves based on strain corresponding to specific compositions of UV resin composite with magnetic iron oxide particles in different ratios. The machine learning predictions demonstrated consistency with experimental data, indicating significant potential for further development in advanced additive manufacturing. However, the model exhibited some limitations due to unintended artifacts resulting from interpolation. Overall, machine learning techniques showed promising results, suggesting potential scalability for further physical properties of materials.

Using computer vision recognition, Hrechuk et al. [125] investigated a U-Net-based AI model for predicting hole defects in flax-reinforced PLA composites. The study revealed that hole quality was related to material anisotropy, and the model helped detect drilling defects in less than 11 milliseconds.

Cui et al. [164] explored the ML techniques, such as random forest and artificial neural networks, to optimize natural fiber-reinforced polypropylene manufacturing. The model considered the influence of 3D printing parameters, such as extrusion flow rate, printing temperature, layer thickness, and printing speed, on the interfacial properties of the material. While the artificial neural network model demonstrated high accuracy for predicting material processing properties, the random forest model still provided acceptable accuracy with parameter importance.

Moore et al. [165] studied fracture growth using machine-learning approaches through random forests, decision trees, and artificial neural network algorithms. Based on input regarding the location and timing of material fracture, the created models allowed for predicting the size and dynamics of fractures, with further applicability to diverse conditions and materials.

.

II.Objectives and planning

1. Preamble

Naturally occurring fibers, such as wool, have grown a high interest in material science as easily reproducible, sustainable substances for multiple products. A considerable number of fibers, like the Merino sheep wool, is used in the textile industry. However, some species of sheep are valued for their milk and produce cheese but create undesired quality wool fibers. Therefore, wool fibers from such species are treated as byproducts that require strategies for their utilization.[94] Natural fibers serve as suitable alternative for conventional fibers due to environmental and economic perspectives. The area of usage of the fibers can be broadened by fiber modification.[166]

For a few decades, high and still increasing demand for polymeric thermoplastic materials has been observed. However, in recent years, limited petroleum sources have intensified research on biodegradable and bio-based materials. Biomaterials are especially favorable for short-term applications, where utilization of petroleum-based materials is not desired due to non-renewability and limited petroleum sources. In addition to renewable resources, biodegradable materials offer additional material disintegration in composting conditions, which ensures a material circular economy and a positive environmental aspect. [22,107,113]

One of the most popular and commonly used biodegradable polymers is polylactic acid (PLA). The material can be synthesized from simple sugars derived from biomass, lactic acid, rise, or corn. [167,168] PLA presents similar mechanical and thermal characteristics to PS or PET; nevertheless, PLA's biodegradability and biocompatibility allow it to be applied in food packaging and medical sectors. The PLA's high transparency and resistance to moisture and fats are also advantageous for such applications.[169] However, the spectrum of pure PLA applications is constrained due to its insufficient thermal stability, elongation at the break, and high brittleness. Several strategies, such as blending or copolymerization, are applied to overcome those disadvantages.[93,168,170,171]

Production of modern construction materials often requires reinforcement. Thermoplastic polymeric materials are widely modified with fibers, creating fiber-reinforced polymers (FRPs) with synthetic and naturally occurring fibers. Such modification allows the manufacturing novel materials with designed properties for prior specified application field.[134] Although reinforcement with fibers may be beneficial for polymeric materials, low fiber/matrix interaction often restricts the usage of FRPs. Hence, several strategies can be applied to overcome the negative aspects of FRP production and maintain the satisfactory mechanical properties of the material. An enhancement in adhesion of the components in FRPs can be accomplished mainly by surface treatment, functionalization, and incorporation of compatibilizer agents.[172,173]

FRP compatibility can be achieved with polymer grafting, plasticizers, or fiber surface modification. [174] Among the strategies in the study, fiber modification was considered with the simultaneous use of a bio-based plasticizer. Natural oils, like linseed oil, can be successfully applied for thermoplastic materials, which can be further enhanced with oil functionalization. Maleinized linseed oil (MLO), an example of modified vegetable oil, increases polymer chain mobility, providing a compatibility effect and increasing material flexibility. [168,171,175] Wool fibers can be modified on their surface, allowing better fiber/matrix contact. Through chemical and physical modification, wool

fiber can obtain new, multiple functional groups or better roughness, increasing the contact surface.

The outlined aspects of the study will be further and broader described in the objectives of the thesis.

2. GENERAL OBJECTIVE

The doctoral thesis's main objective is to use dairy industry-derived wool fibers to design and characterize biodegradable polymeric materials, specifically polylactic acid (PLA)/maleinized linseed oil (MLO) polymeric system, and the research of interactions within the fiber-reinforced polymeric composites and their influence on material properties.

Biomaterial selection in the study shows a desire for research on alternative material sources such as conventional non-bio-based and fossil-dependent fiber-reinforced composites.

Therefore, this work's achievement can aim to design and develop composite materials obtained from bio-based and biodegradable materials with simultaneous recovery of industrial bio-wastes.

3. SPECIFIC OBJECTIVES

The main objective has been clarified with specific objectives, which are:

- Determination of the methodology for wool fiber cleaning and purification
- Formulation of biodegradable fiber-reinforced polymers based on short wool fibers.
- Characterizing biodegradable fiber-reinforced polymers with unmodified wool concerning thermal, mechanical, and microstructural properties.
- Determination of reaction conditions for wool surface modification with chemical reagents.
- Evaluation of surface pre-treatment on surface modification of wool fibers.
- Characterizing biodegradable polymers reinforced with modified wool concerning thermal, mechanical, and microstructural properties.
- Data analytics for model training and prediction of material characteristics for different compositions.

4. Research plan

The first step of the production process of fiber-reinforced polymers requires selecting materials. As a result, a sustainable and biodegradable material was planned to be achieved. The following materials were selected for usage and evaluation in the research:

- Polylactic acid
- Linseed oil
- Maleinized linseed oil
- Wool fibers
- (3-(2-aminoethylamino)propyl)-trimethoxysilane (ATS)
- trimethoxy (2-(7-oxabicyclo (4.1.0)hept-3-yl) ethyl) silane (TES)
- tris(2-methoxyethoxy)(vinyl) silane (TVS)
- titanium (IV) (triethanolaminate)isopropoxide. (TTI)

In addition, complementary materials or chemicals were used to ease processing or create an environment for reaction, such as water, acetone, and others.

As a biodegradable plastic and a suitable replacement for conventional, widely utilized petrol-based plastics, polylactic acid was selected as a main component of investigated fiber-reinforced composites.

Research on fiber reinforcement in polylactic acid was carried out with the addition of a plasticizer, which allows easy processability of materials and uniform distribution of fiber in bioplastic. Considering the sustainability of plasticizer, bio-origin and compatibility with selected polymer matrix, the maleinized linseed oil was used for fiber-reinforced polymer processing.

A fiber reinforcement was selected as a dairy industry by-product, wool fiber, which fulfills the composite's bio-origin and sustainable aspect of the materials. Fiber surface modification was applied with chemical coupling agents and plasma treatment to enhance the interaction of the fiber and polymeric material.

Characteristics of each material used in the research were described in detail in the experimental part.

Fiber-reinforced polymers produced from the materials mentioned above were characterized concerning several aspects of material properties, among them:

- Thermal properties
  - Differential Scanning Calorimetry (DSC)
  - Thermogravimetric Analysis (TGA)

- Mechanical properties
  - Tensile properties
  - Flexural properties
  - Hardness by Shore
  - Impact Resistance by Charpy
  - Dynamic Mechanical Analysis (DMA)
  - Vicat Softening Temperature (VST)
  - Heat Deflection Temperature (HDT)

- Morphological properties
  - Scanning Electron Microscopy (SEM)

- Physical properties
  - Wettability
  - Color by CIELab

- Structural characterization
  - Fourier Transmittance Infrared Spectroscopy (FTIR)

The research plan was presented in schematic form in Figure *23*.

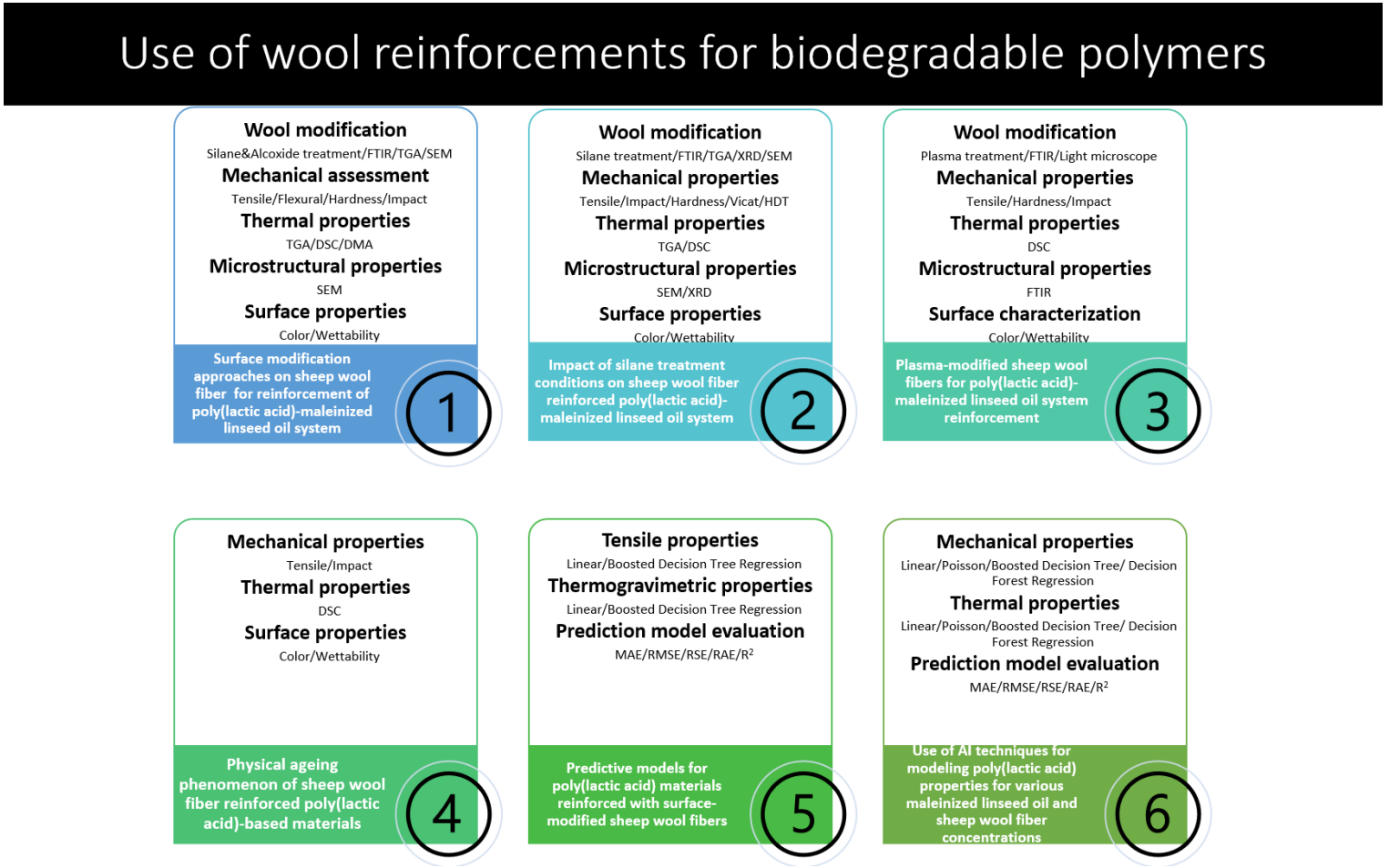

Figure 23 *Schema of research* plan

III. EXPERIMENTAL

1. Materials

The materials utilized in the present doctoral can be distinguished into wool fiber, linseed oil, and polylactic acid, and they are supported by materials used for their preprocessing or modification.

Among materials corresponding to the wool fibers preprocessing are distinguished:

- Sheep wool fibers obtained as a raw material from the cheese manufacturing industry in Basque Country (Spain)
- Sodium carbonate solution in distilled water with the pH=9 and molar concentration of 0.0189 mol/dm^3.
- Commercial detergent in the amount of 20ml for each 1dm^3 of wash solution.

For a surface modification of wool coupling agents were used following substances:

Table 1 Summary of coupling agents applied for modifications.

Name and chemical structure	Abbreviation	Provider	Technical specification
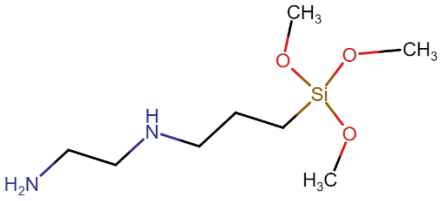 (3-(2-aminoethylamino)propyl)-trimethoxysilane	ATS	Sigma-Aldrich (Schnelldorf, Germany)	CAS: 1760-24-3 Formula: $C_8H_{22}N_2O_3Si$ Molecular weight: 222.36g/mol Appearance: Colorless liquid Density: 1.028g/cm^3 at 25°C Purity: over 98% Flashpoint: 136°C Titration with $HClO_4$: 96.5 – 103.5%
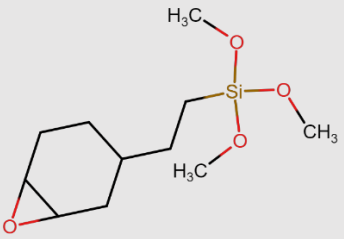 trimethoxy (2-(7-oxabicyclo (4.1.0)hept-3-yl) ethyl) silane	TES	Sigma-Aldrich (Schnelldorf, Germany)	CAS: 3388-04-3 Formula: C11H22O4Si Molecular weight: 246.38g/mol Appearance: Colorless liquid Density: 1.065 g/cm^3 at 25°C Purity: over 97.5% Flashpoint: 136°C Decomposition temperature: over 100°C
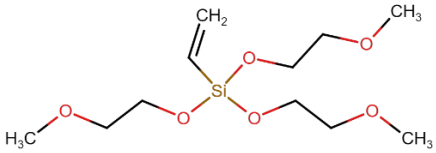 tris(2-methoxyethoxy)(vinyl) silane	TVS	Sigma-Aldrich (Schnelldorf, Germany)	CAS: 1067-53-4 Formula: C11H24O6Si Molecular weight: 280.39g/mol Appearance: dark-yellow liquid Density:1.034g/cm 3 at 25°C Purity: over 97.5% Flashpoint: 113°C
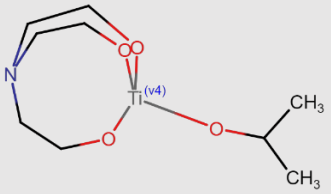 titanium (IV) (triethanolaminate)isopropoxide	TTI	Sigma-Aldrich (Schnelldorf, Germany)	CAS: 74665-17-1 Formula: C9H19NO4Ti Molecular weight: 253.12g/mol Appearance: yellow, viscous liquid Density: 1.087g/cm3 at 25°C Concentration: 80 wt.% in isopropanol

For plasma treatment, nitrogen, and atmospheric air.

MLO

Maleinized linseed oil (MLO) (CAS Nr: 68309-51-3), supplied by Vandeputte Group (Mouscron, Belgium) under a commercial name VEOMER LIN, is chemically modified linseed oil through the introduction of maleic anhydride into oil structure showing enhanced oil`s reactivity. Within the synthesis, maleic anhydride reacts with double bonds in the fatty acids of linseed oil. The chemical properties of MLO include a viscosity 10 dPa·s (at 25°C), an acid value of around 105-130 mg KOH/g, and a density of approximately 0,95-1,00 g/cm^3. A high acidic value regarding unmodified linseed oil (below 1mg KOH/g) corresponds to the presence of cyclic anhydride groups attached to linseed oil macromolecules.

PLA

Polylactic acid (PLA) (CAS Nr 9051-89-2) resin with commercial name Ingeo™ Biopolymer 6201D was brought by NatureWorks LLC (Minnetonka, USA). The PLA is synthesized through the polymerization of lactic acid obtained from the fermentation of renewable resources like corn starch. The chemical properties of the PLA include a molecular weight of approximately 147700 g/mol, density of 1,24 g/cm^3, melting point between 160-170°C and glass transition temperature between 55-60°C. The material exhibits good thermal stability and is suitable for high-temperature melt processing and extrusion techniques. The Ingeo 6201D has a semi-crystalline structure, providing favorable mechanical strength and flexibility. The PLA is characterized by tensile strength between 50-70 MPa, elongation at break 3-10%, and flexural strength between 3500-4000MPa.

2. Characterization techniques

2.1. Mechanical analysis

2.1.1. Tensile properties

The tensile properties were evaluated using the Ibertest ELIB-50-W universal test machine manufactured by Ibertest in Madrid, Spain. The Ibertest ELIB050-W is an electromechanical, universal testing machine designed for low-load applications, as the machine is designed for 50kN of maximum load capacity. Force resolution of 0,1N, measuring range between 1%-100%, and movement speed range of 0,001 to 500 mm/min make the machine suitable for precision material testing. For the tensile test, the machine attachment configuration requires several key components such as grips, extensometer, load cell, or crosshead. Specimens used for testing are held in place using mechanical or hydraulic grips, specifically body-over-wedge grips, which ensure proper

alignment and secure holding during the dynamic measurement. An extensometer is attached to the specimen for accurate elongation measurement, especially at low specimen strains. It also allows precise measurement for Young modulus calculations. A crosshead is a movable part of the universal testing machine that applies tensile force to the specimen. The appropriate load cell is selected between the grip and crosshead based on the maximum force measured during the test.

The machine is suitable for numerous material strength tests, among others, tensile or flexural properties, and complies with international standards such as ISO-527-1:2012, ISO-527-2:2012, ISO-527-3:1996 [176–178] and others where they correspond to the tensile characterization of materials. The Ibertest ELIB-50-W can be successfully applied for material quality control at certified laboratories, universities, or research centers, as it provides high precision and reliability of tests. Among materials that can be tested with the machine are polymers, metals, and composite materials.

The norm of tensile properties characterization is specified within ISO-527 international standards. The ISO 527-1:2012 [176] gives the universal principles for establishing the tensile characteristics of plastics and plastic composites. The standard covers determining the properties of materials with or without and defines dumbbell shape and a maximum thickness of 14mm of specimens used for standard testing. Further to sample shape, the standard defines test parameters such as temperature (23 ± 2°C), relative humidity (50 ± 10%), or minimal premeasurement conditioning time of 16 hours. The norm also specifies that high-precision extensometers, such as Ibertest ELIB-50-W, must accurately determine tensile properties, especially for fiber-reinforced polymers that typically show high stiffness. The recommended number of test specimens for anisotropic fiber-reinforced polymers should be at least 5. Concerning data interpretation, the tensile test results are usually presented in the easy-to-interpret stress-strain curve. That allows us to compare specimens and formulations with each other favorably. A standard course of the stress-strain curves has been presented in Figure 24. Additionally, if any specimens exhibit any failure, such as fiber breakage or matrix cracking, it should be noted in the test results.

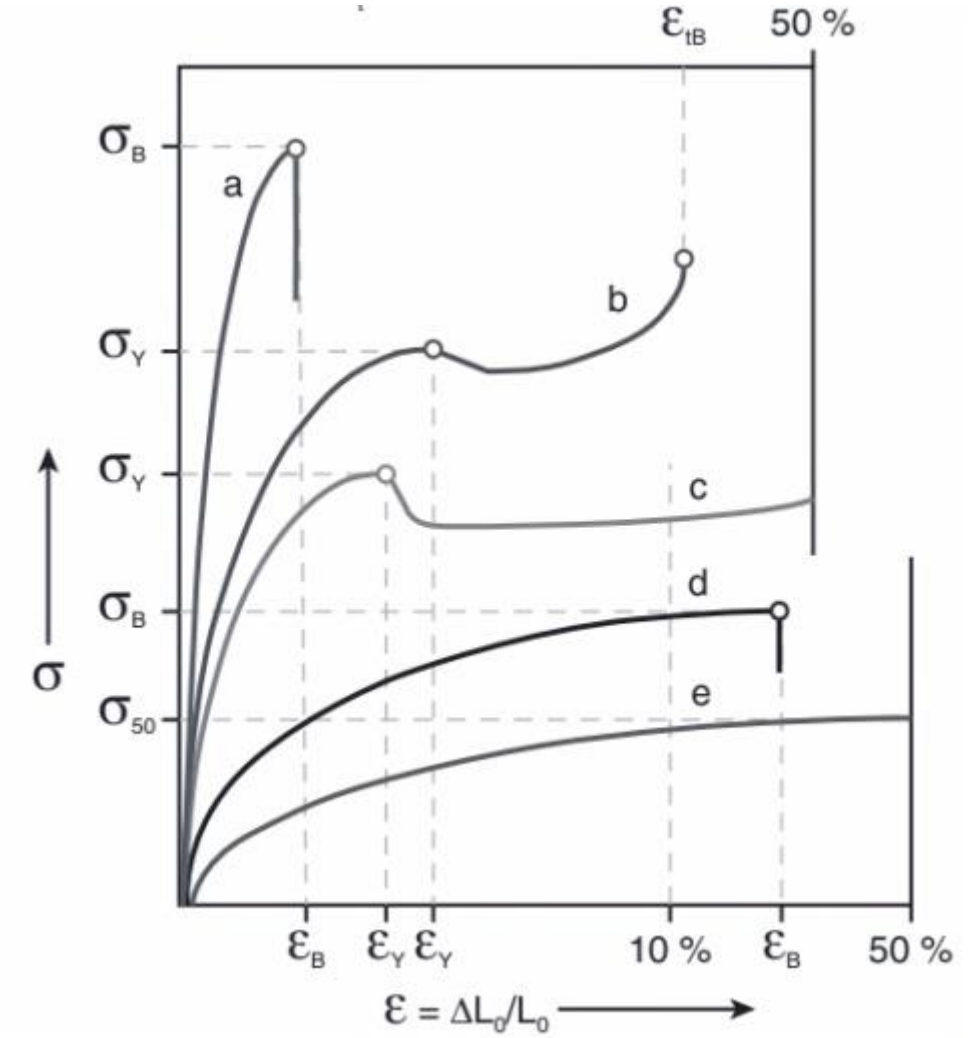

Figure 24 Typical stress-strain curves for polymers: a) brittle, b) ductile, c) stretched plastic, d,e) plasticized plastic, where δ_B - stress at break, δ_Y – yield stress, ε_B – strain at break, ε_Y – yield strain. [176,179]

As the ISO 527-1:2012 [176] has focused on general standards for determining the tensile characteristics of plastics and their composites and serves as a foundational standard, the ISO 527-2:2012 [177] focuses on tensile properties of molding and extrusion plastics. It can be applied to rigid and semi-rigid polymer materials, including compounds filled with short fibers. Due to the norm, test specimens can be either directly molded into the required dimensions or compressed molded and cut afterward to the dimensions. The standard references standards covering specimen preparation for thermoplastic material using specific methods such as compression molding (ISO 293) or injection molding (ISO 294-1). Although a supplementary standard ISO 527-2:1996[176] exists for tensile properties, it specifies test procedures for plastic composite plates or films below 1mm. As for tensile properties in the studies, prepared specimens exceeded 1mm thickness; the norm is not considered in detail.

2.1.2. Flexural properties

Similarly to the tensile properties of evaluated materials, the Ibertest ELIB-50-W universal test machine was used to determine flexural properties in Madrid, Spain. However, compared to tensile measurement, a 3-point bending machine attachment is used for flexural properties. Such test arrangement comprises two parallel lower supports and one centrally positioned upper support; for the measurement, specimens are placed horizontally on the two lower supports, where the upper loading anvil applies force to the center of the specimens, creating a specimen bending, as presented in Figure 25.

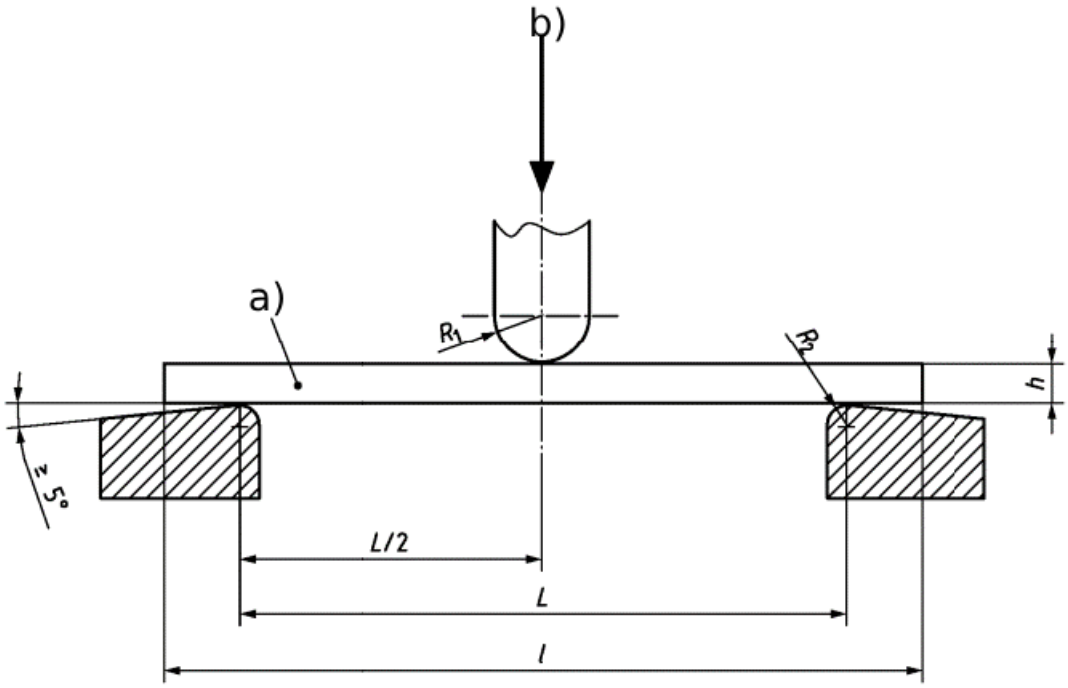

Figure 25 Principal of flexural bending of specimen [179,180]

Prior measurement specimens must be prepared according to standard requirements like tensile test, where temperature and humidity must be controlled, and specimens must be conditioned for minimum 16 hours. Regular test conditions for flexural measurement are temperature at 23 ± 2°C and relative humidity at 50 ± 10%.

The procedure and conditions of flexural measurement are described in international standard ISO 178:2010 [180]. The recommended dimensions for thermoplastic materials with molded specimens are length of l=80mm, thickness h=4mm, and width of 10mm. Similarly, tensile test specimens can be molded directly or cut from molded parts or plates, as defined specifically in ISO 293 or ISO 294-1, to ensure that test specimens are produced reproducible. The recommended distance between lower supports for such specimens should equal 64mm. Likewise, for the tensile test, the flexural measurement between the above-described machine attachment and crosshead is included in the load cell, which measures the load put to the specimen. However, the deflection of a specimen is measured by crosshead displacement. As a result, flexural

stress, strain, and modulus are calculated based on measured force, deflection, and specimen dimension.

2.1.3. Hardness by Shore

The Shore Durometer Model 673-D, produced by Instruments J. Bot S.A. in Barcelona, Spain, is a precision instrument designed for measuring the hardness of materials. On the Shore D scale, it is suitable for hard materials such as rubber or polymeric. The Shore D scale allows for measuring medium to rigid materials, ranging from 0 to 100 points, with an accuracy of 1 point. The durometer uses a conical indenter with an angle of 30° designed to penetrate hard materials effectively. Figure 26 shows the indenter for hard materials measurement with the Shore D characteristics. Consistency and repeatability of the measurement are ensured by 50N force, which is applied by the indenter on a specimen.

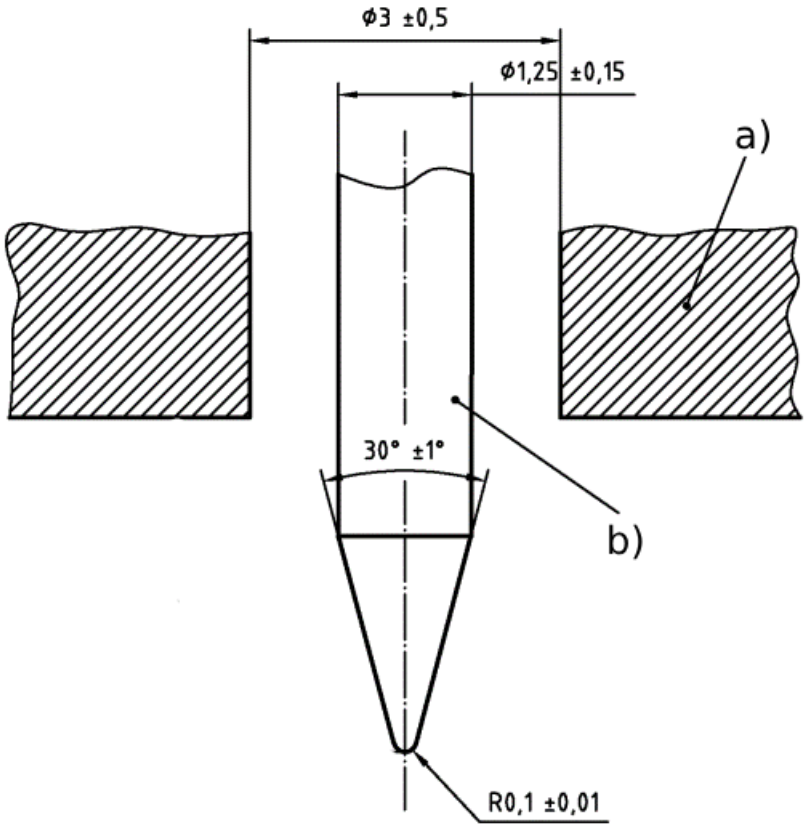

Figure 26 Conical indenter for Shore D scale with a) support material, b) indenter.[181]

The use of a durometer for determining the indentation hardness of plastics is specified by the international standard ISO 868:2003. [181] Hardness is the indentation depth made by the durometer`s indenter under a specified force. Two hardness scales are distinguished contingent on the tested material: Shore A, utilized for softer materials like soft plastics or rubber; and Shore D, utilized for more rigid materials like hard plastics and ebonite. The A and D methods also differ by their indenter, where Shore A

durometers use a truncated cone-shaped indenter, and Shore D durometers use a sharper, conical indenter with a smaller tip radius. Furthermore, a lower force (1kg) is applied on the specimen for Shore A durometers than for Shore D durometers (5kg).

Prior to the measurement, the polymer specimen required proper preparation and conditioning. The material sample should be prepared to ensure a uniform thickness and surface finish. For accurate measurements, specimen thickness should be at least 6mm, whereas thinner samples should be reinforced with additional layers of the same material to comply with the required thickness. The surface of the specimen should be flat and defect-free to mitigate the influence of irregularities on the measurement. The measurement samples must be conditioned for at least 24 hours at a standard laboratory temperature of 23 ± 2°C and relative humidity of 50 ± 5%.

2.1.4. Impact by Charpy

The Charpy impact resistance equipment, manufactured by Metrotec and located in San Sebastian, Spain, assessed the materials' impact properties. The machine's primary function is to assess the impact resistance of materials based on their capability to absorb energy before the fracture of materials. Therefore, the measurement provides insights into material toughness. From an operation perspective, the testing procedure involves striking a notched or unnotched specimen with a pendulum. The pendulum is freely swung from a predetermined height, and upon impact, energy is measured and absorbed by the specimen during fracture. As a result, the machine provides a direct readout of the absorbed energy, typically in kilojoules per square meter (kJ/m^2).

According to the international standard ISO 179-1 [182], different test parameters are based on material type, specimen type, and notch type. Usually, to test plastics, a pendulum of known energy of 1 or 6J is considered for striking the specimen. Pendulum selection should be based on no expected specimen`s fracture, which should occur with an energy between 10% and 80% of the pendulum`s capacity. Considering specimen placement, it can be placed with either narrow or wide sides. Furthermore, impact resistance is considered two types of notched and unnotched specimens. Figure 27 shows the principle for measuring wide side unnotched samples, as all study samples were evaluated with this specific method type.

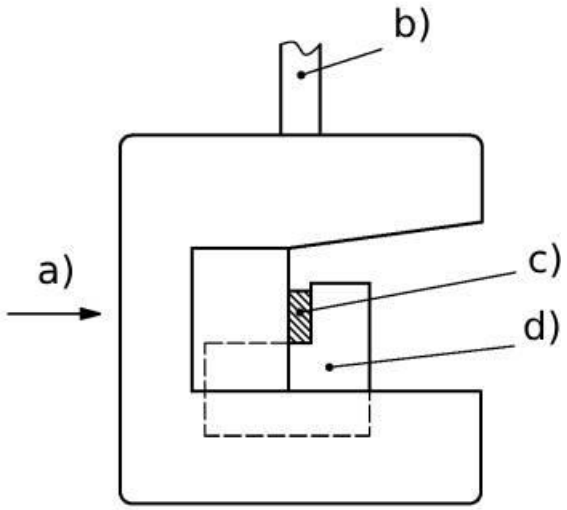

Figure 27 The principle of Charpy impact measurement a) direction of impact, b) pendulum, c) specimen, d) specimens holder [182]

Considering test specimen dimensions, ISO 179-1 specifies for thermoplastic materials length l=80mm±2mm, width b=10mm±0.2mm, and thickness h=4mm±0.2mm. A specimen with the above-specified dimensions, without a notch and with wide side placement, is presented in Figure 28. Further to notched modifications of test specimens, two notch types are distinguished: V-shaped and U-shaped notches. The V-notches create a stress concentration point that facilitates the fracture of the specimens. Such V-notch is characterized by a 45° angle and depth of 2mm with a tip radius of 0.25mm. On the other hand, the U-notches are used for materials that may not fracture easily with a V-notch. Such U-notches are characterized by a centric cut-in specimen with a 1mm radius and 2mm depth.

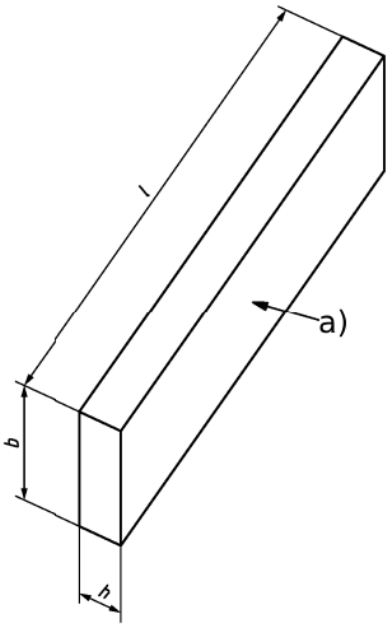

Figure 28 Unnotched specimen for Charpy impact resistance a) direction of impact [182]

2.2. Thermal properties

2.2.1. TGA

The Linseis TGA 100 is a thermogravimetric analyzer manufactured by Linseins GmbH in Selb, Germany. The equipment is designed to operate from room temperature up to 1100°C, making it suitable for characterizing plastic composites and other material groups, such as certain metals or ceramics. Concerning sample capacity, the TGA 1000 can handle a sample mass and crucible up to 5g with a measurement resolution of 0.1µg. However, the heating and cooling rates offered by the device range between 0.001 and 250°C/min. Further to the controlled heating rate, the equipment operates in various gas atmospheres, including inert, oxygen, nitrogen, or vacuum.

Thermogravimetric analysis (TGA) is an analytical method for measuring a sample's mass change as a function of time or temperature in a specific atmosphere. Such a method can provide insight into material composition and thermal stability and monitor material weight changes in specific thermal conditions. The sample is placed in a crucible and heated in a controlled manner in the TGA furnace. The crucible with a sample is placed on a highly sensitive microbalance, and its mass is continuously controlled with changes in time or temperature. During the measurement, several thermal events can be observed, such as evaporation of volatile components, decomposition or degradation of the material, and others. Such thermal events can be observed due to the mass loss of a sample, which is noted as a decrease in the weight signal. At the end of the analysis, the remaining mass of the sample is named either a residual mass or an ash content.

As an outcome of the measurement, two curves are provided: the thermogravimetric curve and its derivative curve. The thermogravimetric (TG) curve shows the plot mass loss or mass gain as a function of time or temperature. Based on its shape, this curve allows for the determination of thermal stability and assists with assessing material composition. On the other hand, the TG curve's first derivative, as a function of time or temperature, provides insights into maximum rates of weight change, helping identify and quantify thermal events.

The international standard ISO 11358-1:2022 [183] specifies the general principles for the thermogravimetry of polymers. The samples can occur in various forms, including pellets, granules, powders, or fabricated shapes that are reduced to appropriate size and fit into the crucible. The typical size of the material sample ranges between 5mg to 20mg for accurate measurement. Prior to the measurement, samples should be conditioned for at least 24 hours in laboratory conditions at a temperature of 23°C±2°C and relative humidity of 50%±5%. The crucibles used for analysis should be made of materials that are inert to the polymeric sample and in the test temperature range. Commonly, polymeric materials are used in platinum or ceramic crucibles. The analysis should be performed over a temperature range between room temperature up to 600°C or higher, depending on the tested material. The heating rate is commonly set between 1°C/min and 20°C/min; however, it should be explicitly considered for tested material to achieve the desired resolution of thermal events. Within the test atmosphere, it should be specified whether it is an inert or oxidizing atmosphere and whether vacuum conditions are applicable for the measurement. To ensure repeatability and reliability, at

least three specimens should be tested under the same conditions. Additionally, an equipment calibration should be performed for specified heating and atmospheric conditions to ensure accurate temperature and weight measurements.

2.2.2. DSC

The Mettler DSC 821e is a differential scanning calorimeter (DSC) manufactured by Mettler Toledo in Toledo, Spain. The equipment can operate in temperature ranges from 150°C to 500°C, with heating and cooling ranges between 0.02°C/min and 200°C/min. The machine is equipped with a heat flux sensor that detects differences in heat flow between the sample and reference. The sensor is designed to detect small thermal events with high sensitivity, which allows precise heat capacity and enthalpy changes to be measured. Moreover, the sensor presents a rapid response to temperature changes, which is critical for capturing fast thermal events during the measurement. Towards specimen, the device is designed to measure samples between 0.1mg and 50mg across different material types. The system can operate under various gas atmospheres and pressures during the measurement. Among the accessories for the DSC 821e can be distinguished Intracooler, which allows for extending the lower temperature limit and rapid cooling after the heating cycle.

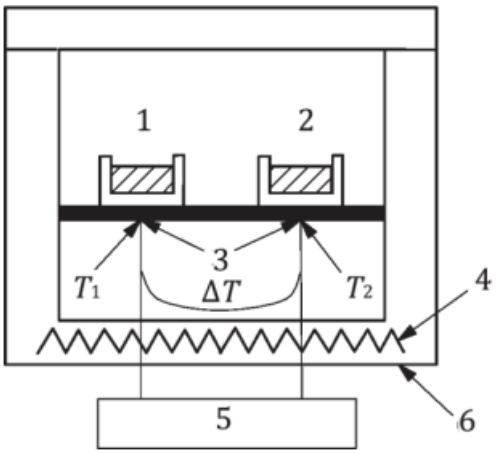

Figure 29 Principle of the DSC measurement: 1) test sample, 2) reference sample, 3) heat flux sensor, 4) heating source, 5) temperature measuring circuit, 6) stove[184]

As shown in Figure 29, the DSC measurement principle focuses on the difference in heat flow between a sample and a reference material as they are heated, cooled, or held at a constant temperature. This allows for observation of thermal events, as the instrument records the energy required to maintain the exact temperature of the sample and reference. Change in the heat flow detected by DSC is caused by thermal transitions, like melting, of the sample. The temperature measuring circuit continuously monitors the temperature of the samples and heating source, guaranteeing accurate control of the measuring system.

General principles for differential scanning calorimetry (DSC) assessment of plastics are described in ISO 11357-1[184] international standard. However, additional guidelines for result analysis and properties determination for plastics serve a series of ISO 11357, where several were applied in the presented studies' results. The ISO 11357-2[185] is a specified method for determining polymers' glass transition temperature (Tg) using DSC. The Tg is identified by observing the change in heat capacity as the sample transitions from a glassy state to a rubbery state. A change in the slope of the heat flow curve characterizes this. However, ISO 11357-3 [186] specifies a method for determining the temperatures and enthalpies of melting and crystallization of crystalline or partially crystalline polymers. The melting temperature (Tm) and crystallization temperature (Tc) are determined by analyzing the endothermic and exothermic peaks in the DSC curve, which corresponds to melting and crystallization thermal events.

Towards the measurement itself, first, a sample and measurement procedure require preparation as specified in ISO 11357. A recommended size of the sample ranges typically between 5mg and 20mg to ensure enough sample for measurement and minimize any potential thermal effects from crucibles. The measurement of polymers is conducted in aluminum-sealed pans. As for the measurement procedure, a temperature range must be specified after carefully considering the temperatures at which thermal events should occur. Furthermore, both heating and cooling rates must be specified, together with the atmospheric conditions of the measurement. For defined measurement conditions, instrument calibration is recommended to ensure accurate temperature and heat flow.

2.2.3. DMA

The AR G2 Rheometer is a high-performance instrument designed for advanced rheological measurement manufactured by TA Instruments in New Castle, Delaware, USA. The device is utilized for flow analysis and the deformation behavior of polymeric materials. As the instrument supports various measurement modes such as oscillatory, rotational, and creep tests, it provides viscoelastic properties of materials. Furthermore, the instrument allows measurement in controlled thermal conditions, providing insights into temperature-dependent material behavior.

The Dynamic Mechanical Analysis (DMA) measurement general principles for determining properties of rigid plastics are described in the ISO 6721-1 international standard, whereas the ISO 6721 series describes methods for determining the dynamic mechanical properties of plastics. [187,188] The standard ISO 6721-1 focuses on the DMA subjecting a material oscillatory stress or strain and measuring its response to an applied force. This technique evaluates mechanical properties like storage modulus, loss modulus, and damping factor (tan δ). Depending on the sample mounting, the standard recognizes tensile and flexural yield results, which may not be directly compared. The tensile vibrations produce stress across the specimen`s thickness, whereas flexural tests show surface stress on a specimen.

The ISO 6721-4 part specifies a method for determining plastics' dynamic mechanical properties, providing insights into thermomechanical performance, glass transition temperature (Tg), and damping behavior. This method is commonly applied to illustrate the viscoelastic properties of thermoplastic resins or composite systems.

Towards measurement principle, rectangular specimens are subjected to tensile vibration, and the storage modulus (E'), loss modulus (E"), complex modulus (E*), and loss factor (tan δ) are measured in respect to changing temperature. In the measurement setup, rectangular specimens of polymeric material are clamped at both ends to ensure that they are held securely during the test. The measurement typically covers frequencies up to 100 Hz and is performed in a temperature range covering the examined material's thermal effects. As previously described, several material properties can be derived from the measurement in specified range of temperatures. Storage Modulus (E') represents the elastic response of the material, indicating how much energy is stored during deformation. Loss Modulus (E") represents the viscous response, indicating how much energy is thrown away as heat during deformation. "Complex Modulus" (E*), as a combination of E' and E" provides a comprehensive view of the material`s viscoelastic behavior. Finally, the Loss Factor (tan δ) is a relation of loss modulus to storage modulus, providing insights into the damping characteristics of the material.

2.2.4. Heat Deflection Temperature (HDT)

The DEFLEX 687-A2 is an HDT testing station designed to measure the heat deflection temperature of plastics. It was manufactured by Metrotec S.A. from San Sebastian, Spain. The equipment complies with ISO 75 [189] international standards for HDT and allows testing at conditions specified in the norm. The measurement specimens must fulfill specific dimensions varying whether the test is performed edgewise or flatwise. Additionally, to ensure consistency of the measurement, the material specimen must be defect-free. Towards the measurement, the HDT load is determined on the specimen, and, as a result, the temperature where deflection is reached is recorded.

The method for determining the Heat Deflection Temperature of plastics with applied load is specified in the ISO 75 industrial norms. [189–191]. The standard is crucial for evaluating material performance when exposed to elevated temperatures. The HDT test assesses at which temperature material deforms under a specified load. Method B was selected for the measurement in the current study, where 0.45 MPa load was applied to a specimen; for the flatwise testing, were prepared specimens with 80 mm length, 10 mm width, and 4 mm thickness. In the test, the specimen is placed in a three-point bending apparatus. The HDT temperature is obtained for flatwise testing once the specimen deflects 0.32 mm upon the load. The test helps define the material's ability to maintain its shape under performance and thermal stresses.

2.2.5. Vicat softening temperature

Similarly to the HDT, the DEFLEX 687-A2 testing station was used for Vicat softening temperature, manufactured by Metrotec S.A. from San Sebastian, Spain. The machine allows for testing according to the international standard for VST, the ISO 306. [192] For the VST measurement, several conditions concerning load (10 N or 50 N) and heating rate (50°C/h or 120°C/h) can be selected. Similarly to the HDT measurement, the specimen must fulfill a specific thickness diameter between 3 mm and 6.5 mm and a

minimum length and width of 10 mm and be defect-free; the test results in temperature when the needle penetrates a specified depth.

Vicat softening temperature (VST) can be measured in various load and heating rate conditions. Method B50 was applied in the current study, indicating a load of 50 N and a heating rate of 50°C/h. Prior to the measurement, according to the ISO 306 [192] standard, the specimen needs to fulfill specific dimensions, especially in thickness. The standard allows up to three layers of stacked material if a single layer does not fulfill a 3 mm thickness. The prepared specimen is placed in the apparatus, typically with an ambient temperature of 23 °C, and the flat needle with a 1 mm^2 edge is placed on the specimen. The Vicat Softening Temperature is recorded once the needle reaches 1 mm depth into the specimen. The method is designed for thermoplastic materials known to soften in elevated temperatures.

2.3. Microstructural properties

2.3.1. FTIR

Fourier Transform Infrared (FTIR) spectroscopy was conducted with the Perkin Elmer BX Spectrometer, which was manufactured in Beaconsfield, United Kingdom, and was coupled with a Pike MIRacle™ ATR accessory equipment for the FTIR-ATR measurement. The Ekmer BX spectrometer is designed for infrared spectroscopy for solid and liquid materials and gas testing. The Fourier Transform technology allows for obtaining high-resolution spectra for detailed chemical analysis. The Pike MIRacle™ accessory is designed for FTIR spectrometers, allowing simplified sample analysis due to high-refractive-index ATR crystal, typically made from diamond, zinc selenide, or germanium. Such attenuated total reflectance (ATR) crystal facilitates effective infrared light interaction with the sample.

During the measurement, the sample is located on the ATR crystal, and the sample does not require prior special preparation. The ATR technique involves total internal reflection of infrared light within the ATR crystal. A passing wave penetrates a short distance into the sample, causing molecular vibrations, which result in the absorption of specific wavelengths of infrared light. The resulting spectrum represents the molecular “fingerprint” of the sample, enabling the identification of the chemical composition of the tested material. The spectrum consists of peaks that correspond to vibrations between atoms, showing chemical composition in a qualitative way, as well as the intensity of the peaks showing quantitative analysis of tested material. Although principles for FTIR measurements are outlined in several international standards, the international standards are usually not directly related to FTIR measurement but describe FTIR as a supplementary method in specific applications or for specific material characterization.

2.3.2. SEM

The Emitech SC7620 Sputter Mod Coater is an instrument manufactured by Quorum Technologies that is designed for the deposition of thin conductive coatings. The coatings can be applied to various materials, such as plastics, to enhance surface conductivity during electron microscopy analysis. The equipment utilizes a sputtering method to deposit thin films of metals onto the surface of samples. The layer is created by bombarding a target metal with high-energy ions, which eject atoms and deposit them on the sample surface. The equipment allows for covering samples of various sizes and shapes, making it versatile for the analysis of fractures in polymeric materials.

The Phenom SEM electron microscope is a tabletop laboratory microscope designed by Thermo Fisher Scientific, formerly FEI Company, in Eindhoven, the Netherlands. The equipment offers high image resolution down to 14 nm, making it appropriate for various applications in material science, biology, or nanotechnology. Among the machine applications can be distinguished analysis of material surface morphology and composition, investigation of nanostructures, and quality assessment of materials after manufacturing processes. The Phenom SEM can produce images quickly, making it suitable for research and quality control.

The Scanning Electron Microscopy measurement involves a focused beam of electrons generated from an electron gun focused on an evaluated sample. Before the measurement, materials such as non-conductive polymers are coated with gold conductive layer to ensure proper surface conductivity and improve image quality. Furthermore, as a sample is placed in a holder, a high vacuum environment is prepared to mitigate the electron scattering by air molecules and achieve high-resolution images. As a focused electron beam strikes the sample, due to the electron beam impact, the secondary electrons are ejected from the material surface, forming an image of the surface. As secondary electrons create an micrograph of the surface, the intensity of the image corresponds to the number of electrons collected. The sample's topography can also be obtained based on backscattered, primary electrons reflected from the material surface.

2.3.3. XRD

The Bruker AXS D5005 X-ray diffraction (XRD) system, used to analyze structural properties of materials, was manufactured by Bruker AXS from Karlsruhe, Germany. The equipment is widely used to determine the crystalline structures of materials and identify the sample's phases. The D5005 has a high-intensity X-ray tube with copper (Cu) Kα as a radiation source, a goniometer for precise sample positioning, and an X-ray radiation detector.

Towards the measurement, X-rays are generated as electrons are accelerated into the copper target emitting radiation. The radiation is directed into the sample and prepared in solid or powder form for polymeric composite materials. The crystalline phase of the material scatters the X-rays at different angles and intensities, providing insights into the crystalline characteristics of the sample. The characteristics of crystal structure can be derived based on Bragg`s Law, which is described in Equation 5:

$$n\lambda = 2d \sin(\theta)$$

Equation 5 Bragg`s Law as a principle for XRD measurement, where n - number, λ – wavelength of X-rays, d – distance between crystal planes, θ – angle of occurrence.

Measurement data is collected over a range of goniometer rotation angles and selected based on the expected crystal structure occurrence. The resulting diffraction pattern is recorded as a function of angle (2θ).

2.4. Surface properties

2.4.1. Wettability

The EasyDrop-FM140 optical goniometer measures the contact angle on solid surfaces. Krüss GmbH manufactured it in Hamburg, Germany. The contact angle measurement provides information about material wettability and its surface energy. The goniometer has a high-resolution camera, the Drop Shape Analysis tailored software, and a precise dosing system. The camera captures images of the liquid droplet on the solid surface of the tested material. Using the DSA software, the shape of the liquid droplet is measured with a coupled goniometer, and the contact angle is determined. However, the precise dosing system allows for control droplet deposition on a sample surface, ensuring repeatable measurement conditions. By determining surface energy, the optical goniometer can provide valuable insights for material adhesion or coating and for the monitory consistency of surface properties in manufacturing.

Towards the wettability measurement, the material testing surface of the sample needs to be cleaned from contaminants that may impact the measurement result. Subsequently, a controlled volume of liquid, usually a distilled water droplet, is gently placed on the sample to avoid distortion. Directly after droplet placement, the camera captures images of the droplet on the surface, containing both a horizontal view of the sample surface and the shape of the placed droplet. Based on the image, the Drop Shape Analysis software determines the contact angle, defined as the tangent to the liquid droplet and the solid surface as the contact point. Additionally, the contact angle can be calculated based on the geometry of the droplet. Finally, the character of the surface is assessed based on the contact angle value, where a low contact angle indicates high wettability due to a hydrophilic surface, or a high contact angle indicates low wettability corresponding to a hydrophobic surface. The measurement is conducted multiple times for a single sample to ensure the reproducibility and reliability of results, and the average contact angle is calculated.

2.4.2. Color

The ColorFlex-Diff2 458/08 colorimeter is an instrument designed to measure the color of various materials using the CIELab color space. It is manufactured by HunterLab and is located in Reston, VA, USA. The colorimeter utilizes a 45°/0° geometry, miming how the human eye perceives color, providing accurate and consistent color measurement. The sample is illuminated at a 45° angle, and the reflectance is measured at 0°. Further to the color space, the CIELab method measures color based on three indicators for lightness (L*), red-green color intensity (a*), and yellow-blue color intensity (b*). Results provided by the ColorFlex-Diff2 allow for the quantification and comparison of color differences between tested samples.

Before the measurement, samples are cleaned to ensure accuracy and remove surface contaminants or irregularities. From the ColorFlex-Diff2 equipment side, it is recommended that the light source be warmed up and stabilized for around 30 minutes before measurement and calibration are performed. The calibration consists of a white tile as a reference for top-of-scale color measurement and a black tile for a bottom-of-scale reference. Additionally, a reference green tile is assessed as a diagnostic tool for instrument performance over time. The sample is illuminated by a light source at a specified angle and reflected light from the sample is measured by a colorimeter. The spectral reflectance data are distributed into tristimulus X, Y, and Z values, which are converted to CIELab coordinates based on formulas specified in Equation 6:

$$L^* = 116 \sqrt[3]{\frac{Y}{Y_n}} - 16$$

$$a^* = 500 \left[\sqrt[3]{\frac{X}{X_n}} - \sqrt[3]{\frac{Y}{Y_n}} \right]$$

$$b^* = 200 \left[\sqrt[3]{\frac{Y}{Y_n}} - \sqrt[3]{\frac{Z}{Z_n}} \right]$$

Equation 6 CIELab coordination calculations, where X_n, Y_n, and Z_n are the tristimulus values of the reference white tile.

As a result, the sample containing CIELab coordinates' characteristics defines the measured materials' color. The lightness value (L*) ranges from 0 for black color to 100, indicating white, where the negative a* value specifies green color and the positive a* value refers to red. Further, the negative b* value indicates a blue color, whereas positive b* corresponds to yellow. Color and lightness visual presentation are shown in Figure 30:

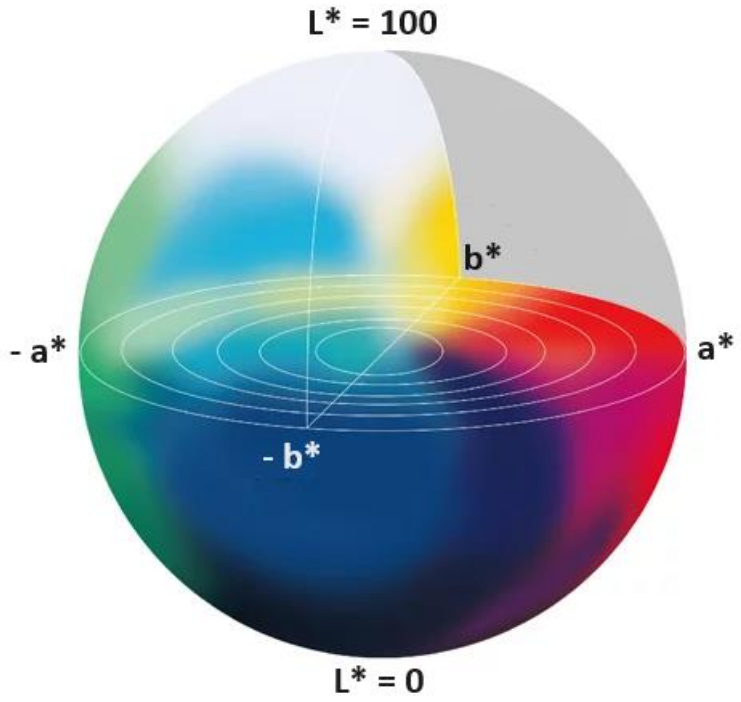

Figure 30 CIELab color presentation

2.5. Computational techniques

2.5.1. Azure Machine Learning studio

Azure Machine Learning Studio is an integrated development environment for constructing and optimizing Machine Learning workflows in Microsoft Azure Cloud, Redmond, WA, USA. The platform allows data-based predictive analytics solutions to be built, tested, and deployed. The Azure ML Studio solution does not require coding knowledge, providing a visual No/Low Code interface. Within the workspace are managed experiments that allow building, training, and deploying machine learning models. The platform allows the publishing trained models as web services and offers automated machine learning capabilities based on specified parameters, i.e., the coefficient of determination (R^2).

To create machine learning models, first, compute and storage resources need to be created in the Microsoft Azure cloud. Once Azure ML Workspace is established, the labeled training dataset can be uploaded for further processing. In the model training pipeline for a suitable regression model configuration algorithm, the training dataset and label column must be selected as prepared data for model training, which can be further evaluated with model performance metrics. Once a model with satisfying performance is

trained, such a model can be deployed by creating an inference pipeline. Such a pipeline requires a dataset used for predictions, which is transformed with a prior trained model and scored accordingly. The inference pipeline can be further deployed as a web service.

2.5.2. Google Colaboratory

Google Colaboratory is a cloud-based tool that enables Python code writing and execution. Google, Mountain View, CA, USA developed the tool. The Colaboratory provides computational and GPU resources without the need for local installation and configuration, enabling the use of Python code for machine learning and data analysis. Its versatile features include the tool's ability to collaborate with multiple users, support various data types, and use Python libraries. Colab notebooks support combinations of executable Python code, text, chart, or images, allowing comprehensive documentation and data analysis presentation. However, for access to libraries, the tool supports popular Python libraries within the environment for data science and machine learning, such as Sklean, PyTorch, NumPy, or Pandas.

3. Proceedings and methodology

3.1. Surface modification approaches on sheep wool fiber for reinforcement of poly(lactic acid)-maleinized linseed oil system

3.1.1. Materials

Poly(lactic acid) (PLA) Ingeo Biopolymer 6201D, sourced from NatureWorks LLC (Minnetonka, Minnesota, USA), was applied in the production of fiber-reinforced polymer (FRP) composites. This commercial-grade PLA contains 2% D-lactic acid, with a density of 1.24 g/cm³ and a melt flow index (MFI) measured at 210 °C ranging from 15 to 30 g/10 min. The material has a molecular weight of approximately 70,000 g/mol. [193] Maleinized linseed oil (MLO), commercially known as Veomer Lin, was incorporated into the formulation and sourced from Vendeputte (Mouscron, Belgium). It possesses a viscosity of 10 dPa·s at 20 °C and an acid value ranging from 105 to 130 mg KOH/g. Wool fibers, sourced from the Basque Country (Spain), were used as the raw material. Prior to use, the wool underwent a multistep cleaning and preparation process. The fibers were washed in a solution containing 0.2 wt% sodium carbonate and 2 wt% of a commercial detergent to remove surface impurities. The cleaned wool fibers were then aligned uniformly and trimmed to 1 cm, getting a length-to-diameter (L/D) ratio of approximately 200.

Surface modification was performed using coupling agents obtained from Sigma-Aldrich (Schnelldorf, Germany), including (3-(2-aminoethylamino)propyl)-trimethoxysilane (ATS), trimethoxy(2-(7-oxabicyclo[4.1.0]hept-3-yl)ethyl)silane (TES), tris(2-methoxyethoxy)(vinyl)silane (TVS), and titanium(IV) (triethanolaminate) isopropoxide (TTI). These silanes and alkoxides were applied to improve the interfacial adhesion between the polymer matrix and the fibers, facilitating enhanced load transfer and thus improving the mechanical properties of the composite, particularly for inorganic fibers. [22]. The chemical structure of all coupling agents is shown in Figure 31:

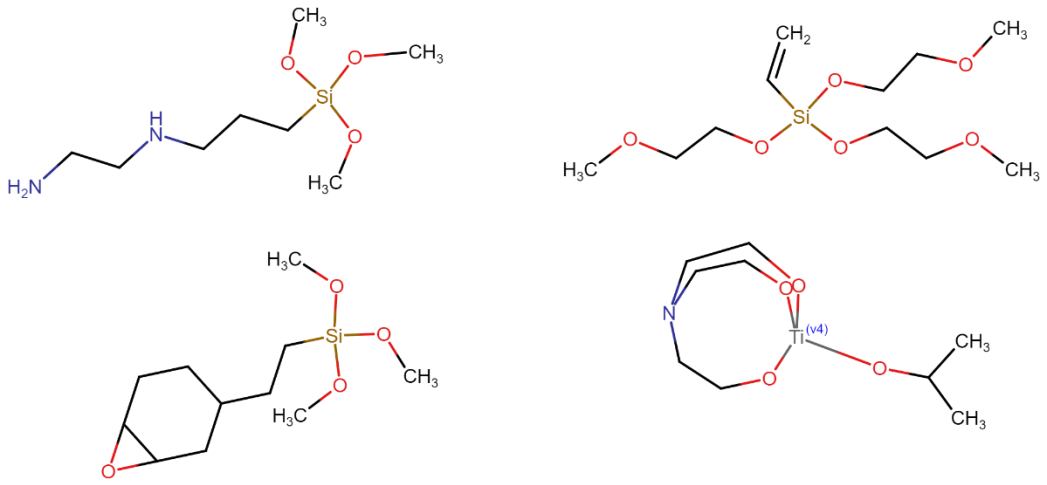

Figure 31 Chemical structures of applied agents: (ATS) (3-(2-aminoethylamino)propyl)-trimethoxysilane; (TES) trimethoxy (2-(7-oxabicyclo(4.1.0)hept-3-yl)ethyl]silane; (TVS) tris(2-methoxyethoxy)(vinyl) silane; and (TTI) titanium (IV) (triethanolaminate)isopropoxide.

3.1.2. Material processing

3.1.2.1. Wool fiber

The study has covered an examination of five distinct types of wool. Firstly, the unmodified wool was selected as a reference reinforcement raw material for the assessment. Further, it was followed by the wool fibers altered with four different coupling agents, prior named ATS, TES, TVS, and TTI, with a concentration of 1phr of each coupling agent about the weight of the wool fibers. For surface modification, 1 phr of the coupling agent was dissolved in a pre-prepared water/acetone solution (50:50 wt%) and stirred for 30 minutes. The use of this water/acetone mixture is preferred because the presence of ethanol may cause the coupling agent to detach. In contrast, acetone is chemically inert in the reaction but effectively dissolves the coupling agent. [194] Next, 100 phr of wool fibers was added to the solution and stirred for one hour at an ambient temperature of 23°C. The treated fibers were then dried at 50°C for 48 hours to ensure all solvents were fully evaporated. A representative chemical reaction diagram for the fiber modification process is provided in Figure 32

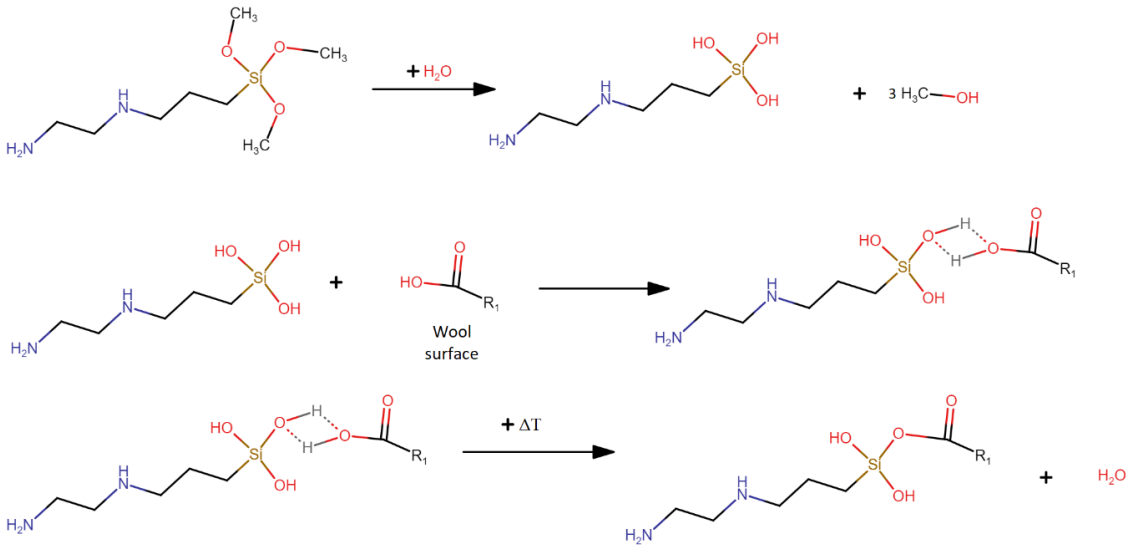

Figure 32 A reaction of wool with coupling with (3-(2-aminoethylamino)propyl)-trimethoxysilane (ATS).

3.1.2.2. PLA

In this process, wool fibers and MLO were added at concentrations of 1 phr and 10 phr, respectively, relative to the amount of PLA pellets (100phr). Six material formulations were prepared for evaluation: PLA with MLO (referred to as PLA–MLO), PLA with MLO and untreated wool (PLA–MLO–UW), and PLA with MLO combined with treated wool using various coupling agents: (3-(2-aminoethylamino)propyl)-trimethoxysilane (PLA–MLO–Wool(ATS)), trimethoxy(2-(7-oxabicyclo[4.1.0]hept-3-yl)ethyl)silane (PLA–MLO–Wool(TES)), tris(2-methoxyethoxy)(vinyl)silane (PLA–MLO–Wool(TVS)), and titanium(IV) triethanolaminate isopropoxide (PLA–MLO–Wool(TTI)). The components were dried, pre-mixed, and processed using a Dupra S.L. (Castalla, Spain) twin-screw extruder (L/D ratio of 25) with temperatures set from 150°C to 185°C (from hopper to die) and a rotation rate of 20 rpm. After extrusion, the materials were ground in a grinder (Silmisa, Onil, Spain) operating at 500 rpm, producing pellet sizes ranging from 3.5 to 4 mm. The ground materials were dried at 50°C for 24 hours and then subjected to injection molding to create test samples. The injection molding process, performed using a Sprinter-11 machine (Erinca S.L., Barcelona, Spain), was conducted with temperatures ranging from 160°C to 180°C (from hopper to die). The molded samples were then prepared for characterization of the fiber-reinforced polymer (FRP) formulations..

3.1.3. Characterization techniques

3.1.3.1. Wool fiber

To assess the effectiveness of wool treatment with coupling agents, attenuated total reflectance Fourier transform infrared spectroscopy (ATR-FTIR) and thermogravimetric analysis (TGA) were performed on untreated wool (Wool) and wool fibers modified with the coupling agents ATS, TES, TVS, and TTI (denoted as Wool(ATS), Wool(TES), Wool(TVS), and Wool(TTI), respectively). FTIR spectra were obtained using a Perkin Elmer Spectrum BX FTIR system (Beaconsfield, United Kingdom) over a spectral range of 4000–650 cm^{-1}, with a resolution of 16 cm^{-1}, and 20 scans were completed. TGA was performed using a Linseis TGA PT1000 (Selb, Germany), heating from 30 to 700°C at a rate of 10°C/min under nitrogen at a flow rate of 20 cm^3/min. The onset degradation temperatures (T_5) were identified at 5% mass loss, while the temperatures corresponding to the maximum decomposition rate (T_{max}) were determined from the peaks of the first derivative of the TGA curves (DTG). TGA measurements were performed in triplicate, and the average values along with standard deviations were reported. Statistical significance of the differences between samples was analyzed using OriginPro 8 software (OriginLab, Northampton, MA, USA). Differences between wool fiber samples were identified at a 95% confidence level through Tukey's test, applied with ANOVA analysis.

3.1.3.2. PLA

Tensile and flexural tests followed the specifications outlined in ISO 527 and ISO 178, respectively. The tests were conducted using a universal testing machine (Ibertest ELIB-50-W, Madrid, Spain), with a 5 kN load capacity and a speed of 10 mm/min. Charpy impact resistance was measured using a Metrotec (San Sebastian, Spain) pendulum impact tester, with a pendulum energy of 6 J. Hardness was evaluated using a Shore D durometer (model 673-D, Instruments J. Bot S.A., Barcelona, Spain). For each testing method, five specimens were assessed, and the mean values along with their standard deviations were recorded. Furthermore, the toughness of each material formulation was determined by calculating the area under the stress-strain curves generated during the tensile tests, with the area calculation performed using the OriginPro 2015 software. [195] The differences in the mechanical results were statistically analyzed with a one-way analysis of variance (ANOVA), as it was conducted using OriginPro 8 software at a 95% confidence level. Tukey's post-hoc test was applied to determine significant differences among the formulations.

Thermogravimetric analyses (TGA) were performed using a Linseis TGA PT1000 instrument (Selb, Germany) operating in dynamic mode. Samples were heated from 30 °C to 700 °C at a rate of 10 °C/min under a nitrogen atmosphere with a flow rate of 20 cm^3/min. The onset degradation temperatures (T_5) were determined at 5% mass loss, while the temperatures corresponding to the maximum decomposition rates (T_{max}) were calculated from the peak temperatures of the first derivative of the TGA curves (DTG). Additionally, mass losses at 300 °C and 350 °C were reported.

Differential scanning calorimetry (DSC) analysis was performed using a Mettler DSC821e instrument (Toledo, Spain) following a thermal cycle that included an initial heating from 30 to 180 °C, a cooling phase from 180 to 30 °C, and a second heating from 30 to 220 °C. A heating rate of 10 °C/min was applied for each cycle, with nitrogen flow set to 20 cm³/min. The second heating cycle was used to assess the thermal properties. The glass transition temperature (T_g), melting temperature (Tm), and cold crystallization temperature (T_{cc}) were determined based on this second heating cycle. T_g was identified at the inflection point between the onset and endset of the DSC curve, while T_{cc} and T_m were determined at the respective peak positions. The degree of crystallinity ($X_{c\%}$) was also determined using Equation 7:

Equation 7 $X_c(\%) = \frac{\Delta H_m - \Delta H_{CC}}{f \times \Delta H_m^c} \times 100$

Where the melting enthalpy is defined as ΔHm, and the cold crystallization enthalpy is defined as ΔHcc . The ΔHcm is the estimated melting enthalpy of a purely crystalline PLA, equal 93 J/g according to [168]

Dynamic mechanical analysis (DMA) was made on rectangular specimens with sizes of 40 × 10 × 4 mm³ via a TA Instruments AR G2 rheometer (New Castle, DE, USA). The analysis was conducted over a temperature range of 30 to 140 °C, with a heating rate of 2 °C/min, an oscillation frequency of 1 Hz, and a maximum strain of 0.1%.

To evaluate the results from DSC, TGA, and DMA, three specimens were evaluated for each testing method, and the mean values along with their standard deviations were reported. Statistical analysis of significant differences in the measured properties was performed using these data.

Scanning electron microscopy (SEM) was conducted on the fractured surfaces of the impact test specimens to analyze their structure. Micrographs were acquired using a Phenon SEM system from FEI (Eindhoven, The Netherlands) operating at an accelerating voltage of 5 kV. Samples were attached to the specimen holder with graphite adhesive and subsequently covered with a gold-palladium alloy to improve conductivity. The coating process was carried out using a Sputter Mod Coater (Emitech SC7620, Quorum Technologies, East Sussex, UK).

Wettability was assessed by measuring the static contact angle, which was used to determine the Theta angle of a distilled water droplet placed on the surface of the sample. The measurement was conducted using an EasyDrop-FM140 optical goniometer (Kruss Equipments, Hamburg, Germany) with Drop Shape Analysis software at room temperature. Color evaluation was carried out using a Colorflex-Diff2 458/08 colorimeter (HunterLab, Reston, VA, USA), based on the CIELab* color model, which provided the L*, a*, and b* values. The L* value represents the lightness or darkness of the color, the a* value indicates the red-green intensity, and the b* value denotes the blue-yellow intensity. For each sample, ten measurements were taken and averaged for both wettability and color properties. The mean and standard deviation were recorded, and a statistical analysis of significant differences was conducted based on the previously aforementioned parameters.

3.2. Impact of silane treatment conditions on sheep wool fiber reinforced poly(lactic acid)-maleinized linseed oil system.

3.2.1. Materials

Poly(lactic acid) (PLA) Ingeo Biopolymer 6201D, supplied by NatureWorks LLC (Minnetonka, MN, USA), was utilized. This material contains 2% D-lactic acid, has a density of 1.24 g/cm³, and a melt flow index (MFI) ranging from 15 to 30 g/10 min (at 210 °C). Maleinized linseed oil (MLO) was employed as a plasticizer, with the commercial-grade product Veomer Lin provided by Vendeputte (Mouscron, Belgium), featuring a viscosity of 10 dPas at 20 °C and an acid value between 105 and 130 mg KOH/g. Wool, obtained from a local source in the Basque Country (Spain), underwent a cleaning process before preparation, following a previously documented method. [196]. In summary, the fibers were cut and cleaned using an aqueous solution containing 0.2 wt% sodium carbonate and 2 wt% detergent. After cleaning, the fibers were carded to align them in a single direction and subsequently cut into 1 cm lengths, achieving a length-to-diameter ratio of 200. Tris(2-methoxyethoxy)(vinyl) silane (TVS) was used as a coupling agent. TVS has a density of 1.034 g/mL at 25 °C and a refractive index (n_{20}/D) of 1.43, and was supplied by Sigma Aldrich (Schnelldorf, Germany). The chemical structures of the components utilized are presented in Figure 33.

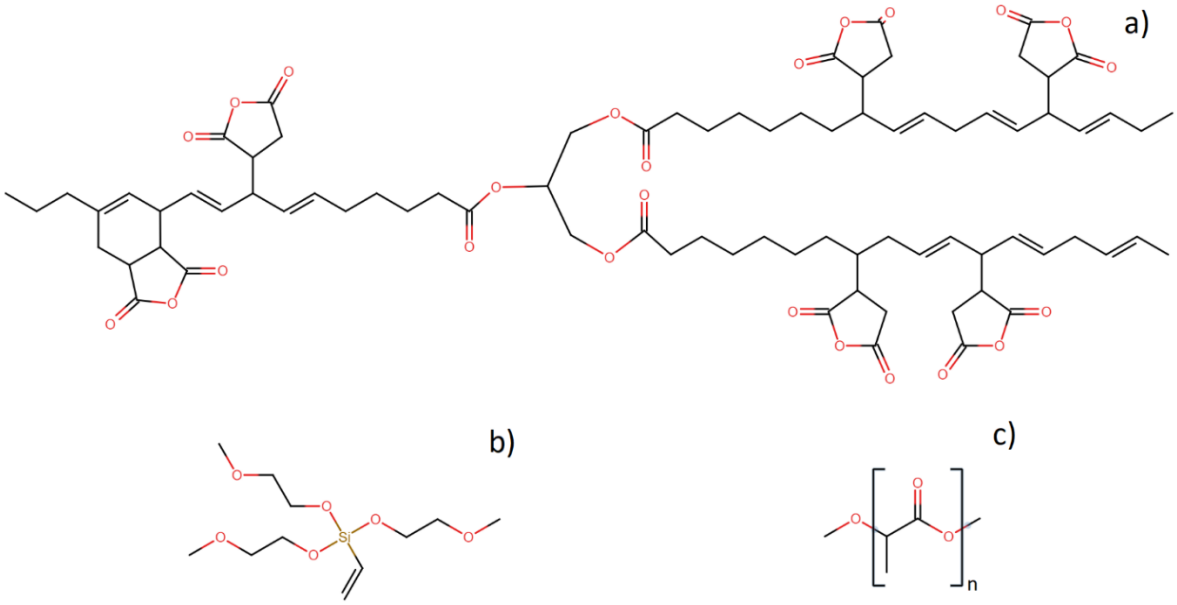

Figure 33 Chemical structure of a) MLO, b) TVS, and c) PLA

3.2.2. Material processing

3.2.2.1. Wool modification

A schematic representation of the silane treatment process applied to the wool fibers is presented in Figure 34. The wool fibers were altered using 1 phr and 2.5 phr of TVS coupling agent per 100 parts of wool fibers. The modification process began by dissolving the TVS in an acetone solution with 99% purity, which was heated to 40 °C and mixed for 30 minutes. The wool fibers were then immersed in the prepared coupling agent solutions and stirred for 2 hours at 1000 rpm. After treatment, the fibers were dried in an air-circulating oven at 80 °C for 48 hours to ensure complete solvent evaporation. Untreated wool fibers were used as a control sample for reference.

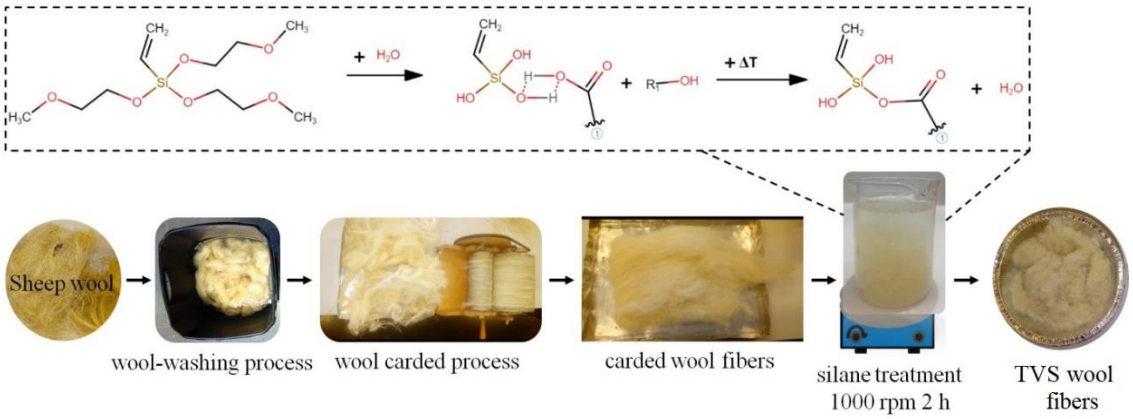

Figure 34 Schematic representation of sheep wool fibers TVS treatment.[174]

The coupling reaction between TVS and the wool fibers is illustrated in the upper section of Figure 34. The coupling process begins with the hydrolysis of the coupling agent in an acetone solution, where water facilitates the hydrolysis reaction while acetone serves as the solvent. Subsequently, the wool fibers, with adsorbed surface moisture, form hydrogen bonds with the hydroxyl groups of TVS. Finally, during heat treatment, the evaporation of water promotes the grafting of the silane molecules onto the surface of the wool fibers. [194,197,198]

3.2.2.2. PLA processing

PLA was plasticized with 10 phr of MLO relative to neat PLA, in accordance with previous studies. [94,168,196]. Composites were developed by incorporating wool fibers into the plasticized PLA/MLO matrix. The PLA/MLO matrix was reinforced with 1, 5, and 10 phr (parts of fiber per 100 parts of neat PLA) of wool fibers and TVS-treated wool fibers. Additionally, composites with untreated wool fibers were prepared and evaluated for comparison. In total, eleven formulations were prepared and designated as indicated in Table 2.

Table 2 Summary of PLA/MLO-wool formulations

Coding of formulation	PLA (phr)	MLO (phr)	Wool (phr)	TVS (phr)
PLA	100	-	-	-
PLA/MLO	100	10	-	-
PLA/MLO -1Wool	100	10	1	-
PLA/MLO -1Wool-1TVS	100	10	1	1
PLA/MLO -1Wool-2.5TVS	100	10	1	2.5
PLA/MLO -5Wool	100	10	5	-
PLA/MLO -5Wool-1TVS	100	10	5	1
PLA/MLO -5Wool-2.5TVS	100	10	5	2.5
PLA/MLO -10Wool	100	10	10	-
PLA/MLO -10Wool-1TVS	100	10	10	1
PLA/MLO -10Wool-2.5TVS	100	10	10	2.5

All components of the formulations were pre-dried and then pre-mixed in a plastic container prior to processing. The materials were subsequently extruded using a co-rotating twin-screw extruder (Dupra S.L, Castalla, Spain) with an L/D ratio of 25. The extrusion was performed with a temperature profile of 150-170-180-180 °C (from hopper to die) and a screw rotation speed of 10 rpm. This temperature profile was selected to ensure proper melting of the PLA while preventing thermal degradation of the wool fibers, which can occur at temperatures above 200 °C. [199,200] Each formulation was subsequently ground using a Silmisa mill (Onil, Spain) to produce pellets measuring between 3.5 and 4 mm. The materials were then re-extruded and milled under identical processing conditions to promote improved interaction among the components in the final compound. Finally, the materials were injection-molded using an Erinca Sprinter-11 injection molding machine (Barcelona, Spain) to produce standard test specimens. The injection molding was performed with a temperature profile of 160-170-180-180 °C (from hopper to die). These molded specimens were used for further characterization of each composite formulation.

3.2.3. Characterization techniques

3.2.3.1. Wool fibers

To confirm the effectiveness of the silane surface treatment on the wool fibers, unmodified wool fibers, along with wool fibers treated with 1 phr and 2.5 phr of TVS coupling agent (denoted as UW, W-1TVS, and W-2.5TVS, respectively), as well as pure TVS, were analyzed using Attenuated Total Reflectance Fourier-Transform Infrared Spectroscopy (ATR-FTIR) (Perkin-Elmer Spectrum BX, Beaconsfield, UK). All samples were examined over the spectral range of 4000 to 600 cm^{-1}, with 20 scans performed at a resolution of 16 cm^{-1}.

The thermal stability of the wool fibers was evaluated using thermogravimetric analysis (TGA) with a Linseis TGA PT1000 instrument (Selb, Germany). The analysis was performed in isothermal mode at 180 °C for 30 minutes under air atmosphere conditions.

The X-ray diffraction (XRD) patterns of both unfunctionalized and silane-treated fibers were acquired using a BRUKER AXS D5005 instrument (SCSIE, Universitat de València). The measurements were performed with a diffractometer employing Cu Kα radiation, with a scanning step size of 0.02° over a 2θ range from 2.5° to 40° at 40 kV, and a collection time of 10 seconds per step. The raw XRD data were subsequently smoothed using the Savitzky–Golay method with a window size of 25 points, processed in OriginPro software.

The fibers were also examined using scanning electron microscopy (SEM) with a Phenon SEM electron microscope (FEI, Eindhoven, The Netherlands) operated at 5 kV. To enhance conductivity, the wool samples were pre-coated with a gold-palladium alloy using a Sputter Coater (Emitech SC7620, Quorum Technologies, East Sussex, UK).

3.2.3.2. PLA

3.2.3.2.1. Mechanical assessment

Tensile tests were conducted using an Ibertest ELIB-50-W universal testing machine (Madrid, Spain) equipped with a 5 kN load cell and a crosshead speed of 10 mm/min, following the ISO 527 standard. [176] Charpy impact resistance was measured using Metrotec equipment (San Sebastian, Spain) with a 6 J pendulum, in accordance with the ISO 179 standard. [201] Hardness was evaluated using a Shore D durometer (model 673-D, Instruments J. Bot S.A., Barcelona, Spain) under the ISO 868 standard. [181]. For each test, five specimens were analyzed, and the mean values along with their standard deviations were reported.

The statistical significance of the differences among the formulations was analyzed using OriginPro 8 software (OriginLab, Northampton, MA, USA). A one-way analysis of variance (ANOVA) was performed at a 95% confidence level, followed by Tukey's test to identify significant differences between the formulations.

The thermomechanical properties were evaluated by determining the Vicat softening temperature (VST) per ISO 306[192], employing a load of 5 kg and a heating rate of 50 $°C \cdot h^{-1}$. The heat deflection temperature (HDT) measurement was performed due to ISO 75 [189–191] standards, using a load of 196 g and a heating rate of 120 $°C \cdot h^{-1}$.

3.2.3.2.2. Thermal assessment

Differential scanning calorimetry (DSC) was carried out using a Mettler DSC 821e calorimeter (Toledo, Spain). The thermal program consisted of an initial heating phase from 30 to 180 °C, followed by a cooling cycle from 180 to 30°C, and a final heating phase from 30 to 220 °C. All phases were done under a nitrogen atmosphere, with a temperature change of 10 °C/min and a nitrogen feed of 30 cm³/min. The glass transition temperature (T_g), melting temperature (T_m), and cold crystallization temperature (T_{cc}) were evaluated based on the second heating cycle to eliminate the influence of thermal history. The degree of crystallinity ($X_{c\%}$) was determined based on Equation 8:

Equation 8 $X_c(\%) = \frac{\Delta H_m - \Delta H_{CC}}{f \times \Delta H_m^c} \times 100$

where ΔH_m (J/g) represents the melting enthalpy and ΔH_{CC} (J/g) corresponds to the cold crystallization enthalpy of the material. The ΔHcm (J/g) is the reference melting enthalpy for fully crystalline PLA, taken as 93 J/g [202], and f denotes the weight fraction of PLA in the formulation.

Thermogravimetric analysis (TGA) was performed using a Linseis TGA 1000 instrument (Selb, Germany). The thermal profile was evaluated from 30 °C to 700 °C at a heating rate of 10 °C/min under a flow rate of 30 cm³/min of nitrogen. The onset degradation temperature (T_5) was determined at 5% mass loss, while the temperatures corresponding to the maximum decomposition rate (T_{max}) were identified as maximum temperatures from thermal events observed at the first derivative of the TGA curves (DTG). Additionally, the mass losses at 300 °C and 350 °C were recorded.

In the DSC and TGA analyses, three specimens of each tested material were evaluated, and the mean values along with their standard deviations were obtained. Significant differences in the properties were statistically evaluated using aforementioned parameters.

3.2.3.2.3. Microstructural assessment

The crystalline phases of the nanocomposites were investigated using X-ray diffraction (XRD) with a BRUKER AXS D5005 system (SCSIE, Universitat de València). The analysis was performed on the materials` film surfaces (15 mm × 15 mm) placed in a sample holder. The diffraction patterns were recorded using Cu Kα radiation source, with a scanning step of 0.02° across a 2θ range from 2.5° to 40°, and a collection time of 10 seconds per step, while maintaining a voltage of 40 kV. The raw data were smoothed using the Savitzky–Golay method with a 25-point window in the OriginPro software.

3.2.3.2.4. Surface assessment

Scanning electron microscopy (SEM) was utilized to analyze the fracture surfaces of the impact specimens. The examination was conducted using a Phenon SEM electron microscope (FEI, Eindhoven, The Netherlands) operating at an accelerating voltage of 5 kV. To enhance conductivity, the fractured samples were pre-coated with a gold-palladium alloy using a Sputter Coater Emitech SC7620 (Quorum Technologies, East Sussex, UK).

Wettability was assessed by measuring the static contact angle using an EasyDrop-FM140 optical goniometer equipped with a camera and Drop Shape Analysis software (Kruss Equipments, Hamburg, Germany). The contact angle, also known as the wetting contact angle (WCA—theta angle), was determined for a distilled water droplet placed on the surface of each sample. The WCA was assessed at room temperature 30 seconds after droplet deposition. The mean values from five samples of the same material were reported, with a maximum standard deviation of 3%. [203].

The color assessment of the specimens were conducted in a Colorflex-Diff2 458/08 colorimeter from HunterLab (Reston, VA, USA) evaluating based on the CIELab color space. This method involves measuring the L*, a*, and b* coordinates, where L* represents the lightness of the color, a* indicates the intensity along the red-green axis, and b* corresponds to the intensity along the yellow-blue axis.

Ten measurements were taken for both the wettability and color assessments, and the mean values along with their standard deviations were evaluated. Statistical analysis of significant differences was conducted using aforementioned parameters.

3.3. Plasma-modified sheep wool fibers for poly(lactic acid)-maleinized linseed oil system reinforcement

3.3.1. Materials

Poly(lactic acid) (PLA), specifically Ingeo Biopolymer 6201D, was procured from NatureWorks LLC in Minnetonka (MN, USA). This material is characterized by a 2% D-lactic acid content, a density of 1.24 g/cm³, and a melt flow index (MFI) ranging from 15 to 30 g/10 min at 210 °C. Veomer Lin, a commercial-grade maleinized linseed oil (MLO) used as a plasticizer, was sourced from Vendeputte (Mouscron, Belgium). It exhibits a viscosity of 10 dPas at 20 °C and an acid value between 105–130 mg KOH/g. Raw wool material was acquired from the Basque Country (Spain) and underwent a comprehensive cleaning and preparation process prior to use.

3.3.2. Material processing

3.3.2.1. Wool fibers

Raw wool material underwent a cleaning process involving cutting and cleaning the fibers employing an aqueous solution containing 0.2%wt. sodium carbonate and 2%wt. cleansing agent. Subsequently, the fibers were carded to align them in desired direction and shorten them into 1 cm lengths, accomplishing a length-to-diameter (L/d) ratio 200. Wool fibers were treated in a sealed container and mixed with a gas flow by air and nitrogen plasma in a voltage of 260V and duration of 2, 4, 6, 8, 10, 15, and 20 seconds.

3.3.2.2. PLA formulations

Polylactic acid (PLA) was prepared as a reference material and plasticized with 10 phr of maleinized linseed oil (MLO). The MLO plasticized PLA material was then reinforced with wool fibers to fabricate fiber-reinforced polymers (FRPs). The PLA/MLO matrix was loaded with varying amounts of untreated and plasma-modified (WA8) wool fibers, specifically at 1 and 5 phr (parts of fiber for 100 parts of the PLA). All components of the formulations were pre-dried and pre-mixed in a sealed package before processing. The mixtures were processed using a co-rotating twin-screw extruder (Dupra S.L., Castalla, Spain) with an L/D ratio of 25, operating at a temperature profile of 150-170-180-180 °C (from hopper to die) and a screw rotation speed of 10 rpm, chosen to prevent wool fiber degradation. After extrusion, the formulations were ground in a Silmisa mill (Onil, Spain) to produce pellets with an approximate diameter of 4 mm. The materials

were subsequently injection-molded using an Erinca Sprinter-11 (Barcelona, Spain) to produce uniform test specimens, with a temperature profile of 160-170-180-180 °C (from hopper to die). These injection-molded samples were utilized for the characterization of each composite formulation.

3.3.3. Characterization techniques

3.3.3.1. Wool fibers

To confirm the value of the plasma surface treatment on wool, various samples were analyzed, including untreated wool fibers (labeled WU), wool fibers treated with air plasma (labeled WA[time]), and wool fibers treated with nitrogen plasma (labeled WN[time]). The analysis was conducted using an ATR-FTIR analyzer supplied by Perkin-Elmer Spectrum BX from Beaconsfield (UK), covering the spectral range from 4000 to 600 cm^{-1} with 20 scans and a resolution of 16 cm^{-1}. Furthermore, wool fibers were observed under a light microscope with a magnitude of 5.6x.

3.3.3.2. PLA formulations

Differential scanning calorimetry (DSC) analyses were conducted using a Mettler DSC 821e calorimeter manufacture in Toledo (Spain). The thermal program consisted of at first heating cycle from 30 to 180 °C, followed by a cooling phase from 180 to 30 °C, and finally a second heating cycle from 30 to 250 °C. All cycles were performed with a temperature change of 10 °C/min and a nitrogen flow of 30 cm^3/min. Tensile tests were performed on an Ibertest ELIB-50-W machine manufacture in Madrid (Spain), equipped with a 5 kN load cell, using a crosshead speed of 10 mm/min in accordance with the ISO 527 standard [177]. Charpy's impact characteristics was evaluated using Metrotec equipment manufactured in San Sebastian (Spain) with a 6 J pendulum, adhering to the ISO 179 [182]. Wettability was assessed with an EasyDrop-FM140 optical goniometer manufactured by Kruss Equipments in Hamburg (Germany). A camera, being part of the goniometer was supported by Drop Shape Analysis software, focusing on the drop forming static contact angle of distilled water created on each sample surface; the WCA of every drop was measured with 30 s delay at room temperature to ensure comparable test conditions. Color measurements were conducted using a colometer Colorflex-Diff2 458/08 manufactured by HunterLab in Reston (VA, USA), applying the CIELab color model, which involves assessing the L, a*, and b* coordinates.

3.4. Physical ageing phenomenon of sheep wool fiber reinforced poly(lactic acid)-based materials

3.4.1. Materials

Polylactic acid Ingeo Biopolymer 6201D (PLA) was supplied by NatureWorks LLC (Minnetonka, Minnesota, USA). The plasticizer utilized in the manufacturing was maleinized linseed oil (MLO) Veomer Lin, sourced from Vendeputte (Mouscron, Belgium). A blend of the PLA with 10phr MLO was used as a base for further modification with wool fibers. Raw wool material was acquired from the Basque Country (Basque Country, Spain) and subjected to prior cleaning and preparation through a multi-step procedure described in prior studies [174,196]. Surface modification with silane coupling agent was executed using tris(2-methoxyethoxy)(vinyl)silane provided by Sigma-Aldrich manufactured in Schnelldorf (Germany). The study encompassed various formulations: PLA blended with 10 phr of MLO, PLA-MLO blends reinforced with unmodified wool, and silane-treated wool at 1 and 5 phr concentrations. Silane treatment was applied on wool in a concentration of 2.5phr of the tris(2-methoxyethoxy)(vinyl)silane with a procedure described in prior study[200].

3.4.2. Material processing and conditioning

Each formulation underwent processing in a co-rotating twin-screw extrusion machine with the screw L/D=25 manufactured by Dupra S.L from Castalla (Spain) at dynamic temperature along the screw (hopper-150-170-180-185°C-die) and a rotation speed of 20 rpm. Subsequently, the obtained materials were processed through molding with a temperature set between 160-170-180-180°C to produce test samples using the Sprinter-11 manufactured by Erinca S.L. in Barcelona (Spain).

Table 3 List of evaluated formulations

Sample name	Wool concentration (phr)	Silane-treatment concentration (phr)	Sample ageing
PLA_0_N	0	Not applicable	No
PLA_0_A	0	Not applicable	Aged
PLA_1_0_N	1	0	No
PLA_1_0_A	1	0	Aged
PLA_1_2.5_N	1	2.5	No
PLA_1_2.5_A	1	2.5	Aged
PLA_5_0_N	5	0	No
PLA_5_0_A	5	0	Aged
PLA_5_2.5_N	5	2.5	No
PLA_5_2.5_A	5	2.5	Aged

Table 3 summarizes formulations obtained in the current study. All formulations were examined directly after injection molding processing and after four years of aging. Aged specimens were placed in dedicated containers sheltered from direct sunlight and airflow. The temperature of 23 ± 2 °C and moisture of 50 ± 5% were maintained in the laboratory environment and controlled by air conditioning.

3.4.3. Characterization techniques

Tensile characterization were conducted using an Ibertest ELIB-50-W machine manufactured by Ibertest in Madrid (Spain), with a 5 kN load cell and 10 mm/min crosshead rates, following ISO 527 standard [176]. Charpy's impact strength was evaluated employing Metrotec equipment (San Sebastian, Spain), utilizing a 6 J pendulum defined in the ISO 179 [182]. Each mechanical test comprised five specimens; mean measurements with standard deviations were reported. Differential scanning calorimetry (DSC) was executed using a Mettler DSC 821e calorimeter (Toledo, Spain), with thermal profile involving initial heating (30-180 °C), followed by cooling (180-30 °C) to ensure equal measurement conditions for every formulation. As the measurement a heating in range of 30 to 250 °C was conducted in nitrogen flow of 30 cm^3/min a heating rate of 10 °C/min.As an outcome glass transition (T_g), melting (T_m), and cold crystallization (T_{cc}) temperatures were determined, alongside with corresponding degree of crystallinity (X_c%). The degree of crystallinity (X_c%) was calculated according to *Equation 9:*

Equation 9 $$X_c(\%) = \frac{\Delta H_m - \Delta H_{CC}}{f \times \Delta H_m^c} \times 100$$

Wettability was assessed by an EasyDrop-FM140 goniometer manufactured by Kruss Equipments in Hamburg (Germany), and color measurements were obtained using a Colorflex-Diff2 458/08 from HunterLab in (Reston, VA, USA), with the CIELab color space. Ten measurements were averaged for wettability and color evaluation, and significant differences were statistically assessed applying ANOVA analysis.

3.5. Predictive models for poly(lactic acid) materials reinforced with surface-modified sheep wool fibers

3.5.1. Data selection

In the prior studies, polylactic acid (PLA) was modified with maleinized linseed oil (MLO) and with either unmodified or modified sheep wool fibers with four coupling agents. Labeling of coupling agents remained as follows: (3-(2-aminoethylamino)propyl)-trimethoxysilane (ATS marked as coupling agent A), trimethoxy (2-(7-oxabicyclo(4.1.0)hept-3-yl)ethyl)silane (TES marked as coupling agent B), tris(2-methoxyethoxy)(vinyl) silane (TVS marked as coupling agent C) and titanium (IV) (triethanolaminate)isopropoxide (TTI marked as coupling agent D). The experimental phase of this study involved collecting raw data from prior studies, specifically experiments conducted following industrial testing standards.[94,174,176]

The outcomes derived from the tensile test, specifically the maximum resistance, and the thermogravimetric analysis, precisely the 5% mass loss temperature, were gathered and written down in the dataset as a CSV file. The gathered data was based on various variables for characterization, including the presence of maleinized linseed oil (MLO) in a formulation, the concentration of sheep wool fiber or its surface modification type, and the concentrations of a coupling agent used for modification. A comprehensive summary of the formulations involved within the database is provided, offering a structured representation of the relevant experimental variables and their corresponding labeling.

Table 4 The formulations collected in the database

Label	PLA [phr]	MLO [phr]	Wool [phr]	Coupling agent type	Coupling agent concentration [phr]
PLA-MLO-1W	100	10	1	n.a.*	0
PLA-MLO-5W	100	10	5	n.a.*	0
PLA-MLO-10W	100	10	10	n.a.*	0
PLA-MLO-1W-1C	100	10	1	C (TVS)	1
PLA-MLO-5W-1C	100	10	5	C (TVS)	1
PLA-MLO-10W-1C	100	10	10	C (TVS)	1
PLA-MLO-1W-2.5C	100	10	1	C (TVS)	2.5
PLA-MLO-5W-2.5C	100	10	5	C (TVS)	2.5
PLA-MLO-10W-2.5C	100	10	10	C (TVS)	2.5
PLA-MLO-1W-1A	100	10	1	A (ATS)	1
PLA-MLO-1W-1B	100	10	1	B (TES)	1
PLA-MLO-1W-1D	100	10	1	D (TTI)	1

3.5.2. Data processing

In the subsequent phase of the study, preprocessing of the prepared data was conducted to adjust its suitability for regression Machine Learning (ML) algorithms. Initially, a targeted selection of columns was performed, focusing on material composition and the experimentally obtained characterization values. All data were converted into numerical form to comply with a supervised regression model type. To achieve this, the selected columns underwent analysis to identify and subsequently eliminate entries that were either empty or non-numerical. Following the process, experimental results were normalized to standardize the data within a range of 0 to 1, regardless of the actual numerical values derived from experiments. The rational values between 0 and 1 maintained the original scale between the experimental results, preserving the relative relationships among the data points.

Conclusively, the prepared data underwent a final step of random partition into two subsets: 75% of the data, comprising 115–116 records, was allocated for model training, while the remaining 25%, consisting of 37–38 records, was reserved for model evaluation. This thorough preprocessing and division of the dataset into training and evaluation subsets aimed to ensure the effectiveness of the subsequent machine learning models developed for selected material properties and their modeling approaches. An example of a created pipeline is shown in Figure 35.

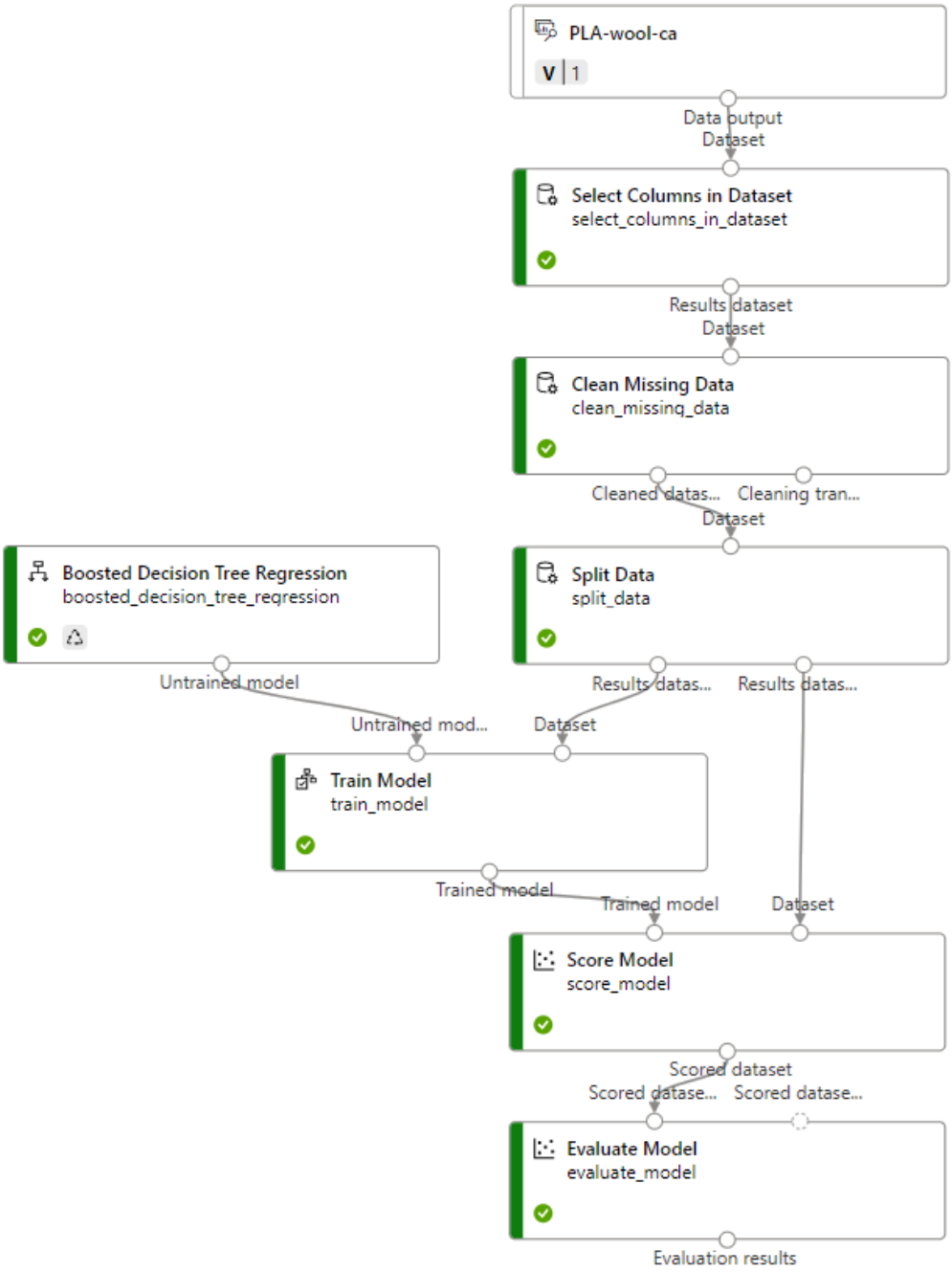

Figure 35 Training pipeline in Microsoft Azure Machine Learning Studio

For model training were used two types of models were: linear least square regression with a regularization rate equal to 0.001 and with an intercept term and boosted decision tree with a single parameter training mode, maximum of 20 leaves per tree, minimum of 10 samples per leaf node, a 0.2 learning rate and 100 trees constructed per model. The evaluation, as an additional outcome of the machine learning pipeline, included mean absolute error (MAE), root mean squared error (RMSE), relative absolute error (RAE), relative squared error (RSE), and coefficient of determination (R^2). [150]

Subsequently, prepared training pipelines were deployed into batch inference pipelines, as presented in Figure 36. In this scenario, a structured CSV data file,

organized in a tabular form, was created with a similar structure to the original database used for training. The database used for predictions of degradation temperature (T_5) and tensile strength contained variable wool concentration (from 1 to 15phr, with 1phr step), coupling agent concentration (from 0 to 5phr, with 0.5phr step), and coupling agent type (the A, B, C, and D). The prepared prediction dataset was transformed using the previously trained models, and the scoring process followed. The outcome of this scoring procedure involved obtaining predictions for material characteristics based on the updated input parameters, contributing to an enhanced understanding of the influence of wool and coupling agent concentrations on the estimated material properties.

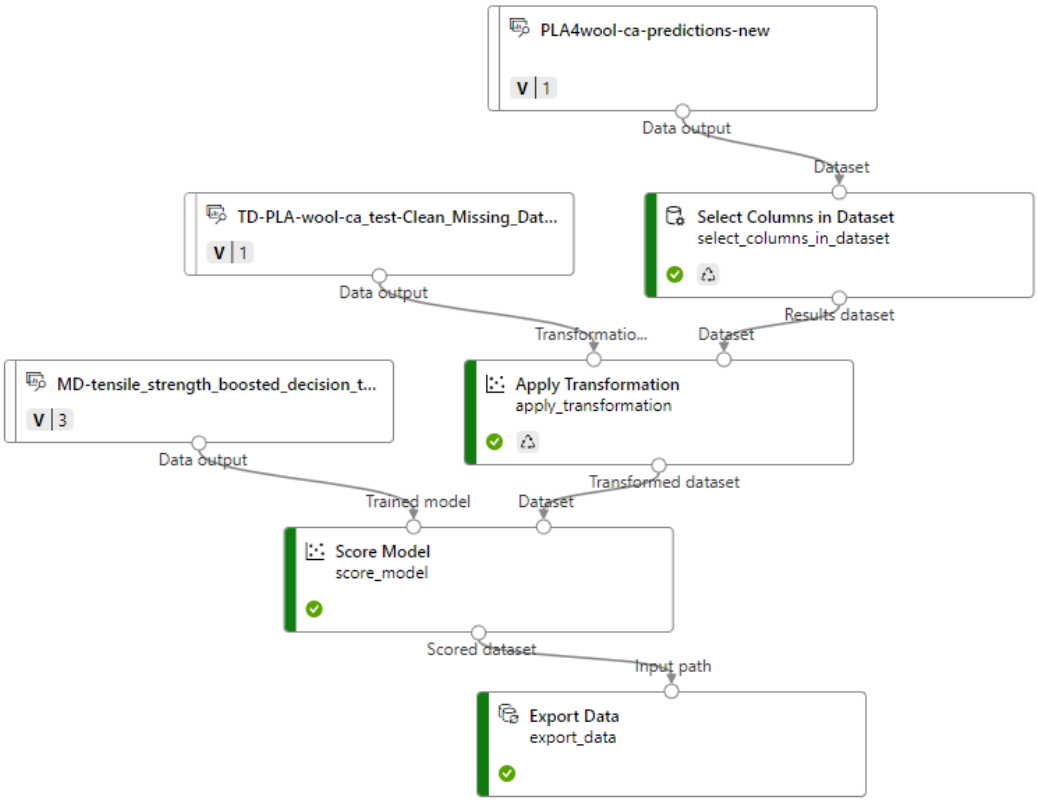

Figure 36 Batch inference pipeline

3.6. Use of AI techniques for modeling poly(lactic acid) properties for various maleinized linseed oil and sheep wool fiber concentrations.

3.6.1. Data selection

The experimental section utilized raw data collected from previous studies [94,171,174,196]. Among the collected materials are distinguished neat PLA, PLA modified with several MLO concentrations, and PLA-MLO blend modified with several sheep wool fiber concentrations, as summarized in Table 5. Material characteristics data, focusing on mechanical and thermal properties of PLA-based Fiber-Reinforced Polymers (FRPs), were obtained following industrial testing standards related to tensile properties, specifically tensile strength, Young modulus, and elongation at break[176], flexural properties specifically flexural strength and flexural modulus [180], impact resistance by Charpy [182], hardness by Shore and differential scanning calorimetry [184].

The characterization process specifically addressed mechanical properties, encompassing the evaluation of tensile strength, elongation at break, Young's modulus, flexural strength, flexural modulus, and impact resistance. Additionally, thermal properties were assessed based on the glass transition temperature, cold crystallization temperature, melting temperature, and degree of crystallinity.

Table 5 Formulations used for training ML models for predictions of MLO and wool fiber impact on properties

PLA [phr]	MLO [phr]	Wool [phr]
100	0	0
100	5	0
100	10	0
100	10	1
100	10	5
100	10	10
100	15	0
100	20	0

3.6.2. Data processing

Data in tabular form from a .csv file, specifying PLA type, MLO, wool fiber concentration, and the corresponding material characterization for each of the 110 samples, was inputted into Microsoft Azure ML Studio for further processing.

Subsequently, the prepared data underwent preprocessing to optimize its suitability for machine learning algorithms. The first step involved selecting the desired columns for modeling, focusing on material composition and experimentally obtained characterization values. As a supervised AI regression model was intended for use, all data must be presented numerically. Therefore, columns were examined to identify those that were either empty or non-numerical, and they were excluded from further analysis. The second step involved normalizing experimental results to bring the data within the range of 0 and 1, irrespective of the actual numerical values derived from experiments. Here, 0 indicated the lowest received value, and 1 indicated the highest. Rational values between 0 and 1 corresponded to the remaining experimental results, maintaining the original scale between the results. Finally, the prepared data was randomly split into two subsets: 75% of the data (81-82 records) were used for model training, and 25% (27-28 records) were reserved for model evaluation.

The selection of the machine learning algorithm was based on the expected outcome of the model. As a numerical result was required, supervised AI regression algorithms were considered. Among the algorithms offered within Azure ML Studio, two groups were selected: Linear Least Square and Poisson regression, which were applied to explore whether the data could be modeled as a linear function. In contrast, boosted decision tree and decision forest algorithms were applied for model training to investigate correlations between decisions, obtaining specific values and providing a similar representation of input data into the model.

The prepared data for each characteristic of PLA-based FRPs was trained by the abovementioned models, resulting in 40 models representing various material properties with different modeling approaches.

The evaluation of the models was assessed based on performance factors such as mean absolute error (MAE), root mean square error (RMSE), relative squared error (RSE), relative absolute error (RAE), and coefficient of determination (R2). The parameters were defined by equations as follows:

Equation 10 $$\boldsymbol{MAE} = \frac{1}{n}\sum_{i=1}^{n} |\boldsymbol{Ai} - \boldsymbol{Pi}|$$

Equation 11 $$\boldsymbol{RMSE} = \sqrt{\boldsymbol{MSE}} = \sqrt{\frac{1}{n}\sum_{i=1}^{n}(\boldsymbol{Ai} - \boldsymbol{Pi})^2}$$

Equation 12 $$\boldsymbol{RSE} = \frac{\sum_{i=1}^{n}(\boldsymbol{Pi} - \boldsymbol{Ai})^2}{\sum_{i=1}^{n}(\boldsymbol{Ai} - \frac{1}{n}\sum_{i=1}^{n}\boldsymbol{Ai})^2}$$

Equation 13 $$\boldsymbol{RAE} = \frac{\sum_{i=1}^{n}|\boldsymbol{Pi} - \boldsymbol{Ai}|}{\sum_{i=1}^{n}|\boldsymbol{Ai} - \frac{1}{n}\sum_{i=1}^{n}\boldsymbol{Ai}|}$$

Equation 14 $$\boldsymbol{R^2} = \mathbf{1} - \frac{\boldsymbol{SSr}}{\boldsymbol{SSm}}$$

Where A_i represents the actual value, P_i represents the predicted value, SS_r represents the squared sum error of the regression line, and SS_m represents the squared sum error of the mean line. [155]

Following the evaluation and deployment of the trained models, a subsequent step involved introducing another dataset to predict material properties. In this scenario, a structured tabular form CSV data file was prepared, maintaining the same structure as the original database used for training but with new values for wool (between 0-15phr) and MLO (between 0-25phr) concentrations. The prepared prediction dataset was then transformed using the previously trained models and subsequently scored, resulting in the prediction of material characteristics.

IV. RESULTS AND DISCUSSION

1. Surface modification approaches on sheep wool fiber for reinforcement of poly(lactic acid)-maleinized linseed oil system

1.1. Wool modification

FTIR spectra of unchanged and altered wool fibers (treated with coupling agents ATS, TES, TVS, and TTI, respectively) are illustrated in Figure 37. All the wool samples show a peak around 3275 cm^{-1} corresponding to hydroxyl (-OH) group, which is typical for this region even after wool fiber modifications.[204] Wool fibers treated with coupling agents exhibit a slight reduction on this peak intensity, suggesting a decrease in the number of hydroxyl groups, likely due to their reactivity with the coupling agents. This phenomenon has been previously described, where modifications with agents like methacrylate grafting reduce the hydroxyl group peak intensity. This reduction implies fewer available hydroxyl groups due to their reaction with the coupling agent.[205] The most significant decrease in -OH peak intensity was noted for wool treated with the ATS coupling agent, resulting in a sharper peak. A similar shift toward a sharper -OH peak was spotted in the FTIR spectrum of oxidized wool fiber treated with [3-(methacryloyloxy)propyl]trimethoxysilane [197].

Notable differences can also be observed in the peaks associated with $-CH_3$ groups, appearing around 2930 cm^{-1} and 2950 cm^{-1}. As Jiang et al. [206]observed, surface modifications of wool fibers may lead to alterations in the peak corresponding to the methyl group. The surface modification may influence the intensity and position of the -CH3 group, indicating changes in the molecular structure and interactions within the fiber matrix. In this study, the peaks associated with $-CH_3$ groups differ slightly in wool samples modified with treatment agents (Wool ATS, Wool TES, Wool TVS, Wool TTI) in reference to those in untreated wool. Both peaks exhibit a slight shift in the treated samples towards higher wavelength: the peak in untreated wool appears at 2926 cm^{-1}, whereas after treatment, it shifts to 2929 cm^{-1} for Wool TVS and 2931 cm^{-1} for Wool TES. According to the findings of Conzatti et al. (2014) [197], this behavior indicates the occurrence of minimal quantities of coupling agents, as the region corresponds to bands linked with silicon and titanium agents.

The occurence of silicon or titanium compounds on the fiber surface is further supported by the increased intensity of peaks in the 900 to 1400 cm^{-1} range, corresponding to -Si-O-R- and -Si-O-Si- bonds [197]. Relating to the FTIR spectrum of untreated wool, the treated wool samples exhibit a slight increase in peak intensity within this region, particularly near 1450 cm^{-1} and 1100 cm^{-1}, which are associated with the Si- and Ti-based coupling agents applied for fiber altering. This behavior aligns with observations by Yang et al. [207], where the formation of -Si-O-R- bonds led to the appearance of new peaks and shifts in existing ones after coupling, assigned to the existence of organic groups from silanes. Additionally, the reduction in the hydroxyl group peak, as previously noted, suggests the attachment of silane compounds to the fiber structure.

The minimal changes in peak intensity observed in the FTIR spectra are attributed to the minimal amount of silanes and alkoxides used in the fiber modification, with treatment agents applied at 1 phr per 100 parts of wool. Conzatti et al. [197] reported a more pronounced change in band intensity when a significantly higher concentration of the coupling agent (10 wt%) was used for wool modification.

Most importantly, as observed in the study presented by Jiang et al. [206], although silane modification has a markable influence on the surface, the keratin molecular structure of wool fibers is retained. Surface modification influences the surface topography and wool fiber absorption capacity; however, the initial secondary structure is retained.

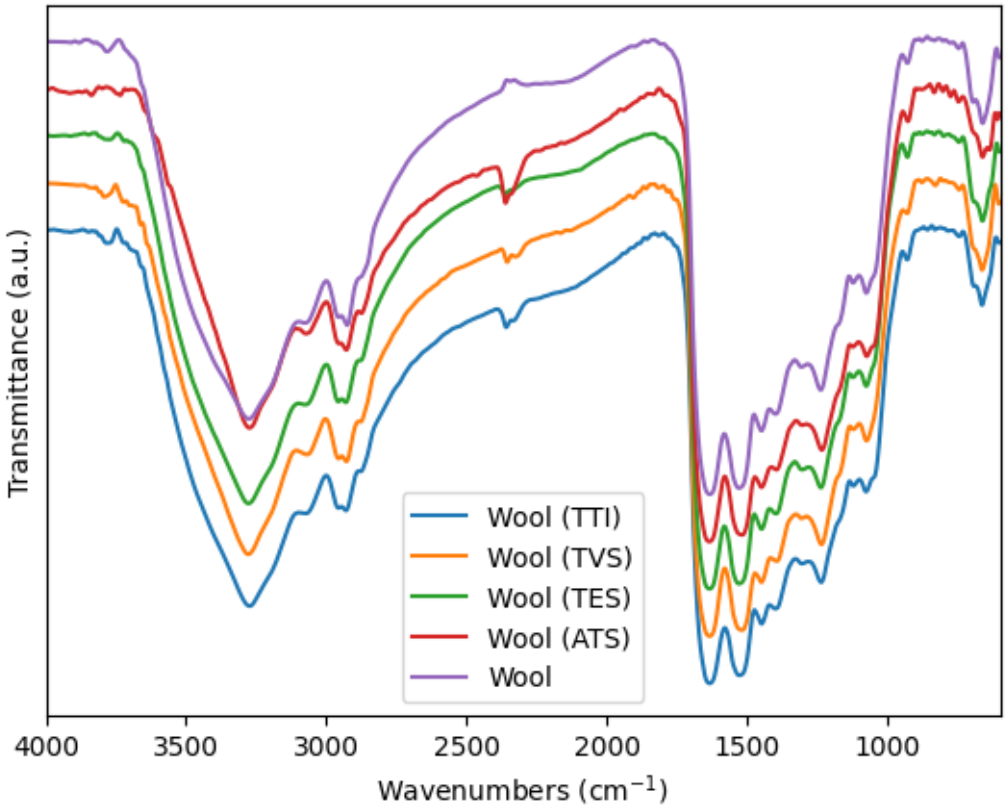

Figure 37 FTIR spectra of unmodified wool and wool modified with studied coupling agents: Wool (ATS), Wool (TES), Wool (TVS), Wool (TTI).

As the whole FTIR spectra of wool fibers are shown in Figure 37, a focused views of most crucial from modification point of view were presented in Figure 38. As prior written, although low concentrations of silanes and alkoxide coupling agents were applied in modification procedure, in the FTIR analysis there are visible changes in intensity of peaks, or in wavelength shifts between unmodified wool fibers, are fibers after treatments.

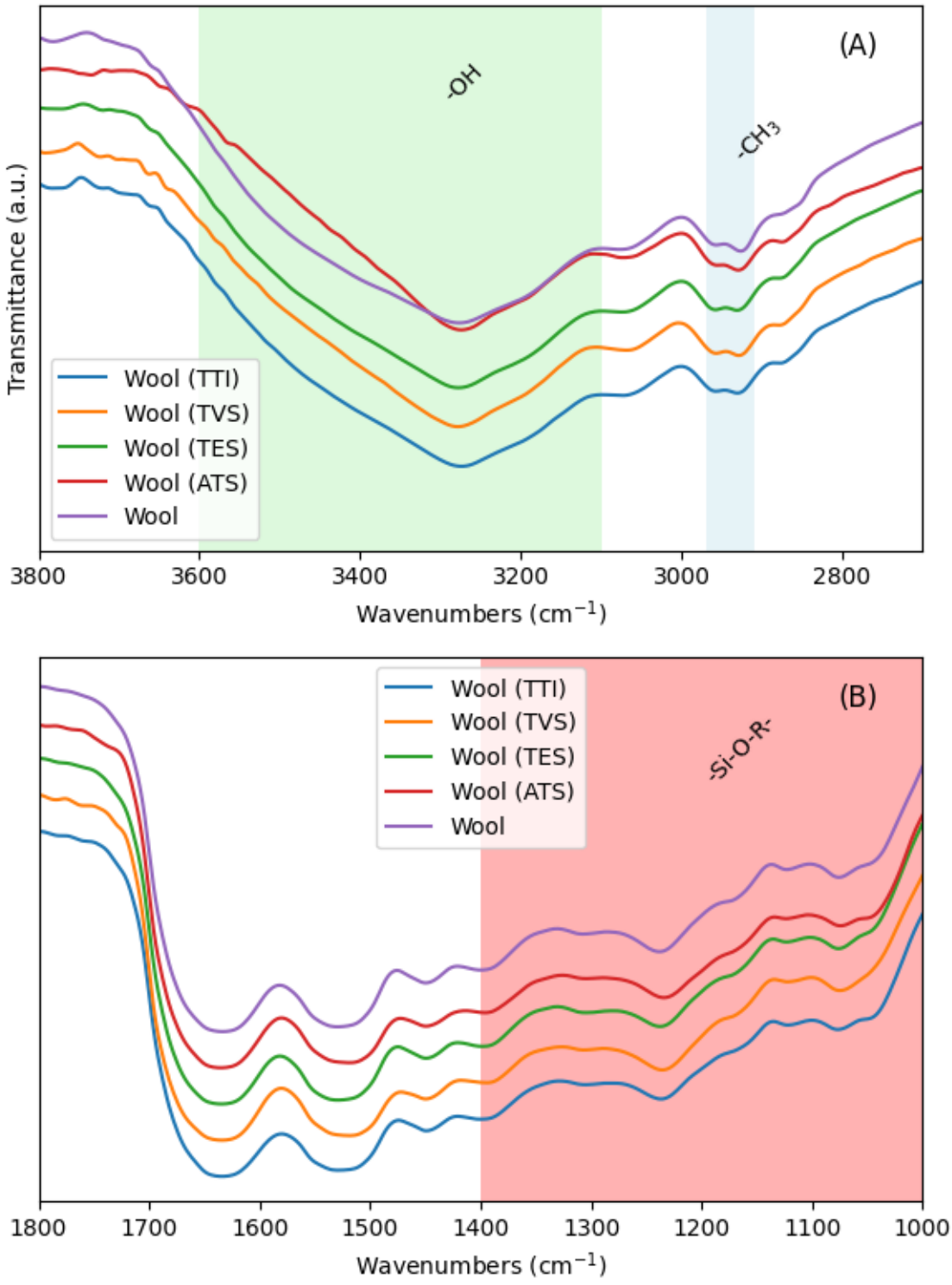

Figure 38 Focused FTIR spectra of examined formulations: A) hydroxyl and methyl groups, B) silicon compounds.

Thermogravimetric analysis (TGA) was performed on wool fibers prior and after modification, with the results presented in Figure 39 showing both the TGA curve and its first derivative. The initial mass loss stage appears around 100 °C, corresponding to water evaporation. As noted by Xie et al. [208], the thermogravimetric measurement of

wool fiber shows up to 250°C mass changes resulting from volatilization of moisture and perspiration in the wool fiber. Additionally, a temperature of 250°C is considered the temperature of the initial processes of thermal degradation of keratin, the core histological component of wool fiber. [60] Water molecules are appearing in the samples as wool fibers' natural tendency to absorb moisture. Variations in this temperature point between samples can be credited to differing levels of humidity absorbed on the wool surface. Additionally, the wool fiber modification process was carried out in both aqueous and organic solvent environments, what acts as a potential source of the molecules. Despite drying the fibers after modification, small amounts of residual molecules may still desorb from the wool fibers during the initial stages of the thermogravimetric analysis.

Additionally, neither the TGA nor DTG curves exhibit any changes between 136 and 185 °C, corresponding to the minimum boiling point of the used coupling agents and the processing temperature, respectively. The absence of changes in this range indicates that both untreated and treated wool can be utilized as reinforcement and manufactured under the chosen (180 °C) conditions. Moreover, since no substantial mass loss is spotted at temperatures up to 250 °C, these types of reinforcement may also be suitable for use with other thermoplastic polymers, among others polyethylene or polypropylene. Concerning intensive wool fiber decomposition observed around 300°C and 570°C, no clear tendency in decomposition was observed between untreated and treated wool fibers. From a decomposition kinetics point of view, silane or titanium-based coupling agents should cause higher activation energy for thermal decomposition, suggesting decomposition in higher temperatures, but such an effect was not spotted. That could result from low coupling agent concentration causing a minor impact on the occurrence of thermal effects in the considered temperature range. Gashti et al. [60] have concluded that colloidal clay dispersion treatment of wool fiber resulted in the shift of mass loss into higher temperatures than untreated wool fibers. Such shift was explained by higher heat resistance and heat insulation effect, as the particle created due to surface treatment played the role of a mass transport barrier.

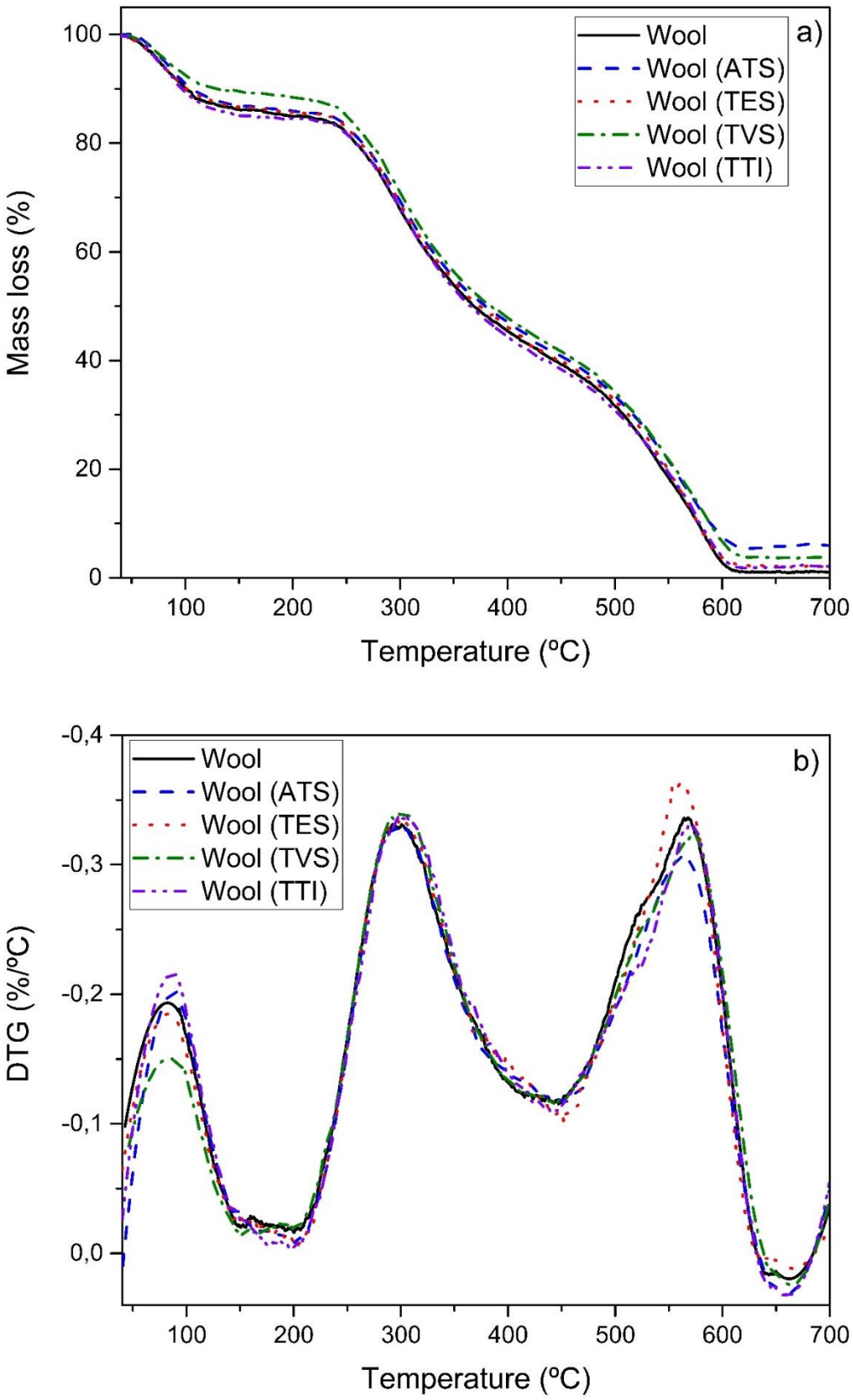

Figure 39 The a) TGA and b) DTG of unmodified wool and modified wool fibers with ATS, TES, TVS and TTI.

In the 600–700 °C temperature range, differences in the residual mass between unmodified and modified wool fibers become apparent. At this stage, the mass stabilizes for all wool types, indicating decomposition of organic matter in full. This stability enables the evaluation of additional inorganic content present in the modified wool samples. The TES-treated wool exhibited the lowest increase in inorganic matter, ranging from 0.98% to 1.08% compared to unmodified wool, while the ATS-treated wool showed the highest increase, between 4.57% and 4.92%. These changes indicate the introduction of silicon and titanium-based compounds through the modifications made.

1.2. Mechanical assessment

The tabular summary of the mechanical characterization data for the materials is presented in Table 6 :

Table 6 Tensile, flexural, hardness, and impact resistance properties of PLA-wool FRP

	Tensile Properties			Flexural properties		Impact resistance	Hardness
Formulation	Tensile strength (MPa)	Young's modulus (MPa)	Elongation at break (%)	Maximum resistance (MPa)	Flexural modulus (MPa)	Charpy's impact energy (kJ/m^2)	Shore D
PLA-MLO	54.1±1.5^{a}	1816±283^{a}	6.8±1.1^{a}	27.4±2.5^{a}	3216±131^{a}	27.4±2.5^{a,c}	81.4±2.1^{a}
PLA-MLO-Wool	36.5±1.5^{b}	1712±64^{a}	21.2±5.1^{a,b}	17.4±1.9^{b}	3206±75^{a}	17.4±1.9^{b}	74.2±0.8^{b}
PLA-MLO-Wool (ATS)	39.5±1.3^{c}	1903±201^{a}	36.4±7.8^{b}	18.6±5.2^{b,c}	3139±132^{a}	18.6±5.2^{b}	79.6±0.5^{a,c}
PLA-MLO-Wool (TES)	41.6±1.8^{c}	1723±340^{a}	34.0±11.5^{b}	23.6±5.2^{c,d}	3053±115^{a}	23.6±5.2^{b,c}	77.0±1.6^{c}
PLA-MLO-Wool (TVS)	41.8±1.3^{c}	1923±216^{a}	25.2±11.2^{b}	20.1±3.6^{d}	3220±25^{a}	20.1±3.6^{b}	80.4±1.3^{a}
PLA-MLO-Wool (TTI)	40.9±1.2^{c}	1947±129^{a}	32.4±9.5^{b}	19.0±2.0^{d}	3181±33^{a}	19.0±2.0^{b}	81.0±1.2^{a}

$^{a-d}$ Different letters within the same property show statistically significant differences between formulations ($p < 0.05$).

According to tensile properties results, shown in Table 6, PLA modified with a plasticizer (PLA-MLO) has significantly higher resistance ($p < 0.05$) compared to other FRP, treated and unmodified wool. This is the opposite observation; nevertheless, PLA-MLO-Wool presents lower resistance than silane and isopropoxide-treated wool materials. The Young's modulus, in all studied materials, presents comparable values (values are not significantly different, $p > 0.05$). However, there is a visible increase in FRP containing coupling agents ATS, TVS, and TTI, a decrease in the materials with unmodified wool fibers and with wool treated with coupling agent TES. A similar effect has been observed for epoxy resin with basalt fibers [175] or epoxy resin with jute additive [209], where surface-modified fibers showed higher tensile strength or Young's modulus. Comparing the results in the tensile properties of materials with treated wool with the PLA-MLO-Wool formulation, it is possible to confirm that the fiber surface was modified, and therefore, treated wool fibers interact better with the polymer matrix. The bibliography attributes this interaction to the silane or alkoxide bonds [209].

On the other hand, if the values of elongation at break are compared (Table 6), it is possible to see a significant improvement of the FRP with treated wool provided by the coupling agents (values are significantly different, $p < 0.05$). Even though MLO plasticizer is known for its positive effect on ductile properties [168], conferring a 6.8% elongation at break to PLA-MLO, the incorporation of 1 phr of unmodified wool increases about 15% more in elongation of the material. Similar values of this property are obtained with silane-modified wool for PLA-MLO-WC. Besides, the other modified wool materials (obtained with coupling agents ATS, TES, and TTI) present the highest elongation at break values (34% on average). In addition, the standard deviation of the values of this property reveals that the wool FRP could not present much homogeneity compared to the PLA-MLO, and the statistical analysis shows that there are no significant differences, $p > 0.05$, in the elongation at break of the materials that contain wool. Similar behavior and improvements concerning elongation have been observed in PLA FRPs containing bamboo fibers after alkali surface treatment [210].

Regarding the entire tensile properties, surface treatment with each coupling agent studied (ATS, TES, TVS, and TTI) improves the wool FRP properties concerning unmodified wool material (PLA-MLO-Wool) and the matrix PLA-MLO, being the PLA-MLO-Wool(TTI) (which contains the titanium (IV) (triethanolaminate)isopropoxide) the material that presents the highest combination of tensile properties. It shows that alkoxide coupling agent either provides a stronger bond between wool and PLA or has better reactivity than silane coupling agent.

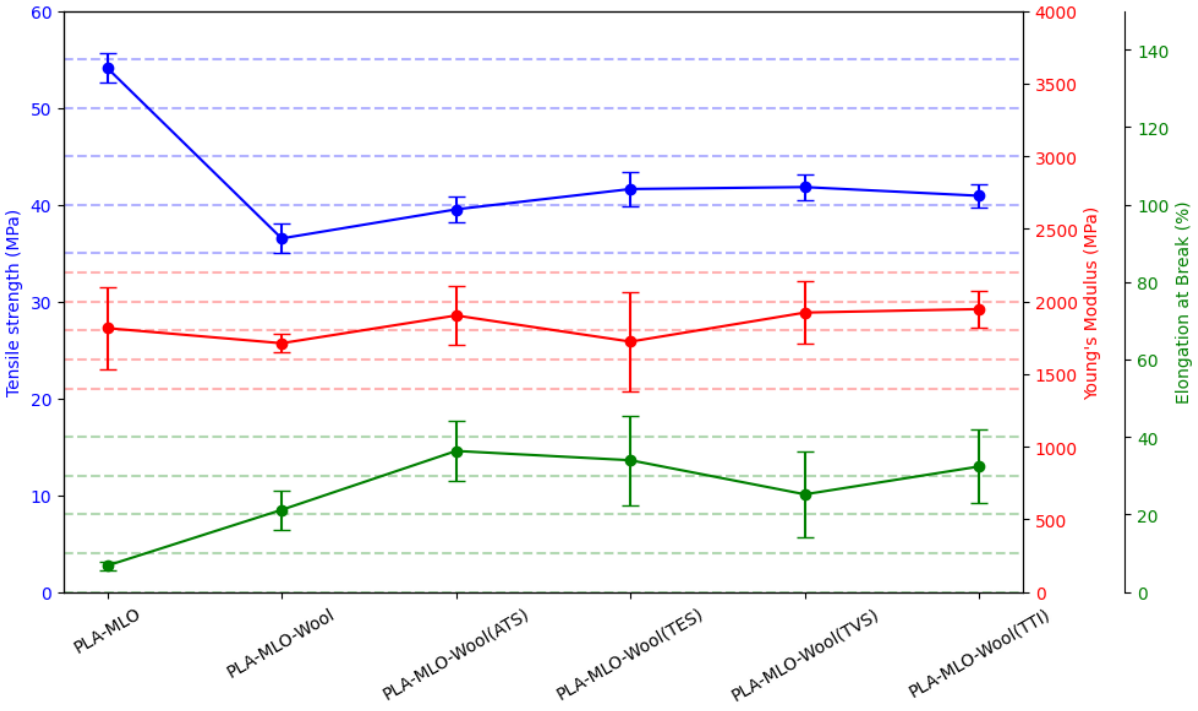

Figure 40 Tensile properties across evaluated formulations

As shown in Figure 40, the graphics shows how tendencies across evaluated formulations changes for all tensile properties. It is easy to spot that once PLA-MLO blend is modified with any type of wool fiber, its tensile strength and elongation at break changes, where Young modulus remains at comparable level. In such way that corresponds to ANOVA analysis specified in Table 6, where relevant ($p < 0.05$) changes were observed between PLA-MLO with wool reinforced formulations for tensile strength

and the elongation, as well between PLA-MLO-Wool with remaining surface modified formulations.

Regarding flexural properties, results in Table 6 show that the tendency of these properties is similar to those from tensile properties, of which the PLA-MLO presents the highest flexural strength of all the studied materials. In this property, all values are significantly different. In addition, the samples containing unmodified wool (PLA-MLO-Wool) exhibit lower flexural resistance than those materials with modified wool. The most significant improvement, compared to unmodified wool FRP, was notified in PLA-MLO-Wool (TES) samples, which were treated with trimethoxy [2-(7-oxabicyclo[4.1.0]hept-3-yl)ethyl]silane. Indeed, a positive impact on flexural strength, attributed to silane even in low coupling agent concentration, was observed for epoxy resin containing modified jute [209] or basalt fibers [22]. On the other hand, the flexural modulus presents similar values in all the material studied groups. No significant effect ($p > 0.05$) of wool or treatment with coupling agents was observed in the values of this property.

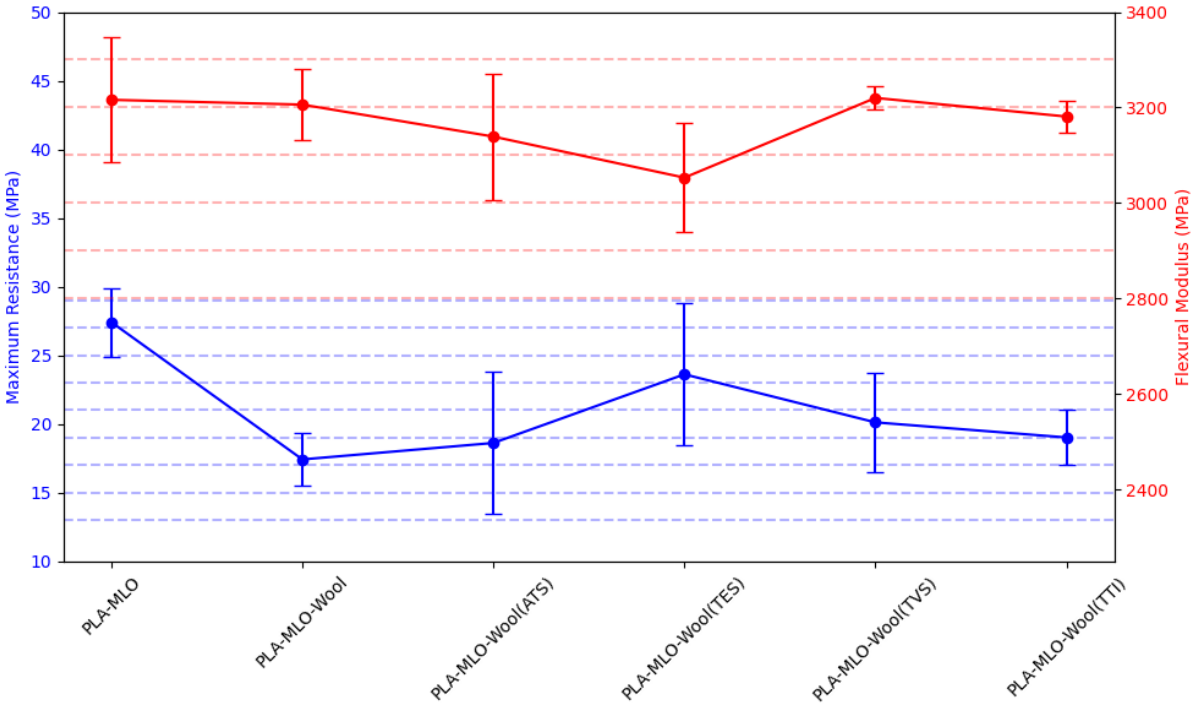

Figure 41 Tendencies in flexural properties across evaluated formulations

Changes across tested formulations for flexural properties were shown in Figure 41. As based on ANOVA analysis there were no significant changes in the flexural modulus across considered materials and irrespective of applied modification of PLA/MLO matrix, the modulus remains constant. However, several significant changes were spotted between PLA/MLO formulation and wool reinforced materials. In general, PLA/MLO reinforcement with wool fiber causes reduced flexural resistance, especially when unmodified wool is applied. Such finding was supported by ANOVA analysis, which results are specified in Table 6. Furthermore, surface treatment helped to mitigate the negative impact, showing for TES, TVS and TTI significant improvement in flexural strength compared to PLA/MLO-Wool. Although ATS modification on average improved

the strength, based on ANOVA analysis the change was not significant, most probably due to high standard deviation of obtained results for PLA/MLO-Wool (ATS).

Charpy's impact energy values, reported in Table 6, reveal the same tensile and flexural properties behavior. This means that the highest impact resistance of all the materials groups is observed for PLA-MLO, which is significantly different from all the wool FRP materials, except for the PLA-MLO-Wool (TES). Meanwhile, this property's highest value is detected in PLA-MLO-Wool (TES) among the materials containing wool. It is already known that modification of the PLA matrix with MLO is prone to increase impact resistance [168]. However, wool fibers offer a negative impact response, decreasing the property to about 10 J/m^2 compared to the PLA-MLO sample.

Nevertheless, wool surface treatment with coupling agents allowed the samples to absorb more energy (1.2 up to 6.2 J/m^2, respectively) than the FRP with unmodified wool (PLA-MLO-Wool). A similar effect of silane coupling on impact resistance was observed for epoxy resin with basalt fiber, although the effect between PLA and wool is significantly lower than the resin and inorganic basalt fiber [211]. Such behavior occurs because the coupling agents provide a better load transfer from the polymer matrix to the fiber [22].

Finally, regarding hardness values reported in Table 6, the tendency of the effect of treated and unmodified wool remains like the other mechanical properties previously discussed. In other words, coupling agent treatment positively affects the FRP properties. In this case, PLA-MLO-Wool (TTI) and PLA-MLO present the highest values of hardness, which are significantly different ($p < 0.05$) from PLA-MLO-Wool. Hardness results present a similar change tendency compared to the tensile test's maximum resistance values.

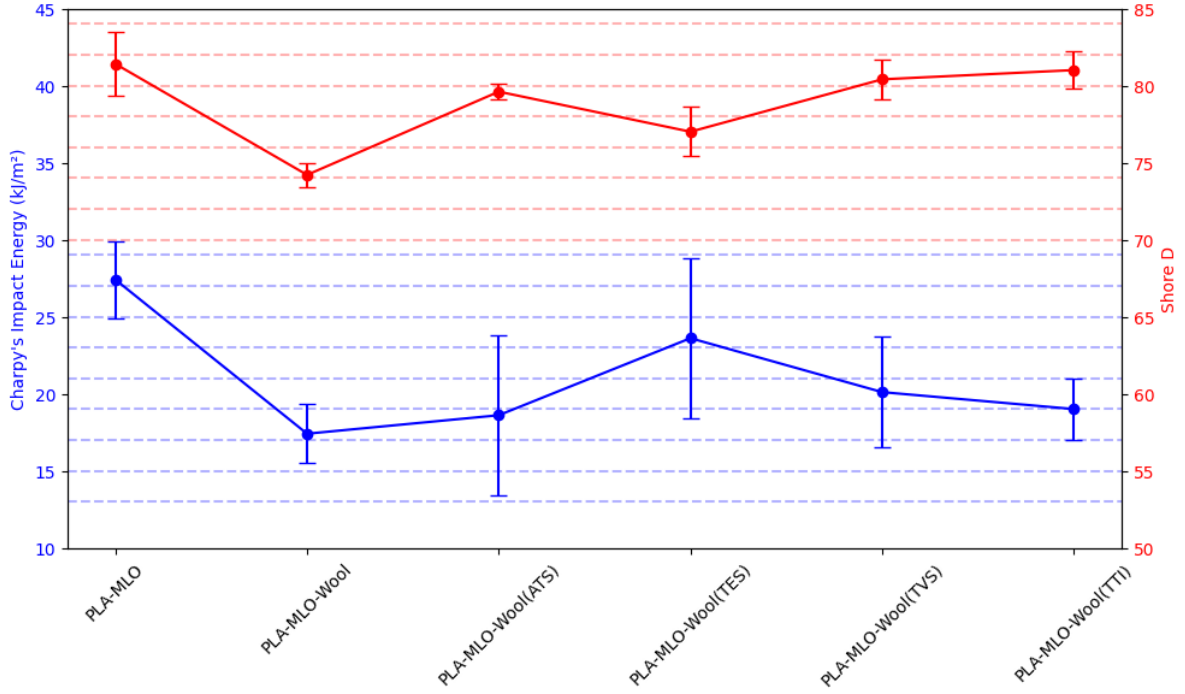

Figure 42 Tendencies in hardness and impact properties across evaluated formulations

Finally the Figure 42 have shown how the tendencies in impact properties and hardness change across evaluated formulations. As in general use of wool fibers for PLA-MLO blends have caused reduced impact resistance, the formulation were TVS treatment was applied have shown lower negative impact of wool fiber on the property reduction. Additionally, as due to ANOVA results provided in Table 6, both PLA-MLO and PLA-MLO-Wool (TVS) blends are placed in same significance group. However taking into consideration all examined formulations it is clear, that wool fiber presence have reduced impact resistance of material and application of various treatments have helped to mitigate the negative effect. Similar observations can be concluded from comparison of hardness results, where across all tested formulations PLA-MLO blend have show highest hardness across the formulations. Similarly, a significant difference in hardness was observed for modification with unmodified wool fiber in the PLA-MLO-Wool. However, in case of reinforcement with silane treated wool, a majority of evaluated treatment compensated the negative effect of neat wool reinforcement showing no significant difference in hardness comparing to PLA-MLO for materials were silane treatment was applied using ATS, TVS or TTI.

Figure 43 shows the typical stress-strain curves of all the formulated materials; however, the corresponding toughness values (T) are shown in Figure 44. Regarding the stress-strain curves, it is possible to notice that the coupling agent A interacts better with the PLA–MLO–wool system. Therefore, the toughness of the PLA–MLO–Wool (ATS) is the highest of all the reported materials. Moreover, PLA–MLO–Wool (TVS) reports lower values of the toughness of all treated materials. Nevertheless, its values are 200% higher than PLA–MLO and 22% higher than PLA–MLO–Wool, which refers to increased ductility of the materials due to the coupling agents' modifications [195].

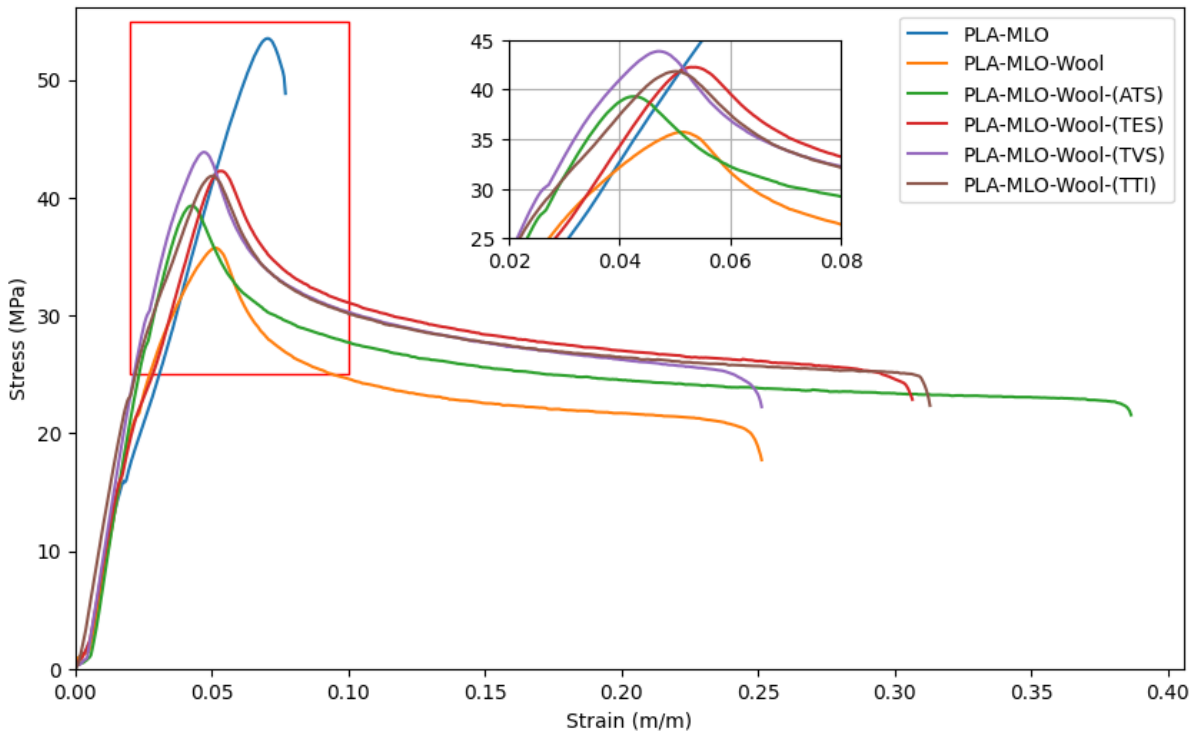

Figure 43 Stress-strain curves of PLA–wool FRPs

As shown in Figure 44 the toughness of all formulations enhanced significantly compared to the PLA–MLO and PLA–MLO–Wool formulations. All values exhibit statistically significant differences ($p < 0.05$), except for PLA–MLO–Wool (TES) and PLA–MLO–Wool (TTI). This suggests that all the studied coupling agents play an active role in the PLA–MLO and wool-based fiber-reinforced polymer (FRP), confirming effective fiber surface modification and improved compatibility, as reflected in the mechanical properties. Notably, even untreated wool fibers contributed to an improvement in toughness compared to the PLA–MLO matrix alone.

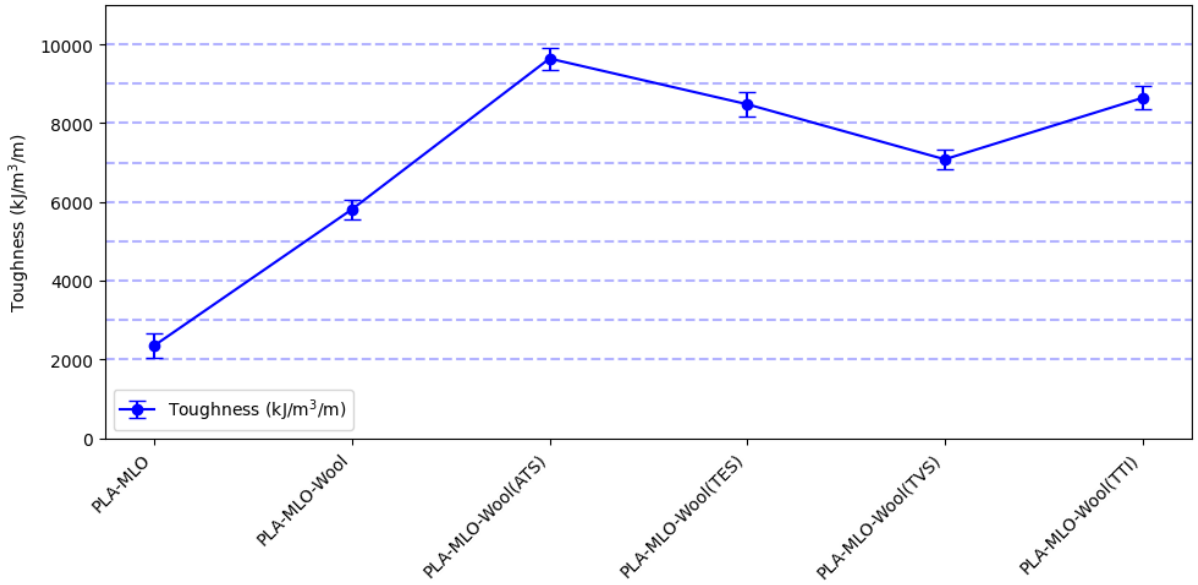

Figure 44 Toughness comparison of tested formulations

The toughness, as a surface measured under stress-strain curves provides single-value, comprehensive indication of tensile properties, showing beneficial impact of wool fiber reinforcement and wool fiber treatment for tensile properties. On Figure 44 is presented tendency in the toughness across examined formulation and it is clear that modification with wool fiber improves toughness of the material. Furthermore, applying silane treatment further enhances the improvement, although the improvement level differentiate between each silane treatment type. However, all examined surface modification have shown that the modification is effective as it increases clearly toughness even corresponding to PLA-MLO-Wool, where neat wool fiber was applied.

1.3. Thermal properties

In the Table 7 are presented the results derived from the TGA and DSC analyses, while Figure 45 illustrates the thermogravimetric graphs for all the formulations studied. All of the formulations exhibited a single step degradation, occurring at temperatures above 300 °C. For the PLA–MLO blend, the temperature at which 5% mass loss occurred (T_5) was observed at 327 °C. The addition of unmodified wool did not significantly alter

the thermal characteristics, as no notable cahnges were observed in the temperatures across all samples, as indicated in Table 7. This behavior is consistent with findings in the literature for PLA systems reinforced with nanocellulose [113] or PLA filled with nanochitin [169] and petroleum-based polymer systems such as PVC modified with lignin, where no sign of degradation was observed below 200°C. These results confirm the applicability of bio-based additives to various polymers based on the thermal stability criteria. However, wool treatment with coupling agents tends to reduce the T_5 temperature in reference to PLA–MLO–Wool, suggesting slightly reduced stability in the fiber-reinforced polymer (FRP), although the differences are not statistically significant. The lowest temperature of 5% mass loss was obtained for PLA–MLO–Wool (TVS).

Table 7 Thermal properties of PLA-wool FRP studied materials.

	TGA evaluation				DSC evaluation			
Formulation	T_5 (°C)	T_{max} (°C)	Mass loss at 300 °C (%)	Mass loss at 350 °C (%)	T_g (°C)	T_{cc} (°C)	T_m (°C)	X_c (%)
PLA-MLO	327.2±0.4[a]	364.9±2.5[a]	2.8±0.2[a]	21.6±0.6[a]	60.7±0.6[a]	105.5±1.2[a]	170.6±0.9[a]	19.9±0.9[a]
PLA-MLO-Wool	327.0±1.8[a]	366.4±2.6[a]	1.9±0.6[a,b]	23.2±1.9[a]	58.6±1.0[a]	105.2±0.5[a]	168.1±1.2[a]	19.2±1.3[a]
PLA-MLO-Wool (ATS)	325.3±1.1[a]	365.9±3.3[a]	1.7±0.4[b]	22.5±0.9[a]	60.1±1.0[a]	111.5±2.0[b]	169.7±0.7[a]	16.7±0.7[b]
PLA-MLO-Wool (TES)	326.8±0.7[a]	366.9±1.9[a]	2.6±0.3[a,b]	21.0±1.2[a]	60.2±1.0[a]	111.3±0.5[b]	170.1±0.5[a]	16.4±0.8[b]
PLA-MLO-Wool (TVS)	324.2±1.6[a]	365.9±0.3[a]	2.4±0.4[a,b]	23.1±1.4[a]	60.4±1.4[a]	111.6±2.5[b]	170.3±1.4[a]	16.1±0.5[b]
PLA-MLO-Wool (TTI)	324.9±1.2[a]	356.9±2.6[a]	1.7±0.2[b]	32.9±5.7[b]	60.2±1.0[a]	110.2±0.6[b]	169.8±0.6[a]	17.5±0.6[b]

[a-b] Statistically significant differences between formulations are indicated by different letters within the same property ($p < 0.05$).

Regarding the temperature of most intensive degradation (T_{max}), as stated in Table 7 and illustrated in Figure 45b, the TTI coupling agent is observed to reduce the thermal stability among all studied formulations, resulting in a T_{max} approximately 10 °C lower than the other formulations. However, these differences are not statistically significant ($p > 0.05$). The PLA–MLO matrix and all wool-containing formulations exhibit similar T_{max} values, ranging between 364 and 367°C.

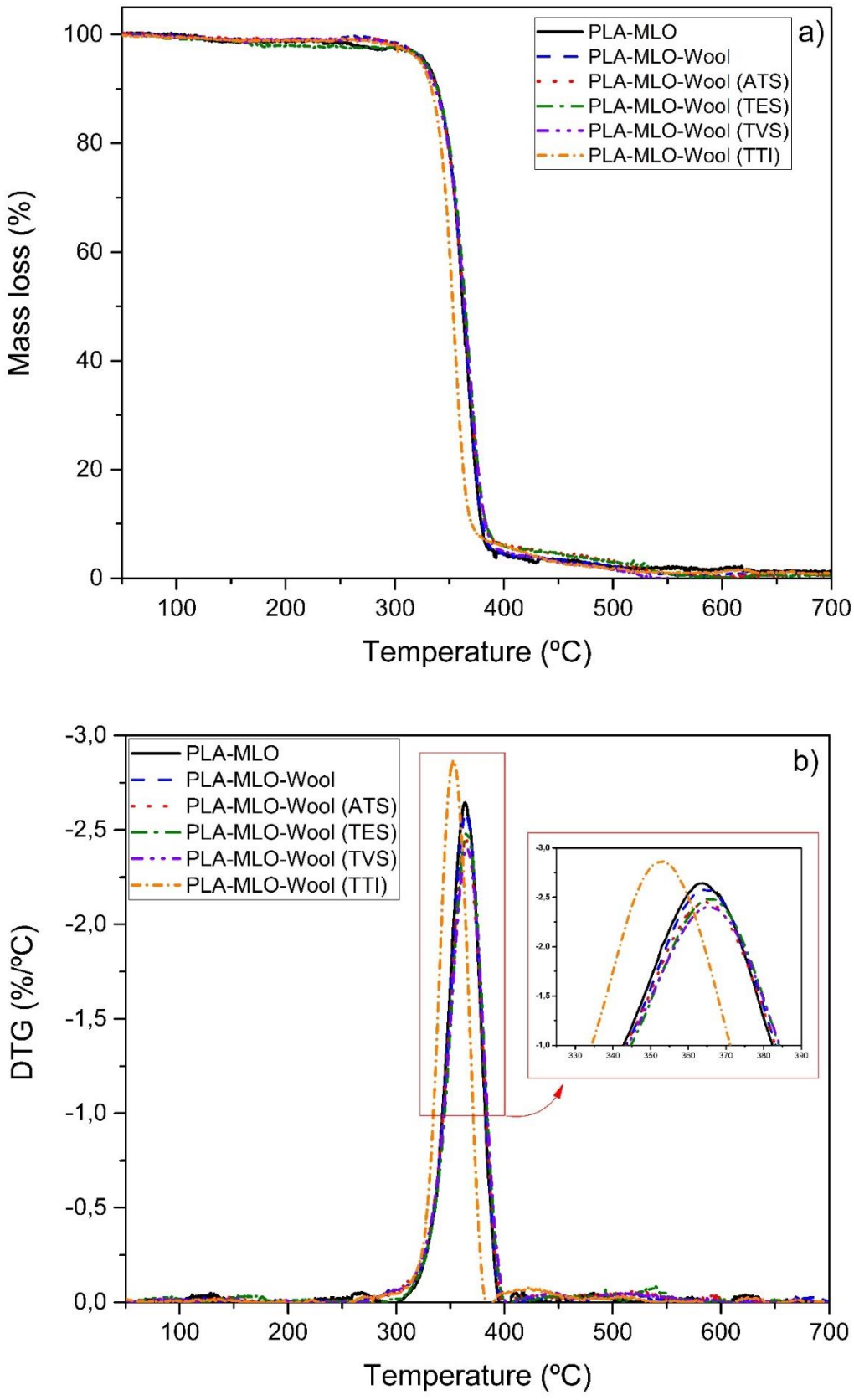

Figure 45 (a) TGA and (b) DTG curves of PLA-wool FRP

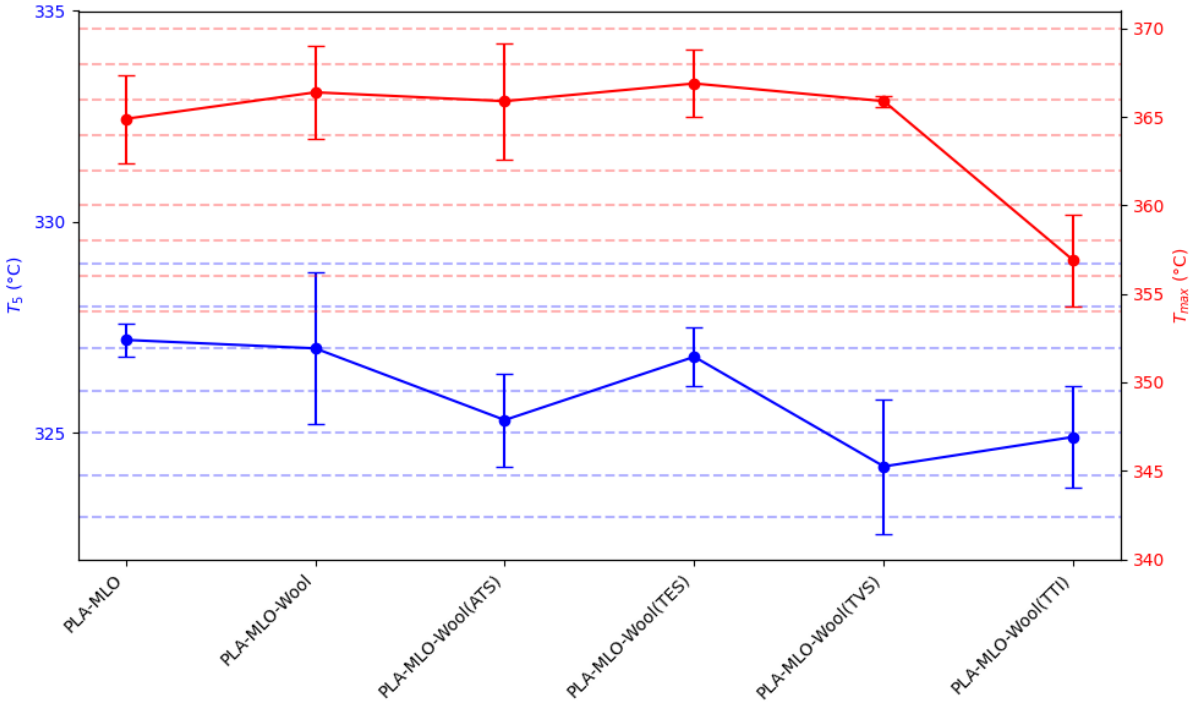

Figure 46 T_5 and T_{max} comparison for evaluated formulations

Based on a comparison across tested formulations shown in Figure 46, for the 5% mass loss temperature (T_5) although slight reduction of the temperature is observed, especially for formulations were ATS, TVS and TTI treatment were applied, from statistical point of view such reduction is not significant, especially as the mass loss occurs in temperatures higher than material processing temperature range. Similarly, the temperature of maximum mass loss (T_{max}) does not change after reinforcement of PLA/MLO matrix. Although for TTI modification lower T_{max} was observed, the result remains at similar temperature level as formulations with other surface coupling agents. Therefore, although minor changes in the 5% mass loss temperature and temperature of maximum mass loss are observed, in general the temperature remains constant, as confirmed by ANOVA analysis with results specified in Table 7.

Interpreting the mass loss at a specific temperature (300 and 350 °C), summarized in Table 7, it can be observed that at 300 °C, the PLA–MLO formulation exhibited the fastest degradation, with a mass loss of 2.8%. In contrast, the lowermost mass loss in the specified temperature was recorded for PLA–MLO–Wool, PLA–MLO–Wool (ATS), and PLA–MLO–Wool (TTI), indicating that both wool fibers ,irrespectively if surface modification was applied, enhanced the thermal stability of the FRPs during PLA decomposition. Materials modified with the TES and TVS coupling agents displayed similar behavior to PLA–MLO, with no significant differences observed. At 350 °C, the mass loss was comparable across all formulations, excluding PLA–MLO–Wool (TTI), which showed a statistically significant change from the remaining formulations, with a mass loss exceeding 30%, compared to 21–23% for the other systems. This outlines the reduced thermal stability in the TTI-treated formulation. Conversely, the formulation with wool modified with the TES coupling agent demonstrated slightly greater stability at 350 °C, with a mass loss of 21%.

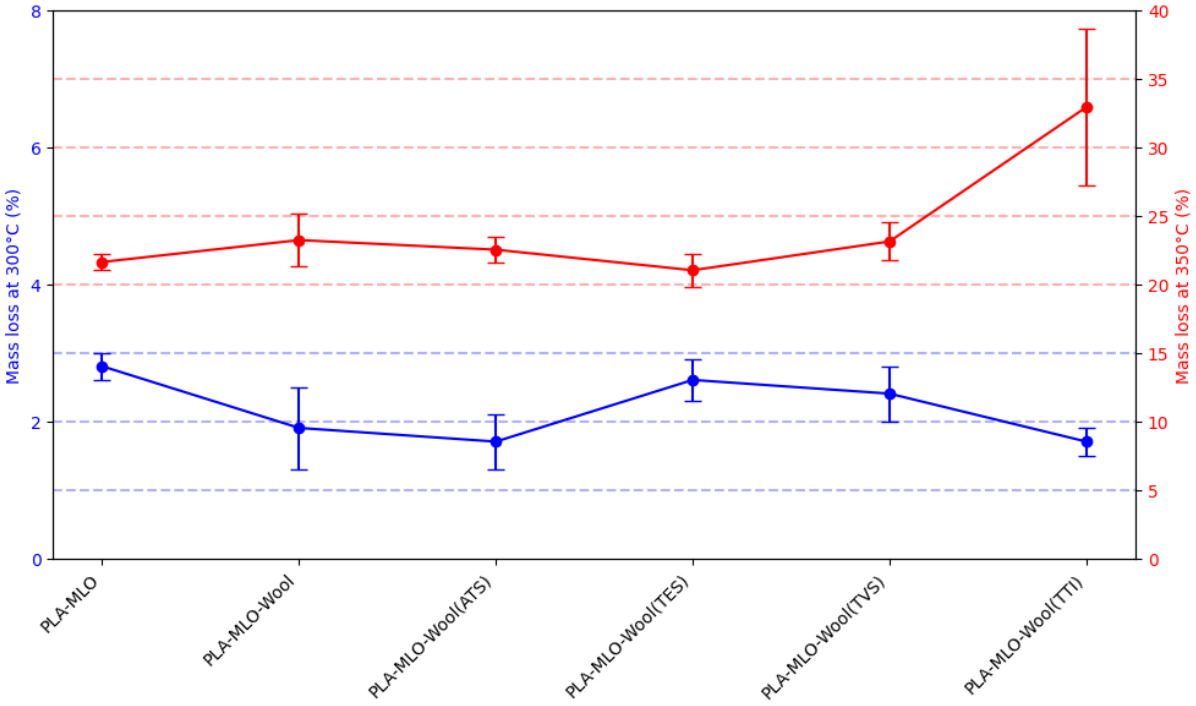

Figure 47 Mass loss comparison for evaluated formulations

As shown in Figure 47, in general minor changes in are spotted for mass loss at specified temperatures, especially at 300°C. As the mass loss results remain constant across the tested formulation, similarly to prior described temperatures of mass loss, for the TTI surface treatment the change was evident at 350°C. Combined, it was possible to observe that in test conditions presence of TTI resulted in slightly faster material decomposition. However, from processing and material applications point of view such property has low impact.

Regarding the DSC analysis, Table 7 presents the results for T_g, T_{cc}, T_m, and X_c for the studied materials, while Figure 48 displays the DSC thermograms. The combination of wool into the FRP and subsequent modifications with coupling agents do not affect the glass transition temperature (T_g) of PLA–MLO, as T_g values remain consistent across all formulations, with no statistically significant differences ($p > 0.05$). A similar stability in T_g was concluded for PLA modified with basalt or carbon fibers [212]. However, PLA–MLO–Wool shows a slight decrease in T_g, approximately 2°C lower than the unmodified matrix. This shift may suggest a merged plasticizing effect of wool fibers and MLO within the PLA matrix, as previous studies have shown MLO reduces the glass transition temperature [168]. Additionally, a similar temperature reduction was linked to plasticization in PLA systems modified with limonene. For T_m, a similar trend to T_g is spotted, with the temperature values remaining comparable to those of PLA–MLO (approximately 170°C), with no significant changes among the formulations. However, a double melting peak is observed in formulations containing modified wool, likely due to the formation of imperfect small crystals that melt at lower temperatures, resulting in a secondary peak [213].

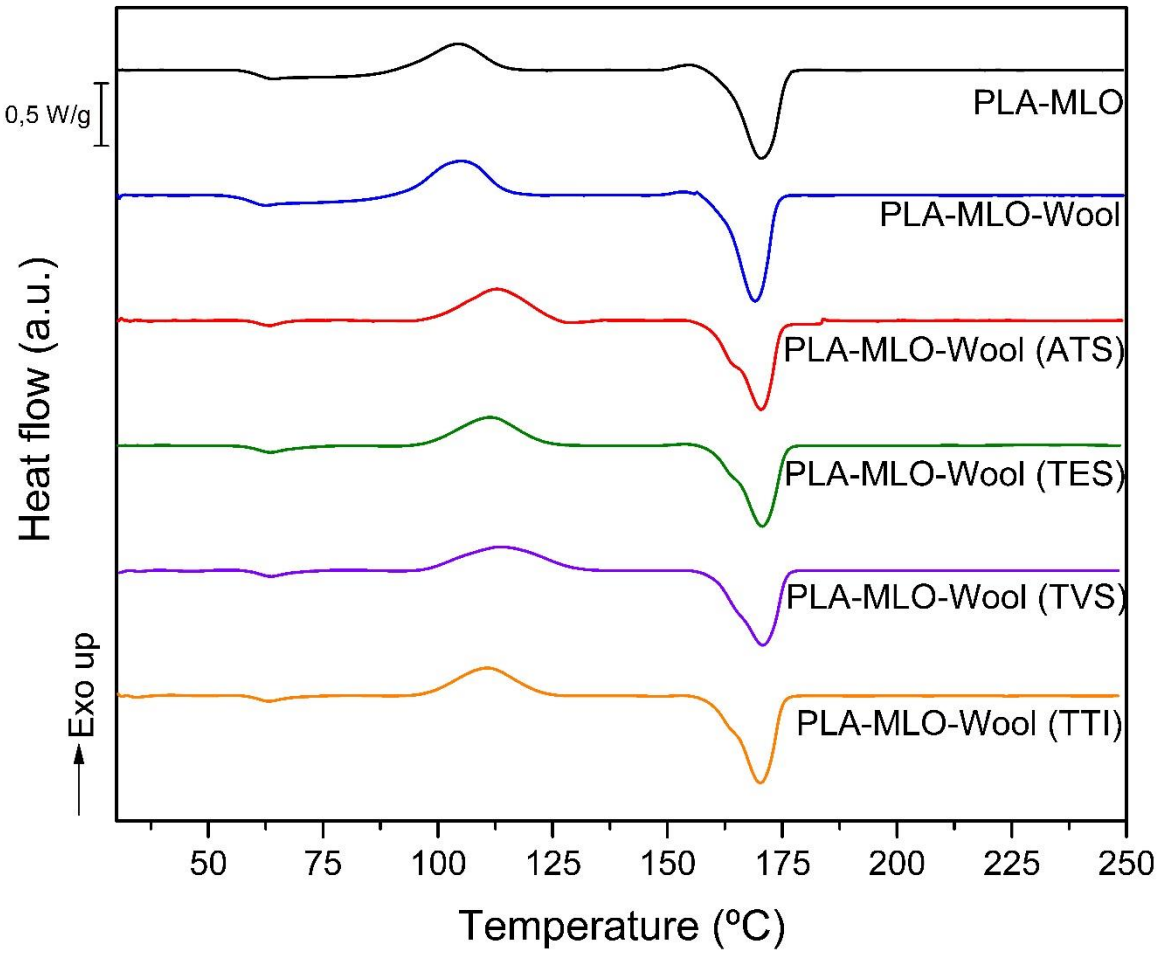

Figure 48 Differential scanning calorimetry (DSC) thermograms of PLA–wool FRPs

An evident effect on the cold crystallization temperature (Tcc) was observed in all composites reinforced with modified wool fibers. As shown in Figure 48 and detailed in Table 7, both PLA–MLO and PLA–MLO–Wool exhibit similar Tcc values (no significant differences, $p > 0.05$). However, the treatment of wool fibers resulted in an enhance in the temperature where peak has occurred, with values rising by 5 to 6 °C. This behavior is likely due to the wool modification, as coupling agents enhance the interaction between wool and PLA, affecting the crystalline regions of the PLA matrix and making cold crystallization more challenging. A similar effect has been reported in the PLA–PHB blend, where composites containing cellulose nanocrystals treated with an acid phosphate ester of ethoxylated nonylphenol also exhibited an increase in T_{cc} [113]. Additionally, X_c (%) values indicate a decrease in crystallinity for the wool formulations modified with ATS, TES, TVS, and TTI coupling agents. These values show significant differences among the formulations ($p < 0.05$).

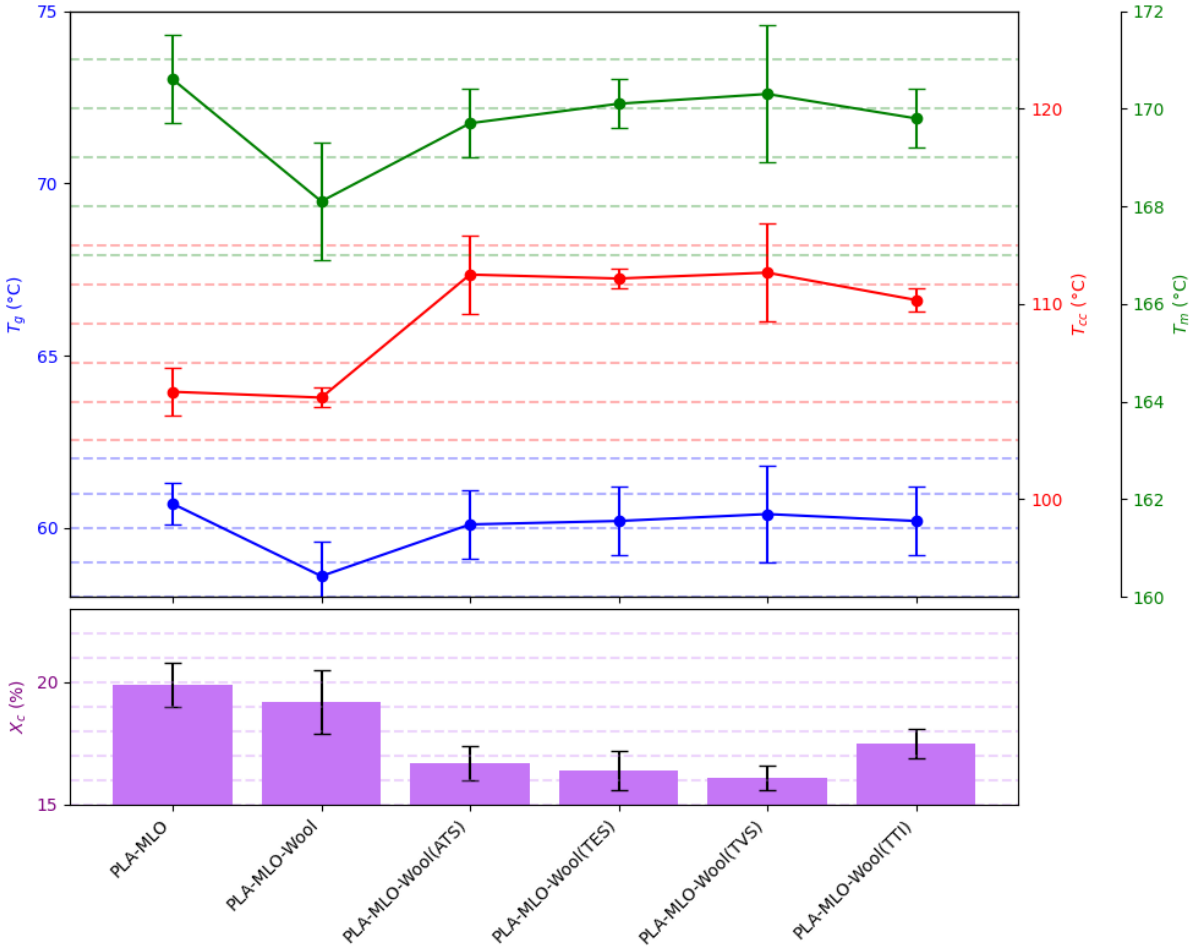

Figure 49 Comparison of DSC-derived material characteristics

As presented in Figure 49, a treatment of PLA-MLO with wool fibers, especially after treatment, alters thermal characteristics of PLA-based materials. In general, a treatment of PLA-MLO blend with untreated wool fiber have cause reduced glass transition and melting temperatures; however, application of surface treatment irrespective of its type among tested modifications, have mitigated the reduction allowing to maintain comparable temperature profile of material. As supported by ANOVA analysis presented in Table 7, the changes in the above-mentioned temperature are not significant as corresponding to the PLA-MLO blend. As previously mentioned, an application of silane and alkoxide treatments have resulted in increased temperatures compared to PLA-MLO-Wool formulations as so similar behavior was spotted for the cold crystallization temperature. However, in that temperature initial reduction after reinforcement of PLA-MLO blend with unmodified wool fibers was not observed, what have led to increase in the T_{cc} for formulations with applied surface treatment. The change appeared to be significant for all surface modifications, as obtained from the results of ANOVA analysis. Finally, a degree of crystallization of material was observed to reduce due to modification of PLA-MLO matrix. Although primarily modification of PLA-MLO blend with neat wool fiber resulted in not significant alterations, the treatment with surface agents have shown a significant reduction in the degree of crystallinity.

1.4. Dynamic Mechanical Analysis

The thermo-mechanical characteristics of the PLA–MLO–wool FRPs is illustrated in Figure 50, which shows the results of storage modulus (G') and the difference between the loss modulus (G'') and G', correspond to the tangent of the gap (tan δ), plotted against temperature. In Figure 50a, the storage modulus evolution for all formulations follows a similar trend. However, analyzing the initial portion of the curves reveals that the PLA–MLO formulation exhibits the lowest storage modulus among tested materials, followed by PLA–MLO–Wool (ATS) and PLA–MLO–Wool (TES). Materials treated with TVS and TTI coupling agents show improved storage modulus values compared to PLA–MLO–Wool, indicating a more elastic behavior up to 45 °C, which is linked to the presence of wool fibers in the FRPs. However, the surface treatment of wool fibers can either decrease or increase the elastic behavior compared to the unmodified PLA–MLO–Wool formulation.

Table 8 Tg temperature determined by DMA analysis from tan δ, wettability, and color measurements results of PLA-wool FRP materials

	DMA assessment	Wettability	Color		
Formulation	T_g from tan δ curve (°C)	Theta angle (°)	L*	a*	b*
PLA-MLO	64.4±0.5^{a}	66.9±3.8^{a}	43.57±0.36^{a}	-1.89±0.05^{a}	2.38±0.08^{a}
PLA-MLO-Wool	62.3±0.3^{b}	66.4±4.3^{a}	47.88±0.41^{b}	1.63±0.22^{b}	19.98±0.75^{b,c}
PLA-MLO-Wool (ATS)	63.7±0.3^{a}	77.3±5.8^{b}	48.36±0.07^{b}	1.23±0.15^{b}	21.32±0.17^{b}
PLA-MLO-Wool (TES)	63.9±0.4^{a}	76.9±1.2^{b}	48.23±0.38^{b}	0.21±0.06^{c}	19.54±0.30^{c}
PLA-MLO-Wool (TVS)	63.6±0.4^{a}	80.8±2.3^{c}	48.86±0.33^{b}	-0.03±0.04^{c,d}	17.21±0.26^{d}
PLA-MLO-Wool (TTI)	63.7±0.2^{a}	75.0±0.4^{d}	49.38±0.45^{b}	-0.36±0.05^{d}	18.05±0.34^{d}

a-d Statistically significant differences between formulations are indicated by different letters within the same property ($p < 0.05$).

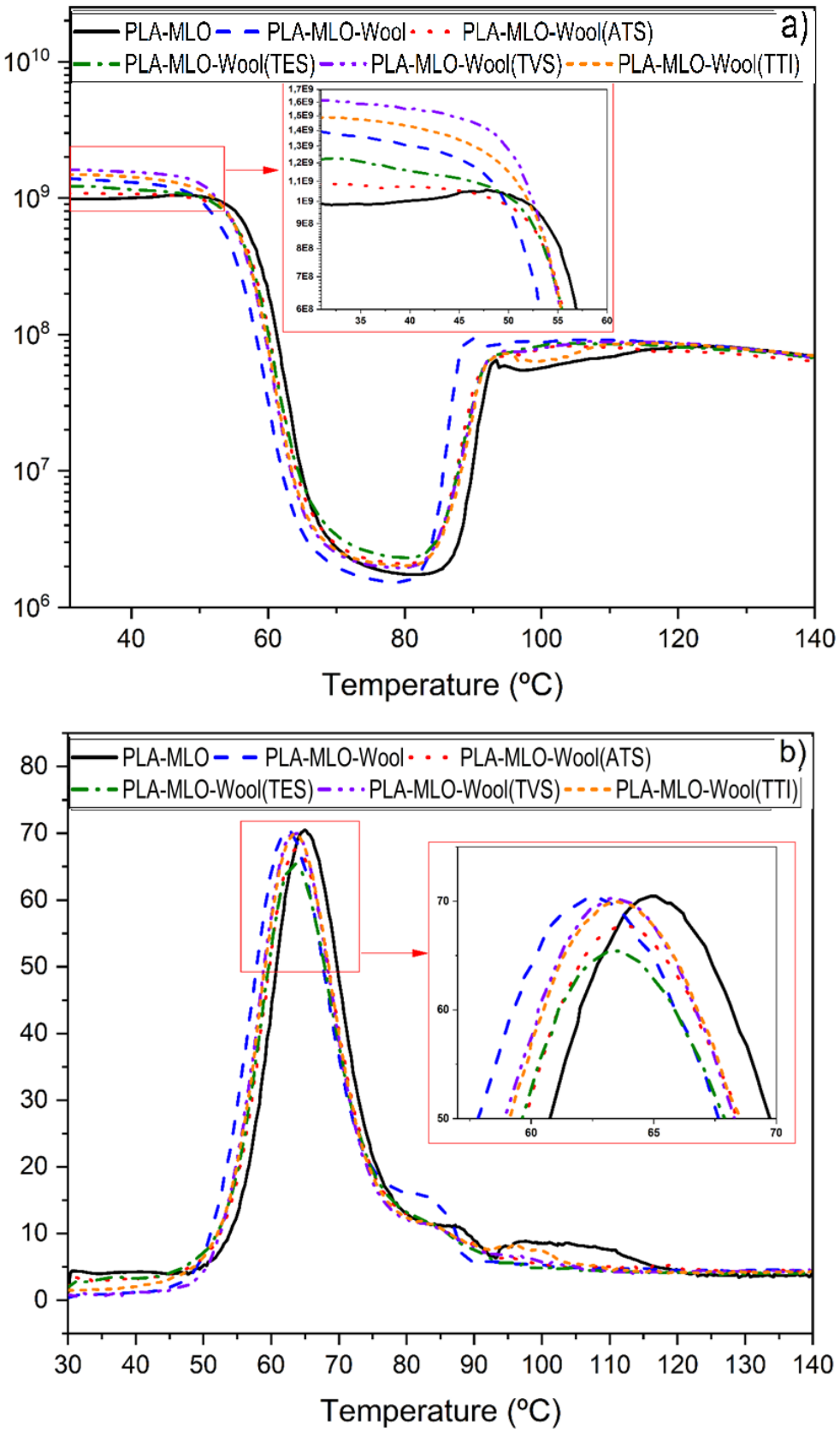

Figure 50 DMA graphs: (a) storage modulus and (b) loss factor for PLA-wool FRPs

Figure 50b illustrates the behavior of the loss factor versus temperature for the studied FRP materials. In the graph, the glass transition temperature (T_g) can be determined alternatively to DSC measurements, based on the peak of the curves. These T_g values are also listed in Table 8. The observed trend in T_g changes aligns with the previously discussed DSC results. Specifically, the incorporation of neat wool into the PLA–MLO system reduces the matrix's glass transition temperature, with significant differences observed between the values. In contrast, the wool systems modified with surface treatment show no significant differences ($p > 0.05$) in Tg compared to the matrix. The highest T_g was recorded for the PLA–MLO formulation at 64.4 °C. The addition of unmodified wool lowered this temperature by over 2 °C, indicating increased macromolecule mobility due to the plasticizing impact of MLO and wool in the PLA matrix [89]. Nonetheless, altering of the wool fibers with surface altering agents slightly heightened T_g compared to PLA–MLO–Wool, yielding temperatures between 63.6 and 63.9 °C.

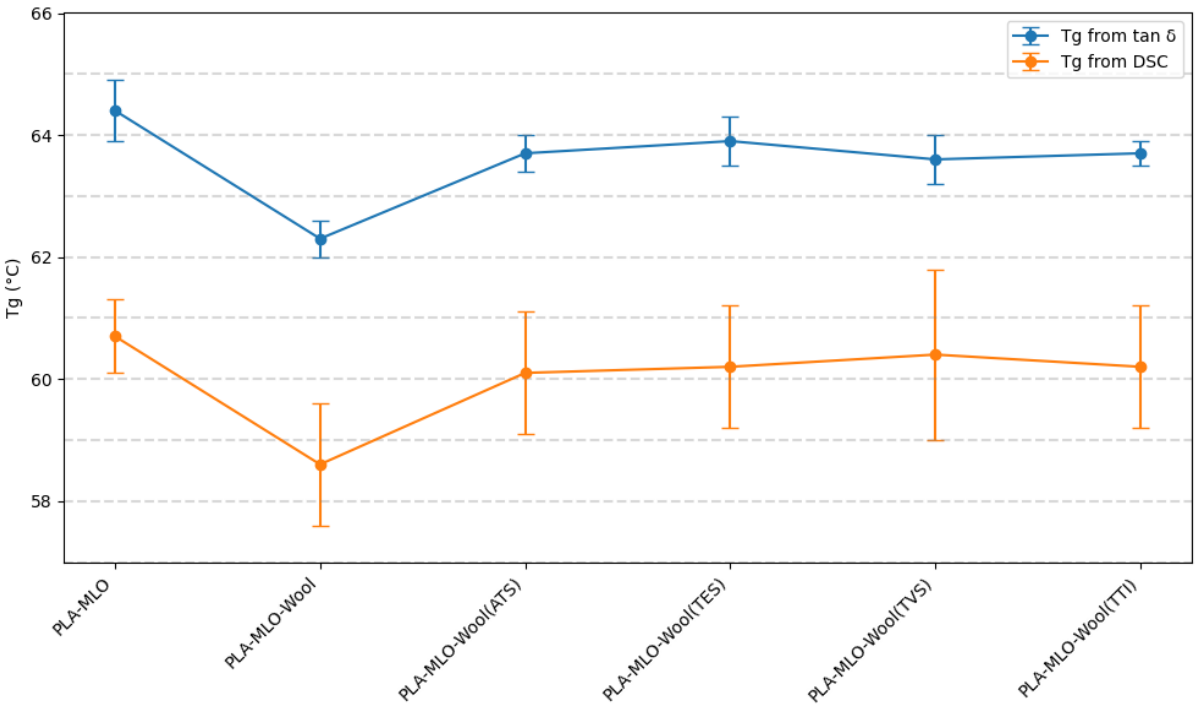

Figure 51 Comparison of glass transition temperature determined with DMA and DSC measurements

As the glass transition temperature was obtained based on two separate methods, a comparison of the results was shown in Figure 51 to visually present a comparison between both methods and across the tested formulations. In general, the results have shown similar behavior, where initial reduction in the glass transition temperature after reinforcement with wool fibers was mitigated by applying surface treatment. However, between both methods a certain shift in the obtained results was observed, which was an object of further analysis using Bland-Altman plot for data analysis.

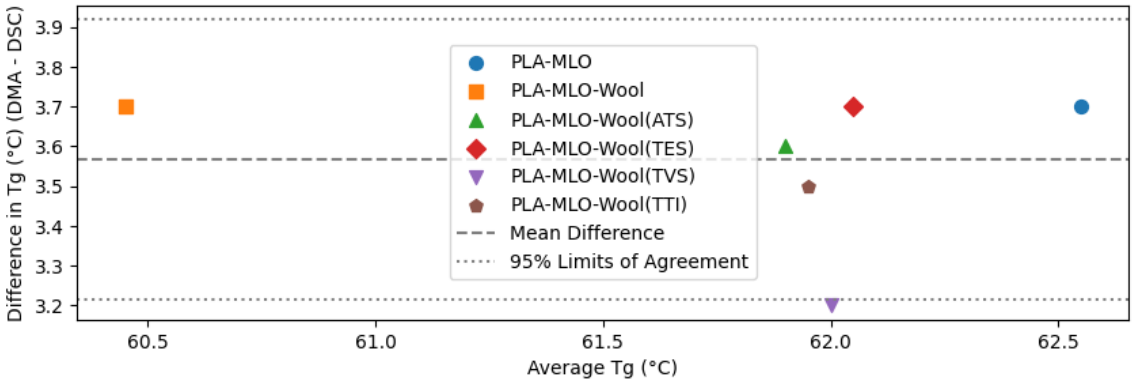

Figure 52 The Bland-Altman plot analysis of differences between DMA and DSC results across tested formulations.

Based on the plot shown in Figure 52 as the Bland-Altman plot, the glass transition temperature determined with DMA and DSC were compared. The diagram shows how, to various formulations, the average glass transition temperature refers to the difference in temperature derived from different methods. The analysis has shown that, on average, DMA shows a temperature around 3.6°C higher than that derived from the DSC measurement. However, across all tested formulations, based on standard deviation from measured temperatures, all samples fit into limits of agreement, and the bias between the two methods is constant. The same bias was observed for all tested formulations, although for the PLA-MLO blend with untreated wool fiber, average Tg was spotted at a lower temperature than the remaining formulations. Despite the bias between those measurements, results obtained with both methods are acceptable.

1.5. Microstructural properties

The microstructural characteristics of the prepared FRPs were examined using scanning electron microscopy (SEM). Figure 53 presents SEM images of the fractured surfaces for all studied materials. The images reveal favorable miscibility between PLA and MLO across all samples, although some domains of the MLO remain as a separate phase within the PLA matrix. These separate MLO phases can be observed in Figure 53 as spherical shapes (indicated by yellow arrows) [168]. The PLA–MLO formulation (Figure 53a) shows a continuous phase with no evident fractures, which aligns with the established understanding that the incorporation of MLO into PLA-based blends enhances material compatibility and miscibility [89,168].

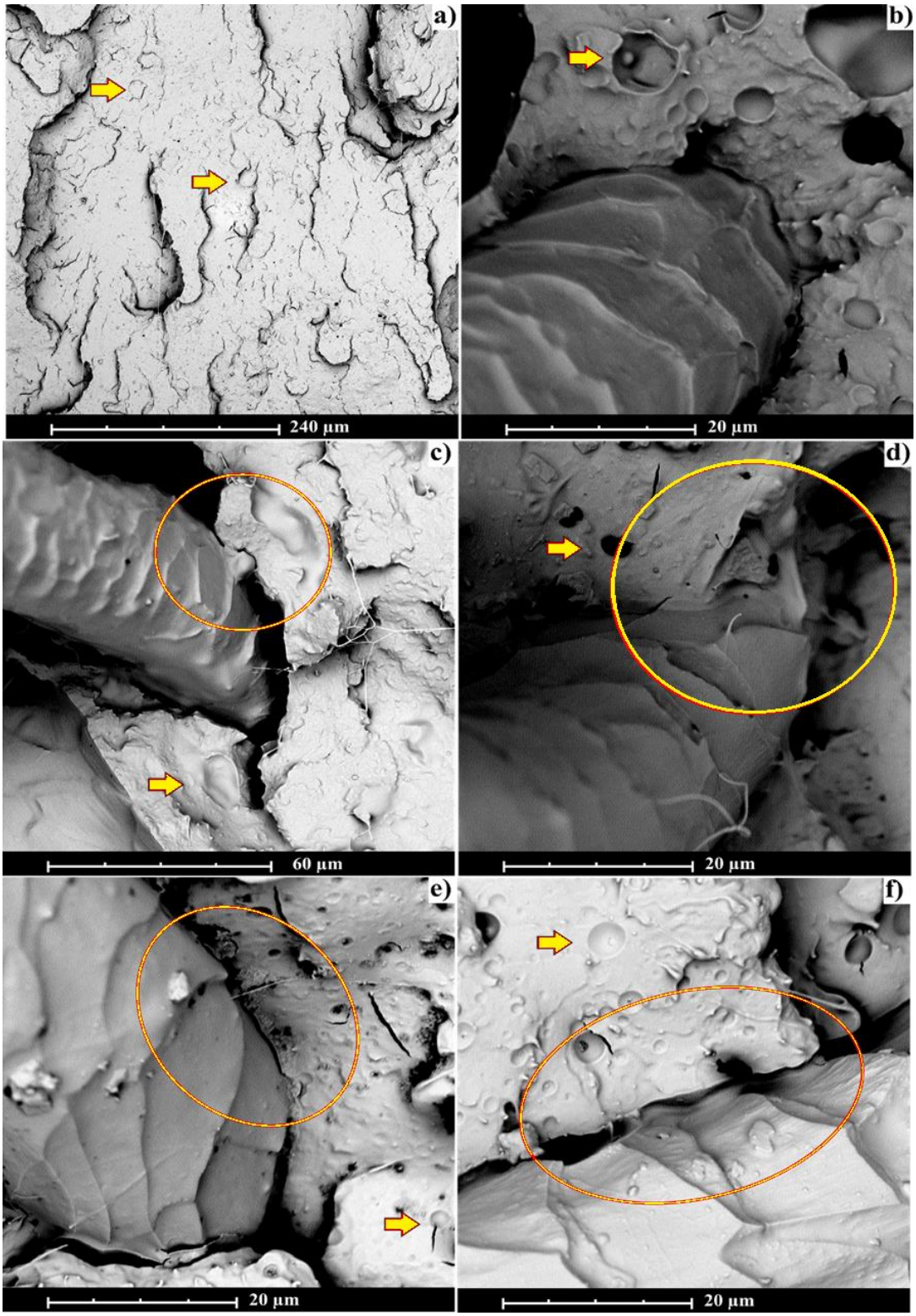

Figure 53 Scanning electron microscopy (SEM) images of (a) PLA–MLO; (b) PLA–MLO–Wool; (c) PLA–MLO–Wool (ATS); (d) PLA–MLO–Wool (TES); (e) PLA–MLO–Wool (TVS); and (f) PLA–MLO–Wool (TTI).

A different behavior is observed in the FRPs containing treated and neat wool fibers. In all samples (Figure 53b–f), a gap is visible between the polymer matrix and the wool fibers, which negatively impacts the mechanical performance and properties of the materials. This gap prevents friction to reinforce material during fiber slippage [214].

Figure 53b illustrates an incompatibility between the polymer matrix and the neat fiber, similar to findings with basalt fibers in epoxidized soybean oil [175] or epoxidized linseed oil [22]. However, the treatment of the wool surface with silanes or alkoxide (ATS, TES, TVS, and TTI) appears to enhance compatibility with the polymer matrix (highlighted by orange marks). The treated wool fibers develop a rougher surface, improving friction on phases contact, as noted in the literature [214]. This effect is due to stronger adhesion between the fiber surface and the polymer matrix, resulting from chemical modification of the fiber surface [209]. In Figure 53b, corresponding to formulation reinforced with unmodified wool, the fiber outer layer appears irregular, with no visible interaction with the PLA matrix. In contrast, coupling agent-treated wool fibers (Figure 53c–f) display smoother fiber superficial, with particles and threads connecting the fiber to the matrix, contributing to improved properties in the treated wool materials compared fibers without grafted silane or alkoxide. This microstructural analysis confirms that wool treatment with coupling agents enhances fiber–matrix compatibility.

1.6. Surface characterization

Table 8 presents the outcome of the color and wettability assessments. Color measurements were conducted using the CIELab* color model. Adding wool fiber affects the sample's lightness, with L* values for the PLA–MLO system showing notable differences ($p < 0.05$) compared to the other formulations. The PLA–MLO formulation exhibited the lowest lightness. The addition of unmodified wool increased the lightness by more than 4 points. Although the L* parameter of wool-reinforced FRPs are insignificantly different ($p > 0.05$), the brightness of treated wool materials increased, reaching 48.23 and 49.38 for formulations with modifications from TES and TTI coupling agents, respectively. Similar increases in lightness have been spotted in PLA-based materials filled with limonene [108].

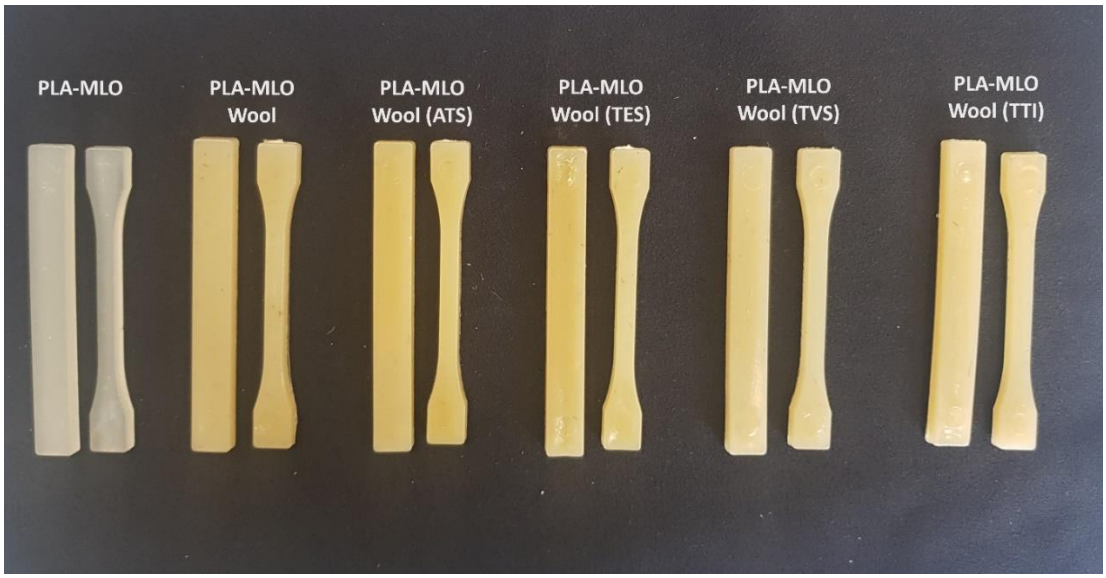

Figure 54 Visual appearance of tested formulations

Concerning the a* value, the PLA–MLO formulation exhibits a slightly green tone equal −1.89. However, incorporating untreated wool and wool treated with coupling agents ATS and TES shifts the color towards the red spectrum, as indicated by the increase in a* values. For PLA–MLO–Wool (TVS) and PLA–MLO–Wool (TTI), a* coefficients are close to 0, indicating that neither red nor green dominates in these samples. Statistical analysis shows significant differences in a* values among all formulations.

Regarding the b* coefficient, representing yellow tones, the PLA–MLO formulation shows the lowest value at 2.38, indicating a slight yellow tint. The addition of unmodified wool increases this value by approximately 20 points. Significant differences in b* values are observed between the PLA–MLO matrix and wool-containing formulations, as shown in Table 8. A similar increase in the b* coefficient was noted in PLA modified with limonene, highlighting the significant impact of natural fillers on color appearance [108]. Furthermore, a shift towards a brownish color was concluded in PLA modified with a bio-origin silica–lignin filler.

Supplementary to result obtained from the CIELab model, a visual appearance of tested materials was shown in Figure 54. From visual appearance a clear color change is spotted between PLA-MLO formulation and remaining wool-reinforced materials. Further, between wool-reinforced formulations slight changes in color are spotted. This correlates with general tendencies observed across formulations, as presented in Figure 55. All three factors considered in the CIELab model (a,b,L) are changing when wool fiber in introduced to PLA-baseed material, as for all factors an increase is observed especially in lightness and yellowish appearance. A modification of PLA-MLO with surface modified wool, although it remains yellowish, have shown slight reduction in yellow and red colors intensity.

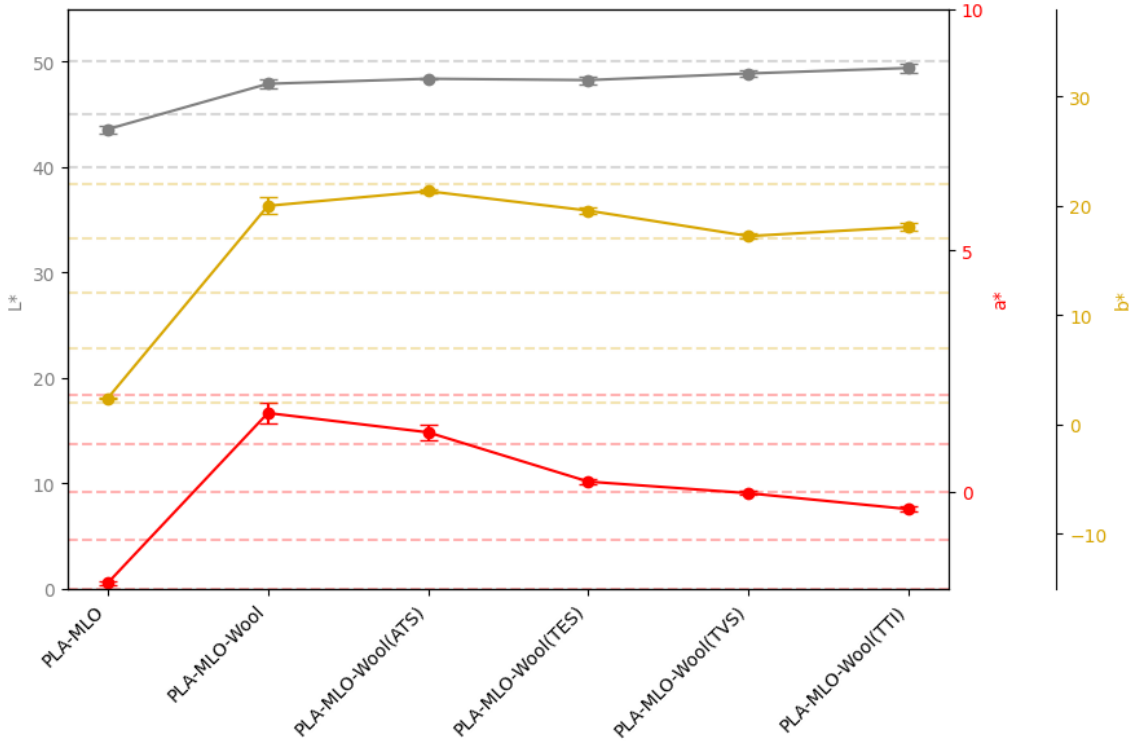

Figure 55 Color results across tested formulations

In the wettability evaluation reported in Table 8, the lowest contact angles were observed for PLA–MLO and PLA–MLO–Wool, with theta angle of 66.9° and 66.4°, respectively, which are insignificantly different ($p > 0.05$). These conclusions suggest that the materials exhibit strong wettability due to the inherently hydrophilic nature of both PLA and wool. The wool modification resulted in reduced wettability, increasing hydrophobicity and making it more suitable for various wet-environment applications. Significant differences in wettability were observed between the treated wool FRPs and the PLA–MLO and PLA–MLO–Wool formulations. A similar increase in hydrophobicity was noted when PLA was filled with limonene [108]. In contrast, surface modification of cellulose nanocrystals improved PLA's wettability [113]. The smallest change in wettability was recorded for the formulation treated with the TTI coupling agent, with a mean theta angle of 75°, while the greatest alteration was observed for PLA–MLO–Wool (TVS), with an average theta angle of 80.8°. These results highlight the significant effect of coupling agents on the surface wettability of PLA–MLO and PLA–MLO–Wool.

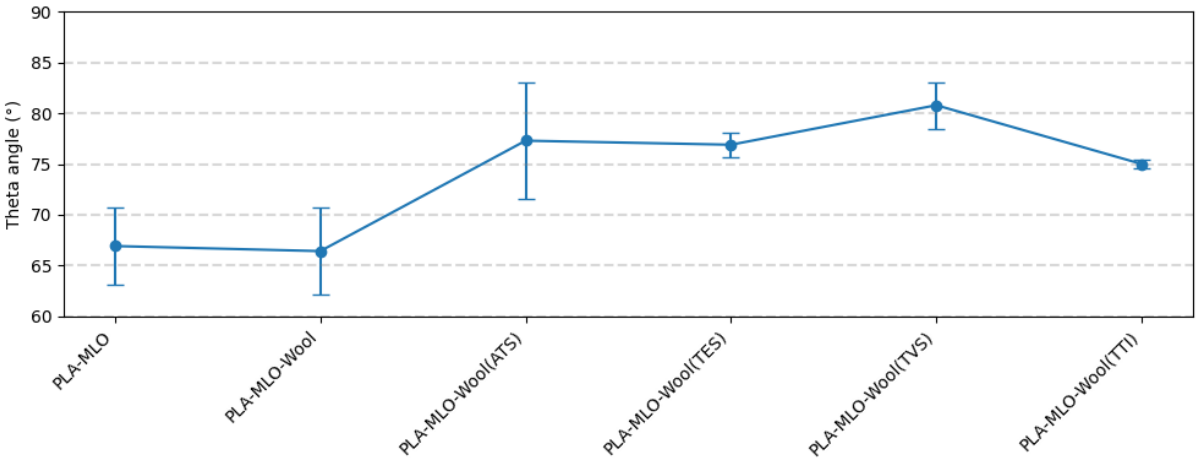

Figure 56 Wettability results across tested formulations

As a visual summary of wettability results, all tested formulations were shown in Figure 56, where impact of coupling agent treatment can be clearly observed. As PLA-MLO blend and formulation reinforced with untreated wool fiber have shown similar theta angle, the hydrophilic characteristics of materials have changed with wool fiber surface modification. Not only surface treatment differentiates with PLA-MLO blend, but also different types of treatment have shown significant changes, as supported by ANOVA analysis shown in Table 8. However, there change of different coupling agents application is not as remarkable as when compared to formulations where no surface treatment was applied.

2. Impact of silane treatment conditions on sheep wool fiber poly(lactic acid)-maleinized linseed oil system

2.1. Wool modification

The FTIR spectra for untreated wool and wool fibers treated with 1 and 2.5 phr of TVS are presented in Figure 57 along with the spectrum of pure TVS shown as a reference. When comparing the treated wool samples (Wool-1TVS and Wool-2.5TVS) to the untreated wool (Wool), no significant reduction is observed in the –OH group peak at 3300 cm^{-1} in the wool fibers. However, modifications in the TVS-treated wool fibers are noticeable between 2880 and 2980 cm^{-1}, where the peak intensities slightly raise after modification. These peaks, correlated with $–CH_3$ bonds [200], also appear in the TVS FTIR spectrum. The most significant intensity rise in this region was observed in wool treated with 1 phr of TVS, aligning with findings from PLA/MLO systems, where silane modification caused only minor changes in peak intensity. [200]. A positive sign of effective grafting TVS on the wool fibers can be observed between 700 and 1300 cm^{-1}, where the peaks are correlated with Si–O–Si and Si–O–R bonds. The most remarkable change in peak intensity has been spotted for wool modified with 2.5 phr of TVS matched to the peaks at 1084 and 763 cm^{-1}, indicating a successful silane grafting to the wool fiber surface. The absorption wavelength at 763 cm^{-1} relates to the –Si–C– symmetric stretching bond [215], shifted to a lower wavenumber (760 cm^{-1}) in the fibers treated with 2.5 phr of TVS, also suggesting a successful coupling reaction.

Furthermore, the asymmetric stretching of Si–O–Si shifted from 1084 to 1120 cm^{-1} in the modified fibers, indicating a strong interaction between the silane structure forming bound to the wool fiber surface, confirmative the achieved the modification treatment [216]. In the neat TVS spectrum, peaks at 1023 and 840 cm^{-1}, correlated with the stretching vibrations of the Si–O–C bond and alkoxy groups, are seen. Analogous bonds were found in vinyltriallyloxysilane monomers when applied for surface modification, and which weaken after an accomplished silane coupling reaction [217]. The absence of these peaks in the Wool-2.5TVS spectrum suggests that no unreacted coupling agent remains.

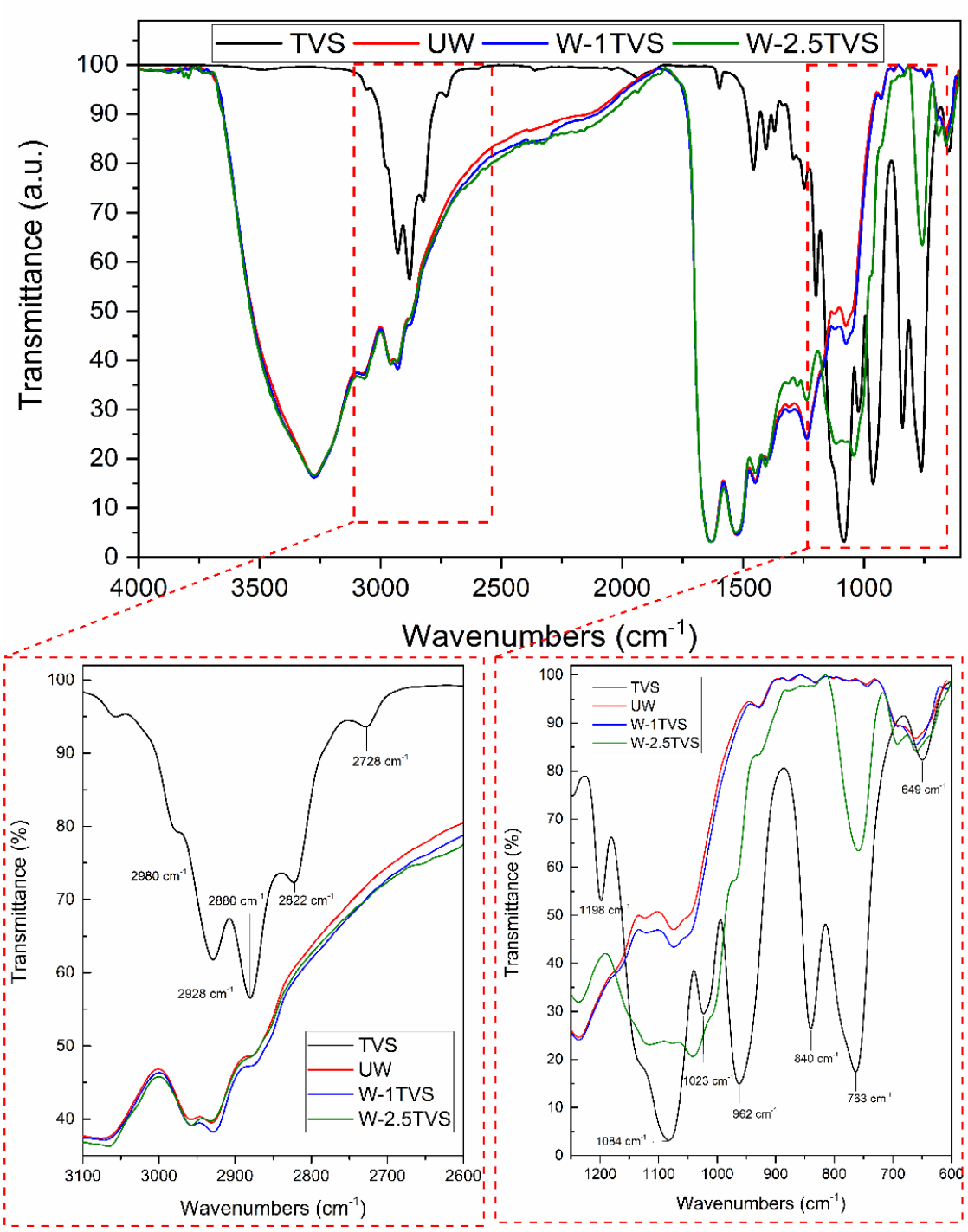

Figure 57 FTIR spectra of TVS and evaluated wool fibers

The thermal properties of untreated sheep wool fibers and TVS-treated wool fibers were evaluated at the composite manufacturing temperature (180 °C) and is presented in Figure 58a. As anticipated, the modified wool fibers exhibited greater stability at the manufacturing temperature compared to unmodified fibers, though both showed typical thermal degradation behavior in atmospheric conditions. For exposure times of less than 3.5 minutes, the untreated and silane-treated fibers demonstrated sufficient thermal stability, with both losing approximately 5% of their initial weight due to moisture evaporation and the evaporation of low molecular weight inpurities. Following

this, the decomposition of wool fiber parts, primarily keratin, begins. Comparing the silane-treated fibers shows that those treated with a higher TVS concentration (2.5 phr) displayed enhanced thermal resistance compared to wool functionalized with 1 phr of TVS.

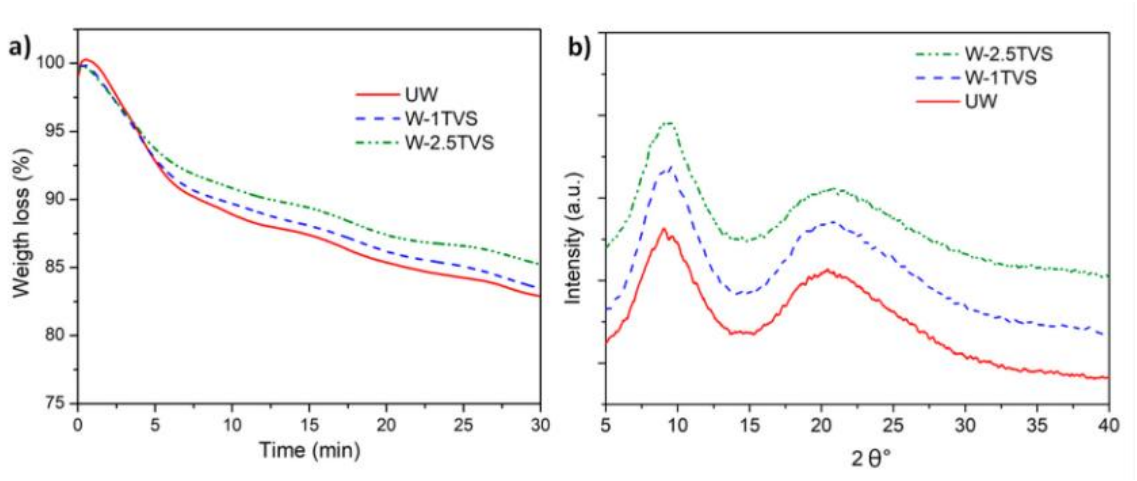

Figure 58: (a) TGA isothermal curves and (b) XRD patterns of evaluated wool fibers

The XRD patterns of evaluated fibers fibers (Figure 58b) reveal two characteristic peaks, corresponding to the α-helix structure at around 9.2° and the β-sheet structure at approximately 20.9°, which are associated with presence of keratin in wool fiber [218]. The broad nature of these peaks also suggests an amorphous crystalline structure of wool. Nonetheless, the modified fibers (W-1TVS and W-2.5TVS) do not exhibit any other crystalline structures, indicating that the attached coupling agent remains in an amorphous state [219]. Furthermore, the XRD patterns confirm that the modification process does not alter the crystalline structure of the wool significantly, as no peak broadening or defective crystalline structure in keratin were detected.

The micrograms of treated sheep wool fibers was further examined using SEM. In neat fibers, cuticle cells remain held to the fiber bulk (Figure 59a); however, with increasing TVS concentration, the silane-treated fibers show greater separation of the cuticle cells from the fiber core (Figure 59b,c). The morphological structure of wool fibers consists of three main parts, including the cuticle, cortex - an outer layer encompassing the fiber bulk, which is linked via the cell membrane complex, also known as intracellular cement. The increased separation of cuticle cells indicates successful grafting of TVS onto the surface, as the treatment selectively interacts with the fiber's structure, causing swelling in the hydrophobic outer layer [197].

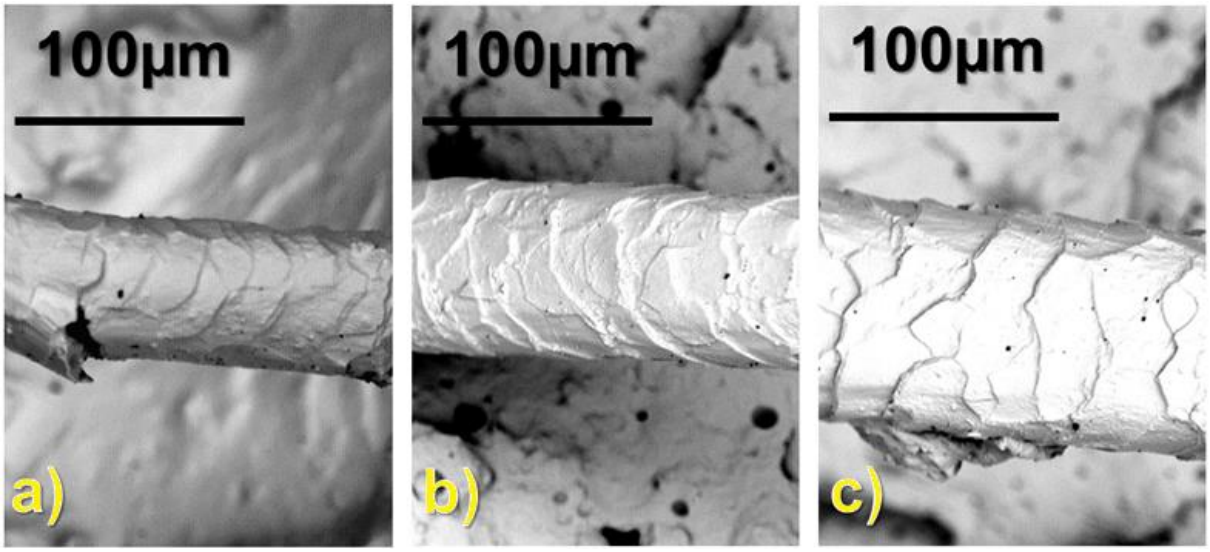

Figure 59 a) Wool, (b) Wool-1phr TVS, (c) Wool-2.5phr TVS micrograms of fibers.

2.2. Mechanical properties

The tensile characteristics of the PLA/MLO-wool FRPs are presented in Figure 60. As anticipated, the tensile strength (Figure 60a) and Young's modulus (Figure 60b) of PLA diminished with the blending of MLO into material, while the elongation at break was improved, validating MLO's plasticizing effect, as previously reported in the literature [171,196].

For composites modified with 1 phr of neat and treated fibers, the tensile strength notably reduced ($p < 0.05$) as the wool concentration increases, indicating vulnerable interaction in the PLA/MLO matrix for neat wool fibers [199]. Furthermore, insignificant differences ($p > 0.05$) were observed between composites with treated and neat wool fibers.

For Young's modulus, adding 1 or 5 phr of untreated or 1 phr TVS-treated wool fibers generally maintained the modulus of the PLA/MLO FRP. However, the use of 2.5 phr TVS-treated wool fibers led to a significant increase, indicating enhanced interaction between the treated fibers and the matrix. When higher wool fiber content (10 phr) was added, the Young's modulus of PLA/MLO was largely preserved at comparable level. In literature negative effects on the modulus with increasing natural filler content in PLA-based composites have been reported for non-compatibilized lignocellulosic fillers [196,200,220,221]

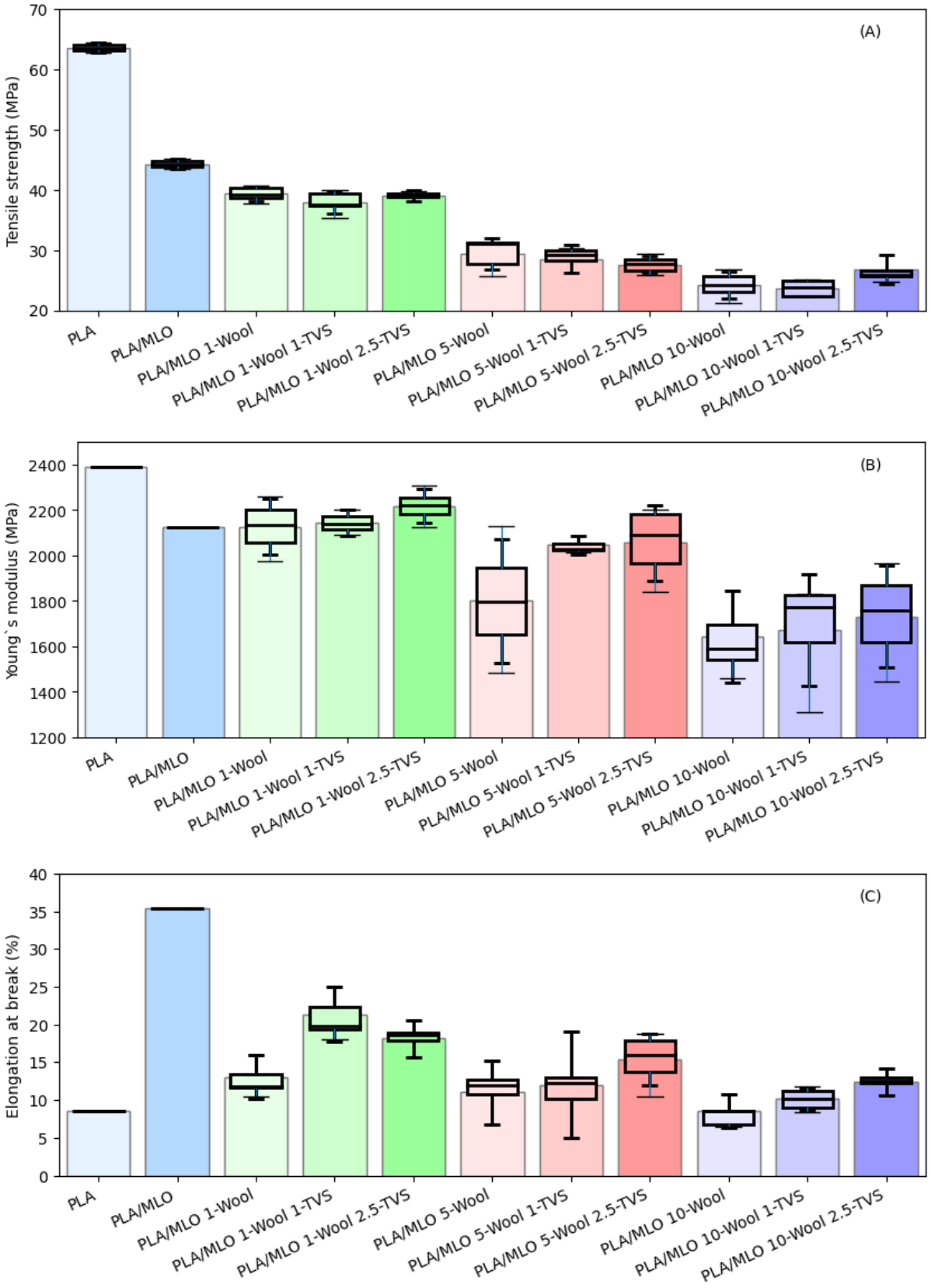

Figure 60 Tensile test results: (A) tensile strength, (B) Young's modulus, and (C) elongation at break.

As wool fiber content increased, the elongation at break of the PLA/MLO FRPs decreased. However, it's important to note that while neat wool fibers provided composites with slightly greater flexibility than PLA, the TVS treatment greatly enhanced their flexibility. A clear improvement in elongation was seen in FRPs containing 1 and 5 phr of wool fibers modified with 1 phr of TVS, with further gains observed at higher TVS concentrations. Specifically, the formulations PLA/MLO-1Wool-1TVS, PLA/MLO-1Wool-2.5TVS, and PLA/MLO-5Wool-2.5TVS ($p > 0.05$) have shown the highest elongation at break among all the evaluated formulations. For the 1 phr untreated wool FRP (PLA/MLO-1Wool), the elongation at break was improved by over 60% with the additive of TVS-treated wool fibers in PLA/MLO-1Wool-1TVS and PLA/MLO-1Wool-2.5TVS. Similarly, for the 5 phr untreated wool composite (PLA/MLO-5Wool), elongation at break increased by almost 40% in PLA/MLO-5Wool-2.5TVS. In composites reinforced with 10 phr of wool, the elongation at break improved from 8.5% to 12.4% in PLA/MLO-10Wool-2.5TVS following TVS treatment, relating to PLA/MLO-10Wool reinforced with neat wool fiber. These findings show that chemical treatment of sheep wool fibers enhances the interaction of wool fibers reinforcement and the PLA/MLO matrix, particularly at minimal fiber concentration (1 and 5 phr) and with the higher TVS concentration of 2.5 phr. However, at higher wool content (10 phr), the effectiveness of the silane agent diminishes, likely due to increased fiber-matrix incompatibility at this concentration [196,199]

Normally, the tensile characteristics of the FRPs tend to improve as the wool content increases up to 5 phr. However, with 10 phr of fibers, the performance begins to decline due to reduced compatibility between the fibers and the PLA/MLO blend. The mechanical properties of the FRP is influenced by the interaction of the polymer and wool, including their compatibility, phase surface adhesion, and fiber content in the material [94,221]. However, statistical analysis indicates that TVS modification of the wool reduces the loss of mechanical performance in the FRP, especially at higher wool and TVS concentrations, due to improved interaction between the components.

Regarding Charpy's impact strength, as shown in Figure 60, the impact strength decreases as the content of neat wool increases. This reduction can be attributed to fiber fracture and material delamination, which lead to reduction in impact resistance at higher fiber contents in the FRPs [222]. When facing the lowest (1 phr) and highest (10 phr) wool contents, it is evident that the TVS modification of the fibers tends to enhance impact strength, although the differences between the wool reinforced formulations are not statistically significant. At higher wool content, surface modification with 2.5 phr of TVS showed better performance compared to lower TVS concentrations or untreated wool. A similar pattern has been observed in fiber-reinforced laminates, where surface modification enhanced the material's overall performance [22]. Although PLA/MLO-1Wool-1TVS exhibited the greatest Charpy's impact strength among all formulations (14.9 kJ/m^2), statistical analysis indicates no significant changes ($p > 0.05$) among evaluated FRPs. PLA/MLO-10Wool-1TVS showed the lowest impact strength. According to the literature, PLA-based FRPs with natural fibers generally show improvements in impact strength.

Regarding hardness (Figure 61), both untreated and treated wool fibers improve the hardness of PLA and PLA/MLO blends, demonstrating effective reinforcement of the PLA matrix with wool fibers. Nonetheless, the Shore D hardness tends to be reduced as the content of neat wool increases. Significant changes ($p < 0.05$) are spotted when comparing materials with untreated wool. Specifically, increasing the wool concentration from 1 to 10 phr results in a decrease in hardness from 78.5 to 76.9. A similar decrease

in hardness was previously observed in PLA combined with untreated wool fibers [196]. In contrast, the surface treatment of the fibers tends to somewhat enhance the hardness, although these differences are statistically insignificant ($p > 0.05$) when comparing modified and unmodified wool fibers at the same content level.

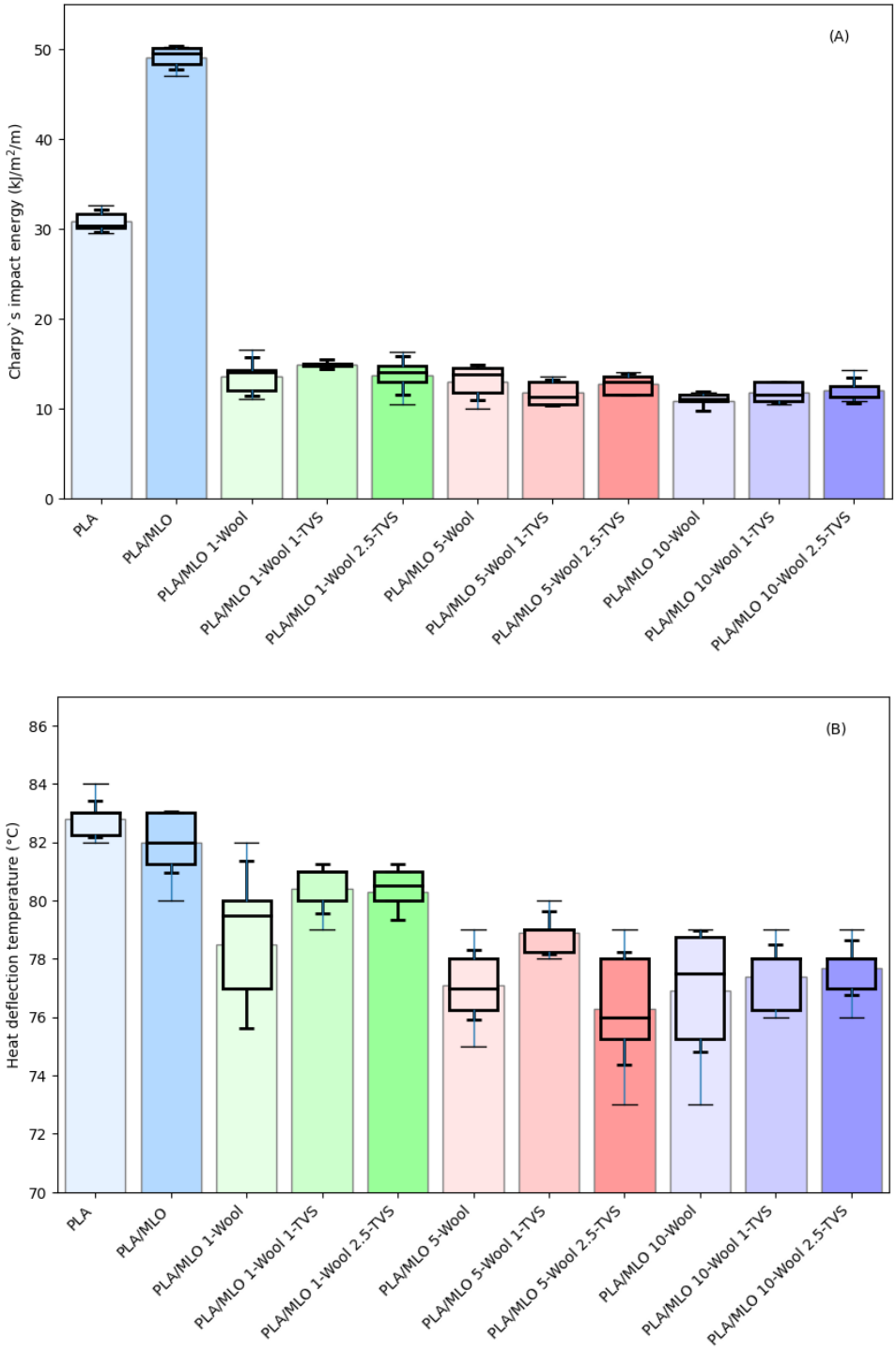

Figure 61 (A) Charpy's impact values and (B) Shore D hardness values of the formulated materials.

In summary, increasing the concentration of neat wool fibers is likely to reduce the tensile properties of FRPs based on the PLA/MLO blend. However, when TVS is applied for surface modification, it improves both stiffness and flexibility, especially in FRPs with lower wool content and higher concentrations of TVS treatment. This improvement confirms the effectiveness of the sheep wool fiber grafting.

On the Figure 62 were presented results of the Vicat softening temperature and the HDT heat deflection for formulations evaluated in the study. Irrespective of the method used, the highest temperature was obtained for the neat PLA material. Furthermore, for both methods blending with MLO as well as reinforcement with wool fibers have further reduced the temperature, indicating material softening in lower temperatures and lowering its liability for construction applications in elevated temperatures.

Concerning the Vicat softening temperature results shown on the Figure 62a, irrespective of amount of unmodified wool used for reinforcement, the temperature remains at comparable level. However, applying surface treatment with the TVS helps to mitigate the reduction in temperature especially at 1phr of the TVS. Although such TVS concentration is shown to compensate for temperature reduction across all tested concentrations of wool fiber in the formulations, the most effective improvement was found for the formulation with lowest wool fiber concentration of 1phr.

Similar findings were observed based on the results for the heat deflection temperature measurements, as presented in Figure 62b. Although MLO incorporation has caused reduction in the temperature between neat PLA and PLA-MLO, the change was not as evident as in the Vicat softening temperature measurement. Furthermore, similarly incorporation on wool fiber to a PLA-MLO blend have cause a decrease in temperature. To compensate the reduction in the HDT, applying TVS coupling agent modification have served beneficially. For all concentrations of wool fibers in a formulation presence of treatment have helped to mitigate negative impact of wool fiber on the heat deflection temperature.

Although results obtained in the Vicat softening temperature and heat deflection temperature have led to similar conclusions towards impact of MLO, wool fiber and TVS treatment, a certain difference between results from the test methods where observed. In order to summarize the result, a Bland-Altman plot have served for data analysis, as presented in Figure 63. An average difference between the Vicat and HDT result across tested formulations was 2.7°C, indicating that Vicat temperature result was on average higher than HDT. By analysing the X-axis, on average highest results were obtained for PLA and PLA-MLO blends. However, as the PLA have shown Vicat and HDT result differentiate between each other in terms of temperature result, for the PLA-MLO blend almost no change in temperature was spotted. For remaining formulations where different wool and TVS concentrations were applied the change in temperature between methods varies between 1 and 5°C higher Vicat temperature, however from significance point of view all of the results remain in the 95% confidence interval. Across all tested formulation only one PLA-MLO result was considered as a bias. It is worth noting that the analysis have confirmed observations described for the results shown in Figure 62.

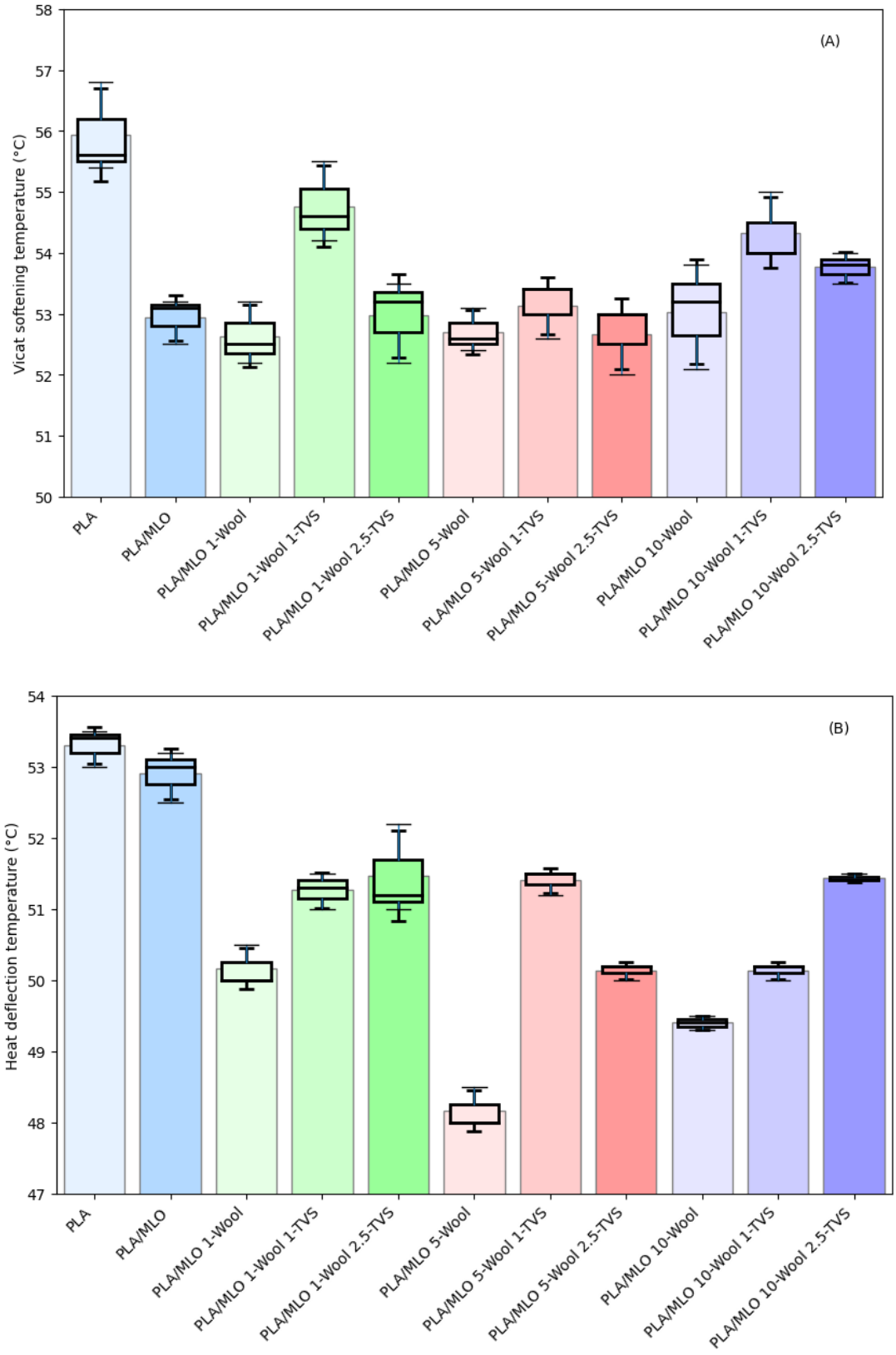

Figure 62 Test results of evaluated formulations for A) Vicat, B) HDT

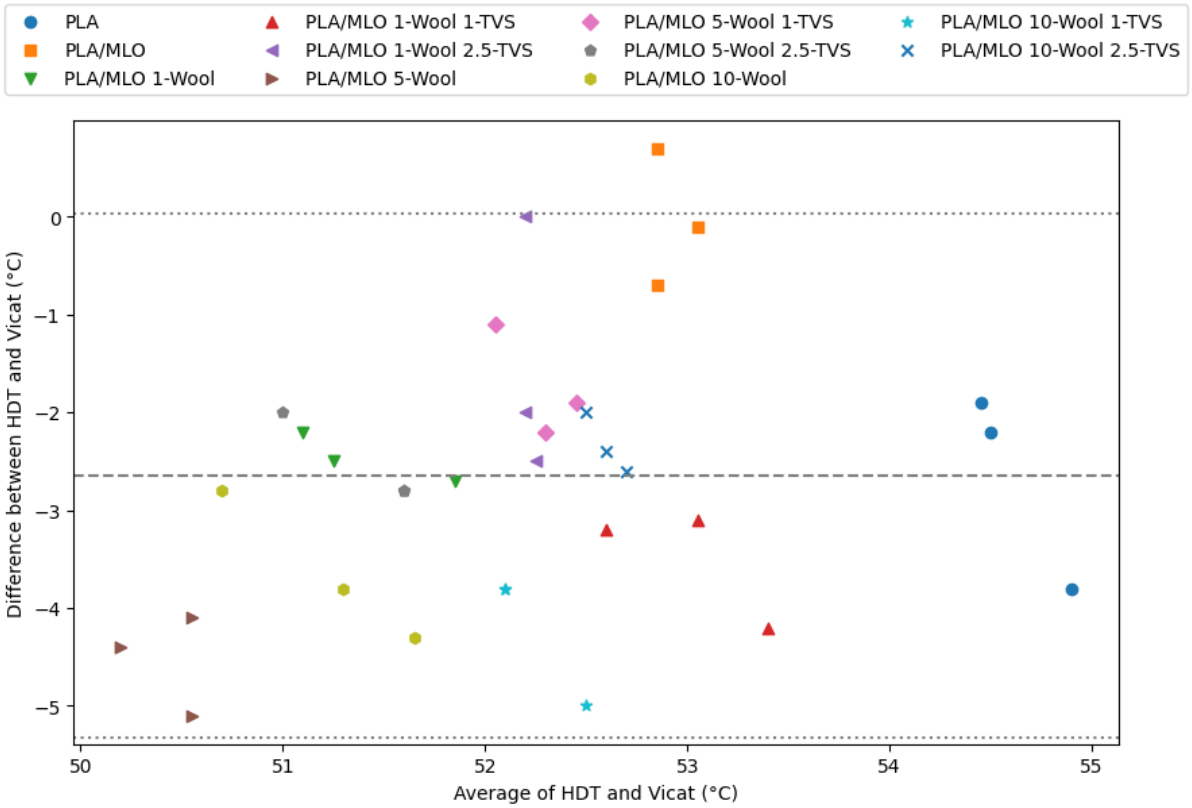

Figure 63 The Bland-Altman plot for HDT and Vicat results

2.3. XRD Diffraction Pattern

The X-ray diffraction (XRD) patterns (Figure 64) exhibit a one broad peak at approximately 16.4°, corresponding to the α-phase crystalline structure of PLA. This confirms that PLA does not undergo polymorphic transitions. The peak's intensity increases for the PLA-MLO blend, which can be justified by enhanced PLA macromolecule mobility and improved crystalline structure formation due to the presence of MLO [223–225]. Reinforcing the PLA-MLO blend with wool fibers produces a crystalline structure comparable to neat PLA, since the fibers limit macromolecule movement. Additionally, wool reinforced composites do not display any novel peaks associated to the crystalline structure of wool, likely due to the low fiber concentrations used.

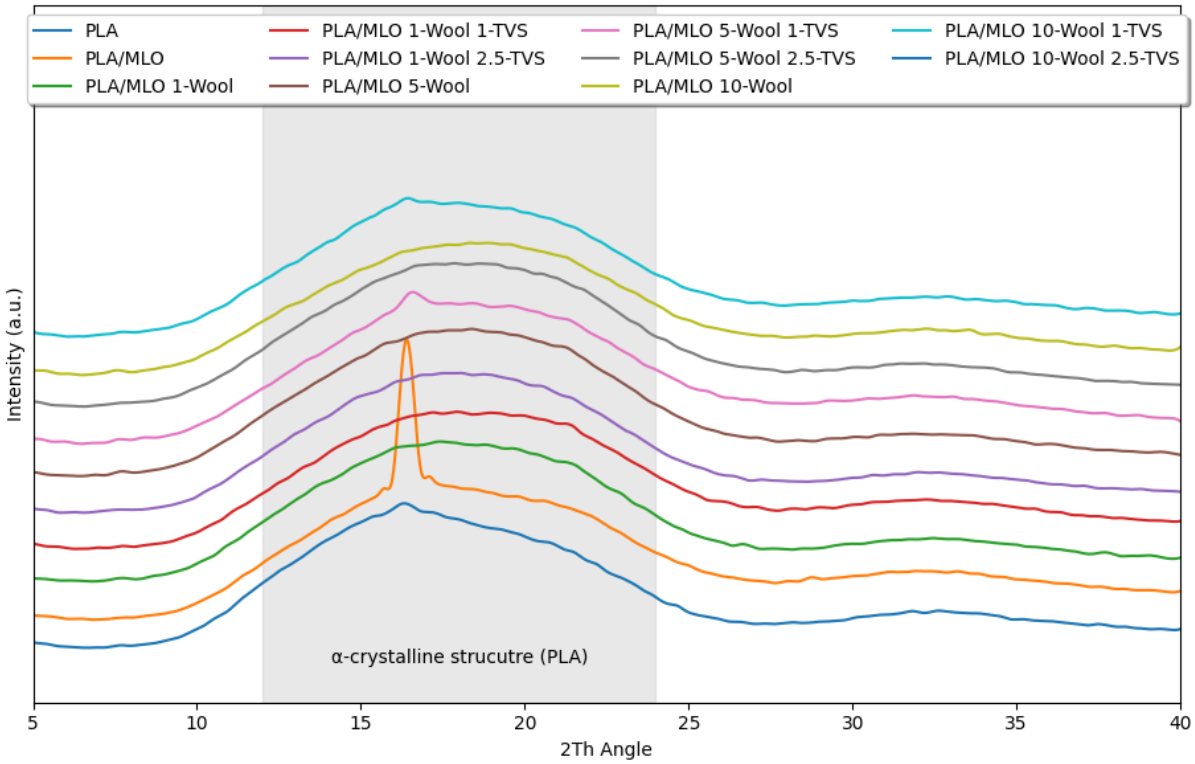

Figure 64 XRD patterns of the formulated materials.

2.4. Thermal properties

The thermal properties derived from the DSC and TGA analyses are presented, with Figure 65 displaying the second heating DSC cycles for evaluated formulations. The PLA matrix plasticization by MLO additive is evidenced by a minor decrease in T_g values across all formulations modified with MLO compared to unmodified PLA. Ferri et al. previously investigated PLA blended with varying concentrations of MLO (from 5 phr to 20 phr) and concluded that, beyond 5 phr of MLO, a slight decrease in T_g occurs caused by saturation with MLO. However, a greater MLO content, such as 10 phr, is necessary to significantly enhance the material's flexibility [89]. The addition of neat and treated wool fibers, their presence was insignificantly for changes in the T_g values ($p > 0.05$).

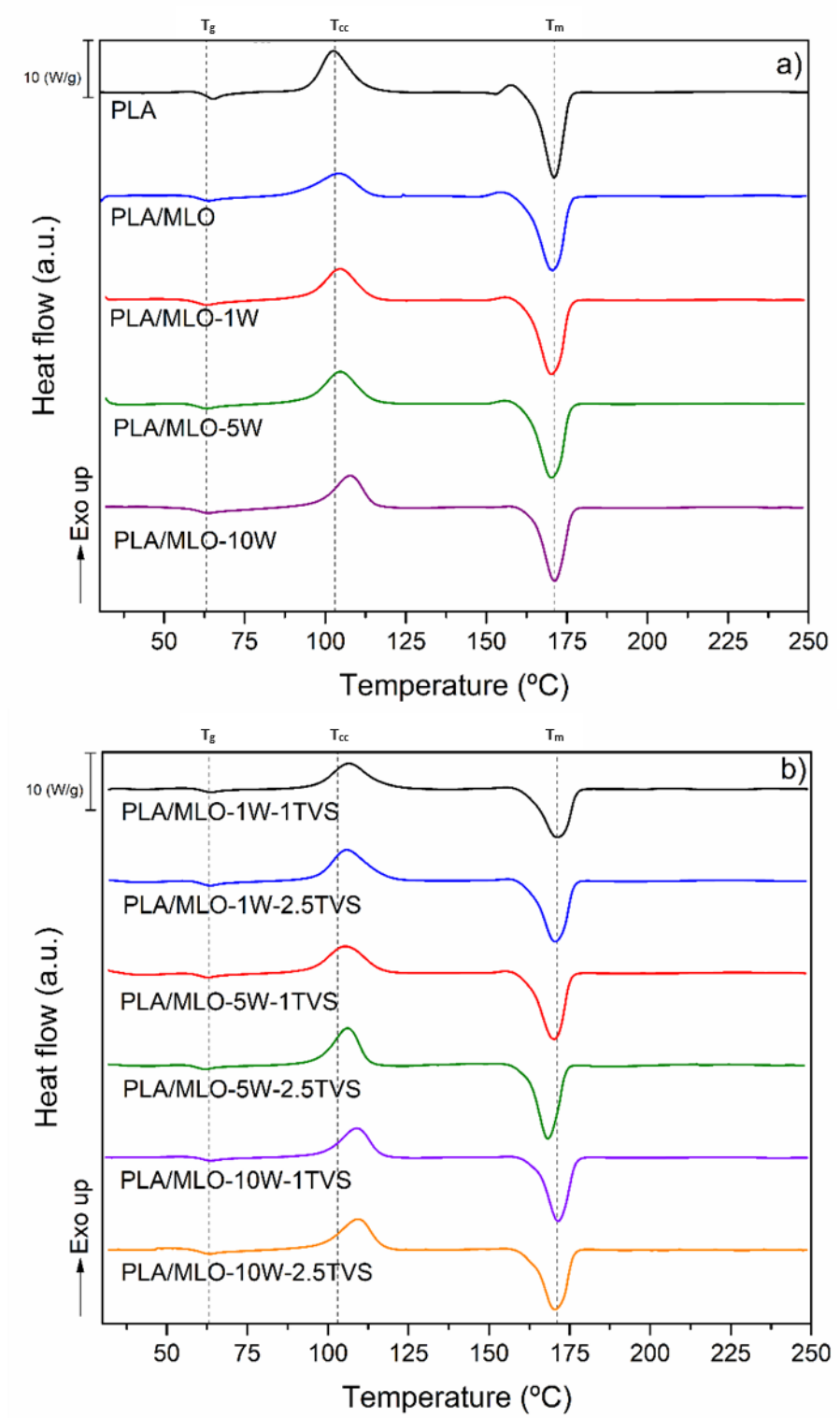

Figure 65 DSC results of (a) neat polymers and untreated wool FRPs and (b) TVS-modified wool FRPs.

The temperature of cold crystallization of PLA was found to be reduced after blending with MLO, as previously spotted for common PLA plasticizers [226] and in earlier studies where PLA blended with MLO [89]. The addition of both untreated and treated wool fibers increases T_{cc}, indicating their capability to influence the crystallization

of PLA by increasing the number of crystal nuclei, thereby expecting additional thermal energy for PLA to re-crystallize. As the wool concentration in the PLA/MLO matrix increases, cold crystallization shifts to greater temperatures (as presented in Figure 65 and summarized in Table 9). Although most T_{cc} results are statistically comparable ($p > 0.5$), materials containing 10 phr of TVS treated wool tend to provide greater cold crystallization temperatures. PLA/MLO-10Wool-1TVS and PLA/MLO-10Wool-2.5TVS exhibit greater T_{cc} temperatures, around 107 °C, whereas the FRP with 1 phr of neat wool provides the lowest among tested materials T_{cc} (103.1 °C for PLA/MLO-1Wool). A analogous change in cold crystallization temperature has been spotted for PLA FRPs with various silane-modified wool fibers [200]. Additionally, a synergistic effect on cold crystallization was observed in earlier studies involving PLA blends with lignocellulosic additives [113,226]. Regarding the TVS silane, increasing its concentration insignificantly affect T_{cc}, as shown in Table 9 and Figure 65b.

Observing the melting temperature, unmodified PLA exhibited a minor baseline shift in the DSC curve, with an exothermic peak appearing before main melting phase (Figure 65a), indicating that the material crystallizes and melts upon heating. Such shift was also present in the PLA/MLO formulation, nonetheless the slight crystallization peak diminished as fiber was introduced into composite and nearly disappeared in the PLA/MLO-10Wool formulation (Figure 65a). In contrast, no aforementioned shifts were detected before melting in the silane-modified FRPs (Figure 65b), suggesting the non-existence of additional crystalline phases. Insignificant changes ($p > 0.05$) were found in the melting temperature (T_m) of the FRPs when relating the results to the temperature for unmodified PLA. Consistent with the XRD results, the plasticized PLA/MLO formulation exhibited a higher degree of crystallinity. Composites based on unmodified wool indicated greater crystallinity ($X_{c\%}$) than reported for unmodified PLA (Table 9) , similar to the findings of Islam et al., who observed that manufacturing PLA with natural fibers can produce hydrogen or covalent linkages after melt processing [227]. Moshiul Alam et al. also reported that treatments such as alkali, ultrasound, and those methods combined can improve the crystallinity of PLA-based FRPs [228]. However, additional surface alteration of wool with the TVS led to crystallinity degrees that were either equal to or lower than those of neat PLA, conditional on the wool concentration. This could be attributed to limited hydrogen bonding of the sheep wool fibers and PLA macromolecules post its manufacturing.

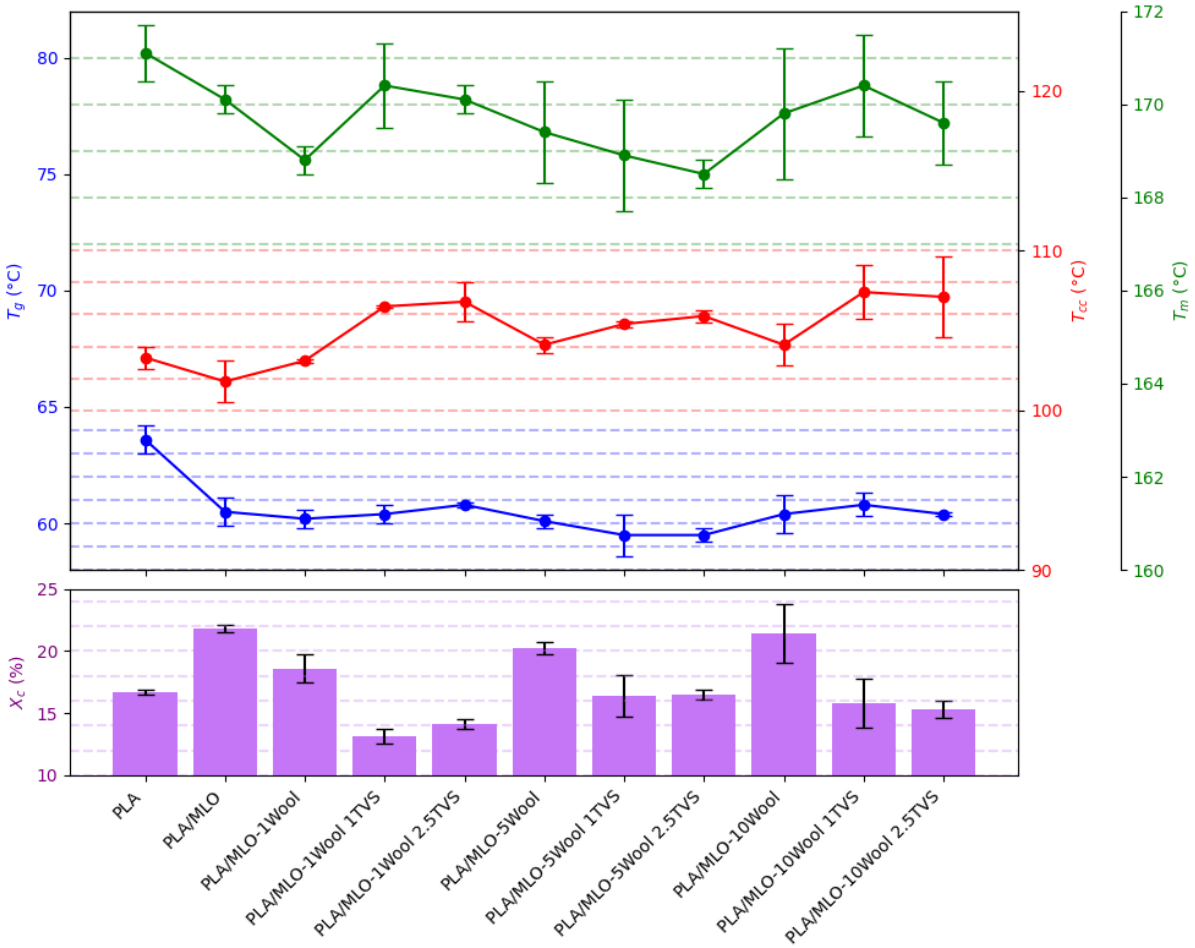

Figure 66 DSC results for evaluated formulations

A general tendencies in DSC results obtained in the study can be formulated based on a comparison presented in Figure 66. From degree of crystallinity point of view, although as expected incorporation of MLO to neat PLA have helped with formation of additional crystalline structures, both presence of wool fiber and coupling agent tends to reduce the amount of crystalline structure in the tested material. However, such reduction is less evident with increasing amount of wool fiber, as the PLA/MLO-10Wool have shown no significant difference to PLA/MLO blend. Concerning glass transition temperature, although presence of MLO, wool fiber and wool surface treatment tends to slightly change the T_g temperature, comparing the the neat PLA after modification temperature is strongly reduced and due to ANOVA analysis shown in Table 9, the change is significant. Furthermore between remaining, modified PLA formulations the changes in temperature are insignificant. For the cold crystallization temperature, almost all of tested formulation have shown slight, insignificant changes between each other. Although in general with presence of wool fiber and TVS treatment increase in the temperature is expected, a significant change in the T_{cc} was observed only between unreinforced formulations and formulations reinforced with 10phr of TVS treated wool fiber. Similar observations were concluded for the melting temperature, were even though the result derived from the measurement changes, it is not significant and did not show clear impact of wool and TVS concentrations on the melting temperature.

Table 9 Thermal properties of the PLA-based FRPs

	DSC				TGA			
Formulation	T_g (°C)	T_{cc} (°C)	T_m (°C)	X_c (%)	$T_{5\%}$ (°C)	T_{max} (°C)	Mass loss at 300 °C (%)	Mass loss at 350 °C (%)
PLA	63.6±0.6 [a]	103.3±0.7 [a]	171.1±0.6 [a]	16.7±0.2 [a,d]	331.0±1.0 [a]	357.3±1.2 [a,c]	0.05±0.0 [a]	21.3±0.9 [a]
PLA/MLO	60.5±0.6 [b]	101.8±1.3 [a]	170.1±0.3 [a,b]	21.8± 0.3 [b]	326.0±1.0 [a,c]	362.7±0.6 [b,d]	1.2±0.1 [a,b]	22.9±2.2 [a]
PLA/MLO-1Wool	60.2±0.4 [b]	103.1±0.1 [a]	168.8±0.3 [a,b]	18.6±1.1 [a,e]	326.3±0.6 [a,c]	361.7±1.6 [b,c,d,e]	1.2±0.1 [a,b]	22.5±2.2 [a]
PLA/MLO-1Wool-1TVS	60.4±0.4 [b]	106.5±0.1 [a,b]	170.4±0.9 [a,b]	13.1±0.6 [c]	313.0±3.0 [b,c]	358.3±1.5 [a,c]	3.3±0.6 [b,c,d]	27.0±6.1 [a,b]
PLA/MLO-1Wool-2.5TVS	60.8±0.1 [b]	106.8±1.2 [a,b]	170.1±0.3 [a,b]	14.1±0.4 [c,d,g]	314.7±4.2 [b,c]	359.3±1.2 [c,e,f,g]	3.3±1.2 [b,c,d]	27.6±6.5 [a,b,d]
PLA/MLO-5Wool	60.1±0.3 [b]	104.1±0.5 [a,b]	169.4±1.1 [a,b]	20.2±0.5 [b,e]	305.7±3.5 [b,c,d]	361.0±1.0 [b,c,e,f]	4.1±0.8 [c,d,e]	29.8±3.5 [a,b,c,d]
PLA/MLO-5Wool-1TVS	59.5±0.9 [b]	105.4±0.2 [a,b]	168.9±1.2 [a,b]	16.4±1.7 [a,g]	316.3±0.6 [c]	364.3±1.5 [d]	2.9±0.1 [b,c]	29.2±1.0 [a,b,c,d]
PLA/MLO-5Wool-2.5TVS	59.5±0.3 [b]	105.9±0.4 [a,b]	168.5±0.3 [b]	16.5±0.4 [a,g]	300.0±3.0 [d,e]	359.0±1.0 [a,e,f,g]	4.6±1.4 [c,d,e]	32.2±2.3 [b,c,d]
PLA/MLO-10Wool	60.4±0.8 [b]	104.1±1.3 [a,b]	169.8±1.4 [a,b]	21.4±2.4 [b,e]	297.3±4.0 [d,e]	358.3±0.6 [a,f,g]	5.3±0.7 [d,e]	37.8±1.1 [c,d]
PLA/MLO-10Wool-1TVS	60.8±0.5 [b]	107.4±1.7 [b]	170.4±1.1 [a,b]	15.8±2.0 [a,c]	296.7±7.6 [d,e]	357.3±0.6 [a,g]	4.6±1.5 [c,d,e]	36.9±1.6 [d]
PLA/MLO-10Wool-2.5TVS	60.4±0.1 [b]	107.1±2.5 [b]	169.6±0.9 [a,b]	15.3±0.7 [c,d,g]	293.0±5.2 [e]	360.0±1.0 [a,b,c]	5.8±0.8 [e]	36.0±1.0 [b,c,d]

[a–d] Statistically significant differences between formulations are indicated by different letters within the same property ($p < 0.05$).

The thermal characteristics of manufactured FRPs was evaluated using TGA, with conclusions presented in Table 9 and Figure 67. The onset degradation temperatures, corresponding to 5% mass loss, were used to assess the initial degradation of the PLA-based materials. A decline in T_5 was spotted across all PLA/MLO formulations, which is usual for PLA plasticized systems [89,113,200]. The greatest T_5 was recorded for PLA/MLO blend reinforced with 1 phr of neat wool (T_5 = 326.3 °C), showing PLA/MLO-1Wool formulation as most stable in terms of temperature resistance among studied FRPs. Increasing the wool concentration tends to remarkably reduce the thermal stability of the FRPs, likely due to the relatively low stability of fibers themself. The surface treatment with TVS of the fibers had a notable impact on FRPs having 10 phr of wool, whereas the T_5 dropped below 300°C. As concluded in similar studies for flax/glass fiber reinforced composites, surface modification can increase the decomposition temperature of natural fibers to above 300 °C, thereby enhancing thermal stability [222]. Still, this increase was noted only in FRPs reinforced with 1 and 5 phr of wool fibers. Despite this, all of evaluated FRPs showed T_5 values exceeding 280 °C, indicating stability under the manufacturing conditions used, without degradation of the fiber or MLO during manufacturing. The mass loss observed between 30 and 250 °C

(Figure 67a,b) corresponds to the early stages of wool fiber mass loss, primarily due to moisture evaporation, especially in neat sheep wool fibers and FRPs with greater fiber concentration (PLA/MLO-5Wool and PLA/MLO-10Wool, Figure 67a). Generally, the T_{max} of unmodified PLA and all evaluated FRPs was lesser than that of PLA/MLO blend, with the exclusion of PLA/MLO-5Wool-1TVS. The addition of MLO increased the T_{max} of neat PLA, indicating a favorable interface between MLO and the PLA polymer.

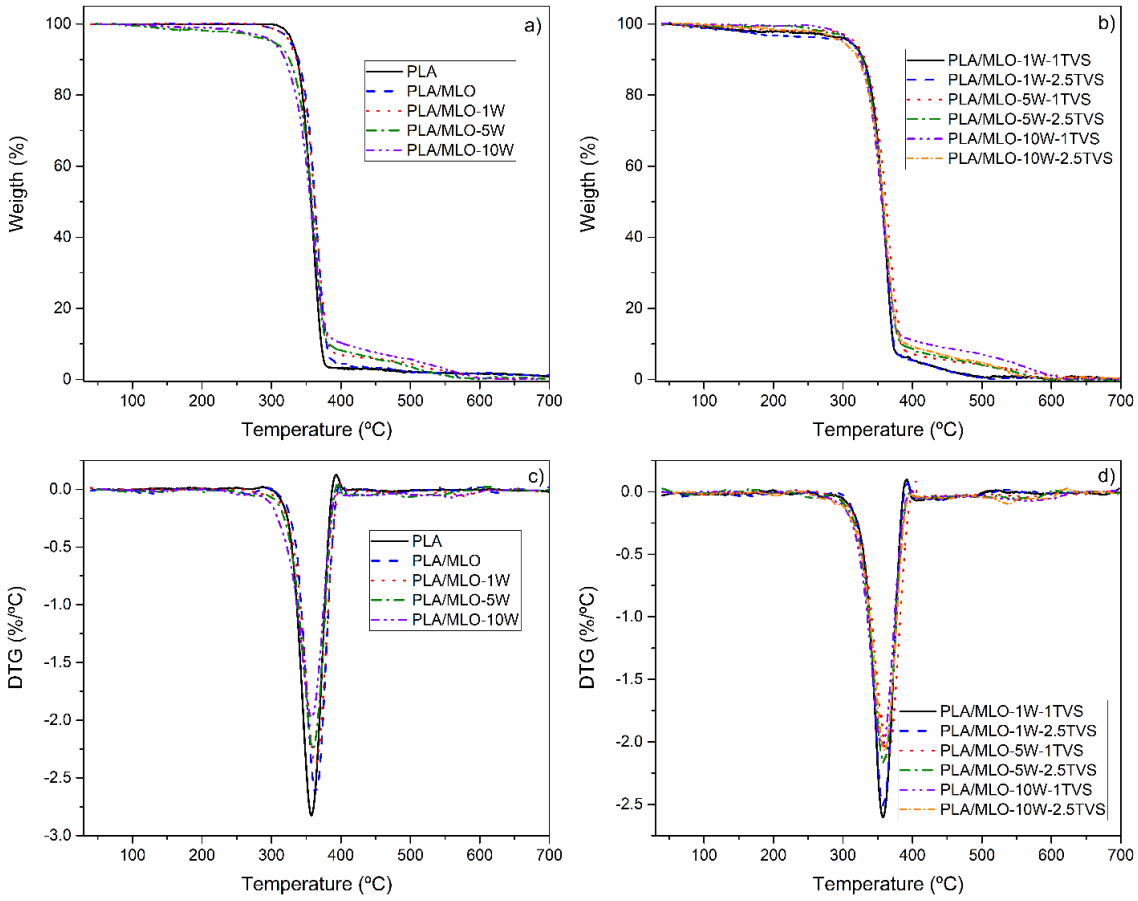

Figure 67 (a) TGA and (c) DTG of PLA, PLA/MLO, and untreated wool composites; (b) TGA and (d) DTG of TVS wool-treated composites.

The reinforcement with low concentrations of the wool fibers (1 and 5 phr) largely kept the T_{max} of PLA/MLO blend, with a slight decrease that showed insignificant changes referring to the neat PLA. In the reinforced materials, where 1phr of wool was utilized (PLA/MLO-1Wool-1TVS and PLA/MLO-1Wool-2.5TVS), the silane treatment marginally reduced T_{max} temperatures, though the changes were statistically insignificant ($p > 0.05$). An opposite trend was spotted for 5 phr wool FRPs, where the silane modification with 1 phr of TVS (PLA/MLO-5Wool-1TVS) increased the T_{max} compared to similar FRPs, but without treatment (PLA/MLO-5Wool), and even exhibited a slightly greater temperature than PLA/MLO ($p > 0.05$), signifying improved fiber compatibility with the plasticized PLA/MLO matrix due to the TVS treatment. For formulations with the highest fiber content (10 phr), the T_{max} temperature decreased to levels comparable to unmodified PLA ($p > 0.05$). However, the TVS modification of 10 phr wool fibers with 2.5 phr of TVS coupling agent mitigated this reduction, indicating that functionalization offset the

negative impact of high fiber content by improving fiber compatibility. These findings suggest that the FRPs are thermally stable during manufacturing cycles, and the reinforcement with either neat or TVS-treated wool fibers insignificantly influence the thermal decomposition of the PLA/MLO matrix.

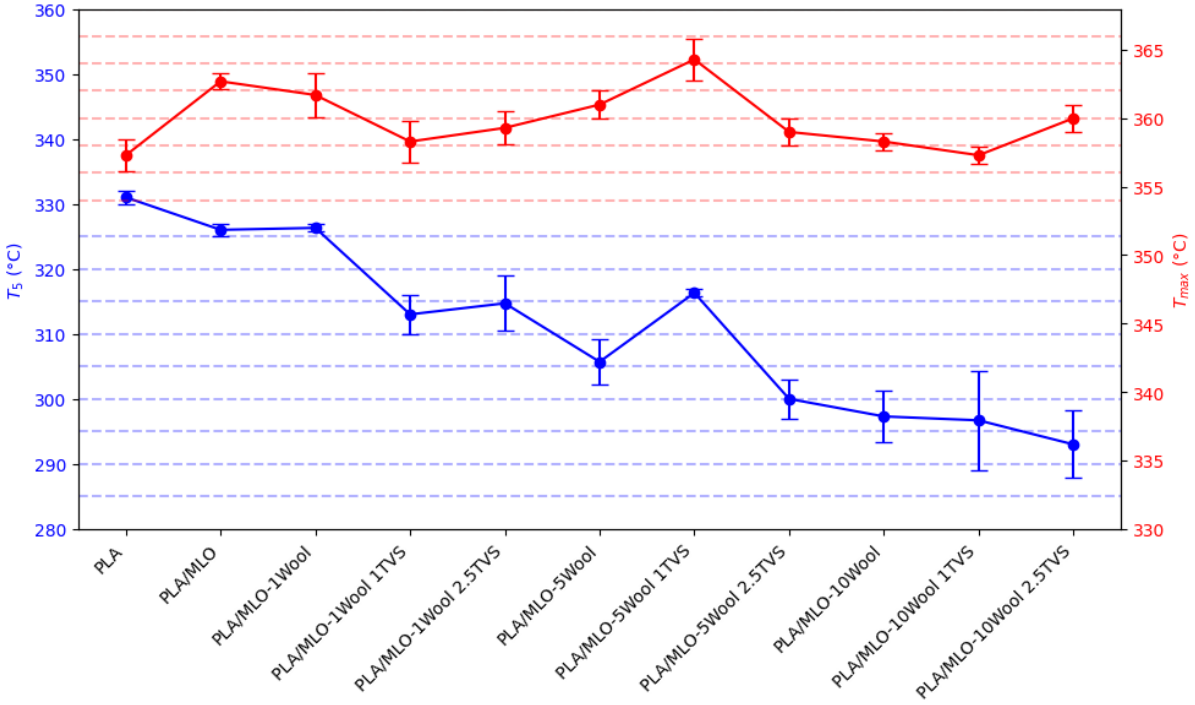

Figure 68 Temperatures of 5% mass loss and most intensive mass loss across formulations

A comparison of TGA results across tested formulations was shown in Figure 69. The mass loss temperature at the most intensive material decomposition was found to be similar across tested formulations and no significant tendency was observed. However, as comparing initial material degradation at 5% mass loss, presence of natural plasticizer and bio-derived fiber is clearly observed. Not only PLA material decompose in lower temperatures after blending with MLO, but also with increasing content of wool fiber. Additionally, presence of TVS treatment did not influence the beginning of decomposition significantly, as result is comparable to unmodified wool fiber formulations, irrespective of the wool concentration in the material.

Mass loss at 300 °C and 350 °C was measured to evaluate further FRPs degradation. Alike to the 5% mass loss analysis, the least mass loss at aforementioned evaluation point was detected for the PLA/MLO-1Wool FRP. At 300 °C, the highest was content of neat wool, the highest change in mass loss was observed, rising from 1.2% for the 1 phr wool in FRP to 5.8% for the 10 phr wool in FRP. Though the mass loss at 300°C varied across evaluated formulations, the effect of higher wool content or TVS treatment insignificantly altered the mass losses. The greatest mass loss was observed in the FRPs with 10 phr of wool, corresponding to the greater fiber content. At 350 °C, increasing wool concentration in the FRPs led to significantly greater mass loss, particularly when comparing FRPs reinforced with 1 phr and 10 phr of wool fiber. Surface

alterations using TVS on the wool fibers, irrespective concentrations of the coupling agent, insignificantly affected mass loss between FRPs with the constant wool content. Overall, all evaluated formulations remained permanent within the temperature ranges used for extrusion and injection molding manufacturing.

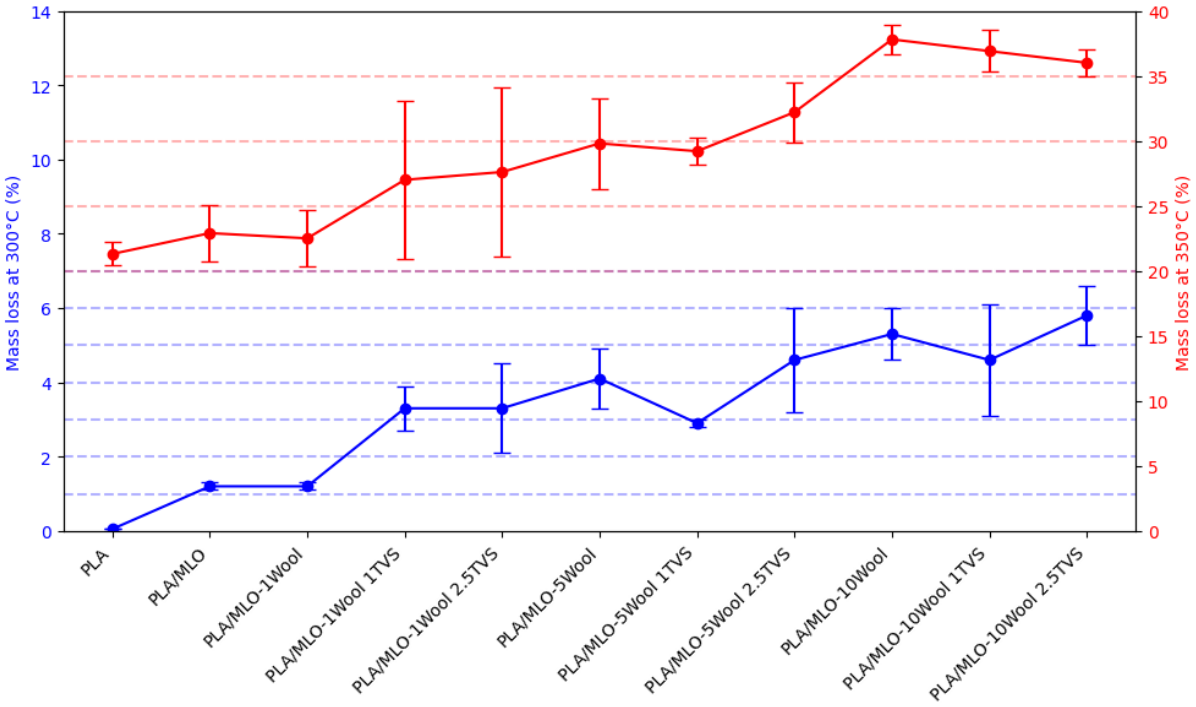

Figure 69 Mass loss results at 300°C and 350°C across tested formulations

The findings described for the 5% mass loss temperature are further supported with tendencies for mass loss at 300°C and 350°C, as shown in Figure 69. A tendency for higher mass loss correlated with presence of natural ingredients in the formulations are clearly spotted. This is especially visible as wool fiber content increases in material, showing that wool fiber decomposes rapidly between 300°C and 350°C. Similarly, no clear impact of silane treatment was observed, as formulations with the same wool content have shown rather similar mass losses at considered temperatures.

2.5. Surface Characteristics

From practical perspective fiber reinforced polymers are subjected to impact-related damages, such as those resulting from free-fall impacts, through blows, or clashes. Since impact strength is an important mechanical property, an SEM analysis was conducted on the specimens derived from impact test showing their fractured surfaces. This analysis aimed to better understand the structural performance of the evaluated FRPs after impact applied to material. While as aformentioned the PLA/MLO phase exhibited a regular fracture superficial based on the excellent miscibility between the two components [89], the SEM evaluation was centered on regions where gaps

between the polymer and fiber were visible, and their interaction was examined in detail (Figure 70). For the formulations where TVS treatment was applied were observed additional linkages between PLA/MLO blend and wool fiber. Such improvement in compatibility in materials, comparing to untreated wool fibers, is considered as a main reason for enhancement mechanical performance of the FRPs.

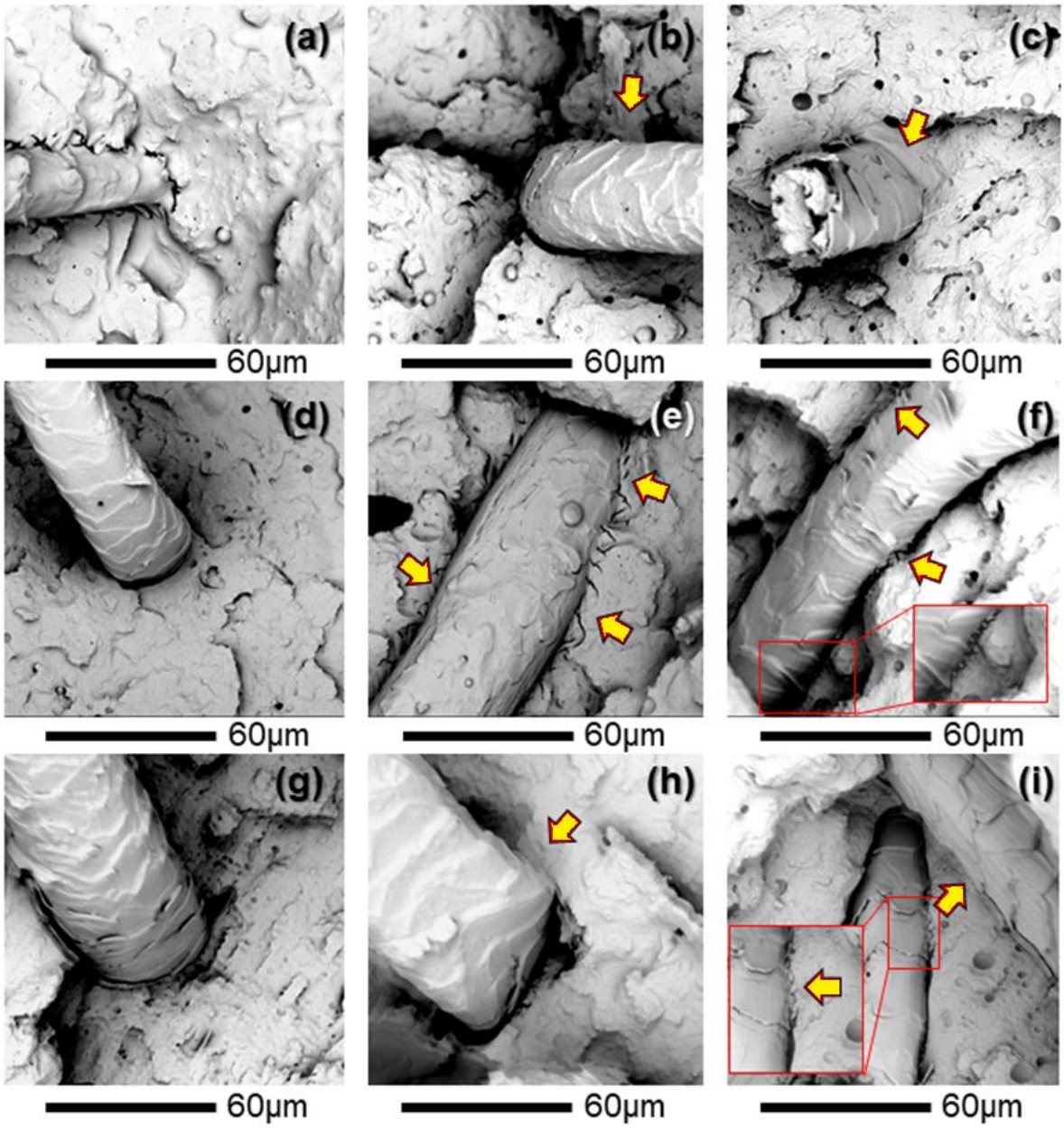

Figure 70 SEM micrographs of (a) PLA/MLO-1Wool, (b) PLA/MLO-1Wool-1TVS, (c) PLA/MLO-1Wool-2.5TVS, (d) PLA/MLO-5Wool, (e) PLA/MLO-5Wool-1TVS, (f) PLA/MLO-5Wool-2.5TVS, (g) PLA/MLO-10Wool, (h) PLA/MLO-10Wool-1TVS, and (i) PLA/MLO-10Wool-2.5TVS.

The wettability and color evaluation of the FRPs` superficial are presented in Table 10. Neat PLA is recognized as a relatively hydrophobic polymer [229] with a fixed

the WCA equal 77°. Though, it demonstrates greater wetting as conventional petroleum-based polymers like polypropylene (PP) [230] and low-density polyethylene (LDPE) [203], which have fixed WCA equal approximatelly 100°. Incorporating MLO to the PLA decreased the water contact angle, which can be attributed to enhanced chain mobility of macromolecule when plasticized, enhancing the diffusion of the polymer [113]. The wettability results, which are summarized in Table 10, show that modifying the PLA/MLO blend with either neat or TVS-treated wool remarkably enhances the hydrophobicity of the FRPs. While increasing the content of unmodified wool in the blend boosts the material's hydrophobicity, the TVS treatment does not show a consistent trend in this regard. Notably, the hydrophobicity of FRPs grew by up to 20% compared to the PLA/MLO blend.

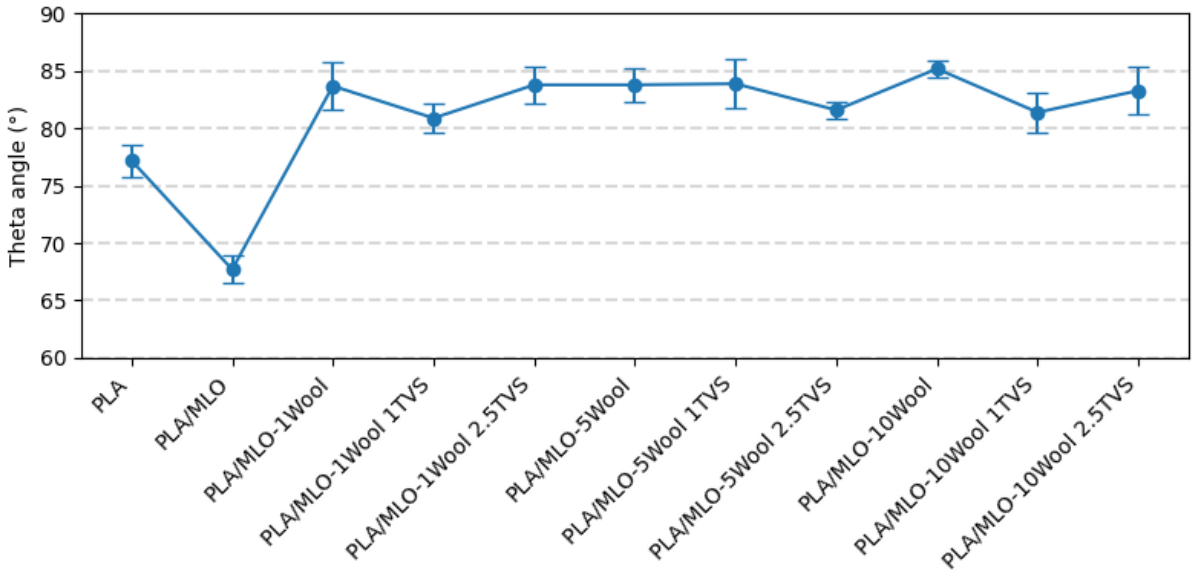

Figure 71 Wettability of tested formulations

As presented in Figure 71, material wettability changes significantly after blending PLA with MLO indicating a reduction in the property. However, irrespective of wool fiber content and silane concentrations applied, wettability increases after PLA-MLO reinforcement, exceeding even initial wettability of neat PLA polymer.

Color changes were evaluated using the CIELab color space, where L indicates lightness, a* represents red or green hues, and b* corresponds to yellow or blue tones. In terms of lightness, the greatest lightness was recorded for the PLA/MLO-1Wool-1TVS FRP (L = 51.16), while the opposite FRP in that term was PLA/MLO-10Wool (L = 37.73). The formulations with greater wool content exhibited a considerable reduction in L intensity, reflecting the darker presence of PLA-based FRPs as the sheep wool fiber concentration increased. A similar darkening effect has been stated for lignin-modified PLA-based materials, where with increasing lignin content color was appearing darker. Then again, wool fiber modified with TVS significantly increased the L intensity, with the most notable change observed in the PLA/MLO-10Wool-2.5TVS FRP, where lightness amplified by approximately 20% compared to PLA/MLO-10Wool.

Table 10 Wettability and CIELab color properties.

	Wettability	Color			
Formulation	WCA (°)	*L*	a*	b*	ΔE
PLA	77.2±1.4 [a]	37.55±0.81[a]	-0.19±0.04[a]	2.54±0.08[a]	-
PLA/MLO	67.7±1.2 [b]	43.58±0.71[b,e]	-1.91±0.10[a]	2.38±0.18[a]	-
PLA/MLO-1Wool	83.7±2.1 [c,f]	47.23±0.34[c]	0.48±0.97[b]	18.76±0.64[b]	17.0±0.7[c]
PLA/MLO-1Wool-1TVS	80.9±1.3 [d]	51.16±0.46[d]	-1.41±0.83[a]	15.16±0.17[c]	14.9±0.4[d]
PLA/MLO-1Wool-2.5TVS	83.8±1.6 [c,f]	47.18±1.34[c,e]	-0.41±0.85[a]	14.19±0.55[c]	12.5±0.9[e]
PLA/MLO-5Wool	83.8±1.5 [c,f]	44.05±0.55[b,e]	5.35±1.14[c]	22.11±0.43[d]	21.1±0.1[f,g]
PLA/MLO-5Wool-1TVS	83.9±2.1 [c]	44.01±1.54[b,e]	5.66±1.09[c,e]	21.59±0.99[d]	20.7±1.0[f]
PLA/MLO-5Wool-2.5TVS	81.6±0.7 [d]	46.54±1.01[c,e]	4.60±1.09[c]	21.49±0.54[d]	20.4±0.7[f]
PLA/MLO-10Wool	85.2±0.7 [e]	37.73±1.78[a]	8.60±1.02[d,e]	19.46±1.42[b]	21.±0.8[f,g]
PLA/MLO-10Wool-1TVS	81.4±1.7 [d]	45.04±0.98[e]	7.86±1.46[d,e]	22.82±1.32[d,e]	22.7±1.7[g,h]
PLA/MLO-10Wool-2.5TVS	83.3±2.1[f]	45.24±0.35[b,c,e]	7.51±1.07[e]	23.81±0.41[e]	23.5±0.1[h]

Significant alterations in the a* intensity were spotted with rising wool concentrations, shifting from 0.48 in PLA/MLO-1Wool to a color change to a red hue (a* values greater than 0), achieving 8.60 in PLA/MLO-10Wool. Similarly, the b* intensity remarkably intensified with greater wool concentration, with all FRPs exhibiting a yellowish tint. This is consistent with earlier studies, where the PLA/MLO blend reinforced with 1 phr of wool fibers exhibited a yellow appearance [200].

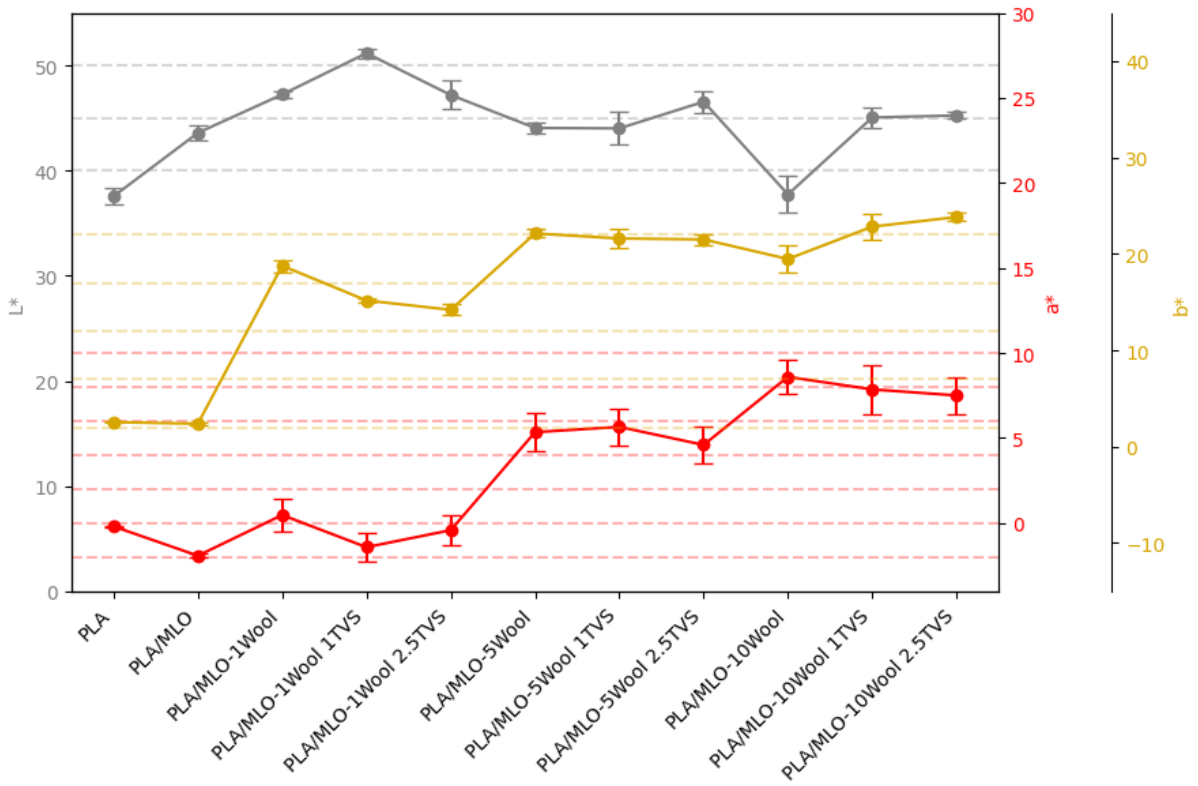

Figure 72 Color of tested formulations

Differences in color appearance (∆E) of the evaluated FRPs indicate a noticeable change between PLA/MLO and the FRPs containing varying amounts of sheep wool fibers. Since color changes are perceptible to the human eye for ∆E exceeding 2 [231], was assumed that all the FRPs differ remarkably from PLA/MLO blend. Adding the wool fiber concentration from 1 to 5 phr resulted in evident color alterations, while the FRPs containing 5 and 10 phr showed no substantial alterations in color. Based on the color analysis, it can be outlined that surface treatment of wool fibers with TVS coupling agent has a substantial effect on the intensity of the composite's yellow color, particularly as wool fiber content increases.

Concerning general tendencies observed across the tested formulations, as shown in Figure 72, a visual appearance of material changes due to its modification. As material lightness is changing while modification with MLO and wool fiber, the most evident changes are visible for a* and b* factors. The change is most remarkable with increasing content of wool fiber, irrespective of TVS concentration applied, both red and yellow color intensity increases with increasing amount of wool fiber.

3. Plasma-modified sheep wool fibers for poly(lactic acid)-maleinized linseed oil system reinforcement

3.1. Wool modification

Wool fiber treatment was undertaken using air and nitrogen plasma, with treatment durations extending up to 20 seconds. Examination of the FTIR spectra, as illustrated in Figure 73, reveals that both types of plasma treatment reveal only minor effects on the measurements. Haque et al. [194] interpreted that numerous FTIR spectra peaks signify bonds characteristic to the wool structure. The presence of Amide, the stretching C=O bond observed at 1630 cm^{-1}, while the presence of Amide II is identified by the bending N-H and stretching C-N bonds at 1530 cm^{-1}. Although a slight reduction in the intensity of these peaks is evident following plasma treatment, their wavelengths remain unchanged.

Furthermore, in the 1300-1450 cm-1 region, a combined peak for Amide III, indicating various bonds such as stretching C-C, C-O, C-N, or N-H, may appear for wool fiber. However, this specific peak was not distinctly observed in the examined wool samples. Another characteristic bond for wool is the C-H vibration bond occurring in the region of 2800-3000 cm^{-1}, representing lipids on the surface of the fibers. Notably, even a brief plasma treatment, regardless of the type of gas employed, demonstrates a reduction in the peak intensity, signifying the cleaning of the wool fiber surface. Notably, some samples exhibited a new peak at 2350 cm^{-1}, attributed to carbon dioxide contamination during measurement; however, this does not significantly impact the overall material analysis.

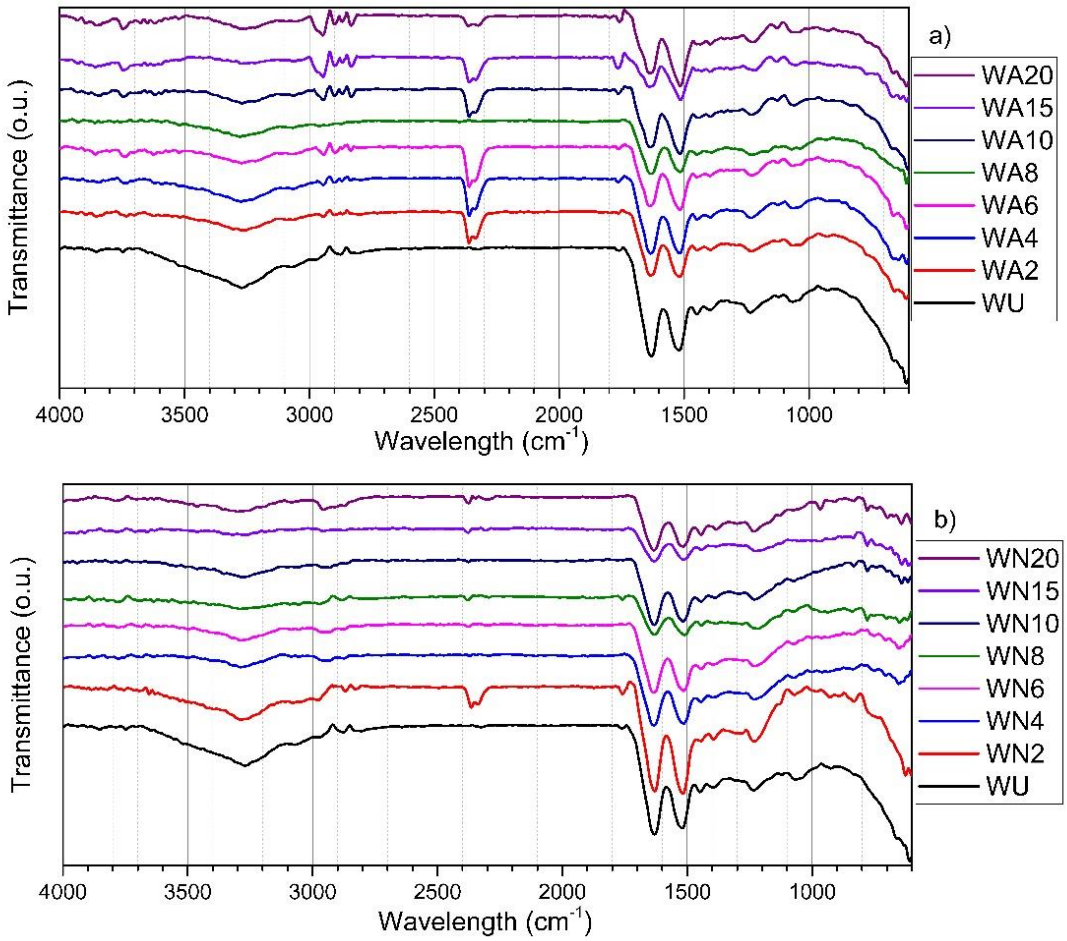

Figure 73 Fourier Transmittance Infrared spectra of a) air plasma treated wool, b) nitrogen plasma treated wool.

In addition to the FTIR analysis, microscopic observations were carried out, and a selected representation of the spectra is illustrated in Figure 73. As predicted, the structure of wool fibers remained intact following the application of both air and nitrogen plasma treatments within the evaluated time, preserving a uniform surface with rounded edges. [232] The impact of the executed plasma treatment can be characterized as a cleaning process, leading to a reduction of the lipid layer and an enhancement in the smoothness of the fiber surface. This pretreatment is recognized for establishing multiple bonding points linking the fiber and the polymer matrix, thereby promoting interlocking and improving interfacial compatibility.[64,65] Among the wool fibers subjected to the plasma treatment, those treated with air plasma for 8 seconds were chosen for further investigations due to their notable reduction in the lipid protective layer and the limited surface erosion associated with prolonged plasma exposure.

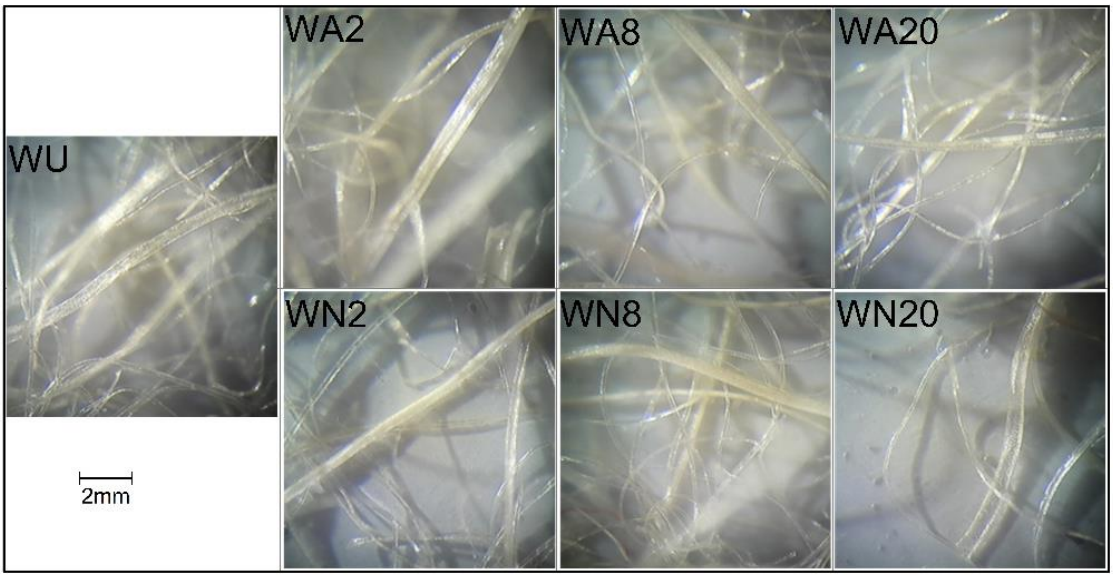

Figure 74 Micrographs of air and nitrogen plasma treated wool fibers.

3.2. Thermal properties

The assessment of fiber-reinforced polymers involved an examination of their thermal, mechanical, and structural characteristics. DSC measurements examined thermal properties, and the heating and cooling curves are illustrated in Figure 75, with the comprehensive results tabulated in Table 11.

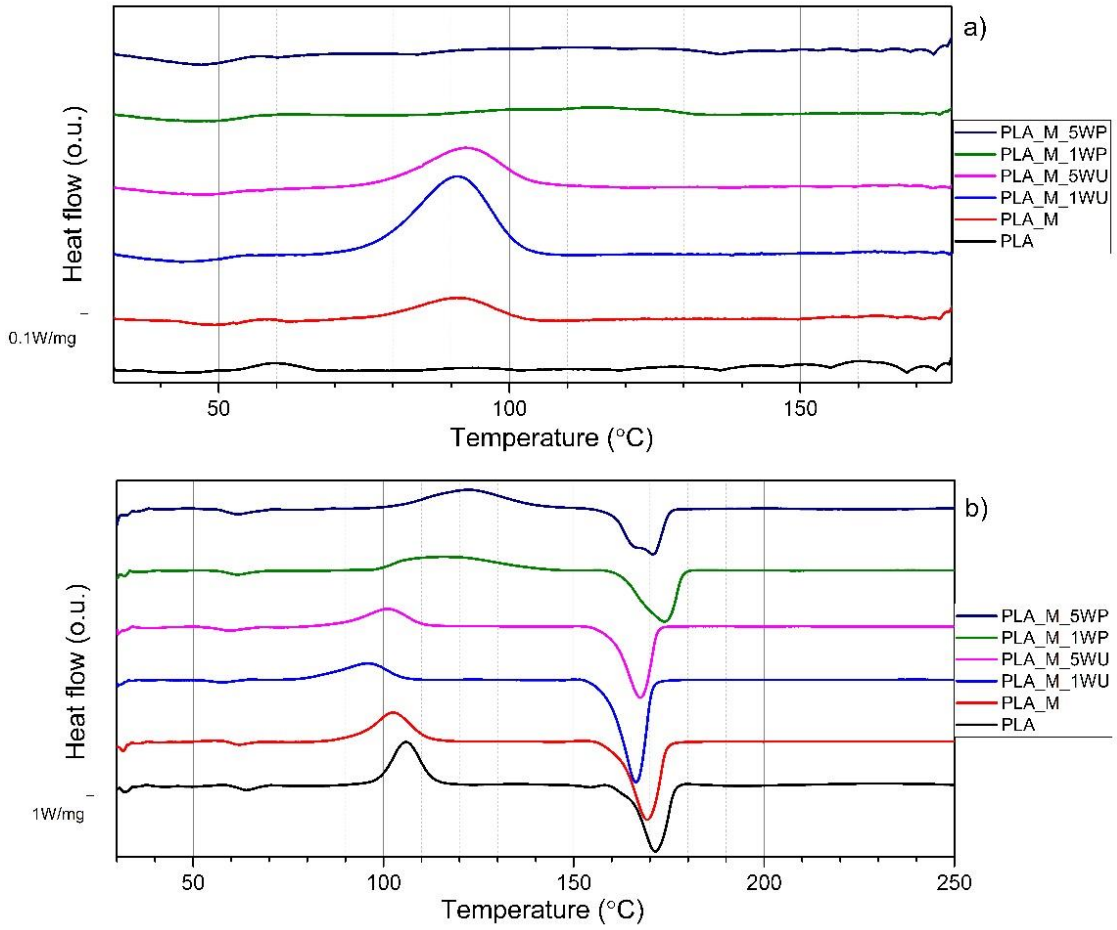

Figure 75 DSC measurements of tested formulations: a) first cooling cycle, b) second heating cycle

The initial cooling cycle exhibited a weak exothermic peak at 91-93°C for PLA_M and samples reinforced with untreated wool, suggesting the formation of a crystalline structure during cooling from the melted state. However, analysis of the heating curve from the second cycle did not reveal any additional crystalline phase resulting from this process. Subsequent samples exhibited no evident changes in material structure during cooling. Following the cooling cycle mentioned earlier, the subsequent heating cycle facilitated the characterization of glass transition, cold crystallization, and melting of the PLA composites developed in this study. For neat PLA, serving as a reference for subsequent modifications, the temperatures of the above transitions were 59.3, 106, and 171.3°C, respectively, with a calculated degree of crystallinity ($X_{c\%}$) of 10.11%. Modifying neat PLA with 10phr of maleinized linseed oil led to a reduction in these temperatures and an raise in $X_{c\%}$ to 23.09%. The addition of the oil additive enhanced PLA chain mobility and facilitated crystallization.

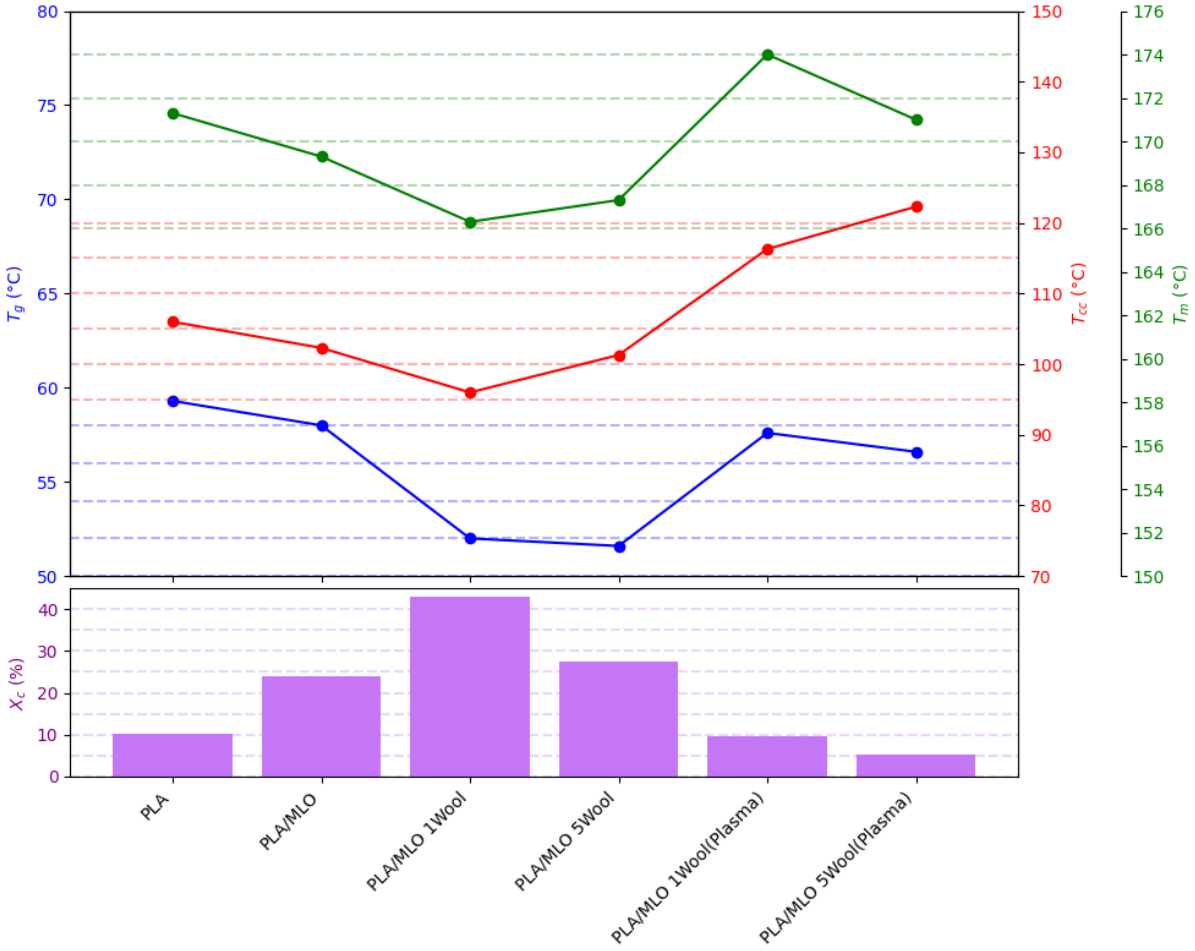

Figure 76 DSC results for evaluated formulations

Furthermore, reinforcement with untreated wool fiber, particularly in the PLA_M_1WU formulation, continued to decrease the temperatures and increase Xc, reaching the highest value of crystalline structure among the tested formulations. Contrary to observations reported by Cao et al.[233] regarding a decrease in cold crystallization temperature and easier crystallization after PLA reinforcement with carbon fiber, such trends were not fully applicable to the tested formulations. The Xc did not increase with higher untreated wool content and for formulations with plasma-treated FRPs.

Plasma treatment exhibited evident influences on the thermal properties of PLA FRPs, as shown in Figure 76. Although the T_g reduced for both tested concentrations, the decrease was not as significant as observed for formulations with unmodified fiber. Additionally, the T_{cc} was determined at significantly higher temperatures for plasma-treated formulations, and the temperature increased with wool fiber concentration. However, the cold crystallization peak was much broader for PLA_M_1WP and PLA_M_5WP than other formulations, affecting the melting temperature. The T_m for PLA_M_5WP exhibited values similar to those of the unreinforced formulation, whereas PLA_M_1WP showed a higher temperature. Notably, plasma-treated wool formulations showed a broader T_m peak, indicating a double maximum peak and the presence of different phases in the PLA crystalline structure. Moreover, $X_{c\%}$ decreased in neat PLA with an increasing concentration of plasma-treated wool fibers, aligning with observations by Enciso et al.[64], where plasma-treated flax fibers increased Tm and

reduced Xc due to the amorphous structure of fibers, limiting the formation of crystalline structure.

Concenring the effect of plasma modification on the DSC result several tendencies could be observed, as shown results of all tested formulations on Figure 76. It is clear that once plasma treatment was applied the degree of crystallinity in the formulation was lowered and it was observed irrespective of the considered wool fiber concentration. However, taking into account temperatures derived from the DSC tests, in case of formulations containing plasma treated wool, a growth in reference to untreated wool fiber was observed for glass transition, cold crystallization and melting temperatures. The increase was also spotted for both tested in the study wool fiber concentrations in formulation.

Table 11 DSC results of PLA formulations

Formulation						
	T_g [°C]	T_{cc} [°C]	T_m [°C]	ΔH_{cPLA} [J/g]	ΔH_{mPLA} [J/g]	$X_{c\%}$ [%]
PLA	59.3	106.0	171.3	26.12	35.52	10.11
PLA_M	58.0	102.3	169.3	25.11	44.44	23.09
PLA_M_1WU	52.0	96.0	166.3	16.85	52.34	42.88
PLA_M_5WU	51.6	101.3	167.3	15.72	37.38	27.40
PLA_M_1WP	57.6	116.3	174.0	28.38	36.25	9.51
PLA_M_5WP	56.6	122.3	171.0	28.42	32.55	5.22

3.3. Mechanical properties

Additionally to the material characteristics, mechanical properties were evaluated through tensile tests and Charpy's impact resistance. The tensile assessment relied on the stress-strain plots depicted in Figure 77.

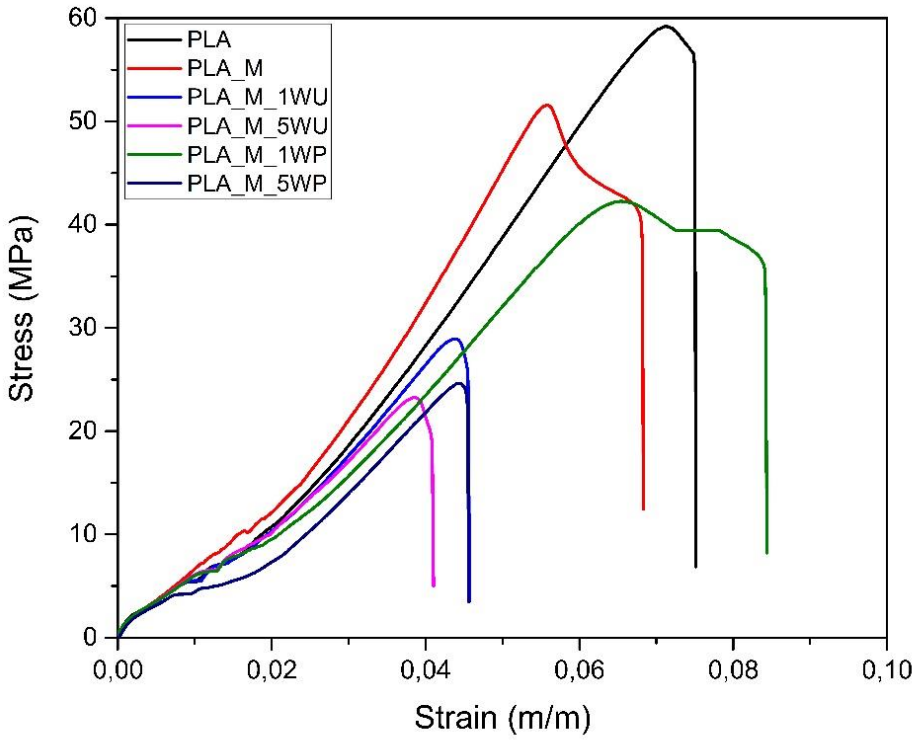

Figure 77 Stress-strain curves of PLA formulations

In the context of tensile properties, the highest tensile strength was obtained for neat PLA, as visible on Figure 78.Both modifications with MLO or wool fibers have lowered the tensile strength, as the modification of PLA introduces weak points in the continuous polymeric structure. Consistent with previous studies [174,200], an increase in wool fiber content in the PLA-MLO blend reduced tensile strength. However, while PLA_M_5WU and PLA_M_5WP exhibited similar results, the PLA_M_1WP formulation demonstrated a notable enhancement compared to untreated fiber, reducing the negative impact of untreated fiber addition to the PLA-MLO blend. Other research has confirmed that plasma treatment improves fiber reinforcement of polymeric materials, as observed in flax-reinforced polyethylene [64] or jute-reinforced PLA [65].

Similarly to tensile strength, elongation at break decreased after the blending of PLA with MLO and the PLA-MLO blend with untreated wool fiber. The concentration of wool fiber also led to a decline in elongation at break. However, considering the influence of plasma treatment, the PLA_M_1WP formulation exhibited a significant improvement in elongation, exceeding, on average, the elongation of neat PLA. This improvement is ascribed to the increased roughness of fibers and improved compatibility, although it was more evident at lower fiber concentrations. Among the Young modulus results, fiber reinforcement of the PLA-MLO blend reduced the modulus, which was further reduced by plasma treatment of fibers. Finally, in terms of toughness, the best tensile properties were demonstrated by the PLA formulation, followed by PLA_M_1WP. Notably, plasma treatment improved toughness compared to FRPs with untreated wool fibers.

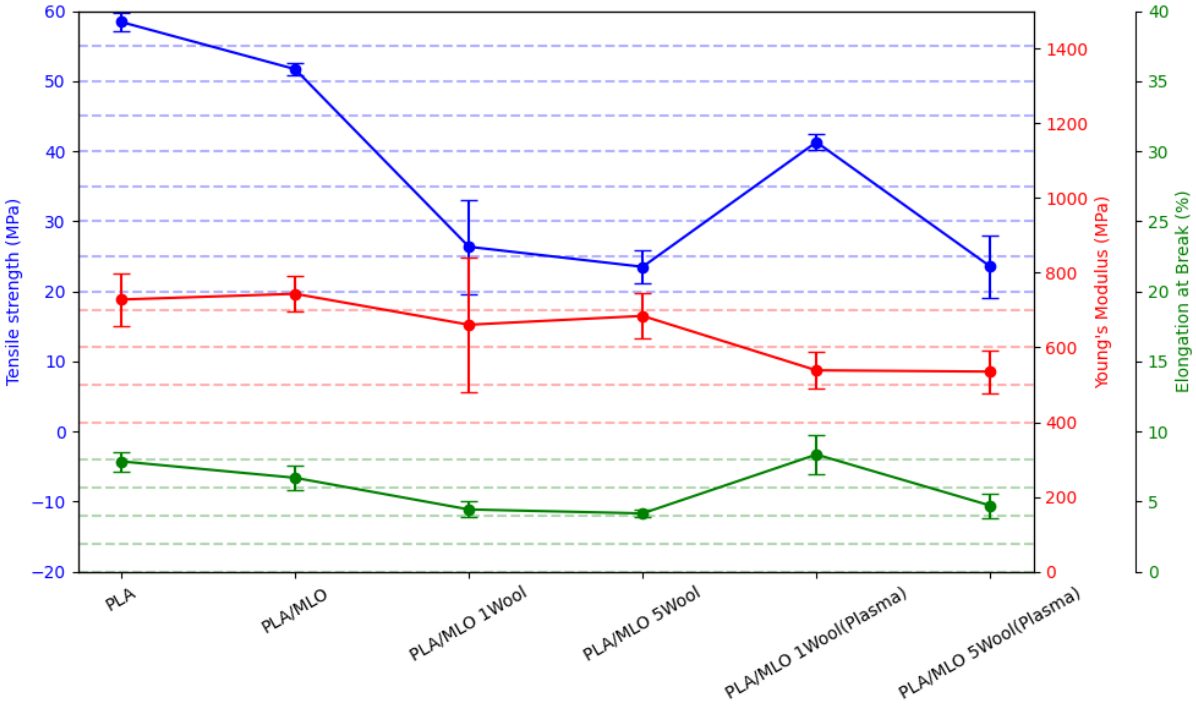

Figure 78 Tensile properties of evaluated formulations

Based on the Figure 78, for both Young modulus and elongation at break plasma treatment did not change the properties significantly, comparing to unmodified wool fibers. However, as wool fiber reinforcement has dropped tensile strength of material, for 1phr of wool fiber treated with plasma the negative effect of reinforcement was partially mitigated.

Mechanical properties were also assessed based on impact resistance. Both PLA and PLA_M formulations showed the highest resistance to impact, with a decrease in impact resistance corresponding to higher concentrations of wool in the formulations. Although the difference between untreated and plasma-treated was insignificant, on average, plasma treatment slightly compensated for the losses in impact resistance caused by wool fiber reinforcement. The observed improvement in impact resistance for FRPs after plasma modification can be attributed to the elimination of superficial impurities from the fiber and the enhanced smoothness of the fiber surface, which is in line with similar observations described by Nguyen et al.[234] for alkali-treated banana fiber used for PLA reinforcement.

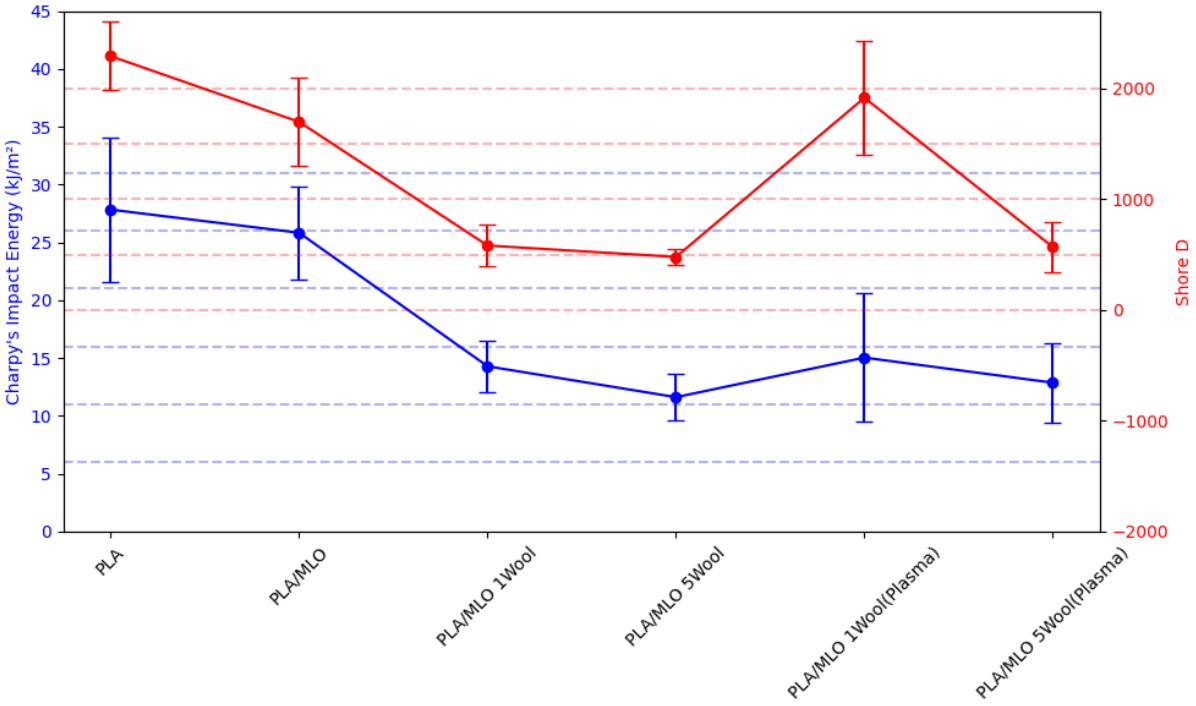

Figure 79 Hardness and impact resistance of tested formulations

As shown in Figure 79, similarly to tensile properties plasma treatment in both considered concentrations have shown rather similar results to formulations reinforced with unmodified wool fiber. However, the formulation with 1phr plasma treated wool have shown slightly higher hardness and impact resistance partially mitigating the negative effect.

Table 12 Mechanical properties of PLA formulations

Formulation	**Impact resistance**	**Tensile properties**			
	[kJ/m^2]	Tensile strength [MPa]	Elongation at break [%]	Young modulus [MPa]	Toughness [kJ/m^3]
PLA	27.83 ± 6.26	58.43 ± 1.36	7.87 ± 0.70	728.1 ± 69.8	2292.0 ± 309.2
PLA_M	25.83 ± 4.04	51.70 ± 0.92	6.70 ± 0.85	743.4 ± 47.3	1698.8 ± 396.8
PLA_M_1WU	14.29 ± 2.22	26.36 ± 6.71	4.44 ± 0.57	660.7 ± 178.9	582.5 ± 190.1
PLA_M_5WU	11.62 ± 2.02	23.50 ± 2.36	4.16 ± 0.24	684.3 ± 61.2	479.5 ± 72.8
PLA_M_1WP	15.04 ± 5.53	41.29 ± 1.12	8.36 ± 1.36	538.7 ± 48.1	1916.6 ± 512.0
PLA_M_5WP	12.87 ± 3.45	23.55 ± 4.42	4.72 ± 0.87	535.3 ± 57.3	568.83 ± 225.0

3.4. Microstructural properties

The FTIR spectra of the examined formulations are presented in Figure 80. In the case of neat PLA, several characteristic peaks were expected. The presence of the C=O

stretching bond is evident at 1780 cm^{-1} and 1680 cm^{-1}, while the peaks at 1750 cm^{-1} and 1180 cm^{-1} correspond to the C-O-C stretching of PLA.[235] Other bonds at 1275 cm-1 and 1020 cm-1 can be attributed to C-O stretching bonds, while the peak at 2950 cm^{-1} indicates C-H stretching bonds. [236] After blending PLA with MLO and wool fiber, whether untreated or treated with plasma, the C-O-related peaks intensified, with a slight shift towards lower wavelengths. Furthermore, as previously suggested, the C-H stretching bond intensified following the reinforcement with wool.

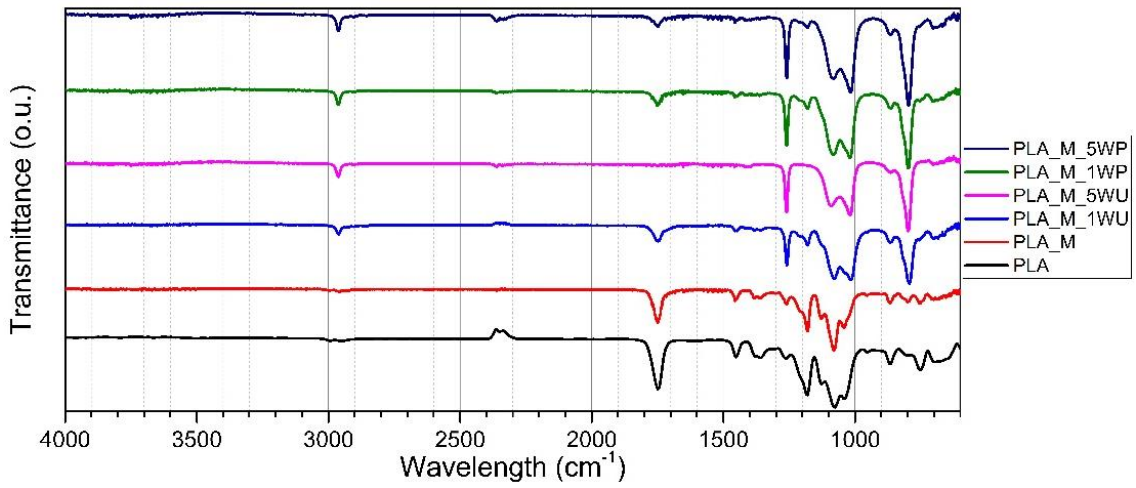

Figure 80 FTIR spectra of PLA formulations

3.5. Surface properties

The material surface characterization involved wettability and color studies, with the results summarized in Table 13. Wetting was assessed through contact angle measurements, representing the angle between a drop of water and the flat surface of the polymeric formulation. All tested formulations exhibited good wettability, with contact angles below 90°. The modification of PLA with MLO facilitated the wetting of the material, which can be associated with increased PLA chain mobility after blending with MLO. [174] Adding untreated wool fibers to the PLA-MLO blend reduced the contact angle, indicating improved wettability. However, no correlation was identified between wettability and fiber concentration in FRPs. In contrast to untreated fibers, plasma-treated wool maintained a similar wettability to the PLA-M formulation. Although previous studies suggested that plasma treatment of wool fabrics [232] or flax fibers [64] significantly enhances the wettability of the fibers, primarily due to the reduction of fatty acids on the surface and partial surface destruction, this observation did not extend to PLA formulations with plasma-treated wool fibers.

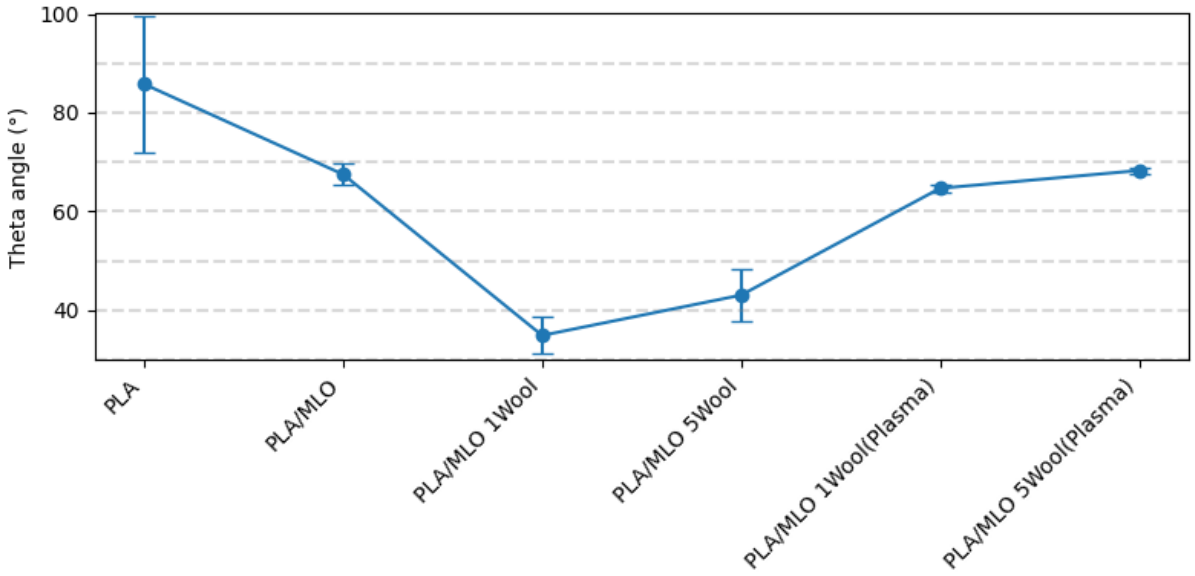

Figure 81 Wettability results of tested formulations

Based on the comparison presented on Figure 81, plasma treatment was found to increase material wettability, comparing to unmodified wool fiber. This is related to surface alterations of wool fiber during the treatment process.

Table 13 Wettability and color of PLA formulations

Formulation	Wettability	CIELab color		
	Contact angle [°]	L*	a*	b*
PLA	85.74 ± 13.74	24.21 ± 1.01	21.78 ± 0.18	-8.37 ± 0.22
PLA_M	67.47 ± 2.19	32.47 ± 1.83	19.54 ± 0.22	-6.17 ± 0.33
PLA_M_1WU	34.87 ± 3.67	45.62 ± 0.35	21.24 ± 0.07	10.28 ± 0.34
PLA_M_5WU	43.03 ± 5.19	36.88 ± 1.58	26.28 ± 0.19	13.35 ± 0.99
PLA_M_1WP	64.66 ± 0.87	27.82 ± 0.24	27.34 ± 0.09	6.03 ± 0.17
PLA_M_5WP	68.26 ± 0.63	23.02 ± 0.61	30.13 ± 0.51	4.62 ± 0.46

The PLA-based formulations were ultimately assessed for their color appearance using the CIELab model. Regarding material lightness (L*), the modification of PLA with MLO resulted in a slightly brighter material, and this change intensified after further modification with untreated wool fibers. However, plasma-treated fibers reduced the lightness caused by the additives, leading to similar lightness between PLA and PLA_M_5WP, resulting in a darker material with an increasing content of plasma-treated fibers.

The a* value also revealed that all formulations exhibited red tonality, although with different intensities. Blending with MLO decreased the red intensity in color for PLA_M, while further reinforcement with wool increased the red color intensity with an increasing wool fiber content. Regarding the influence of plasma modification on the intensity of the red color, it intensified after treatment and with increasing wool content.

Finally, b*, corresponding to blue and yellow colors, indicated slight blue shades for both PLA and PLA_M formulations, as both showed negative b* values. However, FRPs containing untreated wool fiber shifted the color appearance significantly toward

yellow, and this effect increased with increasing content of untreated wool. Thus, the yellowish color of wool was observed to influence the final color of the polymeric material. Although plasma-treated wool fibers also shifted the color toward yellow, the difference was less noticeable than untreated wool. Moreover, an increase in the concentration of plasma-treated wool reduced yellow shades in color.

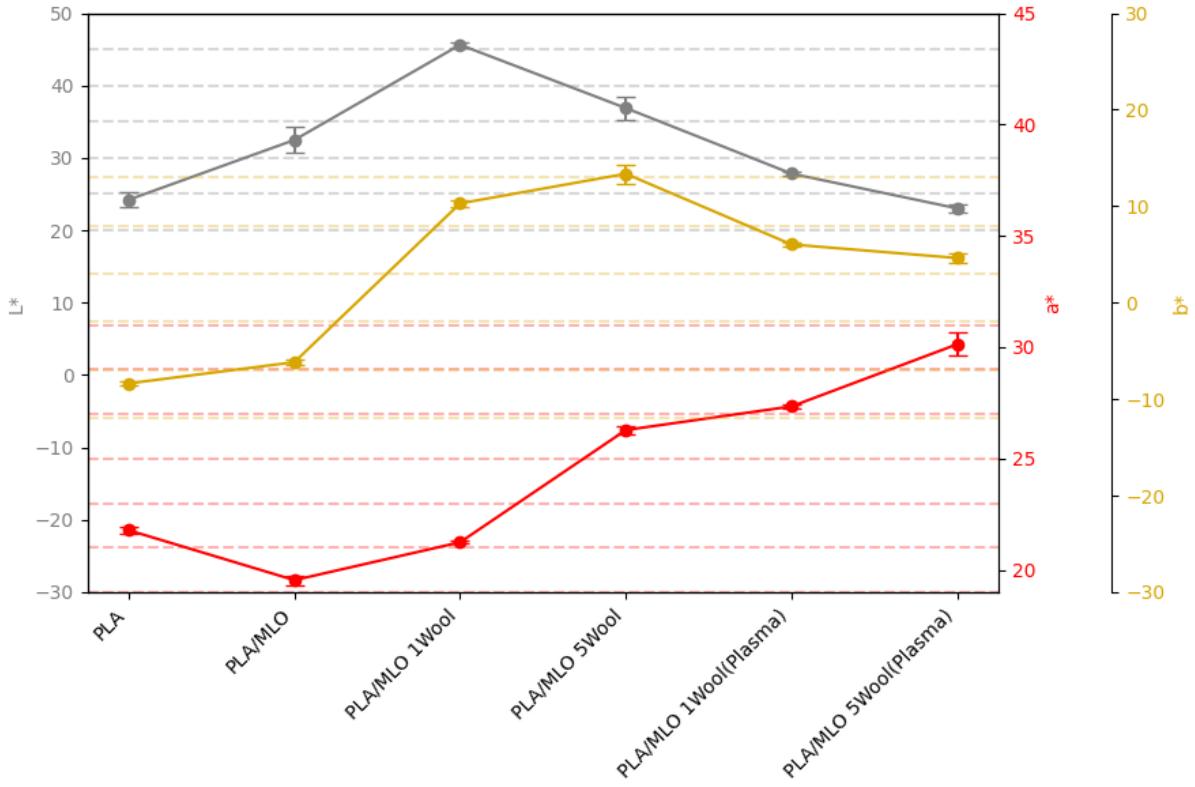

Figure 82 Color results of tested formulations

As compared on Figure 82 across tested formulations, color of materials changes between formulations with untreated and plasma treated samples. As usually presence of wool increases material lightness and intensity of yellow and red colors, plasma treatment of wool fibers slightly alters the appearance of material. A visible decrease in lightness and yellow appearance was found together with further increase in red appearance indicating changes in material color as a result of plasma modification of wool fiber.

4. Physical aging phenomenon of sheep wool fiber reinforced poly(lactic acid)-based materials

4.1. Mechanical properties

Among mechanical properties, formulations were assessed based on tensile and impact characteristics. In the preliminary phase before aging, the tensile properties indicated a ductile behavior in PLA-MLO-based formulations, particularly those reinforced with wool fibers. While PLA_0_N and PLA_0_A formulations exhibited comparable tensile strength and improved elongation at break, the remaining formulations containing wool showed a noteworthy reduction in elongation at break, suggesting a more brittle character in the aged materials. This decline in elongation at break may be attributed to a decrease in free volume and the occurrence of microcracking induced by internal stresses resulting from the aging process.

In the PLA_0 blends, aging led to an increase in elongation at break and a decrease in Young's modulus. While Kumar et al. [121] reported initial improvements in tensile properties during thermal aging, the present study, with a substantially more extended period of physical aging, anticipates a reduction in PLA tensile properties. However, this observed behavior might be influenced by the presence of MLO and its interactions with PLA during aging. Conversely, a decrease in Young's modulus was expected after four years of physical aging due to structural deformations. Such initial changes in mechanical properties are expected for PLA-based materials, leading to material reorganization and a reduction in internal stresses.

Moreover, formulations reinforced with wool exhibited reduced mechanical performance after four years of physical aging. Initially, both formulations reinforced with 1 phr and 5 phr of wool fibers demonstrated an enhanced elongation at break after wool modification with silane treatment. This trend was evident in comparisons between PLA_1_0_N and PLA_1_2.5_N, as well as PLA_5_0_N and PLA_5_2.5_N. Despite a reduction in elongation observed in all formulations, PLA_1_2.5_A, compared to PLA_1_0_A, demonstrated that silane treatment may mitigate the negative impact of aging and reduce material brittleness after aging. However, the mechanical performance of formulations containing 5 phr of wool revealed that PLA_5_0_A and PLA_5_2.5_A exhibited almost identical mechanical properties, with no discernible impact of silane treatment at this wool concentration.

Charpy`s impact energy results are summarized in Figure 84. On average, aging resulted in a slight reduction in impact resistance across the tested formulations, except for PLA-MLO blends reinforced with 1 phr of wool, where a minor increase was observed; nevertheless, these variations fall within the range of statistical error. Despite the known tendency of aging to induce increased brittleness in PLA, a significant reduction in impact resistance was not evident. This phenomenon can be attributed to the intricate nature of the employed formulations, comprising maleinized linseed oil and wool fiber as reinforcement, alongside the surface modification of wool using a silane coupling agent. In formulations PLA_1_0 and PLA_1_2.5, the adverse impact of aging was mitigated at low concentrations of wool reinforcement. Moreover, a positive effect following aging was noted for PLA_1_2.5_A, where silane treatment was applied to the wool reinforcement. However, such a favorable impact on average was not observed for higher wool concentration at 5 phr.

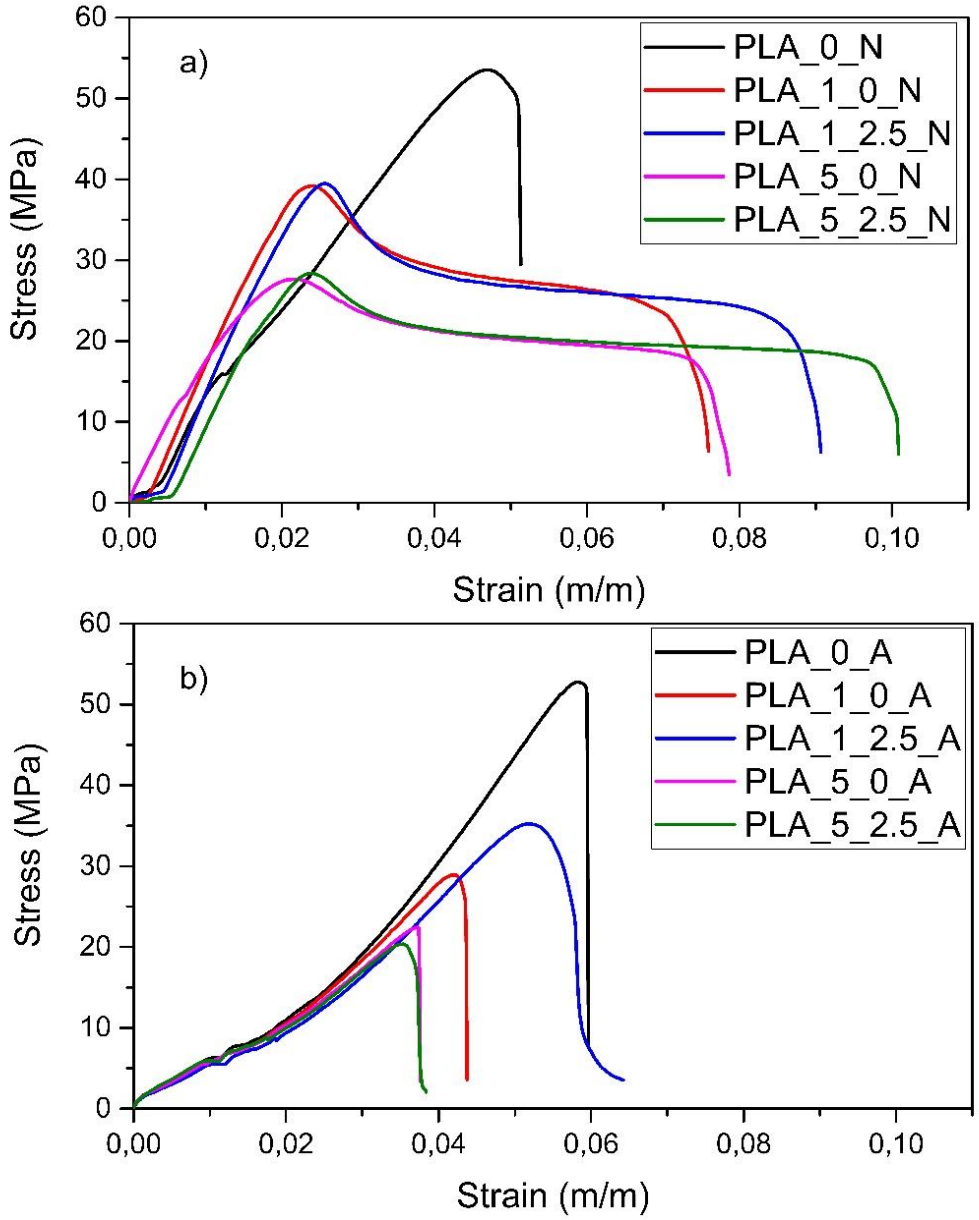

Figure 83 Stress-strain curves of the PLA formulations a) non-altered formulations, b) altered formulations

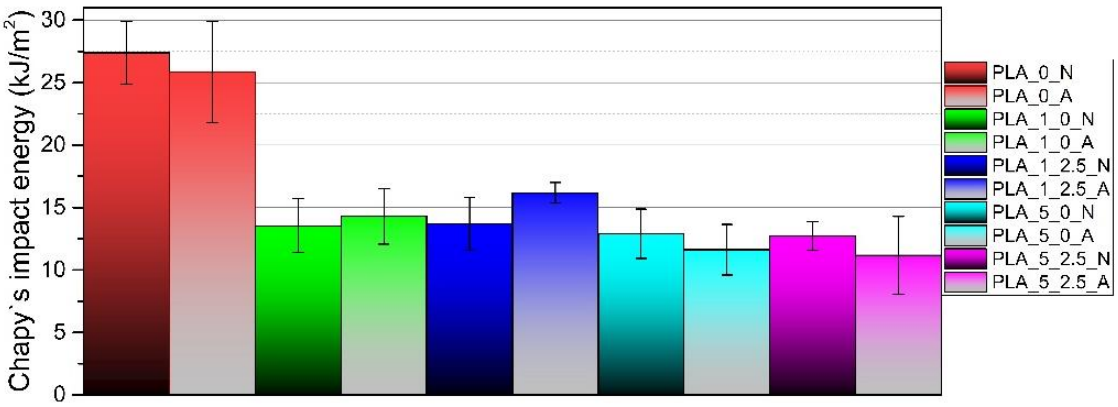

Figure 84 Impact resistance of the PLA formulations

4.2. Thermal properties

The results of DSC are shown in Figure 85. In the thermal characterization of PLA aging, the glass transition temperature (Tg) holds significant importance as it reflects alterations in crystalline structure. While an increase in Tg is commonly observed in many PLA aging studies, some studies indicate a decrease in temperature. These variations are typically attributed to recrystallization and internal stresses within the blend, with factors such as the cooling rate potentially influencing Tg changes during aging. The tested formulations exhibited diverse tendencies after aging; formulations like PLA_0_A or PLA_5_2.5_A increased Tg after four years, whereas PLA_1_0_A demonstrated the opposite decrease trend. Notably, formulations such as PLA_1_2.5_A or PLA_5_0_A showed no significant changes in Tg. Consequently, no distinct aging-related trend was evident based on wool concentration or silane treatment. However, the degree of changes in Tg was at a maximum of 1.3°C for PLA_0_A, whereas Akderya et al. [124] reported temperature changes ranging between 4°C and 10°C after five years of physical aging under comparable conditions for animal-derived fiber-reinforced PLA. Consequently, the aging of the tested formulations does not markedly impact the Tg temperature, maintaining a similar crystalline structure before and after aging.

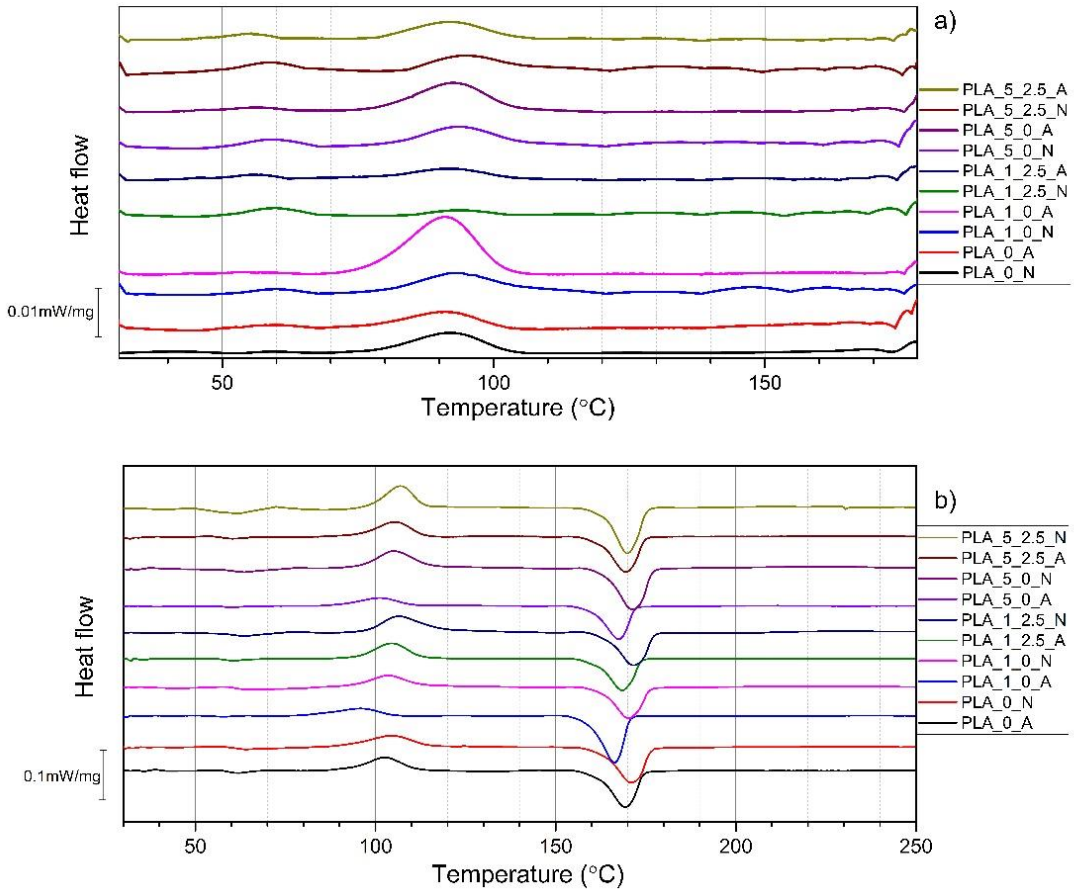

Figure 85 DSC curves of a) first cooling cycle, a) second heating cycle of PLA-based formulations

While the crystalline structure remains similar based on Tg evaluation, the degree of crystallinity (Xc) changes over time under the studied conditions. In contrast to PLA_1_0_A, where an increase in Xc is observed, all other tested formulations exhibited a reduction in the crystalline phase. This implies that the recrystallization of PLA, induced by internal stresses, is less efficient during aging. This observation may be attributed to the complexity of the multi-ingredient formulations, which could impede the recrystallization process. Conversely, the increase in Xc for PLA_1_0_A may be associated with insufficient crystallization during the injection-molding process, as evidenced by the decrease in other values such as Tg, Tm, Tc, and Tcc in comparison to the formulation PLA_1_0_N. Furthermore, among all formulations, PLA_1_0_A exhibited the highest peak of Tcc during the first cooling cycle, potentially explaining the high melting enthalpy in the second heating cycle.

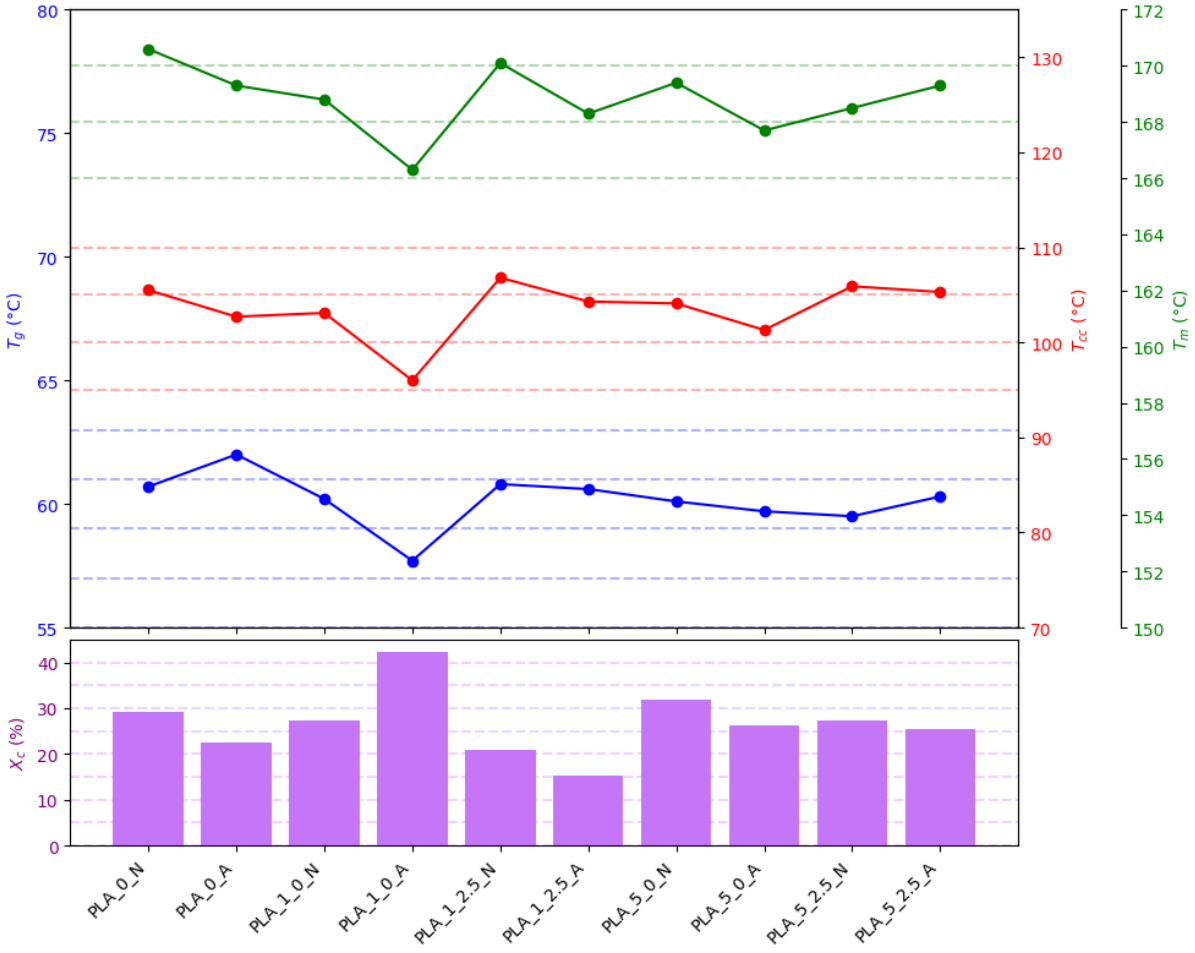

Figure 86 DSC results of tested formulations

Notably, for all formulations, singular peaks were observed in both T_m and T_g, suggesting that although the crystalline structure changes due to aging, no distinct phase separation occurs in the PLA matrix.

As plotted in the Figure 86, thermal characteristics on material changes over time. In general, almost all of the formulation has shown clean reduction in degree of crystallinity, irrespective of wool fiber concentration or treatment applied Additionally, towards glass transition, cold crystallization and melting temperatures no major changes are observed comparing non-altered and altered formulations. However, in general slight reduction in the temperatures is observed as general tendency over time.

Table 14 Results of cooling and heating cycles of DSC measurement

Formulation	DSC cooling cycle	DSC heating cycle					
	Tcc_{PLA} [°C]	Tg_{PLA} [°C]	Tc_{PLA} [°C]	Tm_{PLA} [°C]	ΔHc_{PLA} [J/g]	ΔHm_{PLA} [J/g]	Xc_{PLA} [%]
PLA_0_N	92.0	60.7	105.5	170.6	22.97	47.37	29.15%
PLA_0_A	91.0	62.0	102.7	169.3	24.54	43.31	22.43%
PLA_1_0_N	94.0	60.2	103.1	168.8	17.51	40.09	27.28%
PLA_1_0_A	90.7	57.7	96.0	166.3	16.91	51.87	42.24%
PLA_1_2.5_N	93.7	60.8	106.8	170.1	27.69	44.91	20.80%
PLA_1_2.5_A	91.6	60.6	104.3	168.3	26.31	39.05	15.39%
PLA_5_0_N	93.3	60.1	104.1	169.4	29.18	54.38	31.88%
PLA_5_0_A	92.7	59.7	101.3	167.7	16.24	37.00	26.26%
PLA_5_2.5_N	94.6	59.5	105.9	168.5	30.95	52.44	27.19%
PLA_5_2.5_A	92.0	60.3	105.3	169.3	24.44	44.49	25.36%

4.3. Surface properties

Color studies were conducted using the CIELab model, evaluating three factors: L*, corresponding to lightness on a scale from 0 for black to 100 for white; a*, where negative values represent green color and positive values represent magenta color; and b*, where negative values correspond to blue color and positive values correspond to yellow color. In non-aged formulations, the baseline PLA_0_N exhibited a lightness level of 43 with a slight reflection into green and yellow colors. Modification with wool fibers, as observed in PLA_1_0_N or PLA_5_0_N, led to a slight increase in color lightness, followed by a delicate shift towards magenta and a significant increase in yellow intensity derived from wool fibers. Silane treatment caused a reduction in both a* and b* values, though the change was not significant.

In the context of aged formulations, a consistent impact of aging on color is evident: the lightness of the color decreases, indicating darker shades; the a* value undergoes a significant shift towards magenta color; and the b* value either markedly weakens yellow color or transforms them into blue. While all examined formulations exhibit a darkening effect after aging, the most substantial change was observed for PLA_0_A, where L* decreased by over ten units. Regarding the a* and b* values, aging influences all formulations similarly, with no discernible separate influence based on wool concentration or silane treatment. Consequently, although additives initially influenced the color of the tested formulation, none of the changes, such as wool reinforcement or silane treatment, mitigated the color alterations induced by aging in PLA. Thus, alterations in color must be attributed to structural changes among PLA macromolecules.

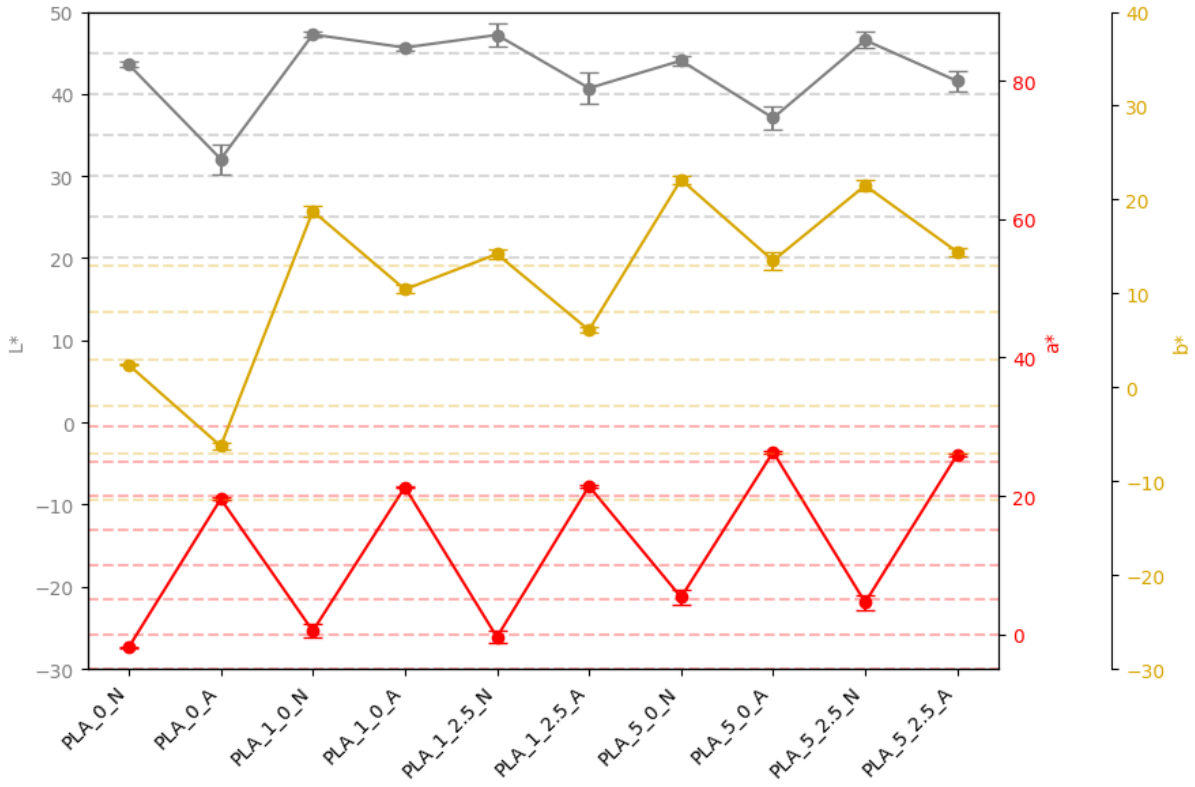

Figure 87 Color results of tested formulations

Based on Figure 87 a comparison of color changes across tested formulations were assessed. A general tendency could be observed, that material appearance changes over time, as material is darker, with decrease intensity of yellow color and increased intensity of red color. Such observation with difference intensity changes was found irrespective of wool fiber concentration or TVS treatment applied.

Wettability was evaluated by measuring how water droplets interacted with the material's surface. Generally, for non-aged formulations, the contact angle significantly increases between PLA_0_N and other wool-reinforced formulations, indicating a higher hydrophilic character of the material. Furthermore, an increase in wool content or silane treatment does not significantly influence wettability. On the other hand, aging did impact the wettability of the predominantly hydrophobic PLA_0_N formulation, where the contact angle increased by about 2° after 4 years of aging. However, wool-reinforced formulations, especially PLA_1_0_A and PLA_5_0_A, exhibited a substantial decrease in the contact angle, indicating a hydrophobic surface of the material. The reduction in wettability was compensated by silane treatment, as formulations PLA_1_2.5_A and PLA_5_2.5_A displayed more hydrophilic characteristics. The decrease in wettability for the wool-reinforced formulation may result from faster material aging alongside wool fiber, allowing water molecules from humidity to penetrate the blend into free spaces between wool fiber and PLA material. Furthermore, silane treatment, which improves compatibility between wool fiber and PLA, impeded water molecule penetration and reduced the impact of aging for the formulations.

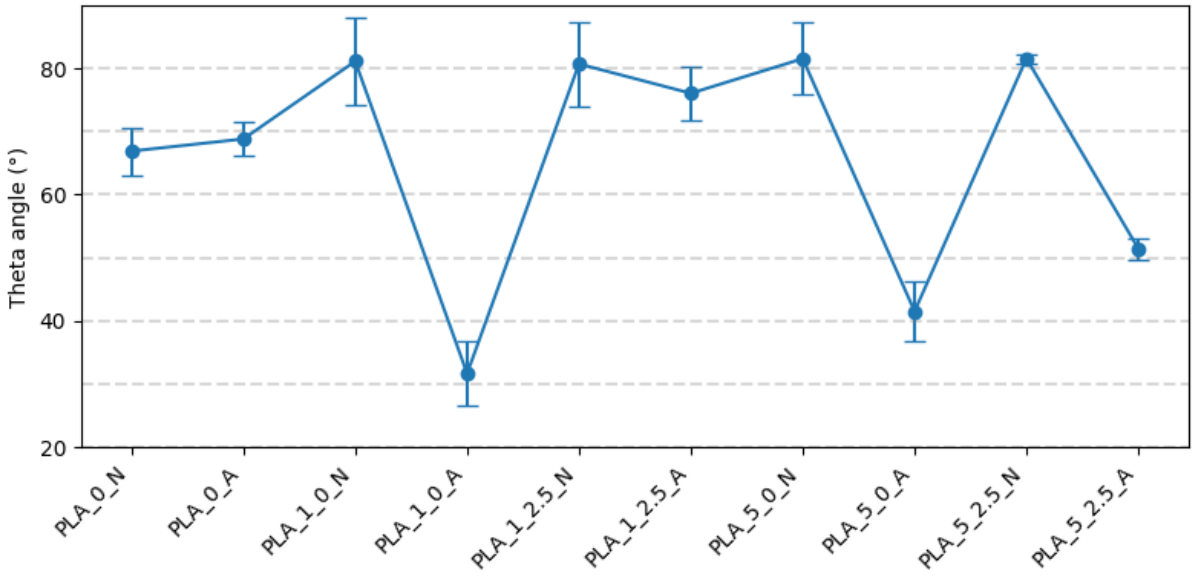

Figure 88 Wettability results of tested formulations

Material wettability was found to decrease over time as a general trend, as shown in Figure 88. Although for PLA-MLO blend wettability remain at comparable level over time, remaining wool fiber reinforced formulations have shown significant decrease in wettability after 4 years of ageing. The change is more evident for formulations where TVS silane treatment was not applied.

Table 15 CIELab color and wettability results of the PLA formulations

Formulation	**Color**			**Wettability**
	L*	a*	b*	[°]
PLA_0_N	43.57±0.36	-1.89±0.05	2.38±0.08	66.90±3.78
PLA_0_A	32.06±1.84	19.56±0.19	-6.27±0.37	68.82±2.71
PLA_1_0_N	47.23±0.35	0.48±0.97	18.76±0.64	81.14±6.84
PLA_1_0_A	45.64±0.31	21.26±0.08	10.42±0.43	31.65±5.12
PLA_1_2.5_N	47.18±1.34	-0.41±0.84	14.19±0.56	80.71±6.66
PLA_1_2.5_A	40.70±1.94	21.40±0.18	6.08±0.30	76.06±4.19
PLA_5_0_N	44.05±0.56	5.35±1.15	22.11±0.43	81.55±5.66
PLA_5_0_A	37.07±1.43	26.34±0.22	13.48±0.90	41.50±4.77
PLA_5_2.5_N	46.54±1.01	4.60±1.09	21.49±0.55	81.59±0.74
PLA_5_2.5_A	41.56±1.28	25.97±0.20	14.41±0.38	51.44±1.69

5. Predictive models for poly(lactic acid) materials reinforced with surface-modified sheep wool fibers

The methodology detailed earlier helped create models capable of simulating numerical values for those, as mentioned earlier, mechanical and thermal properties. The resultant score results were visually represented through graphical presentations for all tested coupling agents. Each coupling agent's evaluation was captured in four plots, corresponding to different properties. These plots, merged with their respective model evaluations, were collectively presented in figures ranging from Figure 89 to Figure 92. Additionally, Figure 93 displays the average measurement results with their standard deviation for selected formulations. [94,174] This figure also incorporated the corresponding scored results derived from the created models, providing a complete visualization of the models' relative performance against experimental measurements.

5.1. Tensile properties

The data export from the inference pipeline summarized simulated tensile strength properties across varied wool and coupling agent concentrations, including different types of coupling agents. The visual representation of tensile strength predictions is illustrated in both Figure 89 and Figure 90, wherein differences between tested algorithms are defined, with separate plots for each coupling agent.

Notably, each model type represents a distinct approach; for instance, the boosted decision tree groups data into a more condensed subset, while linear regression exhibits a linear change with parameter changes; furthermore, regarding the boosted decision tree model, wherein predictions for tensile strength can exhibit sharp differences between adjacent formulations. In contrast, linear regression consistently shows similar tensile strength predictions for adjacent formulations. This difference highlights the behavior of different models in capturing and representing the complex relationships within the data.

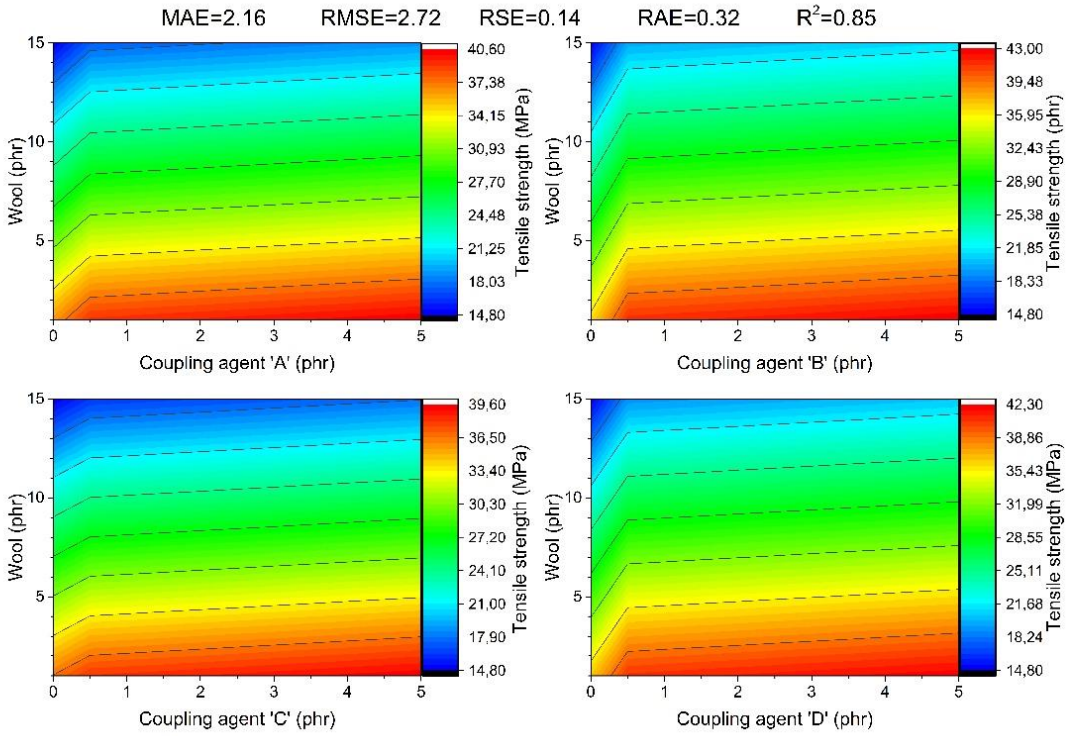

Figure 89 Prediction of tensile strength from linear regression model

The linear regression model, shown in Figure 89, reveals a general trend wherein an rise in the concentration of coupling agents, coupled with a decrease in wool concentration, corresponds to an increase in tensile strength. Nevertheless, this improvement was notable at lower coupling agent concentrations, specifically up to 0.5 phr. Notably, coupling agents B and D, characterized by lower concentrations, demonstrated more significant improvements than other surface modifiers, thereby contributing to the overall enhancement of tensile strength.

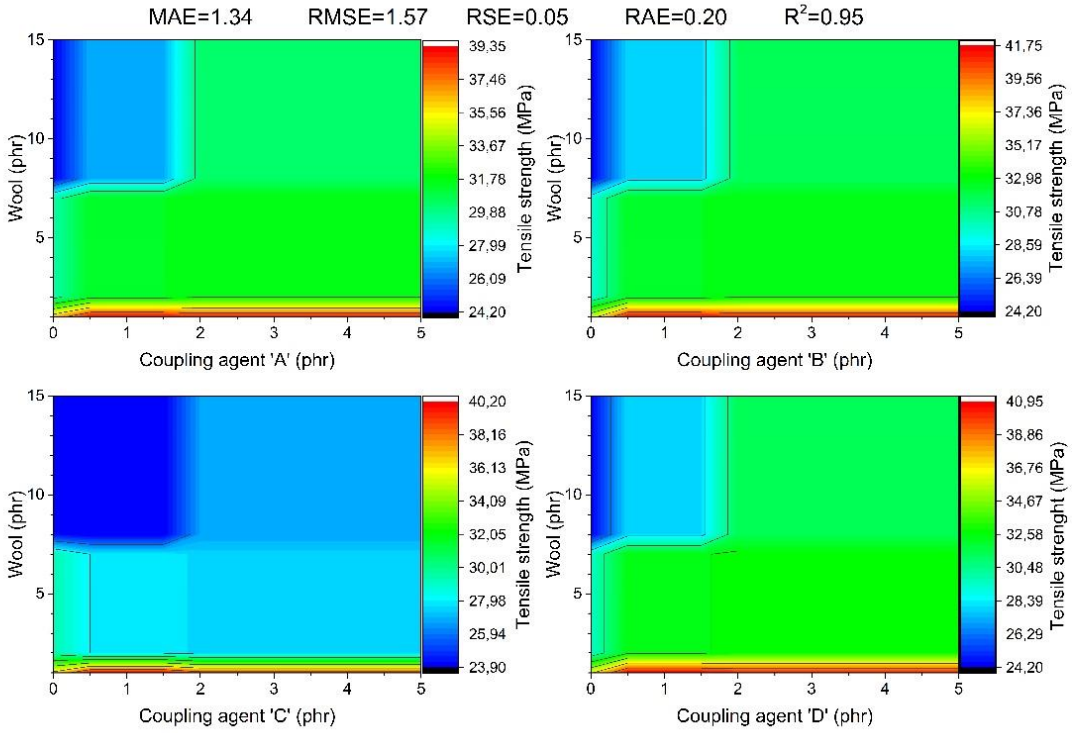

Figure 90 Prediction of tensile strength from boosted decision tree regression model

An alternative approach for simulating tensile strength involved using boosted decision tree regression. The addition of coupling agents enhanced tensile strength across all examined coupling agents and wool concentrations below 1 phr. Notably, changes in the concentration of coupling agents did not lead to changes in this property within the boosted decision tree model. In cases of higher wool concentrations, where an increase in wool content tended to decrease tensile strength, even low concentrations of coupling agents proved beneficial in modifying the adverse impact of wool addition. For wool content exceeding 7 phr, it was concluded that coupling agent concentrations should be used above 2 phr. In line with the assumptions drawn from the linear regression model for tensile strength, both coupling agents, B and D, showed the most effective compensation for the negative effects of wool additives compared to the remaining coupling agents investigated in the study.

The evaluation of the tensile strength models valued their precision and facilitated comparisons between them. Mean Absolute Error (MAE) and Root Mean Squared Error (RMSE) evaluations were provided in MPa units, enabling comparing models about the same property. On the other hand, Relative Standard Error (RSE), Relative Absolute Error (RAE), and Coefficient of Determination (R^2) are absolute values, helping additional comparisons among models across various properties with diverse value ranges and units. The boosted decision tree regression model displayed lower values for both MAE and RMSE, indicative of superior precision compared to the linear regression model. The MAE value of 1.34 MPa for the boosted decision tree model indicated better average model accuracy, whereas the linear regression model exhibited a value of 2.16 MPa.

Although the boosted decision tree model showed higher accuracy, the errors of both MAEs fell within the range of 0.93-2.59 MPa, corresponding to the standard deviation of the original data employed for modeling.[94,174] Additionally, the marginal difference between the MAE and RMSE values for the boosted decision tree regression suggested a similarity in prediction errors. On the contrary, for linear regression, the substantial difference between the MAE and RMSE indicated the presence of more significant errors in the predictions.

Furthermore, the R^2 values demonstrated that the boosted decision tree regression revealed an excellent fit to the input data, suggesting its applicability for predicting data points beyond those used in model creation. However, despite the excellent fitting of linear regression based on the coefficient of determination, more significant errors in tensile strength prediction were observed.

5.2. Thermogravimetric analysis

The 5% mass loss temperature models showed a comparable trend, although the boosted decision tree model tended to group results into subsets more notably than the linear regression model. The conclusions of the assumption for the linear regression model are shown in Figure 91. The model predicts that, following an initial increase, the temperature decrease occurs at coupling agent concentrations higher than 0.5 phr. The model also predicts that increasing coupling agent concentration reduces the initial increase in mass loss temperature observed for 0.5 phr. Depending on the type of coupling agent, the model predicts equal temperatures between 1-2 phr of coupling agent. The highest initial increase in temperature was observed for coupling agent B modification, while 0.5 phr of coupling agent C exhibited the lowest temperature among the modifications.

The boosted decision model exhibits comparable patterns in response to varying coupling agent concentrations, as illustrated in Figure 92. Specifically, the model predicts that treatment with up to 0.5 phr of coupling agent increases temperature. Subsequently, between 0.5 and 1.5 phr, the temperature stabilizes at a stable level, and beyond this range, it experiences a decline. This behavior can be categorized into three subsets of predictions based on wool concentration: below 0.5 phr, between 0.5 and 7 phr, and above 7 phr.

Furthermore, among the tested coupling agents, coupling agent C is generally associated with the most substantial decrease in the predicted temperature. This observation shows the impacts of diverse coupling agents on the predicted thermal characteristics, further contributing to understanding their impact in varying concentration scenarios.

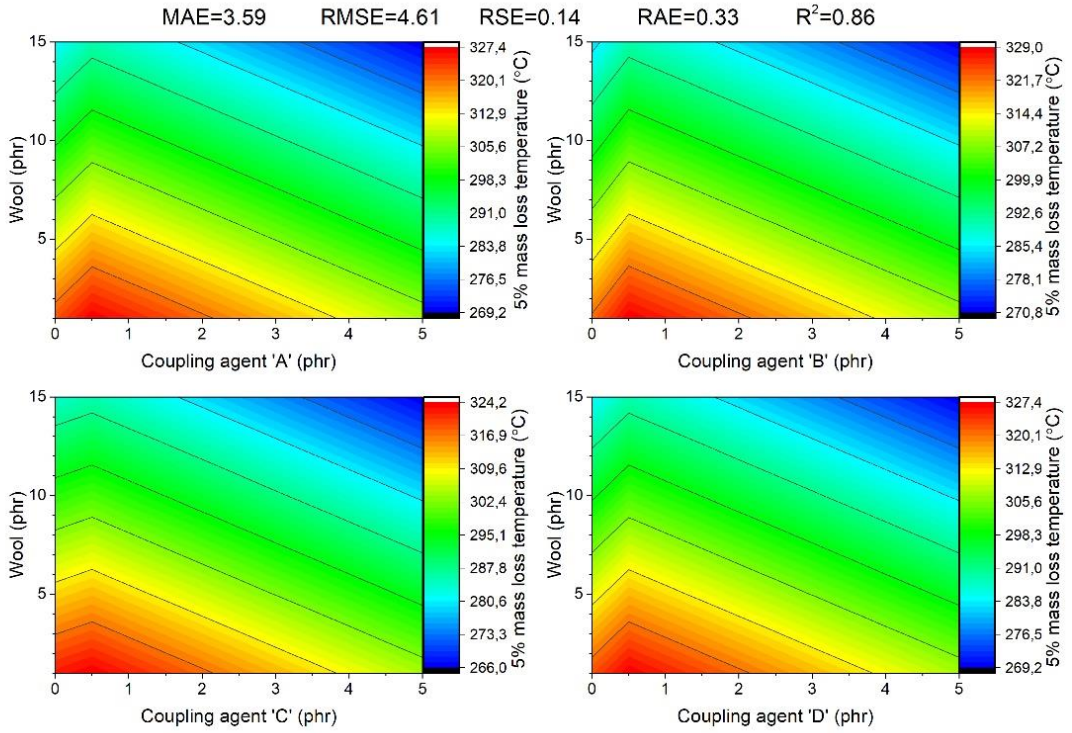

Figure 91 Prediction of 5% mass loss temperature from linear regression model

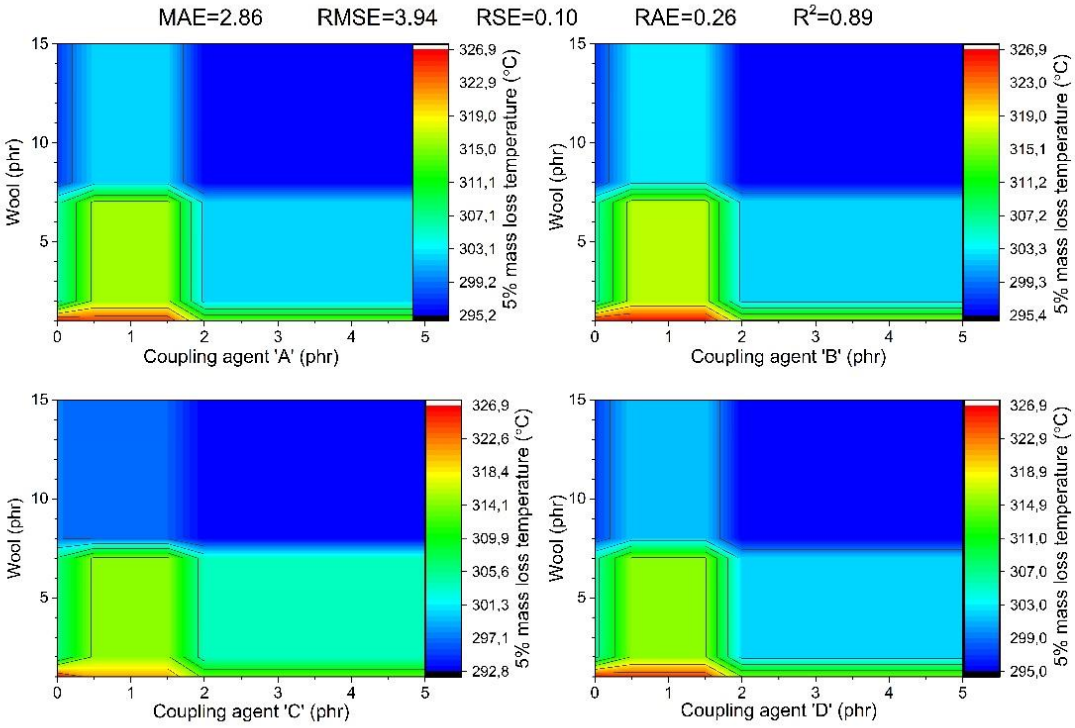

Figure 92 Prediction of 5% mass loss temperature from boosted decision tree regression model

Analogous to the mechanical models for the 5% mass loss temperature, greater accuracy was achieved for the boosted decision tree regression model. This model's Mean Absolute Error (MAE) value was noted at 2.86ºC, while the MAE increased to 3.59ºC for the linear regression model. This difference in MAE values highlights the better precision of the boosted decision tree regression model in predicting the 5% mass loss temperature compared to its linear regression counterpart.

5.3. Prediction evaluation

To compare actual data with modeled data, we selected the results of five representative formulations from Table 4 involving unmodified and modified wool fiber types. As predicted from the model evaluations, both the boosted decision and linear regression models enabled the prediction of results that closely resembled the average outcomes. However, for specific samples such as PLA-MLO-1W or PLA-MLO-1W-1C, predictions generated by both linear and boosted decision tree regressions did not yield satisfactory results when compared to the actual measured values and exceeded mean absolute errors.

Despite the proximity of numerous predictions to the actual values, it is essential to acknowledge that the presented models are not perfectly fitting and should be regarded as reference points. Furthermore, both models should be considered when predicting values to showcase the range of predictions and provide a comprehensive perspective on the potential variations between the modeled and actual outcomes.

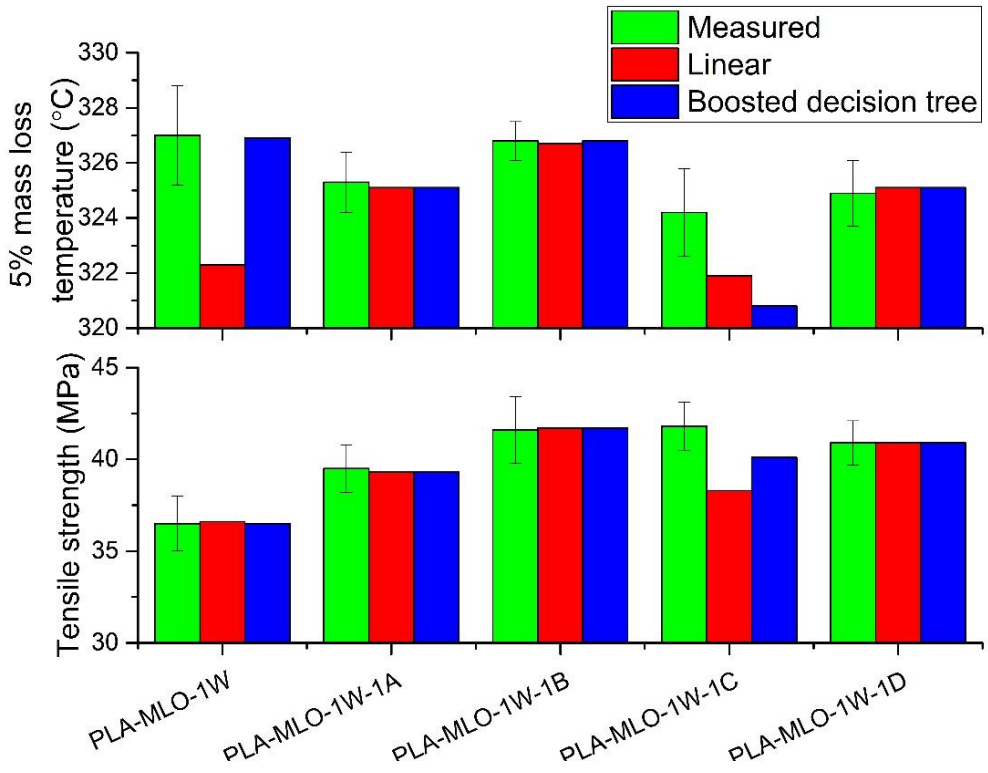

Figure 93 A summary of results from laboratory measurements and modeled values.

In conclusion, considering that the model was developed based on two distinct research studies, it is necessary to define the advantages and drawbacks associated with the models. Firstly, both studies utilized identical raw materials batches comprising polylactic acid (PLA), maleinized linseed oil (MLO), wool fibers, and coupling agents. These materials were processed using the same machinery. Secondly, both tensile strength and 5% mass loss temperature assessments were conducted employing identical equipment, under the same testing conditions, and by the same technician. It is essential, however, that the process of coupling agent modification varied in terms of mixture ingredients and the temperature of modification. Additionally, the investigative phases of both works were separated by a 2-month interval.

Despite the mentioned disadvantages, it is pertinent to highlight that the similarities in raw materials, processing conditions, and testing procedures allow for a relatively accurate comparison between the two studies, minimizing significant errors in assessing the developed models.

6. Use of AI techniques for modeling poly(lactic acid) properties for various maleinized linseed oil and sheep wool fiber concentrations

Based on experimental data, diverse regression models were developed to forecast material characteristics based on varying concentrations of wool fiber and MLO. The significance of these predictions lies in their applicability to the AI-enhanced development and shaping of the FRPs [153,156]. The constructed models underwent evaluation using statistical parameters to assess and characterize the quality of the models and their predictions.

The mean absolute error (MAE) and root mean squared error (RMSE) were calculated in the same units as the predicted characteristic values. The MAE, representing the mean absolute difference between forecasted and actual values, indicates that a lower MAE corresponds to a better-performing model. In contrast, the RMSE provides a summarized error in the model as a singular value, achieved by squaring the difference without distinguishing between under- and over-prediction.

Additionally, relative absolute error (RAE) and relative squared error (RSE) were employed to compare models across different characteristics, given that these measures are unitless. The RAE indicates the relative absolute difference between actual and expected values, while the RSE normalizes the total squared error, providing a single value that correlates predicted and actual values. Similar to mean errors, relative errors are deemed more precise, with lower values indicating greater accuracy, particularly for input data with lower values.

Finally, the coefficient of determination (R^2), a normalized value between 0 and 1, was utilized to showcase the model's effectiveness. A value of 0 signifies a random model, and the nearer is the value to 1, the model fits better within the input data range.

6.1. Mechanical properties

6.1.1. Tensile properties

Four distinct models were formulated for each characteristic, concentrating specifically on mechanical properties. The initial assessments centered on parameters obtained from tensile tests, encompassing evaluations of elongation at break, Young's modulus, and tensile strength.

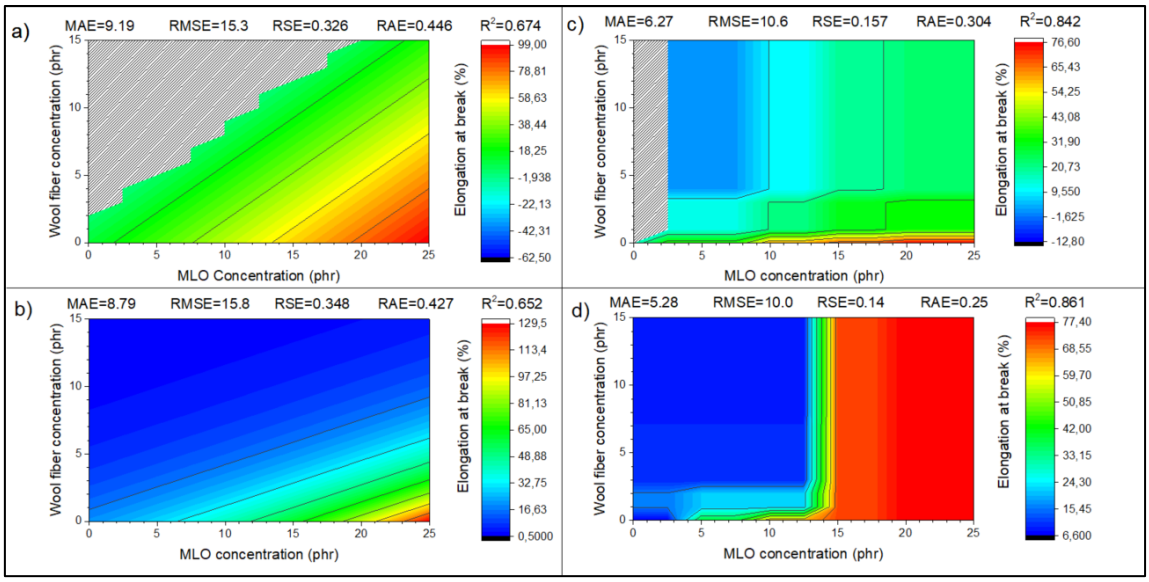

Figure 94 Elongation at break predictions based on a) linear regression, b) Poisson regression, c) Boosted decision tree regression, and d) Decision forest regression models.

In examining various models created for elongation at break, as depicted in Figure 94, the decision forest regression demonstrated the highest coefficient of determination, while boosted decision tree regression exhibited comparable accuracy to the decision forest regression. In contrast, linear and Poisson regression models exhibited notably lower coefficients of determination, a trend supported by higher RMSE values for these models.

Decision tree algorithms, known for their efficiency, are susceptible to overfitting and may disregard feature correlation. [150,155] This overfitting phenomenon was evident in the prediction models for elongation, with linear regressions displaying higher RMSE compared to decision tree regressions. Additionally, linear regression and boosted decision tree models were not universally applicable across the assumed formulations. Specifically, the models predicted negative values for formulations involving more than 2phr of MLO and high wool fiber concentrations.

Among the noteworthy observations from all the generated models, it was discerned that the highest elongation was modeled for formulations with 25phr of MLO without wool reinforcement, irrespective of the specific regression model employed. Decision tree regressions indicated that wool reinforcement tends to be more effective in enhancing elongation above a specific MLO concentration, particularly between 10-15phr. Under such conditions, for MLO concentrations, wool fiber concentrations above 1phr were predicted not to experience significant changes.

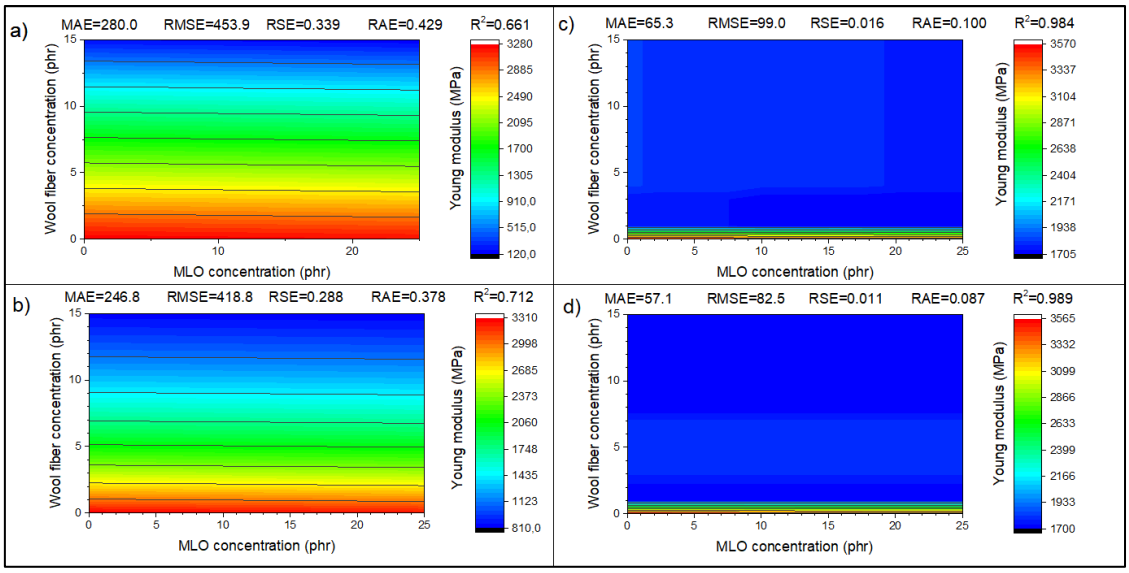

Figure 95 Young modulus predictions based on a) linear regression, b) Poisson regression, c) Boosted decision tree regression, and d) Decision forest regression models.

In addition to the analysis of tensile properties, the Young modulus underwent modeling using the mentioned earlier regression algorithms, as depicted in Figure 95. In the case of linear regression, consistent with the relative errors RSE and RAE, the predictions for Young modulus displayed a similar level of accuracy to the previously described linear models for elongation. The relationship between varying concentrations of MLO and wool fiber and the Young modulus did not align with potential linear functions, whether utilizing least square linear regression or Poisson regression models [157]. The elevated MAE further supports this observation, indicating that the predicted Young modulus is generally imprecise and only reflects a general trend.

In contrast, distinct outcomes were obtained for boosted decision tree and decision forest models, where the coefficient of determination approached an ideal fit, and mean errors were relatively low concerning the predicted Young modulus values. Examining the trends exhibited by all models, it becomes evident that PLA without wool reinforcement consistently demonstrates the highest Young modulus, irrespective of the MLO concentration. The increase in MLO concentration in the polymer blend is predicted not to significantly change the Young modulus at a constant concentration of wool fiber additive. The more precise decision tree-based models reveal that Young modulus predictions exhibit a one-step change between unreinforced and wool-reinforced PLA, unlike the predictions of linear models.

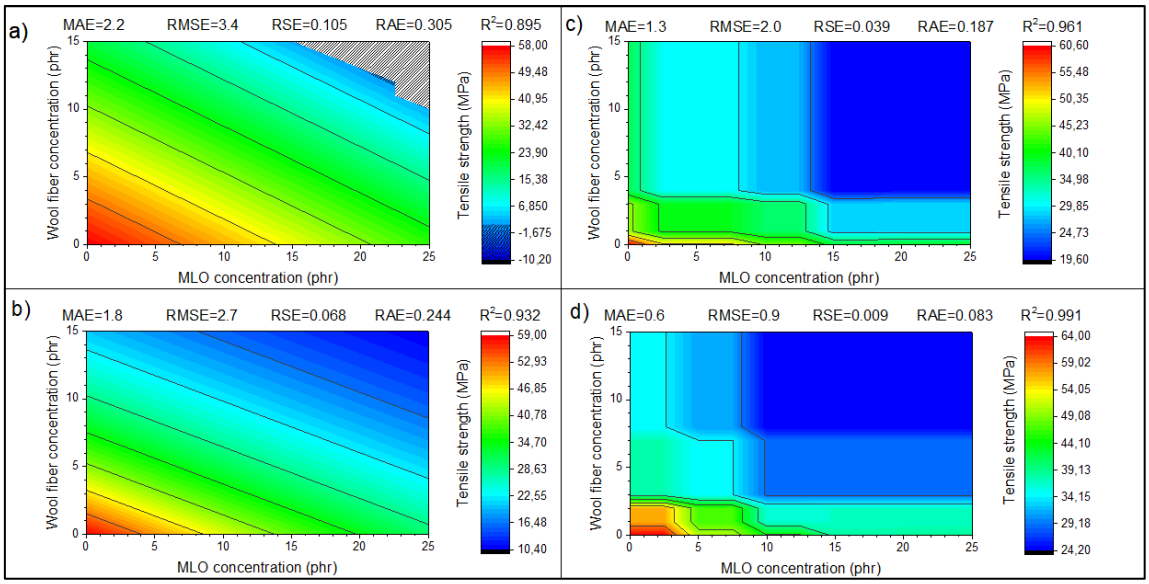

Figure 96 Tensile strength predictions based on a) linear regression, b) Poisson regression, c) Boosted decision tree regression, and d) Decision forest regression models.

The modeling of tensile strength was conducted, and the predictions are visually depicted in Figure 96. All models exhibited satisfactory accuracy, with decision forest regression presenting the highest coefficient of determination. The favorable accuracy of this model is substantiated by a relatively low relative absolute error (RAE), signifying a low total absolute error and underscoring the high precision of the trained model and its predictions. Notably, while boosted decision tree and Poisson regression models displayed similarly good coefficients of determination, their RAE values were double or triple, indicating higher average errors in these models.

In linear regression, although tensile strength can be considered somewhat as a linear function concerning variable MLO and wool concentrations, this linear model exhibits certain inconsistencies by predicting negative values, particularly for high wool and high MLO concentrations. Regarding the predictions for the tensile characteristics, the highest tensile strength was forecasted for neat PLA, regardless of the specific model employed. Moreover, wool fiber reinforcement and blending PLA with MLO were predicted to decrease tensile strength with increased additive content. The interaction between the PLA/MLO blend and wool fiber is insufficient, leading to this outcome [174]. As MLO and wool are incorporated into the polymeric composite, tensile strength experiences a further decline with their content, resulting in the lowest tensile strength prediction for formulations with the highest MLO and wool concentrations among the predicted formulations. Low additive content initially causes a marked decrease in tensile strength, though the reduction becomes less noticeable at higher concentrations.

6.1.2. Flexural properties

Models for mechanical properties were formulated to encompass flexural properties, flexural strength, and modulus.

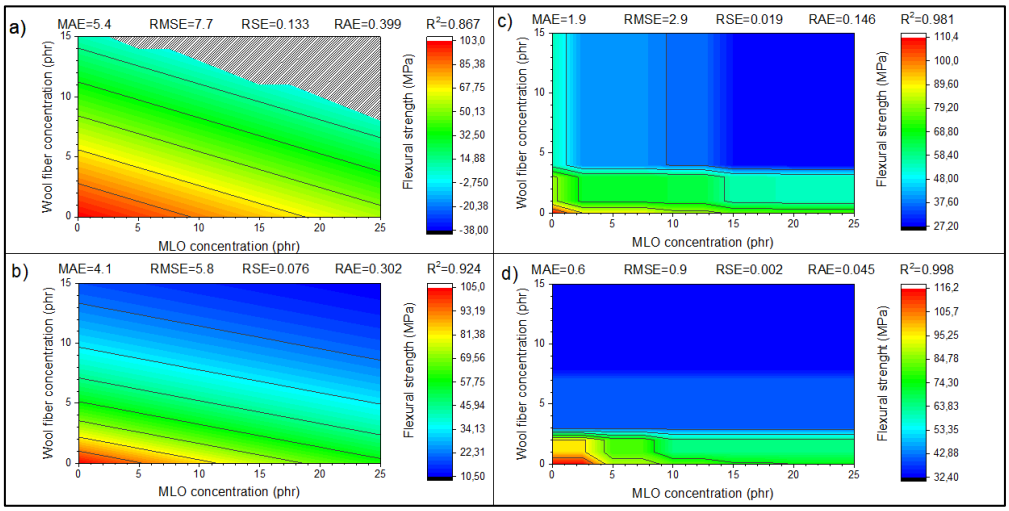

Figure 97 Flexural strength predictions based on a) linear regression, b) Poisson regression, c) Boosted decision tree regression, and d) Decision forest regression models.

As depicted in Figure 97, the models for flexural strength demonstrate comparable accuracies to those observed for tensile strength. Relative errors, such as RSE and RAE, signify a strong fit of the models, particularly evident in decision forest regression, where RSE was calculated to be 0.002. Although the accuracy observed for boosted decision tree and Poisson regressions was slightly lower than that of decision forest regression, they still provide valuable insights into flexural strength predictions. An MAE of 4.1 MPa further supports this for Poisson regression and 1.9 MPa for boosted decision tree regression. Like tensile strength, linear regression could not be fully applied for the investigated MLO and wool concentrations, predicting negative values, especially for high wool and high MLO fiber content.

Consistent with tensile strength predictions, the highest flexural strength was forecasted in all models for unmodified PLA. However, the influence of MLO and wool fiber differs slightly between models. From neat PLA up to 3phr of wool and 10phr of MLO, predictions are consistent across the investigated models, with wool fiber and MLO tending to reduce flexural strength. According to the decision forest model, a further increase in MLO or wool fiber is predicted not to significantly influence flexural strength compared to 3phr of wool fiber or 10phr of MLO. This approach is the most accurate, as the decision forest model evaluation indicates. However, predictions from boosted decision trees and Poisson regressions may complement the decision forest model to estimate flexural strength, especially for extrapolated formulations.

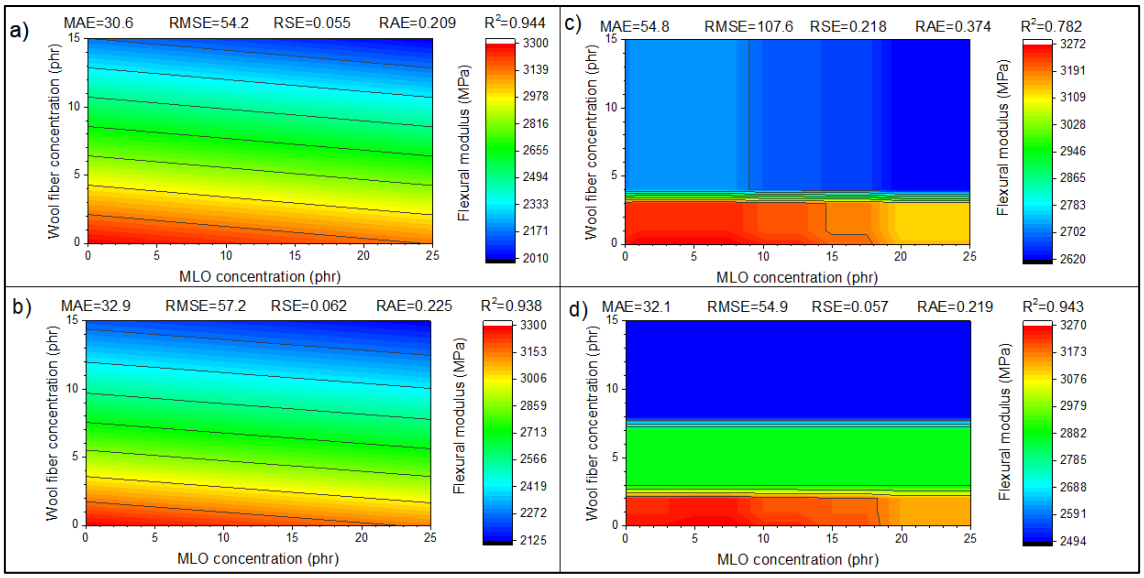

Figure 98 Flexural modulus predictions based on a) linear regression, b) Poisson regression, c) Boosted decision tree regression, and d) Decision forest regression models.

The flexural modulus's prediction outcomes with model evaluation are illustrated in Figure 98. Among the generated regression models, the linear regression model exhibited the highest coefficient of determination, supported by the lowest MAE (30.6 MPa) and RMSE (54.2 MPa). Comparable accuracy was observed for the decision forest and Poisson regressions, even with slightly higher mean absolute errors of 32.1 MPa and 32.9 MPa, correspondingly. The excellent fit of the linear model for flexural modulus suggests that changes in the property are predicted to be linear, dependent on MLO and wool fiber concentrations. The boosted decision tree model demonstrated the lowest accuracy.

In general, the decrease in flexural modulus is more dependent on the increasing concentration of wool fiber, as affirmed by the most accurate models. Furthermore, the boosted decision tree regression suggests that an increase in MLO concentration significantly reduces flexural modulus in addition to wool fiber. However, this correlation was inaccurate and resulted in higher prediction errors. The highest flexural modulus was predicted for neat PLA, a finding supported by research results where neat PLA exhibited a higher flexural modulus than PLA with wool fiber reinforcement without surface treatment.[94]

6.1.3. Impact and hardness characteristics

Additionally to examining tensile and flexural characteristics, modeling was conducted for impact strength using the Charpy method and hardness using the Shore method.

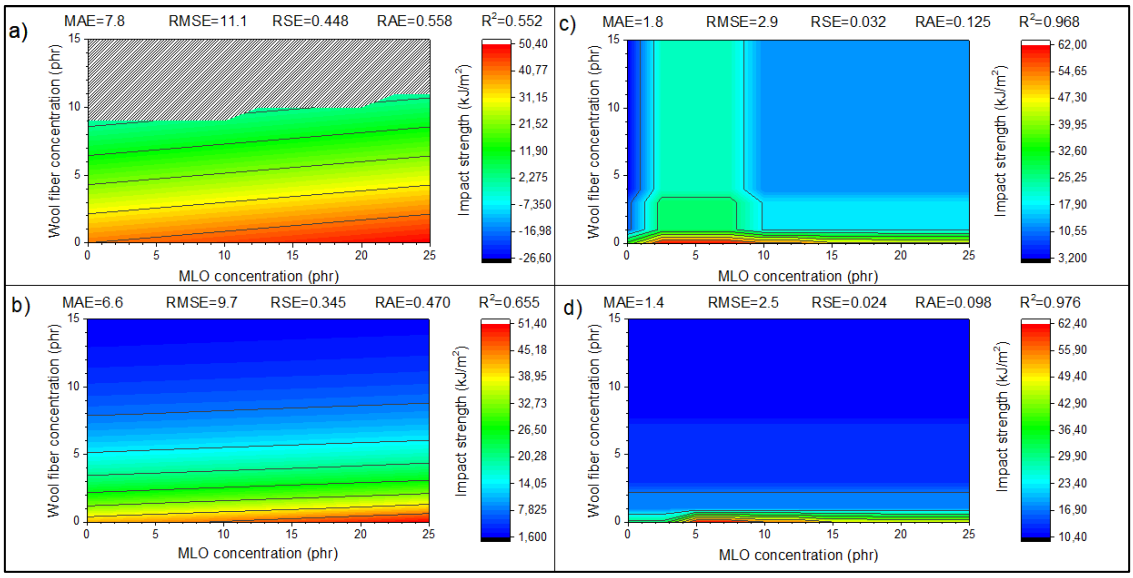

Figure 99 Impact strength predictions based on a) linear regression, b) Poisson regression, c) Boosted decision tree regression, and d) Decision forest regression models.

The summary of impact strength models is presented in Figure 99. Among the trained models, the highest accuracy was observed for decision forest and boosted decision tree regressions. Notably, the boosted decision tree model exhibited similarities with the flexural strength model based on the same algorithm. The flexural strength model was evaluated with a relative absolute error (RAE) of 0.146, while the impact strength model had an RAE of 0.125. In contrast, linear and Poisson regressions displayed high relative squared error (RSE) and mean absolute error (MAE), indicating the randomness of model predictions and relatively high average errors. The linear regression model also proved inadequate beyond 9phr of wool, as it predicted negative values.

According to the boosted decision tree and decision forest regression models, it was predicted that for formulations without wool fiber reinforcement, an increase in MLO concentration improves impact strength, particularly between 2-10phr of MLO. This prediction aligns with laboratory findings where an initial 5phr of MLO doubled the impact resistance of PLA material, but the impact resistance decreased for higher concentrations. [168] The estimation varies slightly for models reinforced with wool. In the boosted decision tree regression, although impact strength is reduced by wool fiber, the positive impact of the MLO additive in the blend is transferred to wool fiber-reinforced formulations. Another approach was modeled for decision forest regression, where the impact strength is not significantly different between the forecasted formulations irrespective of wool fiber concentration above 2phr and the presence of MLO in the formulation. However, the differences between the models above are not substantial.

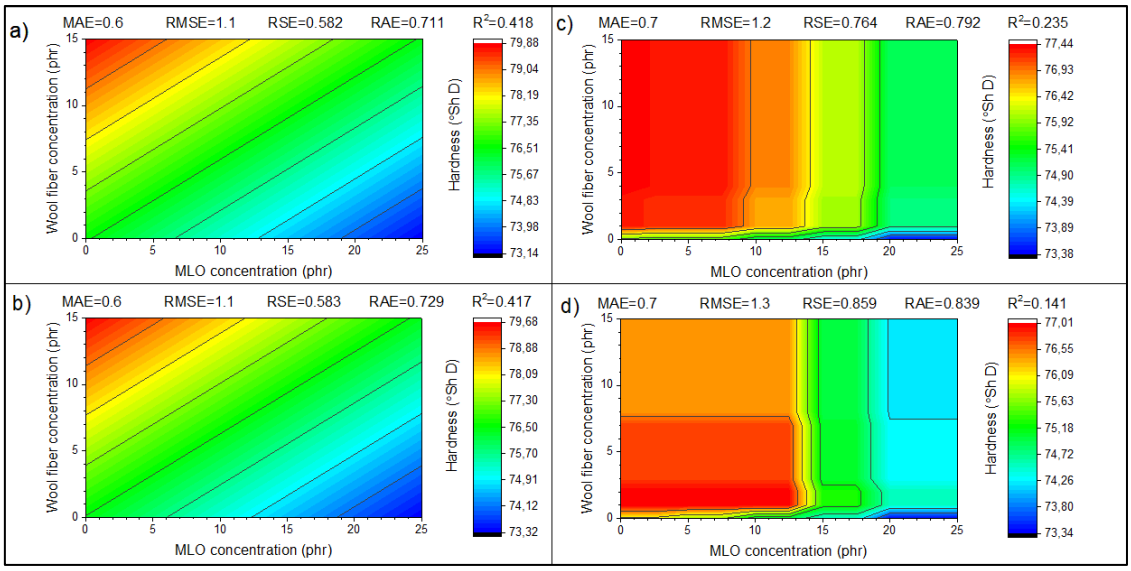

Figure 100 Hardness predictions based on a) linear regression, b) Poisson regression, c) Boosted decision tree regression, and d) Decision forest regression models.

As illustrated in Figure 100, the hardness models exhibited considerable randomness in hardness predictions, particularly evident in the boosted decision tree and decision forest regressions. Pawlak et al. [174] previously reported increased hardness with rising wool fiber concentration, a trend also observed in the linear and Poisson regression models. The suboptimal quality of the prediction models is likely attributed to the minimal differences in hardness among the formulations used for model training in laboratory tests. Another contributing factor to the low quality of the models can be attributed to the relatively high standard deviation of hardness values in laboratory tests. The mean absolute error (MAE) between 0.6-0.7 covers a standard deviation between 0.5-0.7.[168]

6.2. Thermal properties

6.2.1. Differential Scanning Calorimetry (DSC)

In addition to investigating mechanical properties, the thermal characteristics were modeled using the results obtained from Differential Scanning Calorimetry (DSC) measurements. Models were developed for various material characteristics involving glass transition temperature (Tg), cold crystallization temperature (Tcc), melting temperature (Tm), and degree of crystallinity (Xc).

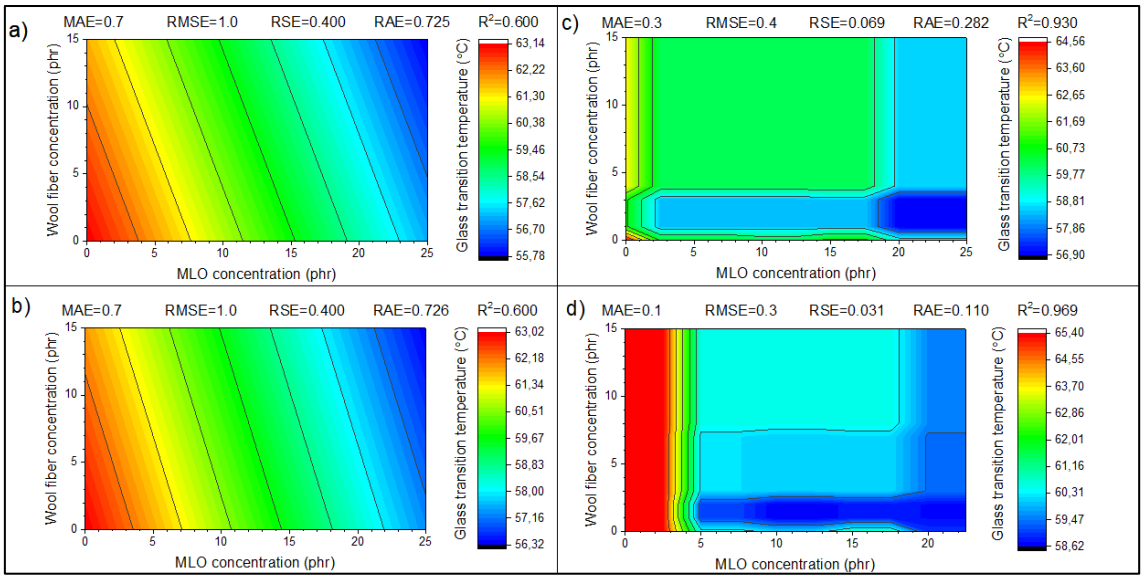

Figure 101 Glass transition temperature predictions based on a) linear regression, b) Poisson regression, c) Boosted decision tree regression, and d) Decision forest regression models.

Among the prediction models developed for the glass transition temperature, high coefficients of determination were achieved for decision forest and boosted decision tree regressions, as illustrated in Figure 101. Based on the Mean Absolute Error (MAE), the average prediction errors for these models were 0.3°C for boosted decision tree regression and 0.1°C for decision forest regression. In contrast, linear and Poisson regression models exhibited significantly lower accuracy, confirmed by MAE values of 0.7°C or Root Mean Squared Error (RMSE) values of 1.0°C for both models.

All models indicated that with an increasing concentration of MLO, the glass transition temperature of PLA decreases. Nonetheless, this change is not linear, as observed in the evaluation results of linear or Poisson regression models, but instead occurs stepwise. According to the boosted decision tree regression, the change in prediction is evident in PLA blended with the addition of 1phr or higher MLO and then after 18phr of MLO. Similarly, the decision forest regression model predicts a decrease in the T_g above 3phr of MLO and subsequently above 18phr of MLO. Concerning wool fiber reinforcement, it is predicted that it will not influence the Tg, except for specific wool concentrations between 1-3phr.

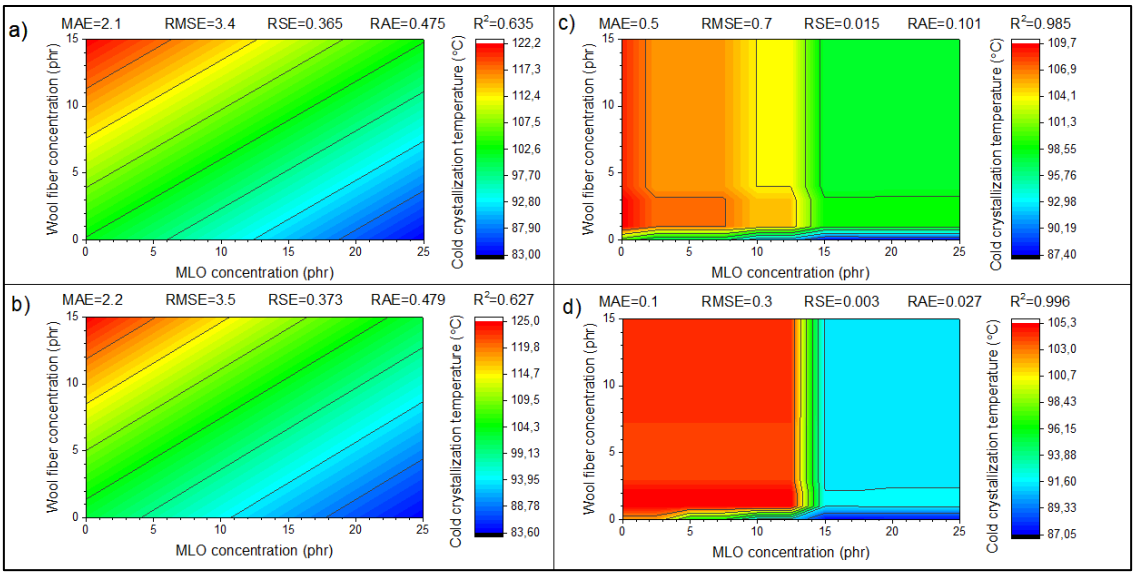

Figure 102 Cold crystallization temperature predictions based on a) linear regression, b) Poisson regression, c) Boosted decision tree regression, and d) Decision forest regression models.

Moreover, the cold crystallization temperature (Tcc) modeling is presented in Figure 102. The most accurate predictions were observed for decision forest regression, showcasing a Mean Absolute Error (MAE) of 0.1°C and a Relative Absolute Error (RAE) of 0.027, the lowest among the models trained based on Differential Scanning Calorimetry (DSC) measurements. Good accuracy was also achieved for boosted decision tree regression, although its MAE was evaluated as 0.5°C, indicating a higher prediction error for that model. Linear and Poisson regression-based models, on the other hand, demonstrated low accuracy and higher randomness in Tcc predictions.

The models suggest that PLA formulations without wool reinforcement predict a lower Tcc than reinforced formulations. However, laboratory characterization indicates that such observations are not significant due to the minimal differences between tested formulations and the relatively high standard deviation of measurements. [174] Additionally, the models predict a decrease in T_{cc} with an raise in MLO concentration in the polymeric blend, significantly above 14phr of MLO in the blend.

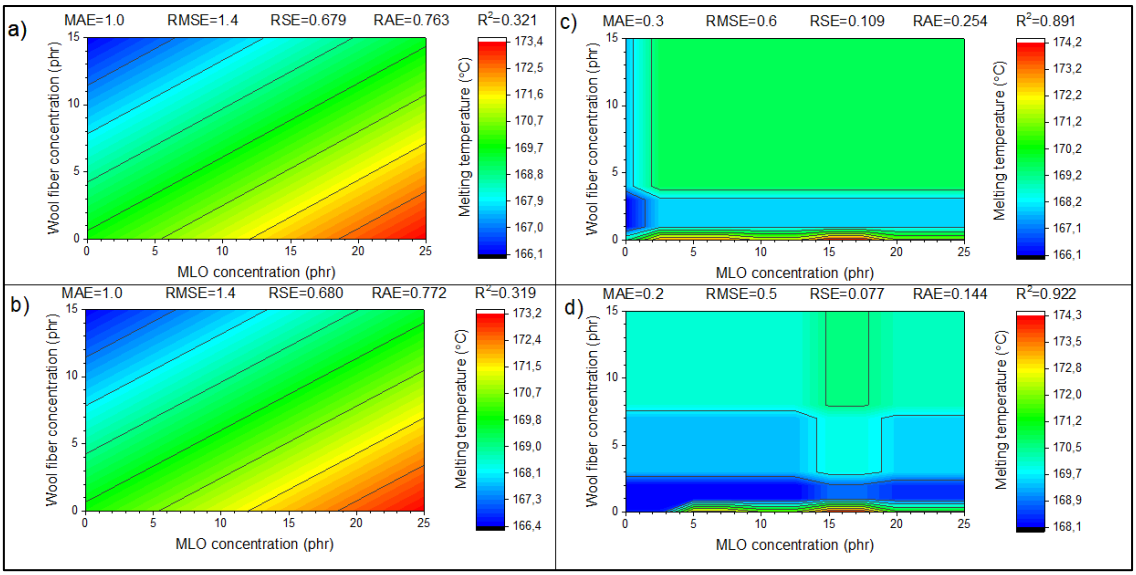

Figure 103 Melting temperature predictions based on a) linear regression, b) Poisson regression, c) Boosted decision tree regression, and d) Decision forest regression models.

The predictions for melting temperature are summarized in Figure 103. Low Mean Absolute Error (MAE) values were achieved for boosted decision tree and decision forest regressions at 0.3°C and 0.2°C, respectively. Although the highest coefficient of determination was observed for the decision forest regression model, its Relative Squared Error (RSE) and Relative Absolute Error (RAE) exhibited relatively high values, indicating a lower fit of the model compared to other values derived from Differential Scanning Calorimetry (DSC) measurements. However, predictions from this model are considerably more accurate than those from linear and Poisson regression, where reported RSE and RAE are several times higher than for the decision forest regression. Despite the lower fit observed in boosted decision tree regression, it can be considered supplementary for predictions of the melting temperature (Tm) of PLA-based formulations with evaluated modifications.

The lowest melting temperature is predicted for neat PLA among all considered formulations. The modification of PLA with wool fibers increases Tm, a trend that also applies to formulations containing MLO in the blend. An increase in MLO concentration is predicted to increase the melting temperature for formulations without wool fiber reinforcement. Further, concerning wool-reinforced formulations, predictions for MLO addition show a relatively constant melting temperature, with exceptions for MLO concentrations between 14phr and 19phr.

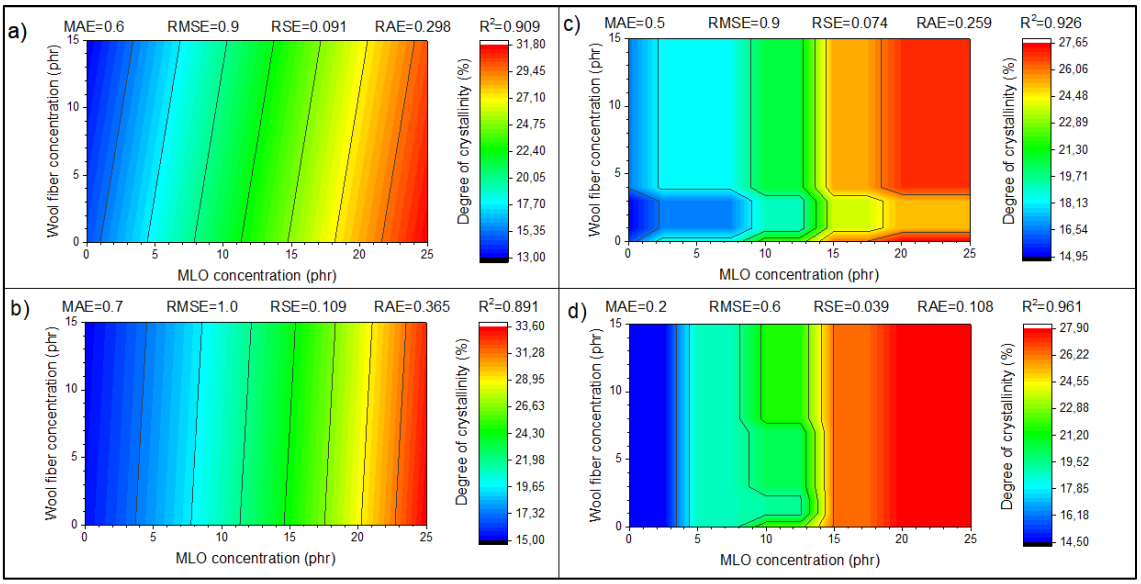

Figure 104 Degree of crystallinity predictions based on a) linear regression, b) Poisson regression, c) Boosted decision tree regression, and d) Decision forest regression models.

Concluding the analysis of Differential Scanning Calorimetry (DSC)-derived characteristics, models for the degree of crystallinity (Xc) are presented in Figure 104. All trained models were evaluated to predict Xc accurately, with the highest precision observed for the decision forest regression. This is further confirmed by a Mean Absolute Error (MAE) of 0.2% for the decision forest, in contrast to a range of 0.5-0.7% for the remaining models.

In general, an increase in wool fiber concentration does not significantly influence the degree of crystallinity. However, the boosted decision tree regression model predicts a slight decrease in Xc between 1-3phr of wool fiber. Furthermore, all models predict that increasing MLO concentration leads to a higher degree of crystallinity. This change in Xc with increasing MLO concentration aligns with observations made by Ferri et al. [168] during the modification of neat PLA.

V. CONCLUSIONS

1. General conclusions

- Sheep wool fibers derived from the dairy industry are sustainable sources from the reinforcement of biodegradable polymers. Before sheep wool fiber application, water-dependent or plasma cleaning approaches are required to remove impurities and promote good interaction between material phases.

- Polylactic acid reinforced with sheep wool fibers can be formulated to ease material processing, especially with maleinized linseed oil.

- The surface treatment of wool fibers, especially with silane coupling agents, is necessary for improving the interaction between the fiber and polylactic acid/maleinized linseed oil blend. Comprehensive material characteristics, including the impact of surface treatment, are described by thermal, mechanical, microstructural, and surface characteristics.

- Over time, the polylactic acid/maleinized linseed oil blend reinforced with sheep wool fiber indicates changes caused by physical aging, in particular, observed in tensile and thermal properties.

- Models trained based on experimental data using machine learning techniques allowed to observe general thermal and mechanical properties tendencies across different additive concentrations and surface treatments.

- The deployment of models delivered predictions of thermal and mechanical properties of polylactic acid/maleinized linseed oil/sheep wool fiber formulations, which were not previously produced in a laboratory. This approach helped to reduce material and energy consumption with simultaneous characteristics of broad material compositions.

2. Specific conclusions

2.1. Conclusions on the surface modification approaches on sheep wool fiber for reinforcement of polylactic (acid)-maleinized linseed oil system

The study has shown the manufacturing of poly(lactic acid) PLA – maleinized linseed oil (MLO) blend reinforced with short wool fiber derived from the dairy industry and a method for fiber`s surface modification using four compatibilizers. Modification of wool fiber surface was applied to improve fiber-matrix interaction due to the reduction or hydrophilic character of fiber surface derived from the presence of hydroxyl groups. Fourier Transmittance Infrared spectroscopy (FTIR) was conducted to measure the changes on a wool fiber surface and thermogravimetric analysis (TGA) to confirm if modified fibers are eligible for processing with poly(lactic acid) (PLA). The modification was found to be effective in tested formulations, whereas titanium (IV) (triethanolaminate)isopropoxide (TTI) has shown good improvement in tensile properties and trimethoxy (2-(7-oxabicyclo(4.1.0)hept-3-yl)ethyl)silane (TES) has shown improvement in impact strength of PLA-based materials. Furthermore, scanning electron microscopy analysis (SEM) of fractured specimens has confirmed improved compatibility after surface treatments.

Thermal properties of PLA-based formulations were assessed in terms of degradation temperatures. For all tested compositions and treatments, material degradation occurred above 300°C. Based on first derivate of the thermogravimetric curve (DTG), except for wool fibers modified with titanium (IV) (triethanolaminate)isopropoxide (TTI), the maximum degradation of the polymeric formulation was found between 364-367°C. However, for TTI treatment, the temperature of thermal degradation of polymeric material was reduced by about 10°C. Differential scanning calorimetry (DSC) has revealed that treated wool fibers have caused a shift from cold crystallization temperature to higher temperatures and have reduced degrees of crystallinity. The reduced crystalline structure for compositions with modified wool fibers is explained by stronger interaction between wool and PLA matrix, impeding crystalline zone formations. The observation revealed in DSC measurements was further supported by dynamic mechanical analysis (DMA).

The materials obtained in the study have shown attractive characteristics from technical, economic, and environmental perspectives and can be considered substitutes for conventional, petroleum-based polyolefins. The environmental aspect is considered an explicit advantage of tested materials, as raw materials are mainly derived from agricultural resources and provide a disposal strategy for by-products derived from the dairy industry.

2.2. Conclusions on the impact of silane treatment conditions on sheep wool fiber for development of poly(lactic acid)-maleinized linseed oil system

The investigation performed in the study has focused on wool fiber functionalization with tris(2-methoxyethoxy)(vinyl) silane (TVS) and the use of fibers for reinforcement of polylactic acid/maleinized linseed oil blend. The effectiveness of surface modification was assessed based on increasing the concentration of TVS in the reaction mixture, up to 2.5phr for wool weight, and increasing the concentration of wool fibers, both unmodified and functionalized, concerning PLA weight. Broad characteristics of processed materials were delivered, focusing on microstructural, thermal, mechanical, and surface properties.

Based on scanning electron microscopy (SEM) observations of fractured specimens, the presence of TVS modification of wool fiber surface has revealed detachment of cuticle cells from fiber bulk, indicating improved interaction with polymer matrix. Such improvement was achieved through the chemical silane treatment of fibers by bonding hydroxyl groups on the surface. Furthermore, the increasing amount of TVS from 1 to 2.5phr has slightly reduced the material's most intense degradation temperature derived from the DTG. A decrease in material thermal stability was also observed with increasing wool fiber content; however, the material showed sufficient stability for melt processing.

Concerning mechanical characteristics, silane treatment with 2.5phr of TVS, especially for polylactic acid-maleinized linseed oil blend reinforced with 1 or 5phr of the wool fibers, has caused notable improvements in Young modulus and elongation at break. As reinforcement with untreated wool fibers was found to present weak interaction and, therefore, a reduction in the material's mechanical performance, the surface treatment partially compensates for the adverse effect. Improved interaction between polylactic acid/maleinized linseed oil blend and TVS-treated wool fibers was confirmed by microscopic observation, as more bonding points between fiber and polymer matrix were observed.

Material appearance in terms of surface color has shown that modification of the polymeric blend with wool fibers intensified the yellowish color, as it is directly derived from the yellowish appearance of wool fibers. However, no significant changes in color were caused by TVS modification of wool fibers. Material wettability has changed for PLA/MLO for reinforced formulations, indicating substantially higher hydrophobicity related to the presence of wool. Although silane treatment was intended to reduce the number of hydroxyl groups on wool fiber surface, TVS treatment was not observed to modify significantly overall material wettability.

2.3. Conclusions on the plasma-modified sheep wool fibers for poly(lactic acid)-maleinized linseed oil system reinforcement

The study summarized the impact of plasma pre-treatment of sheep wool fiber used to reinforce polylactic acid/maleinized linseed oil blend. The impact of pretreatment on formulations without prior plasma application was evaluated. The plasma treatment was evaluated for air plasma applied for 8 seconds, based on the assessment of air and nitrogen plasma modifications up to 20 seconds of treatment. The treatment was intended to clean the fiber surface from the lipid layer with limited destruction of the fiber structure.

Regarding thermal characteristics, plasma treatment reduces the wool-reinforced biopolymer's glass transition temperature (Tg) and affects cold crystallization temperatures. Both tested formulations containing plasma-modified wool fibers at 1phr and 5phr concentrations have shown a double maximum peak for cold crystallization, indicating changes in PLA crystalline structure.

Concerning mechanical properties, among all tested formulations, the neat polylactic acid has shown the highest tensile strength. Further modifications with maleinized linseed oil and wool fibers have impaired the property. However, plasma pretreatment of fibers, primarily for 1phr of modified wool fibers, demonstrated improved tensile strength of untreated wool fibers, mitigating the negative impact of weak interaction between the fiber and polymeric matrix. Similarly, introducing untreated wool fiber to the PLA-MLO matrix decreased elongation at break, which was further reduced with higher wool fiber concentration in a formulation. However, reinforcement with 1phr of plasma-modified has improved elongation at break of PLA-based formulations, which is related to increased fiber roughness and better compatibility between material phases. On the other hand, only a slight improvement of impact strength was observed for formulations with plasma-modified fibers, as, in general, a decrease in the property is correlated with an increase in wool content.

Plasma treatment of wool fibers was found to reflect on the surface appearance of PLA/MLO formulations. As observed in color evaluation, reinforced with wool tends to turn material into yellowish shades, which is notably reduced for formulations where prior plasma treatment was applied on wool fibers. Furthermore, as untreated wool fibers shift into brighter colors, plasma treatment has shown the opposite effect, making the color darker as an unreinforced PLA/MLO blend. Concerning wettability evaluation, irrespective of wool treatment, all of the formulations have shown a water contact angle below 90°.

2.4. Conclusions on the physical aging phenomenon of sheep wool fiber reinforced poly(lactic acid)-based materials

The study examined changes in material thermal, mechanical, and surface properties over time directly after material preparation and four years of aging. Among examined materials were selected the neat polylactic acid and its blend with 10phr of maleinized linseed oil, as well as the PLA-MLO formulations reinforced with unmodified, and tris(2-methoxyethoxy)(vinyl) silane (TVS) treated wool fibers. Two concentrations of wool were examined at 1phr and 5phr of wool reinforcement.

Concerning mechanical performance, a notable decrease in elongation at break over time due to physical aging was observed for wool fiber-reinforced formulations, as initially, ductile PLA-MLO formulations shifted into a brittle character based on stress-strain curves. Such change is potentially explained by internal stresses and decreased free volume, therefore mitigating elongation in test conditions. Furthermore, silane treatment was initially found to improve elongation at break, especially for formulations reinforced with 1 and 5phr of wool fibers, but after aging, a significant decrease in elongation at break was observed, regardless of the silane treatment applied. On the other hand, changes in impact strength for specimens without and after aging were insignificant, and the material impact resistance remained similar across the tested formulations.

Thermal characteristics based on differential scanning calorimetry have shown several material changes over four years of aging. The impact of aging on the glass transition temperature has shown an absence of clear tendencies linked to silane treatment or wool fiber concentrations. As aged formulations of the neat PLA and formulation reinforced with 5phr of TVS-treated wool fiber have shown an increase in glass transition temperature over time, the opposite behavior of decrease in the temperature was observed in PLA reinforced with 1phr of unmodified wool fiber. Although, as reported, glass transition temperature has increased for the neat PLA, contrasting with similar studies, the change was not as evident as for PLA reported in other studies in comparable aging conditions. Concerning the degree of crystallinity (Xc), physical aging has generally caused reduced crystalline structure, implying less efficient crystallization processes due to internal stresses and the complexity of created formulations.

Among surface properties, initially after material preparation, its color was influenced by the wool concentration and TVS treatment's presence. Physical aging has affected all tested formulations similarly, and no distinct impact of wool fibers or TVS treatment presence combined with aging was observed. It suggests that color changes in aged polylactic acid are associated with structural changes in PLA macromolecules. Concerning material wettability, for hydrophilic neat polylactic acid, physical aging over four years has caused an increase in water contact angle by 2 degrees; however, wool-reinforced materials have shown decreased contact angle, resulting in more hydrophobic surface characteristics.

2.5. Conclusions on the predictive models for poly(lactic acid) materials reinforced with surface-modified sheep wool fibers

The study showcased several algorithms for machine learning model training and their application in predicting the mechanical and thermal properties of sheep wool fiber-reinforced polylactic acid-maleinized linseed oil blends. For model training, two machine learning algorithms, linear regression, and boosted decision tree regression, were applied to train on tensile strength and temperature of 5% mass loss from thermogravimetric analysis. The trained models could simulate material properties and graphical presentation of the influence of various wool and coupling agent concentrations based on applied algorithms.

Concerning forecast for tensile strength, among studied surface modifiers, especially coupling agents trimethoxy(2-(7-oxabicyclo(4.1.0)hept-3-yl)ethyl) silane and titanium (IV) (triethanolaminate)isopropoxide have displayed notable enhance in the mechanical property, particularly at lower concentrations. Based on predictions from the boosted decision tree regression model, a notable improvement in tensile strength was observed, significantly below 1phr of coupling agents. However, linear regression models' improvement in tensile strength is already at 0.5phr, providing valuable insights, whereas low doses of coupling agents already acted positively on mechanical performance in the tensile tests. Concerning evaluation metrics, the mean errors have shown superior precision in predicting the boosted decision tree models compared to linear regression.

Among investigated coupling agents, the tris(2-methoxyethoxy)(vinyl) silane has shown a substantial increase in 5% mass loss temperature, especially at lower concentrations, indicating higher material stability. Irrespective of the model training method, the temperature is predicted to initially increase after silane treatment, while concentrations higher than 2phr reduced the temperature, indicating a slight decrease in material stability. Despite differences in specific formulations between obtained and predicted temperatures for both models, low mean absolute error confirms the reliability of models in simulating the thermal characteristics. The presented models serve as helpful reference points for predicting temperature where material mass loss related to degradation processes begins. However, some variation between modeled and actual values should be acknowledged, necessitating cautious interpretation in real-world applications.

2.6. Conclusions on the use of AI techniques for modeling (polylactic acid) properties for various maleinized linseed oil and sheep wool fiber concentrations

The study aimed to assess the mechanical and thermal properties of polylactic acid-based fiber-reinforced polymers modified with maleinized linseed oil and sheep wool fiber. In the assessment were applied supervised machine learning regression models, including linear, Poisson, boosted decision tree, and decision forest regressions for predictions of tensile, flexural, impact, and hardness characteristics of the FRPs, as well as thermal characteristics including transition temperatures based on differential scanning calorimetry results. Prepared regression models allowed to observe general tendencies in material characteristics with variable wool fiber and MLO concentrations.

Among models trained for tensile properties, the most accurate were predictions derived through decision forest regression, whereas, for Young modulus or tensile strength, the coefficient of determination was near 99% fit to experimental data. Comparable accuracy was achieved for flexural properties, where decision forest regressions exhibited the best accuracies; however, a slightly lower coefficient of determination of 94,3% was obtained for the flexural modulus model. Among mechanical properties, irrespective of the training algorithm used, low model accuracies were achieved for hardness predictions, where the coefficient of determination did not exceed 42%.

Models trained for predictions based on differential scanning calorimetry results indicated that, in general, boosted decision trees or decision forest algorithms provided models with accuracy exceeding 92% for at least one of the models. In the case of several linear or Poisson regressions, some of the models showed the coefficient of determination exceeding 90%, as in the case of the degree of crystallinity; however, it was found instead as another approach for modeling the data and supplementary models for prior mentioned decision tree regressions. Finally, transition temperatures modeled with decision tree regressions for various MLO and wool concentrations have shown average mean absolute errors ranging from 0,1 to 0,5°C and were considered satisfactory compared to experimentally obtained results.

VI. REFERENCES

References

[1] Cambridge University Press, Cambridge Dictionary, (2021). https://dictionary.cambridge.org/dictionary/english/fiber (accessed December 27, 2021).

[2] Oxford University Press, Oxford Lerner`s Dictionaries, (2021). https://www.oxfordlearnersdictionaries.com/definition/english/fibre?q=fiber (accessed December 27, 2021).

[3] J. Li, P.J. Lemstra, P. Ma, Chapter 7: Can high-performance fibers be(come) bio-based and also biocompostable?, Adv. Ind. Eng. Polym. Res. 5 (2022) 117–132. https://doi.org/https://doi.org/10.1016/j.aiepr.2022.03.002.

[4] A. Komuraiah, N.S. Kumar, B.D. Prasad, Chemical Composition of Natural Fibers and its Influence on their Mechanical Properties, Mech. Compos. Mater. 50 (2014) 359–376. https://doi.org/10.1007/s11029-014-9422-2.

[5] F. Sadov, M. Korchagin, A. Matetsky, Chemical Technology of Fibrous Materials, Mir Publishers, 1973. https://books.google.pl/books?id=acO9ugAACAAJ.

[6] R. Siakeng, M. Jawaid, H. Ariffin, S.M. Sapuan, M. Asim, N. Saba, Natural fiber reinforced polylactic acid composites: A review, Polym. Compos. 40 (2019) 446–463. https://doi.org/10.1002/pc.24747.

[7] F. Allafi, M.S. Hossain, J. Lalung, M. Shaah, A. Salehabadi, M.I. Ahmad, A. Shadi, Advancements in Applications of Natural Wool Fiber: Review, J. Nat. Fibers. 00 (2020) 1–16. https://doi.org/10.1080/15440478.2020.1745128.

[8] U.S. Bongarde, V.. . Shinde, Review on natural fiber reinforcement polymer composites, Int. J. Eng. Sci. Innov. Technol. 3 (2014) 431–436.

[9] J. Robertson, C. Roux, Fibers: Overview, 2nd ed., Elsevier Ltd., 2013. https://doi.org/10.1016/B978-0-12-382165-2.00088-X.

[10] K.M. Babu, Animal fibers: Silk, Handb. Fibrous Mater. 1–2 (2020) 75–94. https://doi.org/10.1002/9783527342587.ch3.

[11] J.K. Pandey, S.H. Ahn, C.S. Lee, A.K. Mohanty, M. Misra, Recent advances in the application of natural fiber based composites, Macromol. Mater. Eng. 295 (2010) 975–989. https://doi.org/10.1002/mame.201000095.

[12] J. George, M.S. Sreekala, S. Thomas, A review on interface modification and characterization of natural fiber reinforced plastic composites, Polym. Eng. Sci. 41 (2001) 1471–1485. https://doi.org/10.1002/pen.10846.

[13] A. Gholampour, T. Ozbakkaloglu, A review of natural fiber composites: properties, modification and processing techniques, characterization, applications, Springer US, 2020. https://doi.org/10.1007/s10853-019-03990-y.

[14] V.K. Thakur, M.K. Thakur, R.K. Gupta, Review: Raw Natural Fiber-Based Polymer Composites, Int. J. Polym. Anal. Charact. 19 (2014) 256–271. https://doi.org/10.1080/1023666X.2014.880016.

[15] T. Aziz, A. Farid, F. Haq, M. Kiran, A. Ullah, K. Zhang, C. Li, S. Ghazanfar, H. Sun, R. Ullah, A. Ali, M. Muzammal, M. Shah, N. Akhtar, S. Selim, N. Hagagy, M. Samy, S.K. Al Jaouni, A Review on the Modification of Cellulose and Its Applications, Polymers (Basel). 14 (2022). https://doi.org/10.3390/polym14153206.

[16] N.M. Nurazzi, M.R.M. Asyraf, A. Khalina, N. Abdullah, H.A. Aisyah, S.A. Rafiqah, F.A. Sabaruddin, S.H. Kamarudin, M.N.F. Norrrahim, R.A. Ilyas, S.M. Sapuan, A review on natural fiber reinforced polymer composite for bullet proof and ballistic applications, Polymers (Basel). 13 (2021) 1–42. https://doi.org/10.3390/polym13040646.

[17] W. Xu, W. Cui, W. Li, W. Guo, Development and characterizations of super-fine wool powder, Powder Technol. 140 (2004) 136–140. https://doi.org/10.1016/j.powtec.2003.12.010.

[18] C. Vepari, D.L. Kaplan, Silk as a biomaterial, Prog. Polym. Sci. 32 (2007) 991–1007. https://doi.org/10.1016/j.progpolymsci.2007.05.013.

[19] A. Kumar Sahi, S. Gundu, P. Kumari, T. Klepka, A. Sionkowska, Silk-Based Biomaterials for Designing Bioinspired Microarchitecture for Various Biomedical Applications, Biomimetics. 8 (2023) 1–24. https://doi.org/10.3390/biomimetics8010055.

[20] T.F. Cooke, Inorganic Fibers—A Literature Review, J. Am. Ceram. Soc. 74 (1991) 2959–2978. https://doi.org/10.1111/j.1151-2916.1991.tb04289.x.

[21] B. Mahltig, Introduction to inorganic fibers, Elsevier Ltd., 2018. https://doi.org/10.1016/B978-0-08-102228-3.00001-3.

[22] M.D. Samper, R. Petrucci, L. Sánchez-Nacher, R. Balart, J.M. Kenny, New environmentally friendly composite laminates with epoxidized linseed oil (ELO) and slate fiber fabrics, Compos. Part B Eng. 71 (2015) 203–209. https://doi.org/10.1016/j.compositesb.2014.11.034.

[23] A. Carbonell-Verdú, D. García-García, A. Jordá, M.D. Samper, R. Balart, Development of slate fiber reinforced high density polyethylene composites for injection molding, Compos. Part B Eng. 69 (2015) 460–466. https://doi.org/10.1016/j.compositesb.2014.10.026.

[24] P. Senthil Kumar, S. Suganya, 1 - Introduction to sustainable fibres and textiles, in: S.S. Muthu (Ed.), Sustain. Fibres Text., Woodhead Publishing, 2017: pp. 1–18. https://doi.org/https://doi.org/10.1016/B978-0-08-102041-8.00001-9.

[25] N. Vasanthan, 7 - Polyamide fiber formation: structure, properties and characterization, in: S.J. Eichhorn, J.W.S. Hearle, M. Jaffe, T. Kikutani (Eds.), Handb. Text. Fibre Struct., Woodhead Publishing, 2009: pp. 232–256. https://doi.org/https://doi.org/10.1533/9781845696504.2.232.

[26] A. Kausar, Polyacrylonitrile-based nanocomposite fibers: A review of current developments, J. Plast. Film Sheeting. 35 (2019) 295–316. https://doi.org/10.1177/8756087919828151.

[27] L. Cheng, S. Chen, F. Chen, C. Wang, Q. Chen, Research Progress and Performance Evaluation of Polyvinyl Alcohol Fiber Engineered Cementitious Composites, Sustain. 15 (2023). https://doi.org/10.3390/su151410991.

[28] H. Barani, A. Calvimontes, Effects of oxygen plasma treatment on the physical and chemical properties of wool fiber surface, Plasma Chem. Plasma Process. 34 (2014) 1291–1302. https://doi.org/10.1007/s11090-014-9581-x.

[29] J. Fan, X. Yang, Y. Liu, Fractal calculus for analysis of wool fiber: Mathematical insight of its biomechanism, J. Eng. Fiber. Fabr. 14 (2019) 0–3. https://doi.org/10.1177/1558925019872200.

[30] F.M. Kelly, J.H. Johnston, Colored and functional silver nanoparticle-wool fiber composites, ACS Appl. Mater. Interfaces. 3 (2011) 1083–1092. https://doi.org/10.1021/am101224v.

[31] S.M. Liu, D.G. Masters, Amino acid utilization for wool production., Amin. Acids Anim. Nutr. (2009) 309–328. https://doi.org/10.1079/9780851996547.0309.

[32] L. Ammayappan, Eco-friendly Surface Modifications of Wool Fiber for its Improved Functionality: An Overview, Asian J. Text. 3 (2012) 15–28. https://doi.org/10.3923/ajt.2013.15.28.

[33] J.J. Long, C.L. Cui, L. Wang, H.M. Xu, Z.J. Yu, X.P. Bi, Effect of treatment pressure on wool fiber in supercritical carbon dioxide fluid, J. Clean. Prod. 43 (2013) 52–58. https://doi.org/10.1016/j.jclepro.2013.01.002.

[34] E. Wojciechowska, A. Włochowicz, A. Wesełucha-Birczyńska, Application of Fourier-transform infrared and Raman spectroscopy to study degradation of the wool fiber keratin, J. Mol. Struct. 511–512 (1999) 307–318. https://doi.org/10.1016/S0022-2860(99)00173-8.

[35] C.M. Carr, I.H. Leaver, A.E. Hughes, X-Ray Photoelectron Spectroscopic Study of the Wool Fiber Surface, Text. Res. J. 56 (1986) 457–461. https://doi.org/10.1177/004051758605600710.

[36] A. Radzik-rant, M. Wielechowska, W. Rant, Variation in wool characteristics across the body in a herd of alpacas kept in Poland, Animals. 11 (2021). https://doi.org/10.3390/ani11102939.

[37] E. Vujasinović, A. Tarbuk, T. Pušić, T. Dekanić, Bio-Innovative Pretreatment of Coarse Wool Fibers, Processes. 11 (2023) 1–14. https://doi.org/10.3390/pr11010103.

[38] R. Alyousef, H. Mohammadhosseini, A.A.K. Ebid, H. Alabduljabbar, An Integrated Approach to Using Sheep Wool as a Fibrous Material for Enhancing Strength and Transport Properties of Concrete Composites., Mater. (Basel, Switzerland). 15 (2022). https://doi.org/10.3390/ma15051638.

[39] D.O. Sanchez Ramirez, C. Vineis, I. Cruz-Maya, C. Tonetti, V. Guarino, A. Varesano, Wool Keratin Nanofibers for Bioinspired and Sustainable Use in Biomedical Field, J. Funct. Biomater. 14 (2023). https://doi.org/10.3390/jfb14010005.

[40] H. Barani, A. Haji, Analysis of structural transformation in wool fiber resulting from oxygen plasma treatment using vibrational spectroscopy, J. Mol. Struct. 1079 (2015) 35–40. https://doi.org/10.1016/j.molstruc.2014.09.041.

[41] V. Fombuena, R. Petrucci, F. Dominici, A. Jordá-Vilaplana, N. Montanes, L. Torre, Maleinized linseed oil as epoxy resin hardener for composites with high bio content obtained from linen byproducts, Polymers (Basel). 11 (2019). https://doi.org/10.3390/polym11020301.

[42] S.O. Prakash, P. Sahu, M. Madhan, A. Johnson Santhosh, A Review on Natural Fibre-Reinforced Biopolymer Composites: Properties and Applications, Int. J. Polym. Sci. 2022 (2022). https://doi.org/10.1155/2022/7820731.

[43] W. Xu, G. Ke, J. Wu, X. Wang, Modification of wool fiber using steam explosion, Eur. Polym. J. 42 (2006) 2168–2173. https://doi.org/10.1016/j.eurpolymj.2006.03.026.

[44] F.F. Ferro, M. Rampazzo, A. Beghi, Modelling and simulation of wool steaming for the efficient management of decatizing processes, E3S Web Conf. 128 (2019) 1–6. https://doi.org/10.1051/e3sconf/201912809010.

[45] H. Krizova, J. Wiener, Tannin treatment of sheep wool, Vlakna a Text. 26 (2019) 25–32.

[46] M. Mohammed, R. Rahman, A.M. Mohammed, T. Adam, B.O. Betar, A.F. Osman, O.S.

Dahham, Surface treatment to improve water repellence and compatibility of natural fiber with polymer matrix: Recent advancement, Polym. Test. 115 (2022) 107707. https://doi.org/https://doi.org/10.1016/j.polymertesting.2022.107707.

[47] B. Li, J. Li, Y. Shen, H. Wu, Y. Sun, P. Zhang, M. Yang, Development of Environmentally Friendly Wool Shrink-Proof Finishing Technology Based on L-Cysteine/Protease Treatment Solution System, Int. J. Mol. Sci. 23 (2022) 1–17. https://doi.org/10.3390/ijms232113553.

[48] J. Fan, J.F. Liu, J.H. He, Hierarchy of wool fibers and fractal dimensions, Int. J. Nonlinear Sci. Numer. Simul. 9 (2008) 293–296. https://doi.org/10.1515/IJNSNS.2008.9.3.293.

[49] N. Mao, S.J. Russell, The Thermal Insulation Properties of Spacer Fabrics with a Mechanically Integrated Wool Fiber Surface, Text. Res. J. 77 (2007) 914–922. https://doi.org/10.1177/0040517507083524.

[50] X. Huang, yu J. Wang, yu H. di, Experimental Study of Wool Fiber on Purification of Indoor Air, Text. Res. J. 77 (2007) 946–950. https://doi.org/10.1177/0040517507083519.

[51] C. Selenide, O. Belukhina, D. Milasiene, R. Ivanauskas, Investigation of the Possibilities of Wool Fiber Surface, (2021).

[52] M.Y. Abdellah, M.G. Sadek, H. Alharthi, G.T. Abdel-Jaber, A.H. Backar, Characteristic properties of date-palm fibre/sheep wool reinforced polyester composites, J. Bioresour. Bioprod. 8 (2023) 430–443. https://doi.org/https://doi.org/10.1016/j.jobab.2023.09.003.

[53] M. Vasina, P. Straznicky, P. Hrbacek, S. Rusnakova, O. Bosak, M. Kubliha, Investigation of Physical Properties of Polymer Composites Filled with Sheep Wool, Polymers (Basel). 16 (2024). https://doi.org/10.3390/polym16050690.

[54] C.M. Pederneiras, R. Veiga, J. de Brito, Rendering mortars reinforced with natural sheep's wool fibers, Materials (Basel). 12 (2019). https://doi.org/10.3390/ma12223648.

[55] I. Ahmad Wani, R. ul Rehman Kumar, Experimental investigation on using sheep wool as fiber reinforcement in concrete giving increment in overall strength, Mater. Today Proc. 45 (2021) 4405–4409. https://doi.org/https://doi.org/10.1016/j.matpr.2020.11.938.

[56] D. Jóźwiak-Niedźwiedzka, A.P. Fantilli, Wool-reinforced cement based composites, Materials (Basel). 13 (2020). https://doi.org/10.3390/MA13163590.

[57] H. Rajabinejad, I.I. Bucişcanu, S.S. Maier, Current approaches for raw wool waste management and unconventional valorization: A review, Environ. Eng. Manag. J. 18 (2019) 1439–1456. https://doi.org/10.30638/eemj.2019.136.

[58] C. Zhang, L. Xia, J. Zhang, X. Liu, W. Xu, Utilization of waste wool fibers for fabrication of wool powders and keratin: a review, J. Leather Sci. Eng. 2 (2020). https://doi.org/10.1186/s42825-020-00030-3.

[59] I. Wojnowska-Baryła, K. Bernat, M. Zaborowska, Strategies of Recovery and Organic Recycling Used in Textile Waste Management, Int. J. Environ. Res. Public Health. 19 (2022). https://doi.org/10.3390/ijerph19105859.

[60] M.P. Gashti, M.P. Gashti, Effect of Colloidal Dispersion of Clay on Some Properties of Wool Fiber, J. Dispers. Sci. Technol. 34 (2013) 853–858. https://doi.org/10.1080/01932691.2012.713248.

[61] S. Chhetri, H. Bougherara, A comprehensive review on surface modification of UHMWPE fiber and interfacial properties, Compos. Part A Appl. Sci. Manuf. 140 (2021) 106146. https://doi.org/10.1016/j.compositesa.2020.106146.

[62] S.J. Meade, J.M. Dyer, J.P. Caldwell, W.G. Bryson, Covalent Modification of the Wool Fiber Surface: Removal of the Outer Lipid Layer, Text. Res. J. 78 (2008) 943–957. https://doi.org/10.1177/0040517507087859.

[63] W. Li, Y. Zhao, X. Wang, Effect of surface modification on the dynamic heat and mass transfer of wool fabrics, J. Therm. Biol. 85 (2019) 102416. https://doi.org/https://doi.org/10.1016/j.jtherbio.2019.102416.

[64] B. Enciso, J. Abenojar, M.A. Martínez, Influence of plasma treatment on the adhesion between a polymeric matrix and natural fibres, Cellulose. 24 (2017) 1791–1801. https://doi.org/10.1007/s10570-017-1209-x.

[65] N. Gibeop, D.W. Lee, C.V. Prasad, F. Toru, B.S. Kim, J. Il Song, Effect of plasma treatment on mechanical properties of jute fiber/poly (lactic acid) biodegradable composites, Adv. Compos. Mater. 22 (2013) 389–399. https://doi.org/10.1080/09243046.2013.843814.

[66] S.F. Hamad, N. Stehling, S.A. Hayes, J.P. Foreman, C. Rodenburg, Exploiting plasma exposed, natural surface nanostructures in ramie fibers for polymer composite applications, Materials (Basel). 12 (2019). https://doi.org/10.3390/ma12101631.

[67] C.W. Kan, C.W.M. Yuen, Low Temperature Plasma Treatment for Wool Fabric, Text. Res. J. 76 (2006) 309–314. https://doi.org/10.1177/0040517506060908.

[68] C.W. Kan, K. Chan, C.W.M. Yuen, Surface characterization of low temperature plasma treated wool fiber, Fibers Polym. 5 (2004) 52–58. https://doi.org/10.1007/bf02875495.

[69] C.W. Kan, K. Chan, C.W.M. Yuen, M.H. Miao, Effect of Low Temperature Plasma, Chlorination, and Polymer Treatments and Their Combinations on the Properties of Wool Fibers, Text. Res. J. 68 (1998) 814–820. https://doi.org/10.1177/004051759806801105.

[70] J. Petkevičiūtė, A. Sankauskaitė, V. Jasulaitienė, S. Varnaitė-Žuravliova, A. Abraitienė, Impact of Low-Pressure Plasma Treatment of Wool Fabric for Dyeing with PEDOT: PSS, Materials (Basel). 15 (2022). https://doi.org/10.3390/ma15144797.

[71] S. Shahidi, A. Rashidi, M. Ghoranneviss, A. Anvari, J. Wiener, Plasma effects on anti-felting properties of wool fabrics, Surf. Coatings Technol. 205 (2010) S349–S354. https://doi.org/https://doi.org/10.1016/j.surfcoat.2010.08.003.

[72] S. Shahidi, M. Ghoranneviss, B. Moazzenchi, A. Rashidi, P. Physics, I. Azad, Study of Surface Modification of Wool Fabrics Using Low Temperature, Plasma Phys. (n.d.) 1–7.

[73] M.M. Hassan, Enhanced thermal stability, hydrophobicity, UV radiation resistance, and antibacterial properties of wool fabric treated with p-aminobenzenesulphonic acid, (2020) 17515–17523. https://doi.org/10.1039/d0ra02267e.

[74] H. Wang, F.I. Farha, H. Memon, INFLUENCE OF ULTRAVIOLET IRRADIATION AND PROTEASE ON SCALE STRUCTURE OF ALPACA WOOL FIBERS, (2019). https://doi.org/10.2478/aut-2019-0039.

[75] A.A. Amara, The cientific WorldJOURNAL Back to Natural Fiber : Wool Color Influences Its Sensitivity to Enzymatic Treatment, 2012 (2012). https://doi.org/10.1100/2012/356239.

[76] S.K. Gomaa, R.A. Zaki, M.I. Wahba, M. Abou, T. Heba, A. El Refai, A.F. El, H. El Sayed, Green method for improving performance attributes of wool fibres using immobilized proteolytic thermozyme, 3 Biotech. 12 (2022) 1–15. https://doi.org/10.1007/s13205-022-03323-y.

[77] K. Ko, J. Braniša, A. Dubec, Prewetting Electron Beam Irradiated and Native Sheep Wool Can Affect Their Sorptivity, (2023).

[78] T.A. Elmaaty, S. Okubayashi, H. Elsisi, S. Abouelenin, G. Gray, Electron beam irradiation treatment of textiles materials : a review, J. Polym. Res. (2022). https://doi.org/10.1007/s10965-022-02952-4.

[79] J. Braniša, A. Kleinová, K. Jomová, R. Malá, V. Morgunov, M. Porubská, Some properties of electron beam-irradiated sheep wool linked to Cr(III) sorption, Molecules. 24 (2019) 1–15. https://doi.org/10.3390/molecules24234401.

[80] X. Li, L.G. Tabil, S. Panigrahi, Chemical treatments of natural fiber for use in natural fiber-reinforced composites: A review, J. Polym. Environ. 15 (2007) 25–33. https://doi.org/10.1007/s10924-006-0042-3.

[81] R. Gogoi, A.K. Tyagi, Surface Modification of Jute Fabric by Treating with Silane Coupling Agent for Reducing Its Moisture Regain Characteristics, J. Nat. Fibers. 18 (2021) 803–812. https://doi.org/10.1080/15440478.2019.1658252.

[82] A. Vinod, M.R. Sanjay, S. Siengchin, S. Fischer, Fully bio-based agro-waste soy stem fiber reinforced bio-epoxy composites for lightweight structural applications: Influence of surface modification techniques, Constr. Build. Mater. 303 (2021) 124509. https://doi.org/10.1016/j.conbuildmat.2021.124509.

[83] S. Flores-Bonano, J. Vargas-Martinez, O.M. Suárez, W. Silva-Araya, Tortuosity index based on dynamic mechanical properties of polyimide foam for aerospace applications, Materials (Basel). 12 (2019). https://doi.org/10.3390/ma12111851.

[84] R.H. Bradley, I. Mathieson, Chemical interactions of ultraviolet light with wool fiber surfaces, J. Colloid Interface Sci. 194 (1997) 338–343. https://doi.org/10.1006/jcis.1997.5122.

[85] Y.H. Muhammad, S. Ahmad, M.A. Abu Bakar, A.A. Mamun, H.P. Heim, Mechanical properties of hybrid glass/kenaf fibre-reinforced epoxy composite with matrix modification using liquid epoxidised natural rubber, J. Reinf. Plast. Compos. 34 (2015) 896–906. https://doi.org/10.1177/0731684415584431.

[86] A. Todorovic, K. Resch-Fauster, A.R. Mahendran, G. Oreski, W. Kern, Curing of epoxidized linseed oil: Investigation of the curing reaction with different hardener types, J. Appl. Polym. Sci. 138 (2021) 12–18. https://doi.org/10.1002/app.50239.

[87] D.L. Motoc, J.M. Ferri, S. Ferrandiz-Bou, D. Garcia-Garcia, R. Balart, Dynamic–mechanical and decomposition properties of flax/basalt hybrid laminates based on an epoxidized linseed oil polymer, Polymers (Basel). 13 (2021) 1–11. https://doi.org/10.3390/polym13040479.

[88] A. Lerma-Canto, J. Gomez-Caturla, M. Herrero-Herrero, D. Garcia-Garcia, V. Fombuena, Development of polylactic acid thermoplastic starch formulations using maleinized hemp oil as biobased plasticizer, Polymers (Basel). 13 (2021). https://doi.org/10.3390/polym13091392.

[89] J.M. Ferri, D. Garcia-Garcia, L. Sánchez-Nacher, O. Fenollar, R. Balart, The effect of maleinized linseed oil (MLO) on mechanical performance of poly(lactic acid)-thermoplastic starch (PLA-TPS) blends, Carbohydr. Polym. 147 (2016) 60–68. https://doi.org/10.1016/j.carbpol.2016.03.082.

[90] P. Liminana, L. Quiles-Carrillo, T. Boronat, R. Balart, N. Montanes, The effect of varying almond shell flour (ASF) loading in composites with poly(butylene succinate (PBS) matrix compatibilized with maleinized linseed oil (MLO), Materials (Basel). 11 (2018). https://doi.org/10.3390/ma11112179.

[91] M.P. Arrieta, M.D. Samper, M. Jiménez-López, M. Aldas, J. López, Combined effect of linseed oil and gum rosin as natural additives for PVC, Ind. Crops Prod. 99 (2017) 196–204. https://doi.org/10.1016/j.indcrop.2017.02.009.

[92] J. Sempere-Torregrosa, J.M. Ferri, H. de la Rosa-Ramírez, C. Pavon, M.D. Samper, Effect of Epoxidized and Maleinized Corn Oil on Properties of Polylactic Acid (PLA) and Polyhydroxybutyrate (PHB) Blend, Polymers (Basel). 14 (2022). https://doi.org/10.3390/polym14194205.

[93] J. Alam, M. Alam, M. Raja, Z. Abduljaleel, L.A. Dass, MWCNTs-reinforced epoxidized linseed oil plasticized polylactic acid nanocomposite and its electroactive shape memory behaviour, Int. J. Mol. Sci. 15 (2014) 19924–19937. https://doi.org/10.3390/ijms151119924.

[94] F. Pawlak, M. Aldas, J. López-Martínez, M.D. Samper, Effect of different compatibilizers on injection-molded green fiber-reinforced polymers based on poly(lactic acid)-maleinized linseed oil system and sheep wool, Polymers (Basel). 11 (2019). https://doi.org/10.3390/polym11091514.

[95] A. Perez-Nakai, A. Lerma-Canto, I. Domingez-Candela, D. Garcia-Garcia, J.M. Ferri, V. Fombuena, Comparative study of the properties of plasticized polylactic acid with maleinized hemp seed oil and a novel maleinized brazil nut seed oil, Polymers (Basel). 13 (2021). https://doi.org/10.3390/polym13142376.

[96] R. Tejada-Oliveros, R. Balart, J. Ivorra-Martinez, J. Gomez-Caturla, N. Montanes, L. Quiles-Carrillo, Improvement of Impact Strength of Polylactide Blends with a Thermoplastic Elastomer Compatibilized with Biobased Maleinized Linseed Oil for Applications in Rigid Packaging, Molecules. 26 (2021). https://doi.org/10.3390/molecules26010240.

[97] M.P. Arrieta, Influence of plasticizers on the compostability of polylactic acid, J. Appl. Res. Technol. Eng. 2 (2021) 1. https://doi.org/10.4995/jarte.2021.14772.

[98] M. Aldas, J.M. Ferri, D.L. Motoc, L. Peponi, M.P. Arrieta, J. López-Martínez, Gum rosin as a size control agent of poly(Butylene adipate-co-terephthalate) (pbat) domains to increase the toughness of packaging formulations based on polylactic acid (pla), Polymers (Basel). 13 (2021). https://doi.org/10.3390/polym13121913.

[99] M.D. Samper, V. Fombuena, T. Boronat, D. García-Sanoguera, R. Balart, Thermal and mechanical characterization of epoxy resins (ELO and ESO) cured with anhydrides, JAOCS, J. Am. Oil Chem. Soc. 89 (2012) 1521–1528. https://doi.org/10.1007/s11746-012-2041-y.

[100] D. Lascano, A. Lerma-canto, V. Fombuena, R. Balart, N. Montanes, L. Quiles-carrillo, Kinetic analysis of the curing process of biobased epoxy resin from epoxidized linseed oil by dynamic differential scanning calorimetry, Polymers (Basel). 13 (2021). https://doi.org/10.3390/polym13081279.

[101] I. Dominguez-Candela, A. Perez-Nakai, E. Torres-Roca, J. Lora-Garcia, V. Fombuena, Development of a novel epoxy resin based on epoxidized chia oil as matrix and maleinized chia oil as bio-renewable crosslinker, J. Appl. Polym. Sci. 140 (2023) 1–14. https://doi.org/10.1002/app.53574.

[102] S.N. Khot, J.J. Lascala, E. Can, S.S. Morye, G.I. Williams, G.R. Palmese, S.H. Kusefoglu, R.P. Wool, Development and application of triglyceride-based polymers and composites, J. Appl. Polym. Sci. 82 (2001) 703–723. https://doi.org/10.1002/app.1897.

[103] J. La Scala, R.P. Wool, Effect of FA composition on epoxidation kinetics of TAG, JAOCS, J. Am. Oil Chem. Soc. 79 (2002) 373–378. https://doi.org/10.1007/s11746-002-

0491-9.

[104] A.E. Gerbase, C.L. Petzhold, A.P.O. Costa, Dynamic mechanical and thermal behavior of thermotropic polyesters based on, Jaocs. 79 (2002) 797–802.

[105] R. Turco, R. Tesser, V. Russo, T. Cogliano, M. Di Serio, E. Santacesaria, Epoxidation of Linseed Oil by Performic Acid Produced in Situ, Ind. Eng. Chem. Res. (2021). https://doi.org/10.1021/acs.iecr.1c02212.

[106] P. V. Elumalai, D. Balasubramanian, M. Parthasarathy, A.R. Pradeepkumar, S. Mohamed Iqbal, J. Jayakar, M. Nambiraj, An experimental study on harmful pollution reduction technique in low heat rejection engine fuelled with blends of pre-heated linseed oil and nano additive, J. Clean. Prod. 283 (2021) 124617. https://doi.org/10.1016/j.jclepro.2020.124617.

[107] S. Kopacic, A. Walzl, U. Hirn, A. Zankel, R. Kniely, E. Leitner, W. Bauer, Application of industrially produced chitosan in the surface treatment of fibre-based material: Effect of drying method and number of coating layers on mechanical and barrier properties, Polymers (Basel). 10 (2018) 1–17. https://doi.org/10.3390/polym10111232.

[108] M.P. Arrieta, J. López, S. Ferrándiz, M.A. Peltzer, Characterization of PLA-limonene blends for food packaging applications, Polym. Test. 32 (2013) 760–768. https://doi.org/10.1016/j.polymertesting.2013.03.016.

[109] G. Coppola, M.T. Gaudio, C.G. Lopresto, V. Calabro, S. Curcio, S. Chakraborty, Bioplastic from Renewable Biomass: A Facile Solution for a Greener Environment, Earth Syst. Environ. 5 (2021) 231–251. https://doi.org/10.1007/s41748-021-00208-7.

[110] V.V. Devadas, K.S. Khoo, W.Y. Chia, K.W. Chew, H.S.H. Munawaroh, M.K. Lam, J.W. Lim, Y.C. Ho, K.T. Lee, P.L. Show, Algae biopolymer towards sustainable circular economy, Bioresour. Technol. 325 (2021) 124702. https://doi.org/10.1016/j.biortech.2021.124702.

[111] S. Nanda, B.R. Patra, R. Patel, J. Bakos, A.K. Dalai, Innovations in applications and prospects of bioplastics and biopolymers : a review, Environ. Chem. Lett. (2021). https://doi.org/10.1007/s10311-021-01334-4.

[112] F. Shukor, A. Hassan, M. Saiful Islam, M. Mokhtar, M. Hasan, Effect of ammonium polyphosphate on flame retardancy, thermal stability and mechanical properties of alkali treated kenaf fiber filled PLA biocomposites, Mater. Des. 54 (2014) 425–429. https://doi.org/10.1016/j.matdes.2013.07.095.

[113] M.P. Arrieta, E. Fortunati, F. Dominici, J. López, J.M.M. Kenny, Bionanocomposite films based on plasticized PLA–PHB/cellulose nanocrystal blends, Carbohydr. Polym. 121 (2015) 265–275. https://doi.org/10.1016/j.carbpol.2014.12.056.

[114] E.M.N. Polman, G.J.M. Gruter, J.R. Parsons, A. Tietema, Comparison of the aerobic biodegradation of biopolymers and the corresponding bioplastics: A review, Sci. Total Environ. 753 (2021) 141953. https://doi.org/10.1016/j.scitotenv.2020.141953.

[115] G. Atiwesh, A. Mikhael, C.C. Parrish, J. Banoub, T.-A.T. Le, Environmental impact of bioplastic use: A review, Heliyon. 7 (2021) e07918. https://doi.org/10.1016/j.heliyon.2021.e07918.

[116] O. Faruk, A.K. Bledzki, H.P. Fink, M. Sain, Progress report on natural fiber reinforced composites, Macromol. Mater. Eng. 299 (2014) 9–26. https://doi.org/10.1002/mame.201300008.

[117] T. Casalini, F. Rossi, A. Castrovinci, G. Perale, A Perspective on Polylactic Acid-Based Polymers Use for Nanoparticles Synthesis and Applications, Front. Bioeng. Biotechnol.

7 (2019) 1–16. https://doi.org/10.3389/fbioe.2019.00259.

[118] M.S. Singhvi, S.S. Zinjarde, D. V. Gokhale, Polylactic acid: synthesis and biomedical applications, J. Appl. Microbiol. 127 (2019) 1612–1626. https://doi.org/10.1111/jam.14290.

[119] K. Hamad, M. Kaseem, M. Ayyoob, J. Joo, F. Deri, Polylactic acid blends: The future of green, light and tough, Prog. Polym. Sci. 85 (2018) 83–127. https://doi.org/10.1016/j.progpolymsci.2018.07.001.

[120] A. Dey, I.N.R. Eagle, N. Yodo, A review on filament materials for fused filament fabrication, J. Manuf. Mater. Process. 5 (2021). https://doi.org/10.3390/jmmp5030069.

[121] X. Song, C. Zhang, Y. Yang, Y. Weng, Effect of oligomers from epoxidized soybean oil and sebacic acid on the toughness of polylactic acid/bamboo fiber composites, J. Appl. Polym. Sci. 139 (2022) 1–12. https://doi.org/10.1002/app.51583.

[122] G. Molins, M.D. Álvarez, N. Garrido, J. Macanás, F. Carrillo, Environmental Impact Assessment of Polylactide(PLA)/Chicken Feathers Biocomposite Materials, J. Polym. Environ. 26 (2018) 873–884. https://doi.org/10.1007/s10924-017-0982-9.

[123] M.K. Lila, K. Shukla, U.K. Komal, I. Singh, Accelerated thermal ageing behaviour of bagasse fibers reinforced Poly (Lactic Acid) based biocomposites, Compos. Part B Eng. 156 (2019) 121–127. https://doi.org/10.1016/j.compositesb.2018.08.068.

[124] T. Akderya, U. Özmen, B.O. Baba, Investigation of long-term ageing effect on the thermal properties of chicken feather fibre/poly(lactic acid) biocomposites, J. Polym. Res. 27 (2020). https://doi.org/10.1007/s10965-020-02132-2.

[125] L. Cui, B. Imre, D. Tátraaljai, B. Pukánszky, Physical ageing of Poly(Lactic acid): Factors and consequences for practice, Polymer (Guildf). 186 (2020) 122014. https://doi.org/10.1016/j.polymer.2019.122014.

[126] O. Gil-Castell, J.D. Badia, T. Kittikorn, E. Strömberg, M. Ek, S. Karlsson, A. Ribes-Greus, Impact of hydrothermal ageing on the thermal stability, morphology and viscoelastic performance of PLA/sisal biocomposites, Polym. Degrad. Stab. 132 (2016) 87–96. https://doi.org/10.1016/j.polymdegradstab.2016.03.038.

[127] A. Le Duigou, A. Bourmaud, P. Davies, C. Baley, Long term immersion in natural seawater of Flax/PLA biocomposite, Ocean Eng. 90 (2014) 140–148. https://doi.org/10.1016/j.oceaneng.2014.07.021.

[128] R. Siakeng, M. Jawaid, H. Ariffin, M.S. Salit, Effects of Surface Treatments on Tensile, Thermal and Fibre-matrix Bond Strength of Coir and Pineapple Leaf Fibres with Poly Lactic Acid, J. Bionic Eng. 15 (2018) 1035–1046. https://doi.org/10.1007/s42235-018-0091-z.

[129] C. Elanchezhian, B.V. Ramnath, G. Ramakrishnan, M. Rajendrakumar, V. Naveenkumar, M.K. Saravanakumar, Review on mechanical properties of natural fiber composites., Mater. Today Proc. 5 (2018) 1785–1790. https://doi.org/10.1016/j.matpr.2017.11.276.

[130] D.N. Saheb, J.P. Jog, Natural Fiber Polymer Composites: A Review, J. Adv. Polym. Technol. 18 (1999) 351–363.

[131] R. Malkapuram, V. Kumar, Y. Singh Negi, Recent development in natural fiber reinforced polypropylene composites, J. Reinf. Plast. Compos. 28 (2009) 1169–1189. https://doi.org/10.1177/0731684407087759.

[132] M.. Begum, K. & Islam, Natural Fiber as a substitute to Synthetic Fiber in Polymer

Composites: A Review, Res. J. Eng. Sci. 2 (2013) 46–53.

[133] L. Wang, K. Okada, Y. Hikima, M. Ohshima, T. Sekiguchi, H. Yano, Effect of cellulose nanofiber (CNF) surface treatment on cellular structures and mechanical properties of polypropylene/CNF nanocomposite foams via core-back foam injection molding, Polymers (Basel). 11 (2019) 1–18. https://doi.org/10.3390/polym11020249.

[134] P. Sormunen, T. Kärki, Compression molded thermoplastic composites entirely made of recycled materials, Sustain. 11 (2019). https://doi.org/10.3390/su11030631.

[135] N. Sgriccia, M.C. Hawley, M. Misra, Characterization of natural fiber surfaces and natural fiber composites, Compos. Part A Appl. Sci. Manuf. 39 (2008) 1632–1637. https://doi.org/10.1016/j.compositesa.2008.07.007.

[136] W. Wang, M. Sain, P.A. Cooper, Study of moisture absorption in natural fiber plastic composites, Compos. Sci. Technol. 66 (2006) 379–386. https://doi.org/10.1016/j.compscitech.2005.07.027.

[137] P.J. Herrera-Franco, A. Valadez-González, A study of the mechanical properties of short natural-fiber reinforced composites, Compos. Part B Eng. 36 (2005) 597–608. https://doi.org/10.1016/j.compositesb.2005.04.001.

[138] R.D.A. Maya Jacob John, Recent Developments in Chemical Modification and Characterization of Natural Fiber-Reinforced Composites, Polym. Compos. 29 (2008) 187–207. DOI 10.1002/pc.20461.

[139] J. Holbery, D. Houston, Natural-fiber-reinforced polymer composites in automotive applications, Jom. 58 (2006) 80–86. https://doi.org/10.1007/s11837-006-0234-2.

[140] S. Harish, D.P. Michael, A. Bensely, D.M. Lal, A. Rajadurai, Mechanical property evaluation of natural fiber coir composite, Mater. Charact. 60 (2009) 44–49. https://doi.org/10.1016/j.matchar.2008.07.001.

[141] S. Taj, M.A. Munawar, S. Khan, Natural fiber-reinforced polymer composites, Pakistan Acad. Sci. (2007) 129–144.

[142] S. V. Joshi, L.T. Drzal, A.K. Mohanty, S. Arora, Are natural fiber composites environmentally superior to glass fiber reinforced composites?, Compos. Part A Appl. Sci. Manuf. 35 (2004) 371–376. https://doi.org/10.1016/j.compositesa.2003.09.016.

[143] J.F. Durodola, Machine learning for design, phase transformation and mechanical properties of alloys, Prog. Mater. Sci. 123 (2022) 100797. https://doi.org/10.1016/j.pmatsci.2021.100797.

[144] A. Gomes, A. Oliveira, J. Nunes, E. Deus, Development of an AI system for characterization of fiber-reinforced polymer composite materials, J. Build. Pathol. Rehabil. 8 (2023) 1–10. https://doi.org/10.1007/s41024-023-00307-0.

[145] K. Choudhary, B. DeCost, C. Chen, A. Jain, F. Tavazza, R. Cohn, C.W. Park, A. Choudhary, A. Agrawal, S.J.L. Billinge, E. Holm, S.P. Ong, C. Wolverton, Recent advances and applications of deep learning methods in materials science, Npj Comput. Mater. 8 (2022). https://doi.org/10.1038/s41524-022-00734-6.

[146] F. Kibrete, T. Trzepieciński, H.S. Gebremedhen, D.E. Woldemichael, Artificial Intelligence in Predicting Mechanical Properties of Composite Materials, J. Compos. Sci. 7 (2023). https://doi.org/10.3390/jcs7090364.

[147] L.E. Vivanco-Benavides, C.L. Martínez-González, C. Mercado-Zúñiga, C. Torres-Torres, Machine learning and materials informatics approaches in the analysis of physical properties of carbon nanotubes: A review, Comput. Mater. Sci. 201 (2022).

https://doi.org/10.1016/j.commatsci.2021.110939.

[148] C. Gomez, A. Guardia, J.L. Mantari, A.M. Coronado, J.N. Reddy, A contemporary approach to the MSE paradigm powered by Artificial Intelligence from a review focused on Polymer Matrix Composites, Mech. Adv. Mater. Struct. 29 (2022) 3076–3096. https://doi.org/10.1080/15376494.2021.1886379.

[149] D. Bishara, Y. Xie, W.K. Liu, S. Li, A State-of-the-Art Review on Machine Learning-Based Multiscale Modeling, Simulation, Homogenization and Design of Materials, Springer Netherlands, 2023. https://doi.org/10.1007/s11831-022-09795-8.

[150] W. Xia, Y. Jiang, X. Chen, R. Zhao, Application of machine learning algorithms in municipal solid waste management: A mini review, Waste Manag. Res. 40 (2022) 609–624. https://doi.org/10.1177/0734242X211033716.

[151] M.S.R. Elapolu, M.I.R. Shishir, A. Tabarraei, A novel approach for studying crack propagation in polycrystalline graphene using machine learning algorithms, Comput. Mater. Sci. 201 (2022) 110878. https://doi.org/10.1016/j.commatsci.2021.110878.

[152] A. Saxena, A. Mehta, H. Vasudev, G. Prashar, N. Yasir Jasim, A short review on machine learning for the purpose of optimizing and predicting the properties of polymeric nanocomposites, Mater. Today Proc. (2023). https://doi.org/10.1016/j.matpr.2023.07.347.

[153] S. Cassola, M. Duhovic, T. Schmidt, D. May, Machine learning for polymer composites process simulation – a review, Compos. Part B Eng. 246 (2022) 110208. https://doi.org/10.1016/j.compositesb.2022.110208.

[154] E. Champa-Bujaico, P. García-Díaz, A.M. Díez-Pascual, Machine Learning for Property Prediction and Optimization of Polymeric Nanocomposites: A State-of-the-Art, Int. J. Mol. Sci. 23 (2022). https://doi.org/10.3390/ijms231810712.

[155] A. Mahajan, S. Bajoliya, S. Khandelwal, R. Guntewar, A. Ruchitha, I. Singh, N. Arora, Comparison of ML algorithms for prediction of tensile strength of polymer matrix composites, Mater. Today Proc. (2022). https://doi.org/10.1016/j.matpr.2022.12.105.

[156] G. Golkarnarenji, M. Naebe, K. Badii, A.S. Milani, R.N. Jazar, H. Khayyam, A machine learning case study with limited data for prediction of carbon fiber mechanical properties, Comput. Ind. 105 (2019) 123–132. https://doi.org/10.1016/j.compind.2018.11.004.

[157] J. Wang, M.A. Ayari, A. Khandakar, M.E.H. Chowdhury, S.M.A.U. Zaman, T. Rahman, B. Vaferi, Estimating the Relative Crystallinity of Biodegradable Polylactic Acid and Polyglycolide Polymer Composites by Machine Learning Methodologies, Polymers (Basel). 14 (2022) 1–17. https://doi.org/10.3390/polym14030527.

[158] M. Hassani Niaki, M. Ghorbanzadeh Ahangari, M. Pashaian, A material-independent deep learning model to predict the tensile strength of polymer concrete, Compos. Commun. 36 (2022) 101400. https://doi.org/10.1016/j.coco.2022.101400.

[159] T. Wen, L. Zhang, H. Wang, E. Weinan, D.J. Srolovitz, Deep potentials for materials science, Mater. Futur. 1 (2022). https://doi.org/10.1088/2752-5724/ac681d.

[160] S. Malley, C. Reina, S. Nacy, J. Gilles, B. Koohbor, G. Youssef, Predictability of mechanical behavior of additively manufactured particulate composites using machine learning and data-driven approaches, Comput. Ind. 142 (2022) 103739. https://doi.org/10.1016/j.compind.2022.103739.

[161] P. Bannigan, Z. Bao, R.J. Hickman, M. Aldeghi, F. Häse, A. Aspuru-Guzik, C. Allen, Machine learning models to accelerate the design of polymeric long-acting injectables, Nat. Commun. 14 (2023) 1–12. https://doi.org/10.1038/s41467-022-35343-w.

[162] E. Menou, F. Tancret, I. Toda-Caraballo, G. Ramstein, P. Castany, E. Bertrand, N. Gautier, P.E.J. Rivera Díaz-Del-Castillo, Computational design of light and strong high entropy alloys (HEA): Obtainment of an extremely high specific solid solution hardening, Scr. Mater. 156 (2018) 120–123. https://doi.org/10.1016/j.scriptamat.2018.07.024.

[163] G. Golkarnarenji, M. Naebe, K. Badii, A.S. Milani, R.N. Jazar, H. Khayyam, Support vector regression modelling and optimization of energy consumption in carbon fiber production line, Comput. Chem. Eng. 109 (2018) 276–288. https://doi.org/10.1016/j.compchemeng.2017.11.020.

[164] R. Cai, W. Wen, K. Wang, Y. Peng, S. Ahzi, F. Chinesta, Tailoring interfacial properties of 3D-printed continuous natural fiber reinforced polypropylene composites through parameter optimization using machine learning methods, Mater. Today Commun. 32 (2022) 103985. https://doi.org/10.1016/j.mtcomm.2022.103985.

[165] B.A. Moore, E. Rougier, D. O'Malley, G. Srinivasan, A. Hunter, H. Viswanathan, Predictive modeling of dynamic fracture growth in brittle materials with machine learning, Comput. Mater. Sci. 148 (2018) 46–53. https://doi.org/10.1016/j.commatsci.2018.01.056.

[166] F. Quartinello, S. Vecchiato, S. Weinberger, K. Kremenser, L. Skopek, A. Pellis, G.M. Guebitz, Highly selective enzymatic recovery of building blocks fromwool-cotton-polyester textile waste blends, Polymers (Basel). 10 (2018). https://doi.org/10.3390/polym10101107.

[167] A. Grzabka-Zasadzińska, L. Klapiszewski, S. Borysiak, T. Jesionowski, Thermal and mechanical properties of silica-lignin/polylactide composites subjected to biodegradation, Materials (Basel). 11 (2018). https://doi.org/10.3390/ma11112257.

[168] J.M. Ferri, D. Garcia-Garcia, N. Montanes, O. Fenollar, R. Balart, The effect of maleinized linseed oil as biobased plasticizer in poly(lactic acid)-based formulations, Polym. Int. 66 (2017) 882–891. https://doi.org/10.1002/pi.5329.

[169] N. Herrera, H. Roch, A.M. Salaberria, M.A. Pino-Orellana, J. Labidi, S.C.M. Fernandes, D. Radic, A. Leiva, K. Oksman, Functionalized blown films of plasticized polylactic acid/chitin nanocomposite: Preparation and characterization, Mater. Des. 92 (2016) 846–852. https://doi.org/10.1016/j.matdes.2015.12.083.

[170] M.P. Arrieta, M.D. Samper, M. Aldas, J. López, On the use of PLA-PHB blends for sustainable food packaging applications, Materials (Basel). 10 (2017) 1–26. https://doi.org/10.3390/ma10091008.

[171] J.M. Ferri, D. Garcia-Garcia, L. Sánchez-Nacher, O. Fenollar, R. Balart, The effect of maleinized linseed oil (MLO) on mechanical performance of poly(lactic acid)-thermoplastic starch (PLA-TPS) blends, Carbohydr. Polym. 147 (2016) 60–68. https://doi.org/10.1016/j.carbpol.2016.03.082.

[172] A. Aluigi, C. Tonetti, F. Rombaldoni, D. Puglia, E. Fortunati, I. Armentano, C. Santulli, L. Torre, J.M. Kenny, Keratins extracted from Merino wool and Brown Alpaca fibres as potential fillers for PLLA-based biocomposites, J. Mater. Sci. 49 (2014) 6257–6269. https://doi.org/10.1007/s10853-014-8350-9.

[173] V. Sessini, I. Navarro-Baena, M.P. Arrieta, F. Dominici, D. López, L. Torre, J.M. Kenny, P. Dubois, J.-M. Raquez, L. Peponi, Effect of the addition of polyester-grafted-cellulose nanocrystals on the shape memory properties of biodegradable PLA/PCL nanocomposites, Polym. Degrad. Stab. 152 (2018) 126–138. https://doi.org/10.1016/J.POLYMDEGRADSTAB.2018.04.012.

[174] F. Pawlak, M. Aldas, F. Parres, J. López-Martínez, M.P. Arrieta, Silane-functionalized

sheep wool fibers from dairy industry waste for the development of plasticized pla composites with maleinized linseed oil for injection-molded parts, Polymers (Basel). 12 (2020) 1–22. https://doi.org/10.3390/polym12112523.

[175] M.D. Samper, R. Petrucci, L. Sanchez-Nacher, R. Balart, J.M. Kenny, Properties of composite laminates based on basalt fibers with epoxidized vegetable oils, Mater. Des. 72 (2015) 9–15. https://doi.org/10.1016/j.matdes.2015.02.002.

[176] International Standards Organization, ISO 527-1:2012 - Plastics - Determination of tensile properties - Part 1: General principles, (2012).

[177] International Standards Organization, ISO 527-2:2012. Plastics - Determination of tensile properties - Part 2: Test conditions for moulding and extrusion plastics, 2012. https://doi.org/10.1039/c0cp01060j.

[178] AENOR, UNE-EN ISO 527-3 Plásticos. Determinación de las propiedades en tracción. Parte 3: Condiciones de ensayo para películas y hojas., 00 (1996) 10.

[179] E. Baur, T.A. Osswald, N. Rudolph, Material Properties and Testing Methods, Plast. Handb. (2019) 45–175. https://doi.org/10.3139/9781569905609.003.

[180] International Standards Organization, ISO 178:2011 - Plastics - Determination of flexural properties, Iso. (2011) 19. https://doi.org/10.1039/c0cp01060j.

[181] International Standards Organization, ISO 868:2003 - Plastics and ebonite -- Determination of indentation hardness by means of a durometer (Shore hardness), 2003. (n.d.).

[182] International Standards Organization, ISO 179-1:2010 - Plastics — Determination of Charpy impact properties/ Part 1: Non-instrumented impact test, (2010).

[183] U. Iso, Norma Española Plásticos Termogravimetría (TG) de polímeros Parte 1 : Principios generales, (2022).

[184] ANAIP, ISO 11357-1. Calorimetría diferencial de barrido (DSC) Parte 1 : Principios generales, (2017).

[185] AENOR, UNE-EN ISO 11357-2. Plásticos. Calorimetría diferencial de barrido (DSC). Parte 2: Determinación de la temperatura de transición vítrea y de la altura del escalón de transición vítrea. (ISO 11357-2:2013), Madrid, AENOR. (2015). www.aenor.es.

[186] U. Asociación Española de Normalización, UNE-EN ISO 11357-3:2018 Plásticos. Calorimetría diferencial de barrido. (DSC). Parte 3: Determinación de la temperatura y de la entalpía de fusión y de cristalización, (2018) 3–5.

[187] U. Iso, E. Del, D.U. Iso, Norma Española Plásticos Determinación de las propiedades mecanodinámicas Parte 2 : Método del péndulo de torsión, (2020).

[188] U. Iso, E. Del, D.U. Iso, Norma Española Plásticos Determinación de las propiedades mecano-dinámicas Parte 1 : Principios generales, (2020).

[189] E.D.E.L.D. Une-en, UNE- EN ISO 75-1 Plásticos Determinación de la temperatura de flexión bajo carga Parte 1: Método general de ensayo (ISO 75-1:2013), Office. (2013) 46. https://doi.org/10.1039/c0cp01060j.

[190] International Standards Organization, ISO 75-3. Plásticos-Determinación de la temperatura de flexión bajo carga. Parte 3: Laminados termoestables de alta resistencia y plásticos reforzados con fibra larga, (2001).

[191] International Standards Organization, ISO 75-2. Plásticos. Determinación de la temperatura de flexión bajo carga (HDT). Parte 2: Plásticos y ebonita, (2013).

[192] International Standards Organization, ISO 306. Plásticos-Materiales termoplásticos. Determinación de la temperatura de reblandecimiento Vicat (VST), (2015).

[193] M. Naeimirad, A. Zadhoush, R. Esmaeely Neisiany, S. Salimian, R. Kotek, Melt-spun PLA liquid-filled fibers: physical, morphological, and thermal properties, J. Text. Inst. 110 (2019) 89–99. https://doi.org/10.1080/00405000.2018.1465336.

[194] M. Abdelmouleh, S. Boufi, A. Ben Salah, M.N. Belgacem, A. Gandini, Interaction of silane coupling agents with cellulose, Langmuir. 18 (2002) 3203–3208. https://doi.org/10.1021/la011657g.

[195] M. Aldas, J.M. Ferri, J. Lopez-Martinez, M.D. Samper, M.P. Arrieta, Effect of pine resin derivatives on the structural, thermal, and mechanical properties of Mater-Bi type bioplastic, J. Appl. Polym. Sci. 137 (2019) 48236. https://doi.org/10.1002/app.48236.

[196] M.F. Aldas Carrasco, N.J. Rouault, J.M. Ferri Azor, J. López-Martínez, M.D. Samper Madrigal, A new bio-based fibre-reinforced polymer obtained from sheep wool short fibres and PLA, Green Mater. (2019) 1–13. https://doi.org/10.1680/jgrma.19.00027.

[197] L. Conzatti, F. Giunco, P. Stagnaro, A. Patrucco, C. Tonin, C. Marano, M. Rink, E. Marsano, Wool fibres functionalised with a silane-based coupling agent for reinforced polypropylene composites, Compos. Part A Appl. Sci. Manuf. 61 (2014) 51–59. https://doi.org/10.1016/j.compositesa.2014.02.005.

[198] Y. Xie, C.A.S. Hill, Z. Xiao, H. Militz, C. Mai, Silane coupling agents used for natural fiber/polymer composites: A review, Compos. Part A Appl. Sci. Manuf. 41 (2010) 806–819. https://doi.org/10.1016/j.compositesa.2010.03.005.

[199] H. Ku, H. Wang, N. Pattarachaiyakoop, M. Trada, A review on the tensile properties of natural fiber reinforced polymer composites, Compos. Part B Eng. 42 (2011) 856–873. https://doi.org/10.1016/j.compositesb.2011.01.010.

[200] F. Pawlak, M. Aldas, J. López-Martínez, M.D. Samper, Effect of different compatibilizers on injection-molded green fiber-reinforced polymers based on poly(lactic acid)-maleinized linseed oil system and sheep wool, Polymers (Basel). 11 (2019) 1–25. https://doi.org/10.3390/polym11091514.

[201] International Standards Organization, ISO 179-1. Pláticos-Determinación de las propiedades al impacto Charpy. Parte 1: Ensayo de impacto no instrumentado, (2010). https://doi.org/10.1039/c0cp01060j.

[202] J.F. Turner, A. Riga, A. O'Connor, J. Zhang, J. Collis, Characterization of drawn and undrawn poly-L-lactide films by differential scanning calorimetry, J. Therm. Anal. Calorim. 75 (2004) 257–268. https://doi.org/10.1023/B:JTAN.0000017347.08469.b1.

[203] V. Fombuena, J. Balart, T. Boronat, L. Sánchez-Nácher, D. Garcia-Sanoguera, Improving mechanical performance of thermoplastic adhesion joints by atmospheric plasma, Mater. Des. 47 (2013) 49–56. https://doi.org/10.1016/j.matdes.2012.11.031.

[204] J. Yao, D. Ph, Y. Liu, D. Ph, S. Yang, J. Liu, Characterization of Secondary Structure Transformation of Stretched and Slenderized Wool Fibers with FTIR Spectra, 3 (2008) 17–21.

[205] P. Zhang, Q. Wang, J. Shen, P. Wang, J. Yuan, X. Fan, Enzymatic Thiol–Ene Click Reaction: An Eco-Friendly Approach for MPEGMA-Grafted Modification of Wool Fibers, ACS Sustain. Chem. Eng. (2019). https://doi.org/10.1021/acssuschemeng.9b02902.

[206] Z. Jiang, Y. Wei, R. Bai, Y. Cui, G. Zheng, Q. Wang, P. Wang, Y. Yu, M. Zhou, The Absorption Accelerating Behavior of Surface Modified Wool: Mechanism, Isotherm, Kinetic, and Thermodynamic Studies, J. Nat. Fibers. 19 (2022) 11858–11869.

https://doi.org/10.1080/15440478.2022.2044965.

[207] M. Yang, J. Su, Y. Zheng, C. Fang, W. Lei, L. Li, Effect of Different Silane Coupling Agents on Properties of Waste Corrugated Paper Fiber / Polylactic Acid Composites, (2023) 1–15.

[208] Q. Xia, Y. Wang, M. Zhang, Z. Zhang, H. Dai, Effects of a Clean Subcritical Degreasing System on Wool Fibers, J. Am. Leather Chem. Assoc. 116 (2021) 162–168.

[209] M.M. Kabir, H. Wang, K.T. Lau, F. Cardona, Chemical treatments on plant-based natural fibre reinforced polymer composites: An overview, Compos. Part B Eng. 43 (2012) 2883–2892. https://doi.org/10.1016/j.compositesb.2012.04.053.

[210] F. Wang, S. Zhou, M. Yang, Z. Chen, S. Ran, Thermo-mechanical performance of polylactide composites reinforced with Alkali-treated bamboo fibers, Polymers (Basel). 10 (2018). https://doi.org/10.3390/polym10040401.

[211] J.M. España, M.D. Samper, E. Fages, L. Sánchez-Nácher, R. Balart, Investigation of the effect of different silane coupling agents on mechanical performance of basalt fiber composite laminates with biobased epoxy matrices, Polym. Compos. 34 (2013) 376–381. https://doi.org/10.1002/pc.22421.

[212] S. Kuciel, P. Romańska, Hybrid composites of polylactide with basalt and carbon fibers and their thermal treatment, Materials (Basel). 12 (2018). https://doi.org/10.3390/ma12010095.

[213] A. Magoń, M. Pyda, Study of crystalline and amorphous phases of biodegradable poly(lactic acid) by advanced thermal analysis, Polymer (Guildf). 50 (2009) 3967–3973. https://doi.org/10.1016/j.polymer.2009.06.052.

[214] J. Jiang, C. Jiang, B. Li, P. Feng, Bond behavior of basalt textile meshes in ultra-high ductility cementitious composites, Compos. Part B Eng. 174 (2019) 107022. https://doi.org/10.1016/j.compositesb.2019.107022.

[215] A. Valadez-Gonzalez, J.M. Cervantes-Uc, R. Olayo, P.J. Herrera-Franco, Chemical modification of henequen fibers with an organosilane coupling agent, Compos. Part B Eng. 30 (1999) 321–331. https://doi.org/10.1016/S1359-8368(98)00055-9.

[216] C. Salgado, M.P. Arrieta, L. Peponi, D. López, M. Fernández-García, Photo-crosslinkable polyurethanes reinforced with coumarin modified silica nanoparticles for photo-responsive coatings, Prog. Org. Coatings. 123 (2018) 63–74. https://doi.org/10.1016/j.porgcoat.2018.06.019.

[217] W.S. Hanoosh, W.S. Hanoosh, Synthesis and Polymerization of New silane Coupling Agent and Used it as Impact Modifier of Silica Filled Unsaturated Polyester, Asian J. Appl. Sci. (2016) 2321–0893. https://doi.org/10.13140/RG.2.2.20077.28640.

[218] X. Liu, Y. Nie, X. Meng, Z. Zhang, X. Zhang, S. Zhang, DBN-based ionic liquids with high capability for the dissolution of wool keratin, RSC Adv. 7 (2017) 1981–1988. https://doi.org/10.1039/c6ra26057h.

[219] M. Montazer, A. Behzadnia, M.B. Moghadam, Superior Self-Cleaning Features on Wool Fabric Using TiO 2 / Ag Nanocomposite Optimized by Response Surface Methodology, (2012). https://doi.org/10.1002/app.36768.

[220] J.M. Raquez, Y. Habibi, M. Murariu, P. Dubois, Polylactide (PLA)-based nanocomposites, Prog. Polym. Sci. 38 (2013) 1504–1542. https://doi.org/10.1016/j.progpolymsci.2013.05.014.

[221] T. Yu, N. Jiang, Y. Li, Study on short ramie fiber/poly(lactic acid) composites

compatibilized by maleic anhydride, Compos. Part A Appl. Sci. Manuf. 64 (2014) 139–146. https://doi.org/10.1016/j.compositesa.2014.05.008.

[222] C.M. Meenakshi, A. Krishnamoorthy, Study on the effect of surface modification on the mechanical and thermal behaviour of flax, sisal and glass fiber-reinforced epoxy hybrid composites, J. Renew. Mater. 7 (2019) 153–169. https://doi.org/10.32604/jrm.2019.00046.

[223] V.S.G. Silverajah, N.A. Ibrahim, W. Zin, W. Yunus, H.A. Hassan, C.B. Woei, A Comparative Study on the Mechanical , Thermal and Morphological Characterization of Poly (lactic acid)/ Epoxidized Palm Oil Blend, (2012). https://doi.org/10.3390/ijms13055878.

[224] Z. Chu, T. Zhao, L. Li, J. Fan, Y. Qin, Characterization of Antimicrobial Poly (Lactic Acid)/ Nano-Composite Films with Silver and, (2017). https://doi.org/10.3390/ma10060659.

[225] M. Maiza, M.T. Benaniba, G. Quintard, V. Massardier-nageotte, Biobased additive plasticizing Polylactic acid (PLA), 25 (2015) 581–590.

[226] M.P. Arrieta, L. Peponi, D. López, M. Fernández-García, Recovery of yerba mate (Ilex paraguariensis) residue for the development of PLA-based bionanocomposite films, Ind. Crops Prod. 111 (2018) 317–328. https://doi.org/https://doi.org/10.1016/j.indcrop.2017.10.042.

[227] M.S. Islam, K.L. Pickering, N.J. Foreman, Influence of alkali treatment on the interfacial and physico-mechanical properties of industrial hemp fibre reinforced polylactic acid composites, Compos. Part A Appl. Sci. Manuf. 41 (2010) 596–603. https://doi.org/10.1016/j.compositesa.2010.01.006.

[228] A.K.M.M. Alam, M.F. Mina, M.D.H. Beg, A.A. Mamun, A.K. Bledzki, Q.T.H. Shubhra, Thermo-mechanical and morphological properties of short natural fiber reinforced poly (lactic acid) biocomposite: Effect of fiber treatment, Fibers Polym. 15 (2014) 1303–1309. https://doi.org/10.1007/s12221-014-1303-8.

[229] M.P. Arrieta, M.A. Peltzer, J. López, L. Peponi, PLA-based nanocomposites reinforced with CNC for food packaging applications: From synthesis to biodegradation, in: Ind. Appl. Renew. Biomass Prod. Past, Present Futur., Springer International Publishing, 2017: pp. 265–300. https://doi.org/10.1007/978-3-319-61288-1_11.

[230] J. Balart, V. Fombuena, T. Boronat, M.J. Reig, R. Balart, Surface modification of polypropylene substrates by UV photografting of methyl methacrylate (MMA) for improved surface wettability, J. Mater. Sci. 47 (2012) 2375–2383. https://doi.org/10.1007/s10853-011-6056-9.

[231] M.P. Arrieta, M.A. Peltzer, J. López, M.D.C. Garrigós, A.J.M. Valente, A. Jiménez, Functional properties of sodium and calcium caseinate antimicrobial active films containing carvacrol, J. Food Eng. 121 (2014) 94–101. https://doi.org/10.1016/j.jfoodeng.2013.08.015.

[232] M.M. El-Zawahry, N.A. Ibrahim, M.A. Eid, The impact of nitrogen plasma treatment upon the physical-chemical and dyeing properties of wool fabric, Polym. - Plast. Technol. Eng. 45 (2006) 1123–1132. https://doi.org/10.1080/03602550600728943.

[233] M. Cao, T. Cui, Y. Yue, C. Li, X. Guo, X. Jia, B. Wang, Preparation and Characterization for the Thermal Stability and Mechanical Property of PLA and PLA/CF Samples Built by FFF Approach, Materials (Basel). 16 (2023). https://doi.org/10.3390/ma16145023.

[234] T.A. Nguyen, T.H. Nguyen, Study on Mechanical Properties of Banana Fiber-Reinforced Materials Poly (Lactic Acid) Composites, Int. J. Chem. Eng. 2022 (2022). https://doi.org/10.1155/2022/8485038.

[235] J.P. Mofokeng, A.S. Luyt, T. Tábi, J. Kovács, Comparison of injection moulded, natural fibre-reinforced composites with PP and PLA as matrices, J. Thermoplast. Compos. Mater. 25 (2012) 927–948. https://doi.org/10.1177/0892705711423291.

[236] B.W. Chieng, N.A. Ibrahim, W.M.Z.W. Yunus, M.Z. Hussein, Poly(lactic acid)/poly(ethylene glycol) polymer nanocomposites: Effects of graphene nanoplatelets, Polymers (Basel). 6 (2014) 93–104. https://doi.org/10.3390/polym6010093.

VII. Appendix

1. List of Tables

2. List of Figures

3. List of equations

4. Abbreviations and terminology

AESO	Acrylated Epoxidized Soybean Oil
AI	Artificial intelligence
ANN	Artificial Neural Network
ANOVA	Analysis of Variance
ATR-FTIR	Attenuated Total Reflectance Fourier-Transformed Infrared Spectroscopy
ATS	(3-(2-aminoethylamino)propyl)-trimethoxysilane - couplig agent A
BPA	Bisphenol A
CIELab	L*a*b* color space defined by International Commission on Illumination
CMC	Complex of membrane cells
CPU	Central Processing Unit
CSV	Comma-Separated Values
DL	Deep Learning
DMA	Dynamic Mechanical Analysis
DOE	Design of Experiment
DSC	Differential Scanning Calorimetry
DT	Decision Tree
DTG	1st Derivate of Thermogravimetric curve
EKO	Epoxidized Karanja Oil
FRP	fiber reinforced polymer
FTIR	Fourier Transmittance Infrared spectroscopy
HAE	High Entropy Alloys
L/D	Length to Diameter ratio
LCA	Life Cycle Assessment
LDPE	Low Density Polyethylene
MAE	Mean Absolute Error
MCSO	Maleinized cottonseed oil
MFI	Melt Flow Index
ML	Machine Learning
MLO	maleinized linseed oil
MSE	Mean Square Error
PEG	polyethylene glycol
PET	polyethylene terephthalate
PHA	polyhydroxyalkanoate
PLA	polylactic acid
PLCL	polylactic-co-caprolactone
PLGA	polylactic-co-glycolic random copolymer
PS	polystyrene
R2	Coefficient of determination
RAE	Relative Absolute Error
RCNN	Region Convolutional Neural Network
RF	Random Forest
RH	Relative Humidity
RMSE	Root Mean Square Error
RSE	Relative Squared Error
SEM	Scanning Electron Microscopy

SVM	Support Vector Machines
TES	trimethoxy (2-(7-oxabicyclo (4.1.0)hept-3-yl) ethyl) silane - coupling agent B
TGA	Thermogravimetric Analysis
TTI	titanium (IV) (triethanolaminate)isopropoxide - coupling agent D
TVS	tris(2-methoxyethoxy)(vinyl) silane - coupling agent C
UNET	U-shaped encoder-decoder Network architecture
UV	Ultraviolet
WCA	Water Contact Angle
XRD	X-Ray Diffraction